AD_____

Award Number:
W81XWH-09-1-0457

TITLE:
Predicting the Toxicity of Adjuvant Breast Cancer Drug Combination Therapy

PRINCIPAL INVESTIGATOR:
Susan F Hudachek, MS, PhD

CONTRACTING ORGANIZATION:
Colorado State University,
Fort Collins, CO 80523-0001

REPORT DATE:
March 2013

TYPE OF REPORT:
Annual Summary

PREPARED FOR:
U.S. Army Medical Research and Materiel Command Fort Detrick, Maryland 21702-5012

DISTRIBUTION STATEMENT: **Approved for Public Release;**
Distribution Unlimited

The views, opinions and/or findings contained in this report are those of the author(s) and should not be construed as an official Department of the Army position, policy or decision unless so designated by other documentation.

REPORT DOCUMENTATION PAGE

Form Approved
OMB No. 0704-0188

1. REPORT DATE	2. REPORT TYPE	3. DATES COVERED
March 2013	Annual Summary	1 September 2009 - 28 February 2013

4. TITLE AND SUBTITLE
Predicting the toxicity of adjuvant breast cancer drug combination therapy

5a. CONTRACT NUMBER

5b. GRANT NUMBER
W81XWH-09-1-0457

5c. PROGRAM ELEMENT NUMBER

6. AUTHOR(S)
Susan F Hudachek

5d. PROJECT NUMBER

5e. TASK NUMBER

5f. WORK UNIT NUMBER

7. PERFORMING ORGANIZATION NAME(S) AND ADDRESS(ES)
Colorado State University
Fort Collins CO 80523-0001

8. PERFORMING ORGANIZATION REPORT NUMBER

9. SPONSORING / MONITORING AGENCY NAME(S) AND ADDRESS(ES)
U.S. Army Medical Research and Materiel Command
Fort Detrick, Maryland 21702-5012

10. SPONSOR/MONITOR'S ACRONYM(S)

11. SPONSOR/MONITOR'S REPORT NUMBER(S)

12. DISTRIBUTION / AVAILABILITY STATEMENT
Approved for Public Release; Distribution Unlimited

13. SUPPLEMENTARY NOTES

14. ABSTRACT

Combination therapy is increasingly utilized for the treatment of metastatic breast cancer. However, co-administration of drugs, particularly agents that are substrates for or inhibitors of p-glycoprotein, can result in increased toxicity. As adverse tissue drug concentrations are not always exposed by plasma drug concentrations, we performed studies in mice to assess both the plasma and tissue levels of the cytotoxics docetaxel and doxorubicinorubicin when administered concomitantly with the p-glycoprotein substrate/inhibitor lapatinibatinib. Both combinations are currently being investigated in clinical trials. First, we determined the tissue distribution of LAPATINIB in mice after an oral gavage dose of 60 mg/kg, which results in an exposure in mice that is equivalent to the exposure in humans when dosed at the recommended dose of 1,250 mg p.o. once daily. Next, we determined the PKs of LAPATINIB after oral gavage doses of 30 and 90 mg/kg. This completed the thorough pharmacokinetic analysis of the biodistribution of single dose LAPATINIB in mice.

Following the elucidation of the pharmacokinetics of LAPATINIB in mice, we conducted time course plasma and tissue distribution studies of concomitant lapatinibatinib and docetaxel or doxorubicinorubicin. Both single and multiple dose lapatinibatinib were evaluated. These studies illustrated that lapatinibatinib, when dosed to achieve human equivalent plasma exposure in mice, did not significantly alter the plasma or tissue pharmacokinetics of doxorubicinorubicin but did increase exposure to docetaxel in the intestine, likely leading to enhanced toxicity. Thus, caution should be taken when docetaxel and lapatinibatinib are administered together, particularly to patients with compromised CYP3A activity.

Finally, we developed a PBPK model of docetaxel in mice that incorporated PGP transport studying docetaxel pharmacokinetics in wild-type FVB and Mdr1a/b constitutive knockout (KO) mice. For all tissues in both the FVB and KO cohorts, the PBPK model simulations closely mirrored the observed data. Furthermore, both models predicted AUC values that were with 15% of the observed AUC values, indicating that our model-simulated drug exposures accurately reflected the observed tissue exposures. Overall, our PBPK model furthers the understanding of the role of ABCB1 in the biodistribution of docetaxel. Additionally, this exemplary model structure can be applied to investigate the pharmacokinetics of other ABCB1 transporter substrates.

15. SUBJECT TERMS- lapatinibatinib, doxorubicinorubicin, docetaxel, p-glycoprotein

16. SECURITY CLASSIFICATION OF:			17. LIMITATION OF ABSTRACT	18. NUMBER OF PAGES	19a. NAME OF RESPONSIBLE PERSON
a. REPORT	b. ABSTRACT	c. THIS PAGE			USAMRMC
U	U	U	UU		19b. TELEPHONE NUMBER *(include area code)*

Table Of Contents

Introduction

When drugs are given in combination, which is common practice in adjuvant breast cancer treatment, interactions can occur that alter an agent's pharmacokinetics (PKs) and pharmacodynamics (PDs) and potentiate the toxicity of the anti-cancer therapies. This is especially true for drugs that are substrates or inhibitors of P-glycoprotein (PGP), including docetaxel (DOCETAXEL), doxorubicinorubicin (DOXORUBICIN) and lapatinibatinib (LAPATINIB). The purpose of the subsequent work is to use physiologically-based pharmacokinetic (PBPK) modeling to determine the changes in both plasma and tissue PKs of DOCETAXEL and DOXORUBICIN when administered in combination with LAPATINIB. PBPK models mathematically incorporate biochemical and physiological principles to determine the pharmacologic disposition of drugs in the body using compartments that represent specific organs or tissue groups. Once the PBPK models have been optimized in humans, variability in patient covariates and PBPK model parameters will be incorporated using Monte Carlo simulation and a virtual population will be created and validated. This population will then be used for population PK analyses to identify the patient covariates that contribute to the variability in the PK data when agents are given in combination. Once these sources of variability are determined, dosing adjustments can be made that will ultimately maximize efficacy and minimize toxicity of combination therapies.

Body

Specific Aim 1. Determine the PKs of LAPATINIB, DOCETAXEL, DOXORUBICIN, combination LAPATINIB and DOCETAXEL, and combination LAPATINIB and DOXORUBICIN in mice.

▪**Task 1a.** Get approval for *in vivo* mouse studies from Colorado State University's Animal Care and Use Committee (IACUC).
TIMEFRAME: Year 1, months 1-3

IACUC approval for the *in vivo* mouse studies was obtained on 7/27/2009.

Milestone #1: IACUC approval.

▪**Task 1b.** Obtain samples for PK analysis. Dose FVB mice with LAPATINIB, DOCETAXEL, DOXORUBICIN, combination LAPATINIB and DOCETAXEL, and combination DOXORUBICIN and LAPATINIB, sacrifice at pre-specified time points, and collect and store plasma and tissue samples. For this study, there will be a total of 600 FVB mice divided into 20 cohorts. In each cohort, there will be a total of 30 mice, as three mice will be sacrificed at each of ten time points.
TIMEFRAME: Year 1, months 3-9

A time course tissue distribution study of LAPATINIB was conducted in eight- to ten-week-old female FVB mice. Single dose LAPATINIB was administered via oral gavage at doses of 30, 60 and 90 mg/kg. Three mice were sacrificed at each time point to get an estimate of the variability in the data. Following dosing, time points included 0.25, 0.5, 1, 2, 4, 8, 12 and 16 hours. Sacrifices were done by cardiac stick exsanguination under isoflurane anesthesia. Blood was collected in a heparanized syringe followed by centrifugation and transfer of plasma to a cryovial for storage at -80°C. Liver, intestine, kidney, lung, heart, brain, muscle, fat and skin were collected, flash frozen in liquid nitrogen and stored at -80ºC until analysis.

LAPATINIB dosing justification: In humans, the recommended dose of LAPATINIB is 1,250 mg p.o. once daily continuously [1]. This dose results in a 24-hour exposure of ~26.7 μg/mL · hr [2,3]. To determine the oral dose that would achieve an equivalent exposure in mice, we used data from an incomplete PK analysis done in mice [4]; the corresponding p.o. dose was calculated to be 60 mg/kg. In HN5 xenograft-bearing mice receiving a cumulative oral dose of 60 mg/kg/day, tumor p-Erk1/2 and p-AKT were inhibited after 2.5 days [5]. In another study with HN5 and BT474 xenograft-bearing mice, LAPATINIB treatment at a cumulative oral dose of 60 mg/kg/day for 21 days inhibited tumor growth substantially, with treatment at a cumulative oral dose of 200 mg/kg/day completely inhibiting tumor growth [6]. Even at this latter high dose, there was <10% weight loss in treated animals. Thus, the clinically relevant dose in mice is both efficacious and nontoxic. In addition to dosing mice at 60 mg/kg, we also dosed mice at 50% of that amount (30 mg/kg) and 150% of that amount (90 mg/kg) for a thorough PK analysis.

A time course tissue distribution study of DOXORUBICIN was conducted in eight- to ten-week-old female FVB mice. Single dose DOXORUBICIN was administered by an i.v. tail vein injection as a bolus dose of 6 mg/kg. Three mice were sacrificed at each time point to get an estimate of the variability in the data. Following dosing, time points included 0.5, 1, 4, 8, and 24 hours. Sacrifices were done by cardiac stick exsanguination under isoflurane anesthesia. Blood was collected in a heparanized syringe followed by centrifugation and transfer of plasma to a cryovial for storage at -80°C. Liver, intestine, kidney, lung, heart, brain, muscle, fat and skin were collected, flash frozen in liquid nitrogen and stored at -80ºC until analysis.

DOXORUBICIN dosing justification: For adjuvant treatment of breast cancer, DOXORUBICIN is typically dosed at 60 mg/m^2. In humans, this dose of DOXORUBICIN is associated with an exposure of 4.76 μg/mL · hr [7]. In mice, DOXORUBICIN PK data indicates that a dose of 6 mg/kg would result in equivalent exposure [8].

A time course tissue distribution study of DOCETAXEL was conducted in eight- to ten-week-old female FVB mice. Single dose DOCETAXEL was administered by an i.v. tail vein

injection as a bolus dose of 3 mg/kg. Three mice were sacrificed at each time point to get an estimate of the variability in the data. Following dosing, time points included 0.25, 0.5, 1, 2, 4, 8, 12, 16, 18 and 24 hours. Sacrifices were done by cardiac stick exsanguination under isoflurane anesthesia. Blood was collected in a heparanized syringe followed by centrifugation and transfer of plasma to a cryovial for storage at -80°C. Liver, intestine, kidney, lung, heart, brain, muscle, fat and skin were collected, flash frozen in liquid nitrogen and stored at -80ºC until analysis.

DOCETAXEL dosing justification: In a phase I PK study of LAPATINIB and DOCETAXEL in patients with advanced solid tumors, the optimally tolerated regimen was LAPATINIB at 1,250 mg p.o. once daily and DOCETAXEL at 75 mg/m^2 i.v. once every 3 weeks [9]. This dose of DOCETAXEL resulted in an exposure (AUC_∞) of 2.47 mg/L · hr. In mice, data from a DOCETAXEL PK study [10] indicates that a dose of 3 mg/kg would result in equivalent exposure.

A time course tissue distribution study of combination LAPATINIB and DOXORUBICIN was conducted in eight- to ten-week-old female FVB mice. LAPATINIB was administered by oral gavage at a single dose of 60 mg/kg and DOXORUBICIN was administered one hour post LAPATINIB administration by an i.v. tail vein injection as a bolus dose of 6 mg/kg. Three mice were sacrificed at each time point to get an estimate of the variability in the data. Following dosing, time points included 0.5, 1, 4, 8 and 24 hours. Sacrifices were done by cardiac stick exsanguination under isoflurane anesthesia. Blood was collected in a heparanized syringe followed by centrifugation and transfer of plasma to a cryovial for storage at -80°C. Liver, intestine, kidney, lung, heart, brain, muscle, fat and skin were collected, flash frozen in liquid nitrogen and stored at -80ºC until analysis.

A time course tissue distribution study of single dose LAPATINIB was conducted in five- to six-week-old female FVB mice. LAPATINIB was administered by oral gavage at a single dose of 600 mg/kg in DMSO. Three mice were sacrificed at each time point to get an estimate of the variability in the data. Following dosing, time points included 1, 5, 9, and 25 hours. Sacrifices were done by cardiac stick exsanguination under isoflurane anesthesia. Blood was collected in a syringe and transferred to a serum separator tube, followed by centrifugation and transfer of serum to a cryovial for storage at -80°C.

A time course tissue distribution study of single dose LAPATINIB was conducted in five- to six-week-old female FVB mice. LAPATINIB was administered by intraperitoneal (IP) injection at a single dose of 600 mg/kg in DMSO. Three mice were sacrificed at each time point to get an estimate of the variability in the data. Following dosing, time points included 5, 9, and 25 hours. Sacrifices were done by cardiac stick exsanguination under isoflurane anesthesia. Blood was collected in a syringe and transferred to a serum separator tube, followed by centrifugation and transfer of serum to a cryovial for storage at -80°C.

A time course tissue distribution study of combination LAPATINIB and DOXORUBICIN was conducted in five- to six-week-old female FVB mice. LAPATINIB was administered by oral gavage at a single dose of 600 mg/kg in DMSO and DOXORUBICIN was administered one hour post LAPATINIB administration by an i.v. tail vein injection as a bolus dose of 6 mg/kg. Three mice were sacrificed at each time point to get an estimate of the variability in the data. Following dosing, time points included 1, 4, 8, and 24 hours. Sacrifices were done by cardiac stick exsanguination under isoflurane anesthesia. Blood was collected in a syringe and transferred to a serum separator tube, followed by centrifugation and transfer of serum to a cryovial for storage at -80°C. Liver, intestine, kidney, lung, heart, brain, muscle, fat and skin were collected, flash frozen in liquid nitrogen and stored at -80ºC until analysis.

A time course tissue distribution study of single dose LAPATINIB was conducted in five- to six-week-old female FVB mice. LAPATINIB was administered by IP injection at a single dose of 60 mg/kg in DMSO. Three mice were sacrificed at each time point to get an estimate of the variability in the data. Following dosing, time points included 1, 2, 4, 8, 16 and 24 hours. Sacrifices were done by cardiac stick exsanguination under isoflurane anesthesia. Blood was collected in a

syringe and transferred to a serum separator tube, followed by centrifugation and transfer of serum to a cryovial for storage at -80°C.

A time course tissue distribution study of single dose LAPATINIB was conducted in five- to six-week-old female FVB mice. LAPATINIB was administered by IP injection at a single dose of 6 mg/kg in 20% hydroxypropyl beta cyclodextrin (HPCD). Three mice were sacrificed at each time point to get an estimate of the variability in the data. Following dosing, time points included 1 and 6 hours. Sacrifices were done by cardiac stick exsanguination under isoflurane anesthesia. Blood was collected in a syringe and transferred to a serum separator tube, followed by centrifugation and transfer of serum to a cryovial for storage at -80°C.

A time course tissue distribution study of single dose LAPATINIB was conducted in five- to six-week-old female FVB mice. LAPATINIB was administered by IP injection at a single dose of 12 mg/kg in 20% HPCD. Three mice were sacrificed at each time point to get an estimate of the variability in the data. Following dosing, time points included 1 and 3 hours. Sacrifices were done by cardiac stick exsanguination under isoflurane anesthesia. Blood was collected in a syringe and transferred to a serum separator tube, followed by centrifugation and transfer of serum to a cryovial for storage at -80°C.

A time course tissue distribution study of single dose LAPATINIB was conducted in five- to six-week-old female FVB mice. LAPATINIB was administered by IP injection at a single dose of 6 mg/kg in DMSO. Three mice were sacrificed at each time point to get an estimate of the variability in the data. Following dosing, time points included 1 and 3 hours. Sacrifices were done by cardiac stick exsanguination under isoflurane anesthesia. Blood was collected in a syringe and transferred to a serum separator tube, followed by centrifugation and transfer of serum to a cryovial for storage at -80°C.

A time course tissue distribution study of single dose LAPATINIB was conducted in five- to six-week-old female FVB mice. LAPATINIB was administered by IP injection at a single dose of 60 mg/kg in 0.5% hydroxypropyl methylcellulose:0.1% Tween 80. Three mice were sacrificed at each time point to get an estimate of the variability in the data. Following dosing, time points included 1 and 4 hours. Sacrifices were done by cardiac stick exsanguination under isoflurane anesthesia. Blood was collected in a syringe and transferred to a serum separator tube, followed by centrifugation and transfer of serum to a cryovial for storage at -80°C.

A time course tissue distribution study of single dose LAPATINIB was conducted in five- to six-week-old female FVB mice. LAPATINIB was administered by IP injection at a single dose of 60 mg/kg in 0.5% hydroxypropyl methylcellulose:0.1% Tween 80. Three mice were sacrificed at each time point to get an estimate of the variability in the data. Following one dose, time points included 1 and 3 hours. Following two doses (one at time 0 and one at 3 hours), time points included 4 hours and 6 hours. Sacrifices were done by cardiac stick exsanguination under isoflurane anesthesia. Blood was collected in a syringe and transferred to a serum separator tube, followed by centrifugation and transfer of serum to a cryovial for storage at -80°C.

A time course tissue distribution study of LAPATINIB was conducted in five- to six-week-old female FVB mice. LAPATINIB was administered by IP injection at a dose of 60 mg/kg in 0.5% hydroxypropyl methylcellulose:0.1% Tween 80. LAPATINIB was dosed every 3 hours for a total of 5 doses (q3hr × 5). Subsequently, three mice were sacrificed at each post-dose Cmax (determined from previous studies to be 1 hr post-dose) and Cmin (3 hrs post-dose). For the fifth dose, we only sacrificed mice at the Cmax. All sacrifices were done by cardiac stick exsanguination under isoflurane anesthesia. Plasma was immediately collected, frozen in liquid nitrogen and stored at -80°C until analysis. A detailed description of the pharmacokinetic study methodology can be found in the appended manuscript titled "Co-administration of lapatinibatinib increases exposure to docetaxel but not doxorubicinorubicin in the small intestine of mice".

Time course plasma and tissue distribution studies of concomitant lapatinibatinib with docetaxel or doxorubicinorubicin were conducted in mice. Intravenous chemotherapy was administered one hour after the first intraperitoneal lapatinibatinib dose. Both single and multiple dose lapatinibatinib were evaluated. Samples were collected up to 12 and 48 hrs post docetaxel and doxorubicinorubicin administration, respectively. A detailed description of the pharmacokinetic study methodology can be found in the appended manuscript titled "Co-administration of lapatinibatinib increases exposure to docetaxel but not doxorubicinorubicin in the small intestine of mice".

Task 1c. Obtain samples for determining the role of PGP in drug PK. Dose mdr1a/b knockout mice with LAPATINIB, DOCETAXEL, DOXORUBICIN, combination LAPATINIB and DOCETAXEL, and combination DOXORUBICIN and LAPATINIB, sacrifice at a pre-specified time point, and collect and store plasma and tissue samples. For this study, there will be a total of 15 mdr1a/b knockout mice divided into 5 cohorts. In each cohort, there will be a total of 3 mice, as three mice will be sacrificed at one time point.
TIMEFRAME: Year 1, months 9-12

A time course tissue and feces distribution study of docetaxel was conducted in both FVB and KO mice. Docetaxel was administered via intravenous tail vein injection as a single bolus dose of 3 mg/kg. A detailed description of the pharmacokinetic study methodology can be found in the appended manuscript titled "Incorporation of ABCB1-Mediated Transport into a Physiologically-Based Pharmacokinetic Model of Docetaxel in Mice".

Task 1d. Obtain samples for determining drug-plasma protein (albumin and α1-acid glycoprotein) binding. Dose FVB mice with LAPATINIB, DOCETAXEL, DOXORUBICIN, combination LAPATINIB and DOCETAXEL, and combination DOXORUBICIN and LAPATINIB, sacrifice at a pre-specified time point, and collect and store plasma samples. For this study, there will be a total of 60 FVB mice divided into 20 cohorts. In each cohort, there will be a total of 3 mice, as three mice will be sacrificed at one time point.
TIMEFRAME: Year 1, months 9-12

The determination of drug-plasma protein binding was for use in the development of PBPK models comprising combination of lapatinibatinib + docetaxel and lapatinibatinib + doxorubicinorubicin . As the combination studies of lapatinibatinib + docetaxel and lapatinibatinib + doxorubicinorubicin did not result in data amenable to PBPK modeling of PGP transport because lapatinibatinib did not alter the pharmacokinetics of docetaxel or doxorubicinorubicin when administered in combination with these chemotherapeutics, it was not necessary to determine the drug-plasma protein binding during combination therapy. For the PBPK model of docetaxel, the fraction of the drug bound to plasma proteins had been previously determined as 0.07 [11] and, thus was simply retrieved from the literature for use in the model.

Milestone #2: Collection of *in vivo* samples.

Task 1e. Determine drug-plasma protein (albumin and α1-acid glycoprotein) binding. Using the samples from Task 1d and the single-use RED (rapid equilibrium dialysis) plate with inserts (Thermo Scientific, Waltham, MA), drug-plasma protein binding and the concentration of free drug (LAPATINIB, DOCETAXEL and DOXORUBICIN) in the plasma will be determined. LAPATINIB and DOCETAXEL levels will be analyzed using LC/MS/MS and DOXORUBICIN levels will be analyzed using HPLC with fluorescence detection.
TIMEFRAME: Year 2, months 1-6.

The determination of drug-plasma protein binding was for use in the development of PBPK models comprising combination of lapatinibatinib + docetaxel and lapatinibatinib + doxorubicinorubicin . As the combination studies of lapatinibatinib + docetaxel and lapatinibatinib + doxorubicinorubicin did not result in data amenable to PBPK modeling of PGP transport because lapatinibatinib did not alter the pharmacokinetics of docetaxel or doxorubicinorubicin when administered in combination with these chemotherapeutics, it was not necessary to determine the drug-plasma protein binding during combination therapy. For the PBPK model of

docetaxel, the fraction of the drug bound to plasma proteins had been previously determined as 0.07 [11] and, thus was simply retrieved from the literature for use in the model.

Task 1f. Analyze drug levels in collected samples. Using the samples from Task 1b and Task 1c, the concentration of drugs in the plasma and tissue samples will be determined. LAPATINIB and DOCETAXEL levels will be analyzed using LC/MS/MS and DOXORUBICIN levels will be analyzed using HPLC with fluorescence detection.
TIMEFRAME: Year 2, months 1-9.

An analytical method for the measurement of LAPATINIB in biological samples using LC/MS/MS was developed. A detailed description of this methodology can be found in the appended manuscript titled "Physiologically based pharmacokinetic model of lapatinibatinib developed in mice and scaled to humans".

The concentration of LAPATINIB in plasma was determined for the 30, 60 and 90 mg/kg cohorts (Figure 1). In addition, the concentration of LAPATINIB in liver, intestine, kidney, lung, heart, brain, muscle, and fat was determined for the 60 mg/kg cohort (Figures 2A, 2B and 2C). These concentration-time results can be found in Figure 2 of the appended manuscript titled "Physiologically based pharmacokinetic model of lapatinibatinib developed in mice and scaled to humans".

An analytical method for the measurement of DOXORUBICIN in biological samples using HPLC with fluorescence detection was developed. The concentration of DOXORUBICIN in plasma was determined for the single agent 6 mg/kg DOXORUBICIN cohort and the combination 60 mg/kg LAPATINIB and 6 mg/kg DOXORUBICIN cohort (Figure 3). However, the analysis of these samples was problematic due to an unforeseen binding interaction between DOXORUBICIN and heparin, the anticoagulent used for blood collection. In subsequent DOXORUBICIN studies, we will collect serum, which does not require the use of an anticoagulent, instead of plasma. The concentration of DOXORUBICIN in liver, gut, kidney, heart and brain was determined for the single agent 6 mg/kg DOXORUBICIN cohort and the combination 60 mg/kg LAPATINIB and 6 mg/kg DOXORUBICIN cohort (Figure 4).

In addition, the concentration of LAPATINIB in plasma, liver and gut was determined for the combination 60 mg/kg LAPATINIB and 6 mg/kg DOXORUBICIN cohort using LC/MS/MS (Figure 5).

The concentration of LAPATINIB in liver, intestine, kidney, muscle, adipose, brain, heart and lung were determined for the 30 and 90 mg/kg cohorts using LC/MS/MS (Figure 6). These concentration-time results can be found in Figure 2 of the appended manuscript titled "Physiologically based pharmacokinetic model of lapatinibatinib developed in mice and scaled to humans".

The concentration of LAPATINIB in serum was determined for mice dosed via oral gavage with 600 mg/kg LAPATINIB in DMSO using LC/MS/MS (Figures 7 and 9).

The concentration of LAPATINIB in serum was determined for mice dosed via IP injection with 600 mg/kg LAPATINIB in DMSO using LC/MS/MS (Figures 8 and 9).

The concentration of DOXORUBICIN in serum, liver and gut was determined for the combination 600 mg/kg LAPATINIB in DMSO and 6 mg/kg DOXORUBICIN cohort using HPLC (Figure 10).

The concentration of LAPATINIB in serum was determined for mice dosed via IP injection with 60 mg/kg LAPATINIB in DMSO using LC/MS/MS (Figure 11).

The concentration of LAPATINIB in serum was determined for mice dosed via IP injection with 6 mg/kg LAPATINIB in 20% HPCD using LC/MS/MS (Figure 12).

The concentration of LAPATINIB in serum was determined for mice dosed via IP injection with 12 mg/kg LAPATINIB in 20% HPCD using LC/MS/MS (Figure 13).

The concentration of LAPATINIB in serum was determined for mice dosed via IP injection with 6 mg/kg LAPATINIB in DMSO using LC/MS/MS (Figure 14).

The concentration of LAPATINIB in serum was determined for mice dosed via IP injection with 60 mg/kg LAPATINIB in 0.5% hydroxypropyl methylcellulose:0.1% Tween 80 using LC/MS/MS (Figure 15).

The concentration of LAPATINIB in serum was determined for mice dosed via IP injection with one dose of 60 mg/kg LAPATINIB in 0.5% hydroxypropyl methylcellulose:0.1% Tween 80 and two doses of 60 mg/kg LAPATINIB in 0.5% hydroxypropyl methylcellulose:0.1% Tween 80 using LC/MS/MS (Figure 16).

The concentration of LAPATINIB in plasma was determined for mice dosed via IP injection with 60 mg/kg in 0.5% hydroxypropyl methylcellulose:0.1% Tween 80 every 3 hours for a total of 5 doses (q3hr × 5) using LC/MS/MS. These concentration-time results can be found in Figure 1 of the appended manuscript titled "Co-administration of lapatinibatinib increases exposure to docetaxel but not doxorubicinorubicin in the small intestine of mice".

Samples from the time course plasma and tissue distribution studies of concomitant lapatinibatinib with docetaxel or doxorubicinorubicin conducted in mice were analyzed and drug concentrations were determined. These concentration-time results can be found in Figures 2 and 3 of the appended manuscript titled "Co-administration of lapatinibatinib increases exposure to docetaxel but not doxorubicinorubicin in the small intestine of mice".

Samples from the time course tissue and feces distribution study of docetaxel conducted in both FVB and KO mice were analyzed and drug concentrations were determined (Figure 17). These concentration-time results can be found in Figure 1 of the appended manuscript titled "Incorporation of ABCB1-Mediated Transport into a Physiologically-Based Pharmacokinetic Model of Docetaxel in Mice".

Milestone #3: Determination of drug concentrations in plasma and tissue samples.

Task 1g. Using the data from Task 1f, plasma and tissue drug concentration versus time data will be modeled by compartmental analysis and PK parameters will be calculated using SAAM II software, version 1.2.1 (Saam Institute, University of Washington).
TIMEFRAME: Year 2, months 1-9.

LAPATINIB plasma, liver, intestine, kidney, lung, heart, brain, muscle, and fat PK parameters were determined for the 60 mg/kg cohort using both noncompartmental modeling and compartmental (2 compartment) modeling (Tables 1-3). These PK parameters can be found in Table 2 and Figure 3 of the appended manuscript titled "Physiologically based pharmacokinetic model of lapatinibatinib developed in mice and scaled to humans".

From the LAPATINIB PK parameter analyses, we determined that the half-life of LAPATINIB is 3.5 hr. For the steady state LAPATINIB studies, this would indicate that we would have to orally gavage mice every 3.5 hours for 24.5 hours to achieve steady state levels of LAPATINIB prior to administration of DOXORUBICIN or DOCETAXEL. As this would likely cause undue stress to the mice, we have decided to use Alzet® osmotic pumps as an alternative LAPATINIB administration route. Approval for the use of the Alzet® osmotic pumps has been obtained from both USAMRMC and Colorado State University's IACUC. The Alzet® osmotic pumps did not work for this study due to formulation incompatibility with the pumps. In order for the pumps to function properly, the compound (in this case, LAPATINIB) must be in solution. However, LAPATINIB is extremely hydrophobic (clogP of 5.1) and to get this drug into solution at a concentration that would result in the necessary PK parameters (human equivalent AUC, C_{max} and C_{min}), we would need to formulate LAPATINIB in 100% DMSO. Unfortunately, the maximum concentration of DMSO that is permissible in the pumps in 50% DMSO, as higher concentrations are not compatible with the pump reservoir. Many other solvents were tried, including methanol, ethanol, Trappsol®, Solutol®, corn oil, sunflower oil, and sesame seed oil, but with no success. If we did manage to get the LAPATINIB in solution in a solvent combination, a common problem we found was that once the pump was implanted *in vivo*, the drug would precipitate out of solution as it exited the pump, thus clogging the pump at the exit port. After many failed attempts, we decided to abandon the Alzet® osmotic pumps and chose a different dose route and schedule in order to maintain LAPATINIB levels between the human C_{max} and C_{min} while either DOXORUBICIN or DOCETAXEL is also on board. We have found that the best alternative will be to dose LAPATINIB via IP injection with 60 mg/kg LAPATINIB in 0.5% hydroxypropyl methylcellulose:0.1% Tween 80 (Figure 16).

The LAPATINIB PK parameters of the 30, 60 and 90 mg/kg cohorts were determined using noncompartmental modeling (Table 4). These PK parameters can be found in Table 2 and Figure 3 of the appended manuscript titled "Physiologically based pharmacokinetic model of lapatinibatinib developed in mice and scaled to humans".

The DOXORUBICIN tissue $AUCs_{0-24}$ of the combination 600 mg/kg LAPATINIB in DMSO and 6 mg/kg DOXORUBICIN cohort were determined using noncompartmental modeling (Table 5).

DOCETAXEL and DOXORUBICIN PK parameters from the biodistribution studies of concomitant lapatinibatinib with docetaxel or doxorubicinorubicin conducted in mice were determined using noncompartmental modeling. These PK parameters can be found in Tables 2 and 3 and Supplementary Tables 1, 2, 3 and 4 of the appended manuscript titled "Co-administration of lapatinibatinib increases exposure to docetaxel but not doxorubicinorubicin in the small intestine of mice".

Milestone #4: PK models of LAPATINIB, DOCETAXEL, DOXORUBICIN, combination LAPATINIB and DOCETAXEL and combination LAPATINIB and DOXORUBICIN.

Specific Aim 2. Using the data from AIM 1, modify DOCETAXEL and DOXORUBICIN PBPK models that have been previously developed and scaled to humans to include parameters that may be affected by drug interactions.

Task 2a. Add organs (and the corresponding organ-specific parameters) that are major sites of toxicity. For the DOCETAXEL model, we will add bone marrow, brain, heart and skin compartments to the model. For the DOXORUBICIN model, we will add brain and skin compartments to the model.
TIMEFRAME: Year 2, months 9-12 and Year 3, months 1-3.

We added organs of relevance to the DOCETAXEL PBPK mouse model. A detailed description of the model development can be found in the appended manuscript titled "Incorporation of ABCB1-Mediated Transport into a Physiologically-Based Pharmacokinetic Model of Docetaxel in Mice". Also, a schematic representation of the PBPK model can be found in Figure 2 of the appended manuscript titled "Incorporation of ABCB1-Mediated Transport into a Physiologically-Based Pharmacokinetic Model of Docetaxel in Mice".

Task 2b. For appropriate organs, include a term for PGP-mediated drug efflux and a term for competitive inhibition of PGP-mediated drug efflux to the equation for the rate of change of the amount of drug in an organ compartment. These terms will be determined from Tasks 1c and 1f. For both the DOCETAXEL model and the DOXORUBICIN model, we will add these terms to the brain, bone marrow, heart, kidney, liver and intestine.
TIMEFRAME: Year 2, months 9-12 and Year 3, months 1-3.

We added PGP-mediated drug efflux terms to relevant tissues in the DOCETAXEL PBPK mouse model. A detailed description of the model development can be found in the appended manuscript titled "Incorporation of ABCB1-Mediated Transport into a Physiologically-Based Pharmacokinetic Model of Docetaxel in Mice". Also, a schematic representation of the PBPK model can be found in Figure 2 of the appended manuscript titled "Incorporation of ABCB1-Mediated Transport into a Physiologically-Based Pharmacokinetic Model of Docetaxel in Mice".

Task 2c. Add a term for competitive binding to plasma proteins (albumin and α1-acid glycoprotein). This term will be determined from the Tasks 1d and 1e.
TIMEFRAME: Year 2, months 9-12 and Year 3, months 1-3.

As the combination studies of lapatinibatinib + docetaxel and lapatinibatinib + doxorubicinorubicin did not result in data amenable to PBPK modeling of PGP transport because lapatinibatinib did not alter the pharmacokinetics of docetaxel or doxorubicinorubicin when administered in combination with these chemotherapeutics, it was not necessary to add a term for competitive binding to plasma proteins for the DOCETAXEL PBPK model.

Task 2d. Validate the PBPK models. Compare the PBPK model-simulated drug concentration versus time data with the actual data from Tasks 1b and 1f. Refine the PBPK model as necessary.
TIMEFRAME: Year 2, months 9-12 and Year 3, months 1-3.

A PBPK model of DOCETAXEL was developed that incorporated PGP transport using the data from the DOCETAXEL pharmacokinetic studies conducted in FVB and Mdr1a/b knockout mice. This work in detailed in the appended manuscript titled "Incorporation of ABCB1-Mediated Transport into a Physiologically-Based Pharmacokinetic Model of Docetaxel in Mice".

Milestone #5: Complete PBPK models for predicting drug interactions between LAPATINIB and DOCETAXEL and LAPATINIB and DOXORUBICIN.

Research Results and Discussion

One of the primary aims of this work was to determine the pharmacokinetics (PKs) of lapatinibatinib (LAPATINIB) in female FVB mice. To our knowledge, LAPATINIB tissue distribution (with the exception of plasma/blood) has not been previously reported. While we found detectable levels of LAPATINIB in all tissues tested, we found high concentrations in the gut, lung, liver and heart, which could impact LAPATINIB toxicity. During the first year of this award, we had determined the tissue distribution of LAPATINIB in mice after an oral gavage dose of 60 mg/kg, which results in an exposure in mice that is equivalent to the exposure in humans when dosed at the recommended dose of 1,250 mg p.o. once daily.

During the second year of this award, we determined the tissue concentrations of LAPATINIB after oral gavage doses of 30 and 90 mg/kg (Figure 6). After we accrued all of this data, we were able to determine the PK of these dose cohorts and compare this data to the PK data of the 60 mg/kg dose cohort determined during year one of this award (Table 1). This comparison indicated that the LAPATINIB exhibits linear PK. Thus, in all tissue examined, exposure to LAPATINIB (as indicated by the $AUC_{0\text{-}24hrs}$) increased linearly with dose. Other characteristics of linear PK include a half-life that is independent of concentration and CL that is independent of dose, both of which were exhibited in this study. The half-life of LAPATINIB was fairly consistent in all tissues and averaged 3.5 hrs. In terms of CL, LAPATINIB was most rapidly cleared from the brain (62430 g/hr/kg) and most slowly cleared from lungs (396 g/hr/kg). This work completed the thorough PK analysis of the biodistribution of single dose LAPATINIB in mice.

During the first year of this award, when we dosed LAPATINIB (60 mg/kg) and DOXORUBICIN (6 mg/kg) in combination, we expected to observe significant alterations in the PKs of tissues with high expression of PGP (liver, gut, kidney and brain), as LAPATINIB is a PGP inhibitor and DOXORUBICIN is a PGP substrate. We did see a statistically significant increase in DOXORUBICIN liver concentrations when DOXORUBICIN was administered in combination with LAPATINIB (24193 ng/g) versus when administered as a single agent (19041 ng/g) ($P = 0.0274$).

To determine if this difference was indeed a result of LAPATINIB PGP inhibition, we increased the LAPATINIB dose to 600 mg/kg and formulated the drug in DMSO so that the LAPATINIB would be in solution as opposed to a suspension. When we dosed this formulation PO in combination with IV DOXORUBICIN at 6 mg/kg, we found increases of 48%, 56% and 29% in the $AUC_{0\text{-}24hrs}$ of serum, liver and gut, respectively (Figure 10 and Table 2).

The next step in this study was to determine if this increase would be amplified when LAPATINIB was at steady state during DOXORUBICIN administration. From the LAPATINIB single dose study, we determined the half-life to be 3.5 hrs; this is a very short half-life in mice, which we did not anticipate. In contrast, the half-life of LAPATINIB in humans is 24 hrs, which is amenable to daily dosing.

For our mouse work, LAPATINIB would have to be dosed every 3.5 hrs 5-7 times to reach steady-state and then every 3.5 hours during the duration of the PK study for DOXORUBICIN or DOCETAXEL. We attempted this dosing schedule via oral gavage but were unsuccessful, as the mice did not tolerate multiple oral gavages well and we ended up puncturing the esophagus in many of the animals.

Our next dosing attempt was to use Alzet® osmotic pumps as another option for LAPATINIB administration. Approval for the use of the Alzet® osmotic pumps was obtained from both USAMRMC and Colorado State University's IACUC. We expected the Alzet® osmotic pumps to be an ideal alternative dosing mechanism, as they would provide continuous administration of LAPATINIB subcutaneously for up to 7 days. However, the Alzet® osmotic pumps did not work for this study due to formulation incompatibility with the pumps. In order for the pumps to function properly, the compound (in this case, LAPATINIB) must be in solution. However, LAPATINIB is extremely hydrophobic (clogP of 5.1) and to get this drug into solution at a concentration that would result in the necessary PK parameters (human equivalent AUC, C_{max} and C_{min}), we would need to formulate LAPATINIB in 100% DMSO. Unfortunately, the maximum concentration of DMSO that is permissible in the pumps in 50% DMSO, as higher concentrations are not compatible with the pump reservoir.

Many other solvents were tried, including methanol, ethanol, Trappsol®, Solutol®, corn oil, sunflower oil, and sesame seed oil, but with no success. If we did manage to get the LAPATINIB in solution in a solvent combination, a common problem we found was that once the pump was implanted *in vivo*, the drug would precipitate out of solution as it exited the pump, thus clogging the pump at the exit port. After many failed attempts, we decided to abandon the Alzet® osmotic pumps and chose a different dose route and schedule in order to maintain LAPATINIB levels between the human C_{max} and C_{min} while either DOXORUBICIN or DOCETAXEL is also on board.

In order to accomplish the goal of maintaining the LAPATINIB levels between the human C_{max} (2430 ng/mL) and C_{min} (1000 ng/mL) for the duration of the combination studies, we decided to explore PO dosing further with alterations in the LAPATINIB formulation. Namely, we formulated LAPATINIB in DMSO so that it would be in solution for the oral gavage dosing (as opposed to the suspension in 0.5% hydroxypropyl methylcellulose:0.1% Tween 80 that we had previously been using). After PO administration of 600 mg/kg, the C_{max} was 23400 ng/mL and the C_{min} measured at 24 hrs was 10365 ng/mL (Figure 7). Thus, this dosing formulation and route resulted in C_{max} and C_{min} values that were roughly 10 times greater than desired.

Next, we chose use the same dose and formulation of LAPATINIB (600 mg/kg in DMSO) but changed the route of administration to IP injection. This resulted in a C_{max} of 13200 mg/mL and a C_{min} of 2770 ng/mL at 25 hrs (Figure 8). Again, these values were much higher than the target C_{max} and C_{min} of 2430 ng/mL and 1000 ng/mL, respectively (Figure 9).

In an attempt to achieve lower C_{max} and C_{min} values, we decreased the IP dose by 10-fold to 60 mg/kg in DMSO. This dose alteration yielded a C_{max} of 22267 ng/mL and the target C_{min} of 1000 ng/mL was reached at ~12 hrs (Figure 11). Again, this dose resulted in significantly greater drug levels than our goal concentrations.

Subsequently, we reduced the dose to 6 mg/kg and changed the vehicle to 20% hydroxypropyl beta cyclodextrin (HPCD), as LAPATINIB goes into solution in 20% HPCD at this low concentration and HPCD is less toxic than DMSO. The C_{max} and C_{min} values that resulted from the IP injections were 1187 ng/mL and 150.3 ng/mL at 6 hrs, respectively (Figure 12). With this dosing regimen, we were below our targeted values.

Therefore, we doubled our dose to 12 mg/kg and achieved our intended C_{max} of 2330 ng/mL with IP injections; however, our target C_{min} of 1000 ng/mL was reached at 1.75 hrs (Figure 13). Consequently, to maintain LAPATINIB levels between these two concentrations, mice would have to be dosed every 1.75 hrs, which is not realistically feasible to do for 24 hrs.

For that reason, we decided to further explore the 6 mg/kg dose given IP using DMSO as a vehicle. The C_{max} at 1 hr was 2247 ng/mL but, again our target C_{min} of 1000 ng/mL was reached at 1.75 hrs (Figure 14), thus making this dosing regimen implausible.

In order to slow the elimination of LAPATINIB such that the dosing interval would be increased to a more practical time period, we chose to administer the drug as a suspension instead of a solution, hypothesizing that the dissolution would prolong the clearance of the drug. Accordingly, we formulated LAPATINIB at 60 mg/kg in 0.5% hydroxypropyl methylcellulose:0.1% Tween 80 and dosed the mice via IP injection. This resulted in a C_{max} at 1 hr of 1967 ng/mL and a C_{min} of 435 ng/mL at 4 hrs (Figure 15). By altering the dosing interval to every 3 hrs, we anticipated that we would be able to achieve our target C_{max} and C_{min}. To verify this, we performed a multiple IP dosing study with LAPATINIB formulated at 60 mg/kg in 0.5% hydroxypropyl methylcellulose:0.1% Tween 80. After one dose, the C_{max} was 2705 ng/mL and the C_{min} was 692 ng/mL. After the second dose, the C_{max} and C_{min} were 2553 ng/mL and 729 ng/mL, respectively (Figure 16). We believe this is sufficiently close to the human values for our studies. Therefore, we have concluded that our best alternative will be to dose LAPATINIB via IP injection with 60 mg/kg LAPATINIB in 0.5% hydroxypropyl methylcellulose:0.1% Tween 80 every 3 hours while the second drug (either DOXORUBICIN or DOCETAXEL) is on board. Approval for this dose route and schedule change has been obtained from both USAMRMC and Colorado State University's IACUC. After this very long road of dose finding, we were able to move ahead with the multiple dose studies, as we did not anticipate all of the LAPATINIB formulation and scheduling challenges that arose.

Using the dose route and schedule determined about, we investigated the combination dosing of lapatinibatinib with docetaxel or doxorubicinorubicin. A detailed description of the methods, results and analysis of this work can be found in the appended manuscript titled "Co-administration of lapatinibatinib increases exposure to docetaxel but not doxorubicinorubicin in the small intestine of mice".

Based on the work presented in the manuscript titled "Co-administration of lapatinibatinib increases exposure to docetaxel but not doxorubicinorubicin in the small intestine of mice", lapatinibatinib did not alter the pharmacokinetics of doxorubicinorubicin and docetaxel to the extent that we hypothesized this PGP substrate/inhibitor would. As detailed in the manuscript, the plasma and tissue pharmacokinetics of doxorubicinorubicin were unchanged by co-administration with lapatinibatinib. However, concomitant lapatinibatinib did increase docetaxel exposure in the intestine but not in plasma or any of the seven other tissues evaluated. Moving forward with this data to Specific Aim 2 was not feasible because we proposed to model differences seen when either docetaxel or doxorubicinorubicin was administered with a PGP

substrate and/or inhibitor. Thus, to continue with Aim 2 and the subsequent Aims that are dependent upon Aim 2, PGP needed to be altered such that there was a resultant PK difference in docetaxel or doxorubicinorubicin. To accomplish this, we could have used a more potent PGP inhibitor, like cyclosporin A, but this had the potential to be problematic because many compounds that are PGP inhibitors also inhibit other pathways important for drug disposition. For example, cyclosporin A also inhibits CYP3A4, the major metabolic enzyme responsible for docetaxel elimination. Therefore, it would be impossible to determine if the altered PK was the result of PGP and/or CYP3A4 inhibition. Consequently, as an alternative to pharmacologic inhibition, we used genetic inhibition. Specifically, we utilized PGP (mdr1a/b) knockout mice as proposed in Task 1c and dosed them with docetaxel to directly evaluate the effect of PGP on docetaxel PK. The plasma and tissue docetaxel concentration profiles in PGP knockout and wild-type mice are presented in Figure 17. Mice without PGP showed significant increases in docetaxel concentrations in intestine, kidney, brain, heart, lung and muscle.

Using the DOCETAXEL PK data from the FVB and PGP knockout mice, we developed a DOCETAXEL PBPK model incorporating PGP transport. A detailed description of the methods, results and analysis of this work can be found in the appended manuscript titled "Incorporation of ABCB1-Mediated Transport into a Physiologically-Based Pharmacokinetic Model of Docetaxel in Mice".

When attempting to scale this mouse PBPK model to humans, we came upon a recent publication titled "Biodistribution and radiation dosimetry of ^{11}C-labeled docetaxel in cancer patients" [12]. This manuscript clearly shows that the whole-body biodistribution of docetaxel is very different in humans than it is in mice. In mice, the exposure ranks, from highest to lowest, lung, kidney, heart, liver, intestine, plasma and brain. However, in humans, this ranking is liver, kidney, intestine, heart, lung and brain. It is currently unclear to us why the tissue distribution of docetaxel is vastly different between the two species. Until we are able to figure this out, which we intend to continue investigating, we cannot scale our mouse PBPK model to humans and continue on with the Monte Carlo simulations and population PK analysis.

Key Research Accomplishments

▪Collection of samples for PK analysis of LAPATINIB dosed at 30, 60 and 90 mg/kg
▪Collection of samples for PK analysis of DOCETAXEL dosed at 3 mg/kg
▪Collection of samples for PK analysis of DOXORUBICIN dosed at 6 mg/kg
▪Collection of samples for PK analysis of combination LAPATINIB (dosed at 60 mg/kg) and DOXORUBICIN (dosed at 6 mg/kg)
▪LC/MS/MS analysis of plasma from study of LAPATINIB dosed at 30, 60 and 90 mg/kg
▪LC/MS/MS analysis of tissues from study of LAPATINIB dosed at 60 mg/kg
▪HPLC analysis of plasma and tissues from study of DOXORUBICIN dosed at 6 mg/kg
▪HPLC analysis of DOXORUBICIN levels in plasma and tissues from study of combination LAPATINIB (dosed at 60 mg/kg) and DOXORUBICIN (dosed at 6 mg/kg)
▪LC/MS/MS analysis of LAPATINIB levels in plasma and tissues from study of combination LAPATINIB (dosed at 60 mg/kg) and DOXORUBICIN (dosed at 6 mg/kg)
▪PK analysis of data from study of LAPATINIB dosed at 60 mg/kg
▪Determined that PO dosing of LAPATINIB in mice results in linear pharmacokinetic behavior.
▪Determined that the dosing of PO LAPATINIB at 600 mg/kg in DMSO in combination with IV DOXORUBICIN at 6 mg/kg results in increased serum, liver and intestine exposure to DOXORUBICIN as compared to DOXORUBICIN alone.
▪Determined the appropriate LAPATINIB dose, formulation, route and schedule for the combination LAPATINIB and DOXORUBICIN and combination LAPATINIB and DOCETAXEL studies (LAPATINIB will be dosed at 60 mg/kg in 0.5% hydroxypropyl methylcellulose:0.1% Tween 80 via IP injection every 3 hours).
▪Further elucidated the plasma and tissue pharmacokinetics of lapatinibatinib
▪Determined that co-administration of lapatinibatinib with doxorubicinorubicin did not alter the plasma or tissue pharmacokinetics of doxorubicinorubicin.
▪Determined that co-administration of lapatinibatinib with docetaxel substantially increased intestinal exposure to docetaxel.
▪Determined that docetaxel concentrations are significantly increased in intestine, kidney, brain, heart, lung and muscle when PGP is absent.
▪Developed a PBPK model of DOCETAXEL that incorporated PGP transport.

Reportable Outcomes

Appended Manuscripts

1. Physiologically based pharmacokinetic model of lapatinibatinib developed in mice and scaled to humans.
Hudachek SF, Gustafson DL. *J Pharmacokinet Pharmacodyn*. 2013 Jan 12.

2. Co-administration of lapatinibatinib increases exposure to docetaxel but not doxorubicinorubicin in the small intestine of mice
Cancer Chemotherapy and Pharmacology (under review)

3. Incorporation of ABCB1-mediated transport into a physiologically-based pharmacokinetic model of docetaxel in mice
Journal of Pharmacokinetics and Pharmacodynamics (under review)

Abstracts

2011 Era of Hope conference (August 2-5, 2011) abstract and poster:

Abstract

When drugs are given in combination, which is common practice in adjuvant breast cancer treatment, interactions can occur that alter an agent's pharmacokinetics (PKs) and pharmacodynamics (PDs) and potentiate the toxicity of the anti-cancer therapies. This is especially true for drugs that are substrates or inhibitors of P-glycoprotein (PGP), including docetaxel (DOCETAXEL), doxorubicinorubicin (DOXORUBICIN) and lapatinibatinib (LAPATINIB). The purpose of the subsequent work is to use physiologically-based pharmacokinetic (PBPK) modeling to determine the changes in both plasma and tissue PKs of DOCETAXEL and DOXORUBICIN when administered in combination with LAPATINIB. PBPK models mathematically incorporate biochemical and physiological principles to determine the pharmacologic disposition of drugs in the body using compartments that represent specific organs or tissue groups. Once the PBPK models have been optimized in humans, variability in patient covariates and PBPK model parameters will be incorporated using Monte Carlo simulation and a virtual population will be created and validated. This population will then be used for population PK analyses to identify the patient covariates that contribute to the variability in the PK data when agents are given in combination. Once these sources of variability are determined, dosing adjustments can be made that will ultimately maximize efficacy and minimize toxicity of combination therapies.

One of the primary aims of this work was to determine the pharmacokinetics (PKs) of lapatinibatinib (LAPATINIB) in female FVB mice. To our knowledge, LAPATINIB tissue distribution (with the exception of plasma/blood) has not been previously reported. While we found detectable levels of LAPATINIB in all tissues tested, we found high concentrations in the intestine, lung, liver and heart, which could impact LAPATINIB toxicity. To further explore LAPATINIB tissue concentrations, we developed a PBPK model for LAPATINIB, which allows us to test the effect of physiological parameters (i.e. altered blood flows, hepatic impairment, etc.) *in silico* to determine their impact on LAPATINIB exposure in specific tissues.

When we dosed LAPATINIB (60 mg/kg) and DOXORUBICIN (6 mg/kg) in combination, we expected to observe significant alterations in the PKs of tissues with high expression of PGP (liver, intestine, kidney and brain), as LAPATINIB is a PGP inhibitor and DOXORUBICIN is a PGP substrate. We did see a statistically significant increase in DOXORUBICIN liver concentrations when DOXORUBICIN was administered in combination with LAPATINIB (24193 ng/g) versus when administered as a single agent (19041 ng/g) ($P = 0.0274$). In future studies, we expect to see more dramatic differences when DOXORUBICIN and DOCETAXEL are administered after LAPATINIB has reached steady state levels. Once this data has been collected, we will then be able to model the drug interactions and determine if there is a significant PK impact when drugs that interact with PGP are given in combination for the treatment of breast cancer.

Poster Number:

Predicting the Toxicity of Breast Cancer Drug Combination Therapy

Susan F. Hudachek and Daniel L. Gustafson
Animal Cancer Center, Colorado State University
Fort Collins CO

Colorado State University
Animal Cancer Center

Abstract

When drugs are given in combination, which is common practice in adjuvant breast cancer treatment, interactions can occur that alter an agent's pharmacokinetics (PKs) and pharmacodynamics (PDs) and potentiate the toxicity of the anti-cancer therapies. This is especially true for drugs that are substrates or inhibitors of P-glycoprotein (PGP), including docetaxel (DTX), doxorubicin (DOX) and lapatinib (LAP). The purpose of the subsequent work is to use physiologically-based pharmacokinetic (PBPK) modeling to determine the changes in both plasma and tissue PKs of DTX and DOX when administered in combination with LAP. PBPK models mathematically incorporate biochemical and physiological principles to determine the pharmacologic disposition of drugs in the body using compartments that represent specific organs or tissue groups. Once the PBPK models have been optimized in humans, variability in patient covariates and PBPK model parameters will be incorporated using Monte Carlo simulation and a virtual population will be created and validated. This population will then be used for population PK analyses to identify the patient covariates that contribute to the variability in the PK data when agents are given in combination. Once these sources of variability are determined, dosing adjustments can be made that will ultimately maximize efficacy and minimize toxicity of combination therapies.

One of the primary aims of this work was to determine the pharmacokinetics (PKs) of lapatinib (LAP) in female FVB mice. To our knowledge, LAP tissue distribution (with the exception of plasma/blood) has not been previously reported. While we found detectable levels of LAP in all tissues tested (**Figure 1 and Table 1**), we found high concentrations in the intestine, lung, liver and heart, which could impact LAP toxicity. To further explore LAP tissue concentrations, we developed a PBPK model for LAP, which allows us to test the effect of physiological parameters (i.e. altered blood flows, hepatic impairment, etc.) *in silico* to determine their impact on LAP exposure in specific tissues.

When we dosed LAP (60 mg/kg) and DOX (6 mg/kg) in combination, we expected to observe significant alterations in the PKs of tissues with high expression of PGP (liver, intestine, kidney and brain), as LAP is a PGP inhibitor and DOX is a PGP substrate. We did see a statistically significant increase in DOX liver concentrations when DOX was administered in combination with LAP (24193 ng/g) versus when administered as a single agent (19041 ng/g) (P = 0.0274) (**Figure 2**). In future studies, we expect to see more dramatic differences when DOX and DTX are administered after LAP has reached steady state levels. Once this data has been collected, we will then be able to model the drug interactions and determine if there is a significant PK impact when drugs that interact with PGP are given in combination for the treatment of breast cancer.

Table 1

Table 1: Tissue pharmacokinetics of lapatinib in 5-6 week old female FVB mice after oral gavage dosing of 30, 60 and 90 mg/kg.

Tissue	Dose mg/kg	AUC_{0-24} ng/g*hr	$t_{1/2}$ hr	CL g/hr/kg	Vz g/kg	T_{max} hr	C_{max} ng/g
Plasma	30	7002.2	3.4	4224.7	20930.3	1.0	2706.7
Plasma	60	13949.1	3.7	4152.4	22206.9	0.5	4790.0
Plasma	90	27196.7	3.7	3261.0	17446.0	4.0	4308.7
Liver	30	47981.9	3.0	621.0	2725.1	1.0	22133.3
Liver	60	90502.5	3.4	643.2	3135.6	0.5	36066.7
Liver	90	145856.0	3.5	608.3	3031.6	1.0	25206.7
Intestine	30	42728.7	3.0	698.6	2985.4	1.0	15133.3
Intestine	60	130006.3	2.9	453.7	1870.3	0.5	115000.0
Intestine	90	147316.9	3.0	606.8	2621.2	0.3	75933.3
Kidney	30	30113.2	3.8	974.3	5275.8	1.0	8976.7
Kidney	60	82178.3	4.2	680.6	4145.8	0.5	19500.0
Kidney	90	131285.5	4.1	668.4	3966.2	4.0	18776.7
Lung	30	55877.6	4.9	507.1	3571.5	1.0	14466.7
Lung	60	136778.0	4.1	422.9	2482.3	1.0	28216.7
Lung	90	346612.3	3.4	256.8	1259.8	4.0	54866.7
Heart	30	4223.3	4.5	6522.3	42338.9	1.0	1897.7
Heart	60	15524.0	4.0	3587.5	20882.3	1.0	5483.3
Heart	90	29980.4	3.2	2944.6	13700.5	1.0	6661.7
Brain	30	335.7	10.7	45944.6	708709.7	1.0	75.8
Brain	60	789.0	4.6	71807.5	477259.0	1.0	160.2
Brain	90	1264.5	3.9	69537.4	390212.0	4.0	219.0
Muscle	30	1488.0	4.8	18003.7	123727.1	1.0	517.3
Muscle	60	5752.4	3.7	10091.9	54431.6	1.0	1848.7
Muscle	90	12892.6	3.8	6864.9	37419.8	1.0	2242.6
Adipose	30	1727.3	3.7	16973.6	91416.4	1.0	743.0
Adipose	60	5280.6	4.0	10926.9	63041.0	0.5	1523.3
Adipose	90	8618.9	3.8	10156.7	55662.3	2.0	1500.3

Figure 1

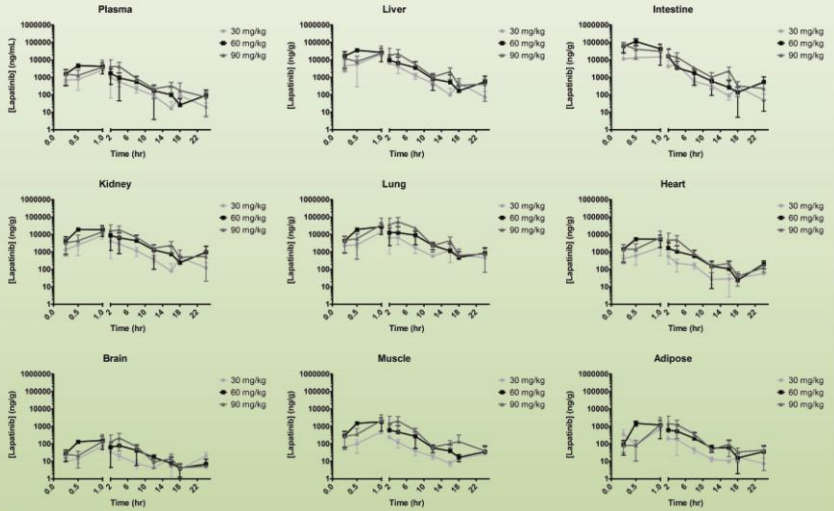

Figure 1: Mean ± standard deviation of tissue concentrations of lapatinib (formulated as a suspension in 0.5% hydroxypropyl methylcellulose: 0.1% Tween 80 in distilled water) in 5-6 week old female FVB mice after oral gavage dosing of 30, 60 and 90 mg/kg. n = 3 per timepoint.

Figure 2

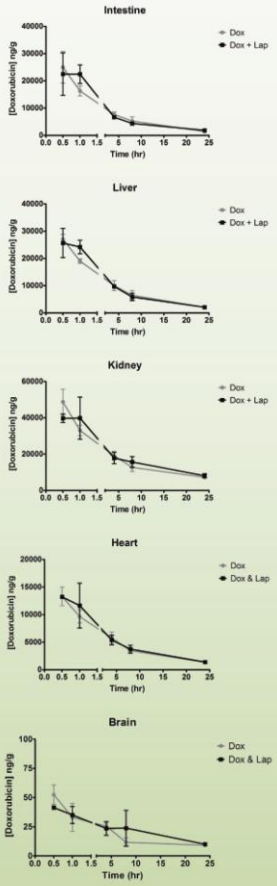

Figure 2: Mean ± standard deviation of tissue concentrations of doxorubicin in 5-6 week old female FVB mice after an oral gavage dose of 60 mg/kg lapatinib followed 1 hr later by an intravenous dose of 6 mg/kg doxorubicin. n = 3 per timepoint.

Figure 3

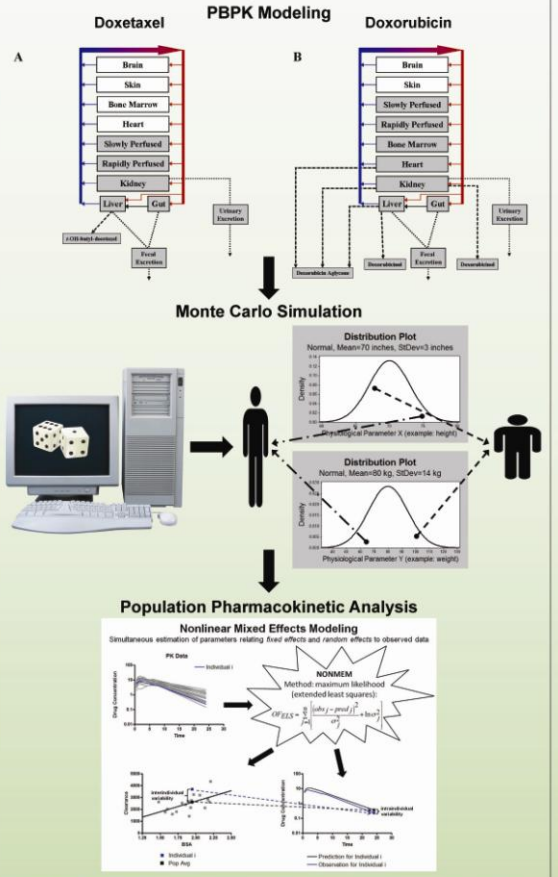

Figure 3: *In Silico* Study Design. Use PBPK modeling to determine the changes in tissue PKs of DTX and DOX when administered in combination with LAP. Incorporate variability in the PBPK parameters using Monte Carlo simulation and create and validate a virtual population. Conduct population PK analyses using the virtual population and identify the patient covariates that contribute to the variability in the PK data. Ultimately, dose adjust based of the identified sources of variability to maximize efficacy and minimize toxicity of combination therapies.

Research Funded by: Department of Defense (DOD)
Breast Cancer Research Program (BCRP)
of the Office of the Congressionally Directed Medical Research Programs (CDMRP)
Award Number: W81XWH-09-1-0457

2012 University of Colorado Cancer Center Retreat Abstract and Poster (Anschutz Medical Campus, Aurora, Colorado):

Abstract

Title: Physiologically-Based Pharmacokinetic Model of Lapatinibatinib Developed in Mice and Scaled to Humans

Authors: Susan F. Hudachek and Daniel L. Gustafson

Program: Animal Cancer Center, Department of Clinical Sciences, Colorado State University

Background: Lapatinibatinib is an oral 4-anilinoquinazoline derivative that dually inhibits epidermal growth factor receptor (EGFR, ErbB1) and human epidermal growth factor receptor 2 (HER2/neu, ErbB2). This drug is a mere decade old and has only been approved by the FDA for the treatment of breast cancer since 2007. Consequently, the intricacies of the pharmacokinetics are still being elucidated.

Material and Methods: In the work presented herein, we determined the biodistribution of orally-administered lapatinibatinib in mouse plasma, brain, heart, lung, kidney, intestine, liver, muscle and adipose tissue. Using this data, we subsequently developed a physiologically based pharmacokinetic (PBPK) model of lapatinibatinib in mice and, by taking into account interspecies differences in physiology and physiochemistry, we then extrapolated the mouse PBPK model to humans.

Results: Our mouse PBPK model accurately predicted plasma and tissue concentrations after doses of 30, 60 and 90 mg/kg. In humans, our model predictions closely reflected lapatinibatinib plasma pharmacokinetics in healthy subjects. Additionally, we were also able to simulate the pharmacokinetics of this drug in the plasma of patients with solid malignancies by incorporating a decrease in liver metabolism into the model. Finally, our human PBPK model also facilitated the estimation of various tissue exposures to lapatinibatinib, which harmonized with the organ-specific toxicities observed in clinical trials.

Conclusions: We have successfully developed a first-generation PBPK model of lapatinibatinib that accurately predicts the pharmacokinetics of this drug in mice, healthy subjects and cancer patients. Additionally, this model improves our understanding of the absorption, distribution, metabolism and elimination of lapatinibatinib in both mouse and man. Potential applications of this model include the prediction of drug interactions with lapatinibatanib as well as determining the sources and magnitudes of exposure variability in specific human populations.

Acknowledgements: This work was supported in part by grant number W81XWH-09-1-0457 from the Department of Defense (DOD) Breast Cancer Research Program (BCRP) of the Office of the Congressionally Directed Medical Research Programs (CDMRP).

Colorado State University
Animal Cancer Center

Physiologically Based Pharmacokinetic Model of Lapatinib Developed in Mice and Scaled to Humans

Susan F. Hudachek and Daniel L. Gustafson at the Animal Cancer Center at Colorado State University

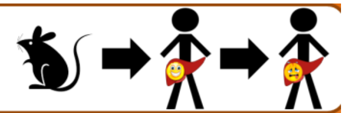

Background

Lapatinib is an oral 4-anilinoquinazoline derivative that dually inhibits epidermal growth factor receptor (EGFR, ErbB1) and human epidermal growth factor receptor 2 (HER2/neu, ErbB2). This drug is a mere decade old and has only been approved by the FDA for the treatment of breast cancer since 2007. Consequently, the intricacies of the pharmacokinetics are still being elucidated.

Material and Methods

In the work presented herein, we determined the biodistribution of orally-administered lapatinib in mouse plasma, brain, heart, lung, kidney, intestine, liver, muscle and adipose tissue. Using this data, we subsequently developed a physiologically based pharmacokinetic (PBPK) model of lapatinib in mice and, by taking into account interspecies differences in physiology and physiochemistry, we then extrapolated the mouse PBPK model to humans.

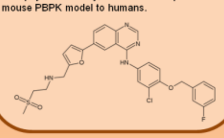

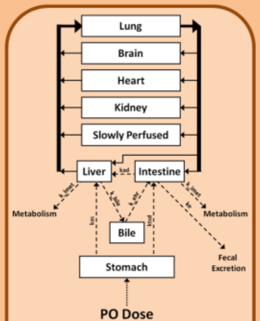

Figure Legend

Schematic representation of a physiologically-based pharmacokinetic (PBPK) model of lapatinib. Solid arrows represent blood flow. Dashed lines represent first-order rate constants for absorption from stomach (kas), absorption from duodenum/intestine (kad), transfer from stomach to duodenum/intestine (ktsd), secretion into bile (k_bile), excretion from bile into intestine (k_ehr), hepatic metabolism (k_lmet), intestinal metabolism (k_imet) and fecal excretion (ke). The dotted line represents lapatinib input into the system via per os (p.o.) dosing.

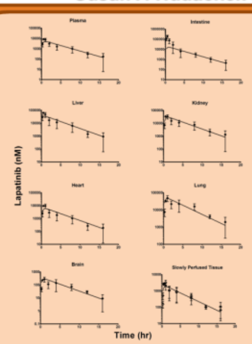

Figure Legend

Observed and model-simulated lapatinib concentrations after oral gavage dosing of 60 mg/kg. In all graphs except the slowly perfused tissue graph, filled diamonds represent the observed data. In the slowly perfused tissue graph, upper half-filled diamonds represent the observed data from adipose tissue and lower half-filled diamonds represent the observed data from muscle tissue. For all observed data, error bars symbolize the SEM. Solid lines represent model simulations.

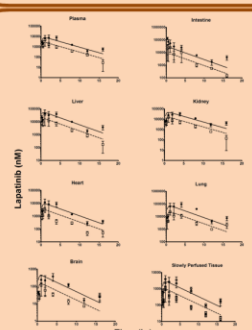

Figure Legend

Observed and model-simulated lapatinib concentrations after oral gavage dosing of 30 and 90 mg/kg. In all graphs except the slowly perfused tissue graph, open squares and filled circles represent the observed data from the 30 and 90 mg/kg dose cohorts, respectively. In the slowly perfused tissue graph, upper half-filled squares and lower half-filled squares represent the observed adipose tissue data and muscle tissue data, respectively, from the 30 mg/kg dose cohort and upper half-filled circles and lower half-filled circles represent the observed adipose tissue data and muscle tissue data, respectively, from the 90 mg/kg dose cohort. For all observed data, error bars symbolize the SEM. Dashed lines and solid lines represent model simulations for the 30 and 90 mg/kg dose cohorts, respectively.

Observed and model-simulated lapatinib pharmacokinetic (PK) parameters in mice[a]

PK Parameter	Dose		Plasma	Intestine	Liver	Kidney	Heart	Lung	Brain	Slowly Perfused
AUC_{0-16hr} (nM*hr)[b]	30	Observed	12008	75885	84546	50440	7158	92409	440.8	2737.5
		Simulated	12483	39357	83754	74067	14608	114551	699.1	4623
		Ratio	0.96	2.03	1.01	0.68	0.49	0.81	0.63	0.59
	60	Observed	24052	235114	157288	137624	26545	233760	1315	9518.5
		Simulated	24966	78713	167508	148135	29217	229102	1398	9246
		Ratio	0.96	2.99	0.94	0.93	0.91	1.02	0.94	1.03
	90	Observed	48230	259808	261237	227184	55179	623277	2261	18930
		Simulated	37449	118070	251261	222202	43825	343654	2097	13869
		Ratio	1.29	2.20	1.04	1.02	1.26	1.81	1.08	1.36
CL (L/hr)[c]	30	Observed	0.09	0.01	0.01	0.02	0.14	0.01	2.34	0.38
		Simulated	0.08	0.03	0.01	0.01	0.07	0.01	1.48	0.22
		Ratio	1.04	0.49	0.99	1.47	2.04	1.24	1.59	1.69
	60	Observed	0.09	0.01	0.01	0.02	0.08	0.01	1.57	0.22
		Simulated	0.08	0.03	0.01	0.01	0.07	0.01	1.48	0.22
		Ratio	1.04	0.33	1.06	1.08	1.10	0.98	1.06	0.97
	90	Observed	0.06	0.01	0.01	0.01	0.06	0.005	1.37	0.16
		Simulated	0.08	0.03	0.01	0.01	0.07	0.01	1.48	0.22
		Ratio	0.78	0.45	0.96	0.98	0.79	0.55	0.93	0.73
$t_{1/2}$ (hr)[d]	30	Observed	2.73	2.79	2.48	2.53	2.59	2.39	3.70	3.88
		Simulated	2.99	2.96	2.96	3.00	2.99	2.99	2.99	2.99
		Ratio	0.91	0.94	0.84	0.84	0.87	0.80	1.24	1.30
	60	Observed	3.42	3.06	2.75	3.57	3.05	3.04	3.12	2.57
		Simulated	2.99	2.96	2.96	3.00	2.99	2.99	2.99	2.99
		Ratio	1.14	1.03	0.93	1.19	1.02	1.02	1.04	0.86
	90	Observed	2.36	2.55	1.91	2.51	2.32	1.72	1.76	1.55
		Simulated	2.99	2.96	2.96	3.00	2.99	2.99	2.99	2.99
		Ratio	0.79	0.86	0.65	0.83	0.78	0.58	0.59	0.52

[a]PK parameters were calculated using noncompartmental modeling.
[b]AUC_{0-16hr} is the area under the concentration-time curve from 0 to 16 hrs.
[c]CL is clearance.
[d]$t_{1/2}$ is the half-life for elimination as calculated from linear regression of the terminal elimination phase.

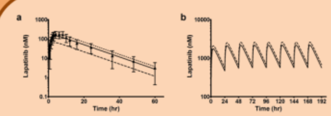

Figure Legend

Observed [13] and model-simulated lapatinib concentrations, AUC and C_{max} values in human plasma. (a) Single oral dose of 100 mg. Filled black triangles represent the observed data with error bars symbolizing the SD. The solid black line represents the model simulation for 27% fecal excretion. The dotted black line and the dashed black line represent model simulations for 3 and 67% fecal excretion, respectively. (b) Multiple doses (q24hr) for 8 days. Solid black line represents the model simulation for daily dosing of 1250 mg. Dashed black line represents the model simulation for daily dosing of 1500 mg.

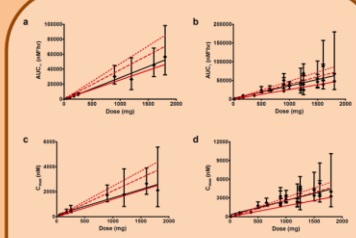

Figure Legend

Observed and model-simulated lapatinib concentrations, AUC and C_{max} values in human plasma. Solid black diamonds represent observed values with error bars symbolizing the 95% CIs. Solid black lines are the corresponding linear regression trendline. Solid red lines represent the model-predicted values. Dashed red lines represent simulated values from the model with moderate hepatic impairment. Dotted red lines represents simulated values from the model with severe hepatic impairment. (a) $AUCs_{\infty}$ after a single dose of lapatinib, (b) $AUCs_{\tau}$ (calculated within the dosing interval from time 0 to 24 hrs) after multiple doses (q24hr) of lapatinib, (c) C_{max} values after a single dose of lapatinib, (d) C_{max} values after multiple doses (q24hr) of lapatinib.

Human tissue AUCs for single and multiple (q24hr) lapatinib doses

	100 mg Single Dose AUC_{0-60hr}[a] (nM*hr)	1250 mg Multiple Dose q24hr AUC_{τ}[b] (nM*hr)	1500 mg Multiple Dose q24hr AUC_{τ}[b] (nM*hr)
Plasma	2536	32155	38586
Intestine	18348	231773	278128
Liver	17132	216986	260383
Kidney	15023	190522	228627
Heart	2967	37622	45146
Lung	23264	295029	354035
Brain	142	1801	2616
Slowly Perfused	938	11897	14277

[a]AUC_{0-60hr} is the area under the concentration-time curve from 0 to 60 hrs.
[b]AUC_{τ} is the steady-state area under the concentration-time curve within the dosing interval (0-24 hr).

Single dose lapatinib observed and predicted human AUC_{∞} and subject characteristics

Dose (mg)	Observed AUC_{∞} (nM*hr)	Predicted AUC_{∞} (nM*hr)	AUC_{∞} PE%[c]	Subjects	Food	Bilirubin[d]	AST[d]	ALT[d]	Age (years)[e]	Reference
50	1170 (756-1817)[a]	1286	9.9%	healthy	fasted	normal	normal	normal	22 (18-53)	[1]
100	2096 (1492-2941)[a]	2572	22.7%	healthy	fasted	normal	normal	normal	22 (18-53)	[1]
100	2459 (2062-2933)[a]	2572	4.6%	healthy	not fasted	normal	normal	normal	28 (20-47)	[2]
175	4206 (2668-6634)[a]	4502	7.0%	healthy	fasted	normal	normal	normal	22 (18-53)	[1]
250	6313 (4550-8758)[a]	6431	1.9%	healthy	fasted	normal	normal	normal	22 (18-53)	[1]
250	6068 (4970-7411)[a]	6431	6.0%	healthy	not fasted	normal	normal	normal	29 (20-46)	[2]
900	30250 (20328-45011)[a]	23151	-23.5%	cancer	fasted	≤1.5X ULN	≤2.5X ULN	≤2.5X ULN	60 (37-73)	[3]
1200	26574 (12763-55375)[a]	30869	16.2%	cancer	fasted	≤1.5X ULN	≤2.5X ULN	≤2.5X ULN	60 (37-73)	[3]
1600	45387 (30150-68263)[a]	41158	-9.3%	cancer	fasted	≤1.5X ULN	≤2.5X ULN	≤2.5X ULN	60 (37-73)	[3]
1800	56519 (32499-98293)[a]	46303	-18.1%	cancer	fasted	≤1.5X ULN	≤2.5X ULN	≤2.5X ULN	60 (37-73)	[3]

[a]AUC_{∞} is the geometric mean (95% confidence interval) of the area under the concentration-time curve calculated from time 0 to infinity.
[b]AUC_{∞} is the geometric mean (range) of the area under the concentration-time curve calculated from time 0 to infinity.
[c]PE% is the prediction error.
[d]Bilirubin, aspartate transaminase (AST) and alanine transaminase (ALT) are measures of liver function. ULN is upper limit of normal.
[e]Median age (range).

Multiple dose lapatinib (25-1200 mg) observed and predicted human AUC_{τ} and subject characteristics

Dose (mg)	Observed AUC_{τ} (nM*hr)[a]	Predicted AUC_{τ} (nM*hr)	AUC_{τ} PE%[b]	Subjects	Food	Bilirubin[c]	AST[c]	ALT[c]	Age (years)[d]	Ref
25	515 (329-809)	643	25.0%	healthy	fasted	normal	normal	normal	22 (19-38)	[1]
100	2566 (1594-4137)	2572	0.2%	healthy	fasted	normal	normal	normal	22 (19-38)	[1]
175	4869 (3313-7154)	4502	-7.5%	healthy	fasted	normal	normal	normal	22 (19-38)	[1]
175	9431	4502	-52.3%	cancer	fasted	≤2 mg/dL	≤3.0X ULN	≤3.0X ULN	61 (25-80)	[4]
375	9878	9647	-2.3%	cancer	fasted	≤2 mg/dL	≤3.0X ULN	≤3.0X ULN	62 (25-81)	[4]
500	23922 (17107-33731)	12862	-46.2%	cancer	not fasted	≤2 mg/dL	≤3.0X ULN	≤3.0X ULN	56 (28-74)	[5]
650	27020 (20480-35797)	16721	-38.1%	cancer	not fasted	≤2 mg/dL	≤3.0X ULN	≤3.0X ULN	60 (37-82)	[5]
675	23578	17364	-26.4%	cancer	fasted	≤2 mg/dL	≤3.0X ULN	≤3.0X ULN	63 (25-82)	[4]
900	21857	23152	5.9%	cancer	fasted	≤2 mg/dL	≤3.0X ULN	≤3.0X ULN	64 (25-83)	[4]
900	40099 (28052-57481)	23152	-42.3%	cancer	not fasted	≤2 mg/dL	≤3.0X ULN	≤3.0X ULN	57 (34-82)	[5]
900	50377 (37204-68217)	23152	-54.0%	cancer	fasted	≤1.5X ULN	≤2.5X ULN	≤2.5X ULN	60 (37-73)	[3]
1000	40615 (35452-46639)	25724	-36.7%	cancer	not fasted	≤2 mg/dL	≤3.0X ULN	≤3.0X ULN	53 (43-69)	[6]
1000	35280 (26847-46295)	25724	-27.1%	cancer	fasted	adequate	adequate	adequate	53 (30-80)	[6]
1200	24610 (16212-37518)	30869	25.4%	cancer	not fasted	≤2 mg/dL	≤3.0X ULN	≤3.0X ULN	54 (37-67)	[5]
1200	44195 (23626-82673)	30869	-30.2%	cancer	fasted	≤1.5X ULN	≤2.5X ULN	≤2.5X ULN	60 (37-73)	[3]
1200	29773	30869	3.7%	cancer	fasted	≤2 mg/dL	≤3.0X ULN	≤3.0X ULN	65 (25-84)	[4]

[a]AUC_{τ} is the geometric mean (95% confidence interval) of the steady-state area under the concentration-time curve calculated within the dosing interval (0-24 hr).
[b]PE% is the prediction error.
[c]Bilirubin, aspartate transaminase (AST) and alanine transaminase (ALT) are measures of liver function. ULN is upper limit of normal.
[d]Median age (range).

Multiple dose lapatinib (1250-1800 mg) observed and predicted human AUC_{τ} and subject characteristics

Dose (mg)	Observed AUC_{τ} (nM*hr)	Predicted AUC_{τ} (nM*hr)	AUC_{τ} PE%[c]	Subjects	Food	Bilirubin[d]	AST[d]	ALT[d]	Age (years)[e]	Ref
1250	62300 (40271-96376)[a]	32155	-48.4%	cancer	not fasted	≤1.5 mg/dL	≤2.0X ULN	≤2.0X ULN	58.3 (2-79)	[7]
1250	68840 (50425-94138)[b]	32155	-53.3%	cancer	not fasted	significant dysfunction excluded			58 (34-78)	[8]
1250	24438 (11769-50941)[b]	32155	31.6%	cancer	fasted	≤1.5 mg/dL	≤2.0X ULN	≤2.0X ULN	59 (19-74)	[9]
1250	40099 (24964-64193)[b]	32155	-19.8%	cancer	not fasted	≤2.0X ULN	≤5.0X ULN	≤5.0X ULN	57.5 (33-74)	[10]
1500	46639 (32699-66430)[b]	38586	-17.3%	cancer	not fasted	≤1.5 mg/dL	≤2.0X ULN	≤2.0X ULN	59.5 (39-73)	[11]
1500	54900 (29601-101833)[b]	38586	-29.7%	cancer	fasted	≤1.5 mg/dL	≤3.0X ULN	≤3.0X ULN	57 (31-73)	[12]
1600	50597 (27364-93450)[b]	41158	-18.7%	cancer	not fasted	≤2.0 mg/dL	≤3.0X ULN	≤3.0X ULN	55 (38-70)	[5]
1600	87941 (49349-156717)[b]	41158	-53.2%	cancer	fasted	≤1.5X ULN	≤2.5X ULN	≤2.5X ULN	60 (37-73)	[3]
1600	39067[b]	41158	5.4%	cancer	fasted	≤2.0 mg/dL	≤3.0X ULN	≤3.0X ULN	66 (25-85)	[4]
1800	47671[b]	46303	-2.9%	cancer	fasted	≤2.0 mg/dL	≤3.0X ULN	≤3.0X ULN	67 (25-86)	[4]
1800	67895 (25858-179656)[b]	46303	-31.8%	cancer	fasted	≤1.5X ULN	≤2.5X ULN	≤2.5X ULN	60 (37-73)	[3]

[a]AUC_{τ} is the mean (90% confidence interval) of the steady-state area under the concentration-time curve calculated within the dosing interval (0-24 hr).
[b]AUC_{τ} is the geometric mean (95% confidence interval) of the steady-state area under the concentration-time curve calculated within the dosing interval (0-24 hr).
[c]PE% is the prediction error.
[d]Bilirubin, aspartate transaminase (AST) and alanine transaminase (ALT) are measures of liver function. ULN is upper limit of normal.
[e]Median age (range).

Results

Our mouse PBPK model accurately predicted plasma and tissue concentrations after doses of 30, 60 and 90 mg/kg. In humans, our model predictions closely reflected lapatinib plasma pharmacokinetics in healthy subjects. Additionally, we were also able to simulate the pharmacokinetics of this drug in the plasma of patients with solid malignancies by incorporating a decrease in liver metabolism into the model. Finally, our human PBPK model also facilitated the estimation of various tissue exposures to lapatinib, which harmonized with the organ-specific toxicities observed in clinical trials.

Conclusions

We have successfully developed a first-generation PBPK model of lapatinib that accurately predicts the pharmacokinetics of this drug in mice, healthy subjects and cancer patients. Additionally, this model improves our understanding of the absorption, distribution, metabolism and elimination of lapatinib in both mouse and man. Potential applications of this model include the prediction of drug interactions with lapatanib as well as determining the sources and magnitudes of exposure variability in specific human populations.

References

1. Bence AK, Anderson EB, Halepota MA, Doukas MA, DeSimone PA, Davis GA, Smith DA, Koch KM, Stead AG, Mangum S, Bowen CJ, Spector NL, Hsieh S, Adams VR (2005) Phase I pharmacokinetic studies evaluating single and multiple doses of oral GW572016, a dual EGFR-ErbB2 inhibitor, in healthy subjects. Invest New Drugs 23(1):39-49
2. Smith DA, Koch KM, Arya N, Bowen CJ, Herendeen JM, Beelen A (2009) Effects of ketoconazole and carbamazepine on lapatinib pharmacokinetics in healthy subjects. Br J Clin Pharmacol 67(4):421-426
3. Nakagawa K, Minami H, Kanezaki M, Mukaiyama A, Minamide Y, Uejima H, Kurata T, Nogami T, Kawada K, Mukai H, Sasaki Y, Fukuoka M (2009) Phase I dose-escalation and pharmacokinetic trial of lapatinib (GW572016), a selective oral dual inhibitor of ErbB-1 and -2 tyrosine kinases, in Japanese patients with solid tumors. Jpn J Clin Oncol 39(2):116-123
4. Burris HA, 3rd, Taylor CW, Jones SF, Koch KM, Versola MJ, Arya N, Fleming RA, Smith DA, Pandite L, Spector N, Wilding G (2009) A phase I and pharmacokinetic study of oral lapatinib administered once or twice daily in patients with solid malignancies. Clin Cancer Res 15 (21):6702-6708
5. Burris HA, 3rd, Hurwitz HI, Dees EC, Dowlati A, Blackwell KL, O'Neil B, Marcom PK, Ellis MJ, Overmoyer B, Jones SF, Harris JL, Smith DA, Koch KM, Stead A, Mangum S, Spector NL (2005) Phase I safety, pharmacokinetics, and clinical activity study of lapatinib (GW572016), a reversible dual inhibitor of epidermal growth factor receptor tyrosine kinases, in heavily pretreated patients with metastatic carcinomas. J Clin Oncol 23 (23):5305-5313
6. Storniolo AM, Pegram MD, Overmoyer B, Silverman P, Peacock NW, Jones SF, Loftiss J, Arya N, Koch KM, Paul E, Pandite L, Fleming RA, Lebowitz PF, Ho PT, Burris HA, 3rd (2008) Phase I dose escalation and pharmacokinetic study of lapatinib in combination with trastuzumab in patients with advanced ErbB2-positive breast cancer. J Clin Oncol 26 (20):3317-3323
7. Chu QS, Schwartz G, de Bono J, Smith DA, Koch KM, Versola MJ, Pandite L, Arya N, Curtright J, Fleming RA, Ho PT, Rowinsky EK (2007) Phase I and pharmacokinetic study of lapatinib in combination with capecitabine in patients with advanced solid malignancies. J Clin Oncol 25 (24):3753-3758
8. Midgley RS, Kerr DJ, Flaherty KT, Stevenson JP, Pratap SE, Koch KM, Smith DA, Versola M, Fleming RA, Ward C, O'Dwyer PJ, Middleton MR (2007) A phase I and pharmacokinetic study of lapatinib in combination with infusional 5-fluorouracil, leucovorin and irinotecan. Ann Oncol 18 (12):2025-2029
9. LoRusso PM, Jones SF, Koch KM, Arya N, Fleming RA, Loftiss J, Pandite L, Gadgeel S, Weber BL, Burris HA, 3rd (2008) Phase I and pharmacokinetic study of lapatinib and docetaxel in patients with advanced cancer. J Clin Oncol 26 (18):3051-3056
10. Molina JR, Kaufmann SH, Reid JM, Rubin SD, Galvez-Peralta M, Friedman R, Flatten KS, Koch KM, Gilmer TM, Mullin RJ, Jewell RC, Felten SJ, Mandrekar S, Adjei AA, Erlichman C (2008) Evaluation of lapatinib and topotecan combination therapy: tissue culture, murine xenograft, and phase I clinical trial data. Clin Cancer Res 14 (23):7900-7908
11. Siegel-Lakhai WS, Beijnen JH, Vervenne WL, Boot H, Keessen M, Versola M, Koch KM, Smith DA, Pandite L, Richel DJ, Schellens JH (2007) Phase I pharmacokinetic study of the safety and tolerability of lapatinib (GW572016) in combination with oxaliplatin/fluorouracil/leucovorin (FOLFOX4) in patients with solid tumors. Clin Cancer Res 13 (15 Pt 1):4495-4502
12. Chu QS, Cianfrocca ME, Goldstein LJ, Gale M, Murray N, Loftiss J, Arya N, Koch KM, Pandite L, Fleming RA, Paul E, Rowinsky EK (2008) A phase I and pharmacokinetic study of lapatinib in combination with letrozole in patients with advanced cancer. Clin Cancer Res 14 (14):4484-4490
13. Castellino S, O'Mara M, Koch K, Borts DJ, Bowers GD, MacLauchlin C Human metabolism of lapatinib, a dual kinase inhibitor: implications for hepatotoxicity. Drug Metab Dispos 40 (1):139-150

Acknowledgements

This work was supported in part by grant number W81XWH-09-1-0457 from the Department of Defense (DOD) Breast Cancer Research Program (BCRP) of the Office of Congressionally Directed Medical Research Programs (CDMRP).

2013 American Association of Cancer Research Meeting Abstract, April 6-10 (Washington DC):

Abstract

Title: Co-administration of lapatinibatinib increases exposure to docetaxel but not doxorubicinorubicin in the small intestine of mice

Authors: Susan F. Hudachek and Daniel L. Gustafson

Abstract:

Combination therapy is increasingly utilized for the treatment of metastatic breast cancer. However, co-administration of drugs, particularly agents that are substrates for or inhibitors of p-glycoprotein, can result in increased tissue toxicity. Unfortunately, determining levels of chemotherapeutics in human tissues is challenging and plasma drug concentrations are not always indicative of tissue toxicokinetics or toxicodynamics, especially when tissue penetration is altered.

The aim of the work presented herein was to determine if concomitant administration of compounds currently being combined in clinical trials for metastatic breast cancer treatment alters plasma and tissue pharmacokinetics in mice if both agents are p-glycoprotein substrates and/or inhibitors. Accordingly, we investigated the pharmacokinetic interactions of the classic cytotoxics and p-glycoprotein substrates docetaxel and doxorubicinorubicin when given concurrently with the targeted agent and p-glycoprotein inhibitor lapatinibatinib.

Our time course plasma and tissue distribution studies showed that co-administration of lapatinibatinib with doxorubicinorubicin did not appreciably alter the pharmacokinetics of this anthracycline in the plasma or six tissues evaluated in mice, presumably because, at doses relevant to human exposure, lapatinibatinib inhibition of p-glycoprotein did not significantly alter doxorubicinorubicin transport out of these tissue compartments.

However, combining lapatinibatinib with docetaxel dramatically increased intestinal exposure to this chemotherapeutic, which has clinical implications for enhancing gastrointestinal toxicity. The significant lapatinibatinib-docetaxel interaction is likely CYP3A4-mediated and thus, our study suggests that caution should be taken when this combination is administered, particularly to patients with compromised CYP3A activity, and recipients should be closely monitored for enhanced toxicity, particularly for adverse effects on the intestine.

Conclusion

One of the primary aims of this work was to determine the pharmacokinetics (PKs) of lapatinibatinib (LAPATINIB) in female FVB mice. To our knowledge, LAPATINIB tissue distribution (with the exception of plasma/blood) has not been previously reported. While we found detectable levels of LAPATINIB in all tissues tested, we found high concentrations in the gut, lung, liver and heart, which could impact LAPATINIB toxicity. To further explore LAPATINIB tissue concentrations, we developed a PBPK model for LAPATINIB, which allows us to test the effect of physiological parameters (i.e. altered blood flows, hepatic impairment, etc.) *in silico* to determine their impact on LAPATINIB exposure in specific tissues.

When we dosed LAPATINIB (60 mg/kg) and DOXORUBICIN (6 mg/kg) in combination, we expected to observe significant alterations in the PKs of tissues with high expression of PGP (liver, gut, kidney and brain), as LAPATINIB is a PGP inhibitor and DOXORUBICIN is a PGP substrate. We did see a statistically significant increase in DOXORUBICIN liver concentrations when DOXORUBICIN was administered in combination with LAPATINIB (24193 ng/g) versus when administered as a single agent (19041 ng/g) ($P = 0.0274$). We expected that when we dosed with LAPATINIB at steady state (using the Alzet® osmotic pumps), the increase would be amplified.

During the second year of this award, we completed the thorough PK analysis of the biodistribution of single dose PO LAPATINIB in mice. From the dosing studies, sample analyses and modeling of the data, we determined that LAPATINIB dosed PO exhibits linear PK, which makes predicting the pharmacology of this drug easier than drugs that exhibit nonlinear PK (PK involving saturable processes).

Following this investigation of LAPATINIB PK, we intended to move forward with the drug combination studies. However, we encountered major obstacles with administering LAPATINIB such that exposure of this drug during the duration of the combination drug PK study would be equivalent to human exposure. After many failed attempts at optimizing formulation, route (including the use of Alzet® osmotic pumps) and schedule to mimic human exposure, we concluded that the best alternative was to dose LAPATINIB via IP injection with 60 mg/kg in a vehicle of 0.5% hydroxypropyl methylcellulose: 0.1% Tween 80 every 3 hours while the second drug (either DOXORUBICIN or DOCETAXEL) was on board.

Subsequently, we conducted mouse studies involving combination LAPATINIB and DOCETAXEL or LAPATINIB and DOXORUBICIN. Our results demonstrated that coadministration of LAPATINIB does not alter the PK of doxorubicinorubicin. In contrast, lapatinibatinib did increase exposure to docetaxel in the intestine, likely leading to enhanced toxicity. The significant lapatinibatinib-docetaxel interaction is likely CYP3A4-mediated and thus, our study suggests that caution should be taken when this combination is administered, particularly to patients with compromised CYP3A activity. As co-administration of these two agents is protocol for clinical trials that are either recruiting or active, we recommend closely monitoring the recipients of combined lapatinibatinib and docetaxel for enhanced toxicity, particularly for adverse effects on the intestine.

Finally, as an alternative to pharmacologic inhibition, we used genetic inhibition. Specifically, we utilized PGP (mdr1a/b) knockout mice to directly evaluate the effect of PGP on docetaxel PK. The plasma and tissue docetaxel concentration profiles were determined. Mice without PGP showed significant increases in docetaxel concentrations in intestine, kidney, brain, heart, lung and muscle. As illustrated by our work, although plasma docetaxel concentrations are virtually the same in FVB and KO mice, there are significant differences in tissue exposure to this taxane that are directly related to PGP transport. And, it is in these tissues that docetaxel-associated toxicities occur. Thus, it is of the utmost importance to understand not only the plasma but also the tissue distribution of docetaxel (as well as other drugs) to truly assess the necessity of dose modifications based on protein functionality.

Using the DOCETAXEL PK data from the FVB and PGP knockout mice, we developed a DOCETAXEL PBPK model incorporating PGP transport. Our data and model suggest that adjusting the dose of docetaxel in relation to ABCB1 function is imperative to minimize detrimental tissue exposure and toxicity related to this compound. To determine the pertinence of this type of dose modification to humans, the present mouse PBPK model can be scaled to humans by taking into account interspecies differences in physiology and physiochemistry. In this way, we can estimate the affect of ABCB1 transport on both the plasma and tissue distribution of docetaxel in humans and subsequently use in silico experimentation prior to clinical trials for optimization of the administration of docetaxel to maximize efficacy and minimize toxicity.

A detailed discussion of the conclusions of this work can be found in the amended manuscripts titled " Physiologically based pharmacokinetic model of lapatinibatinib developed in mice and scaled to humans", "Co-administration of lapatinibatinib increases exposure to docetaxel but not doxorubicinorubicin in the small intestine of mice" and "Incorporation of ABCB1-Mediated Transport into a Physiologically-Based Pharmacokinetic Model of Docetaxel in Mice".

Personnel receiving pay from the research effort include Susan Hudachek.

References

1. GlaxoSmithKline (2012) Tykerb prescribing information. http://us.gsk.com/products/assets/us_tykerb.pdf.

2. Bence AK, Anderson EB, Halepota MA, Doukas MA, DeSimone PA, Davis GA, Smith DA, Koch KM, Stead AG, Mangum S, Bowen CJ, Spector NL, Hsieh S, Adams VR (2005) Phase I pharmacokinetic studies evaluating single and multiple doses of oral GW572016, a dual EGFR-ErbB2 inhibitor, in healthy subjects. Invest New Drugs 23 (1):39-49

3. Burris HA, 3rd, Hurwitz HI, Dees EC, Dowlati A, Blackwell KL, O'Neil B, Marcom PK, Ellis MJ, Overmoyer B, Jones SF, Harris JL, Smith DA, Koch KM, Stead A, Mangum S, Spector NL (2005) Phase I safety, pharmacokinetics, and clinical activity study of lapatinibatinib (GW572016), a reversible dual inhibitor of epidermal growth factor receptor tyrosine kinases, in heavily pretreated patients with metastatic carcinomas. J Clin Oncol 23 (23):5305-5313

4. Gaul MD, Guo Y, Affleck K, Cockerill GS, Gilmer TM, Griffin RJ, Guntrip S, Keith BR, Knight WB, Mullin RJ, Murray DM, Rusnak DW, Smith K, Tadepalli S, Wood ER, Lackey K (2003) Discovery and biological evaluation of potent dual ErbB-2/EGFR tyrosine kinase inhibitors: 6-thiazolylquinazolines. Bioorg Med Chem Lett 13 (4):637-640

5. Xia W, Mullin RJ, Keith BR, Liu LH, Ma H, Rusnak DW, Owens G, Alligood KJ, Spector NL (2002) Anti-tumor activity of GW572016: a dual tyrosine kinase inhibitor blocks EGF activation of EGFR/erbB2 and downstream Erk1/2 and AKT pathways. Oncogene 21 (41):6255-6263

6. Rusnak DW, Lackey K, Affleck K, Wood ER, Alligood KJ, Rhodes N, Keith BR, Murray DM, Knight WB, Mullin RJ, Gilmer TM (2001) The effects of the novel, reversible epidermal growth factor receptor/ErbB-2 tyrosine kinase inhibitor, GW2016, on the growth of human normal and tumor-derived cell lines in vitro and in vivo. Mol Cancer Ther 1 (2):85-94

7. Jacquet JM, Bressolle F, Galtier M, Bourrier M, Donadio D, Jourdan J, Rossi JF (1990) Doxorubicinorubicin and doxorubicinorubicinol: intra- and inter-individual variations of pharmacokinetic parameters. Cancer Chemother Pharmacol 27 (3):219-225

8. Gustafson DL, Rastatter JC, Colombo T, Long ME (2002) Doxorubicinorubicin pharmacokinetics: Macromolecule binding, metabolism, and excretion in the context of a physiologic model. J Pharm Sci 91 (6):1488-1501

9. LoRusso PM, Jones SF, Koch KM, Arya N, Fleming RA, Loftiss J, Pandite L, Gadgeel S, Weber BL, Burris HA, 3rd (2008) Phase I and pharmacokinetic study of lapatinibatinib and docetaxel in patients with advanced cancer. J Clin Oncol 26 (18):3051-3056

10. Bradshaw-Pierce EL, Eckhardt SG, Gustafson DL (2007) A physiologically based pharmacokinetic model of docetaxel disposition: from mouse to man. Clin Cancer Res 13 (9):2768-2776

11. Urien S, Barre J, Morin C, Paccaly A, Montay G, Tillement JP (1996) Docetaxel serum protein binding with high affinity to alpha 1-acid glycoprotein. Invest New Drugs 14 (2):147-151

12. van der Veldt AA, Hendrikse NH, Smit EF, Mooijer MP, Rijnders AY, Gerritsen WR, van der Hoeven JJ, Windhorst AD, Lammertsma AA, Lubberink M Biodistribution and radiation dosimetry of 11C-labelled docetaxel in cancer patients. Eur J Nucl Med Mol Imaging 37 (10):1950-1958

Supporting Data

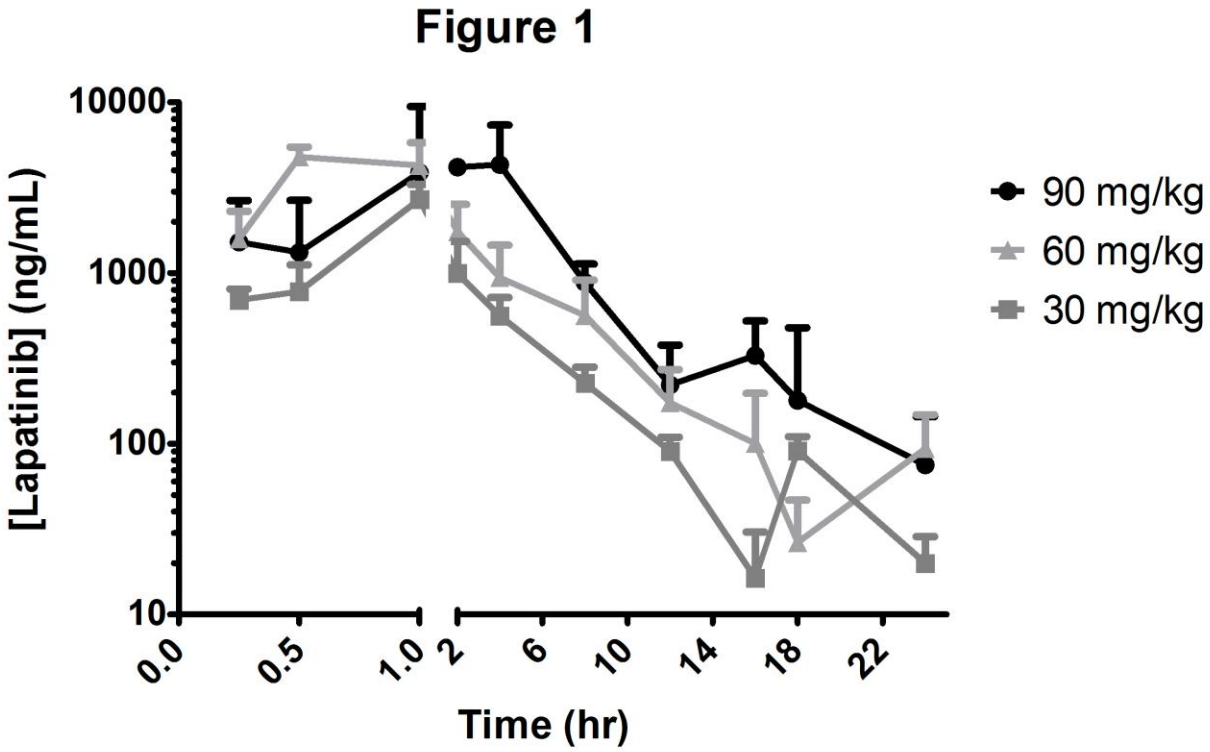

Figure 1: Mean ± standard deviation of plasma concentrations of LAPATINIB after oral gavage doses of 30, 60 and 90 mg/kg. n = 3 per timepoint.

Figure 2A

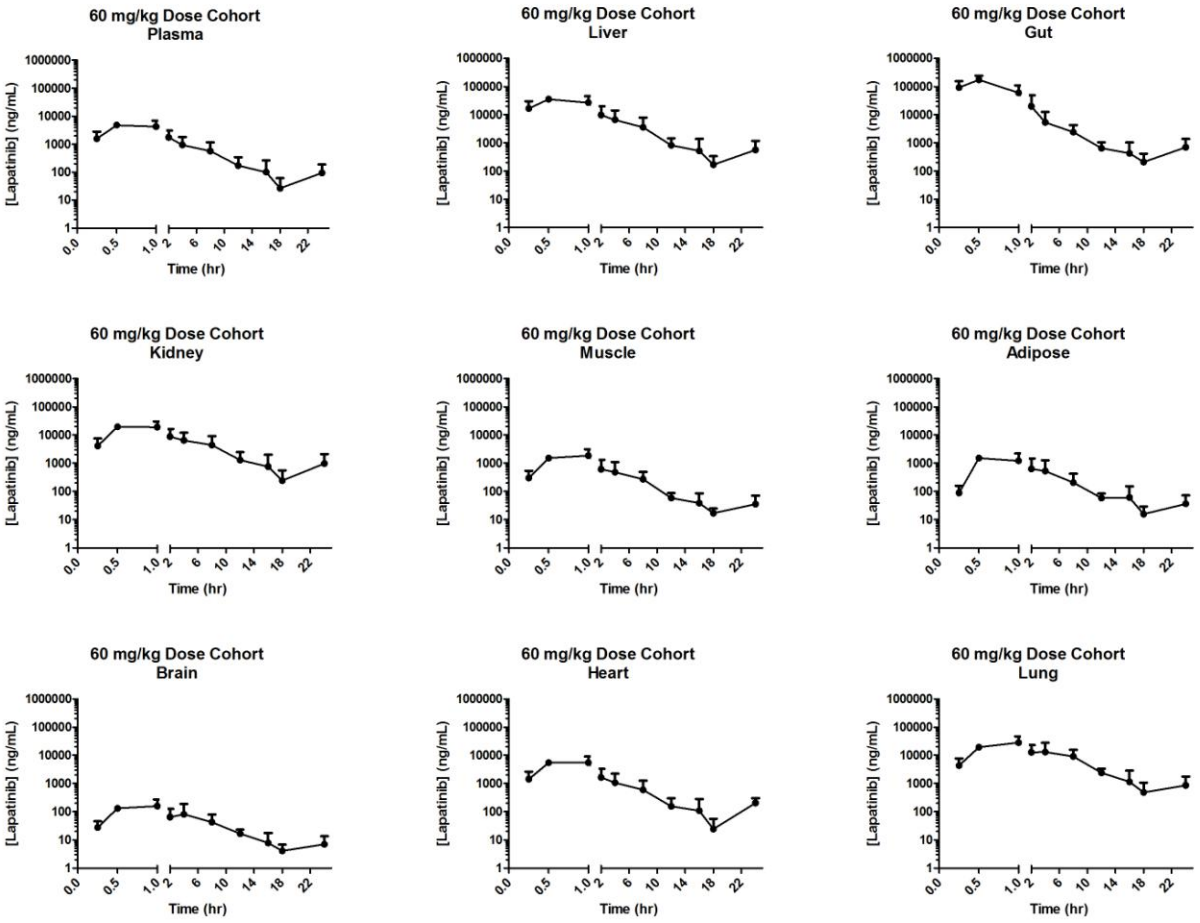

Figure 2A: Mean ± standard deviation of tissue concentrations of LAPATINIB after an oral gavage dose of 60 mg/kg. n = 3 per timepoint.

Figure 2B

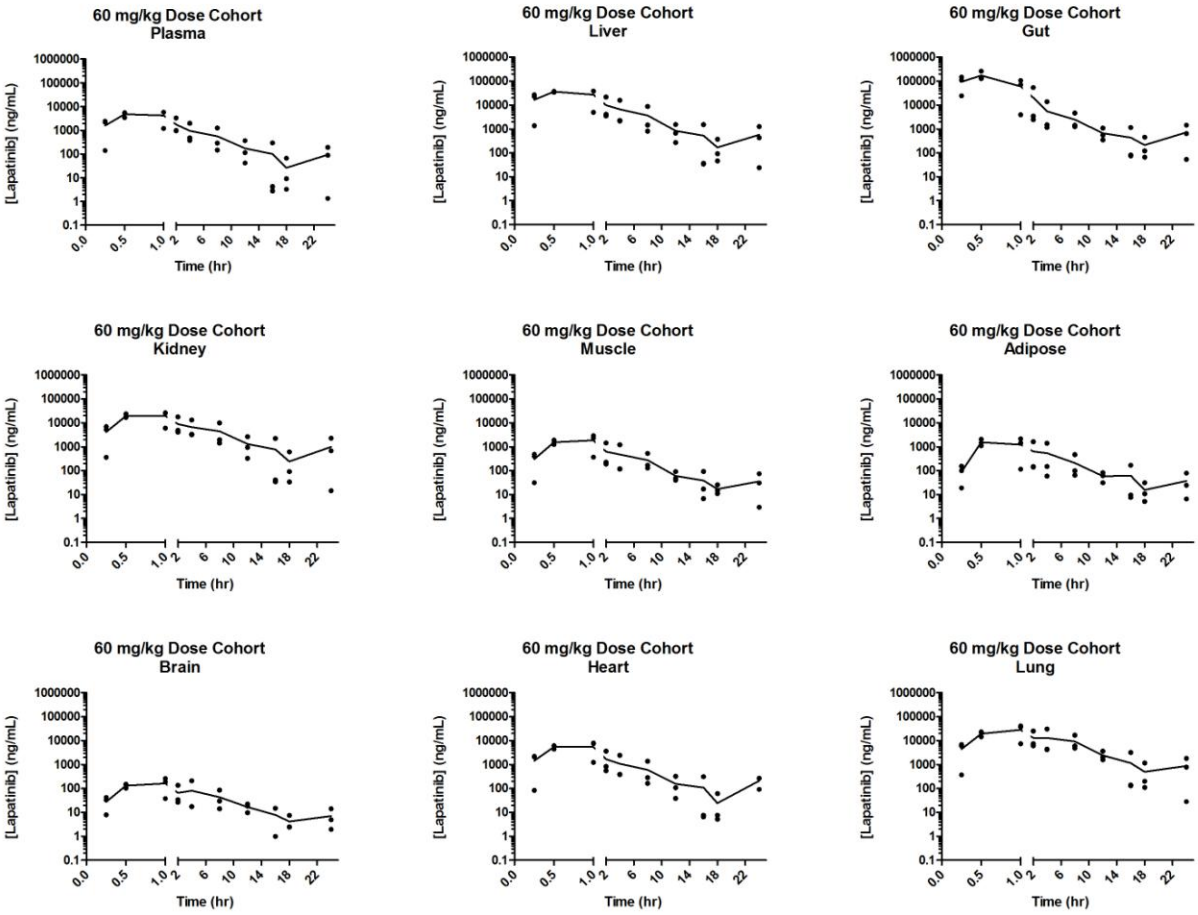

Figure 2B: Mean and scatterplot of tissue concentrations of LAPATINIB after an oral gavage dose of 60 mg/kg. n = 3 per timepoint.

Figure 2C

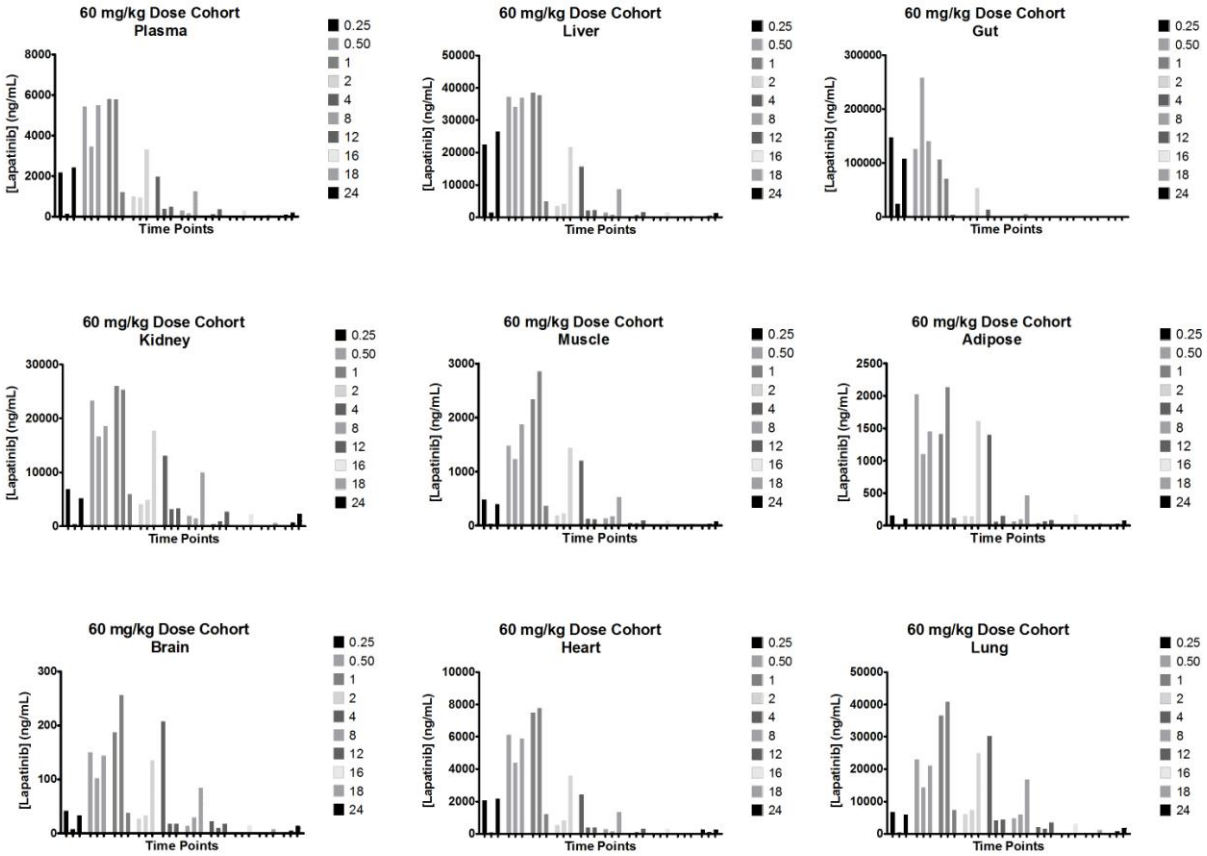

Figure 2C: Individual bar graphs of tissue concentrations of LAPATINIB after an oral gavage dose of 60 mg/kg. n = 3 per timepoint.

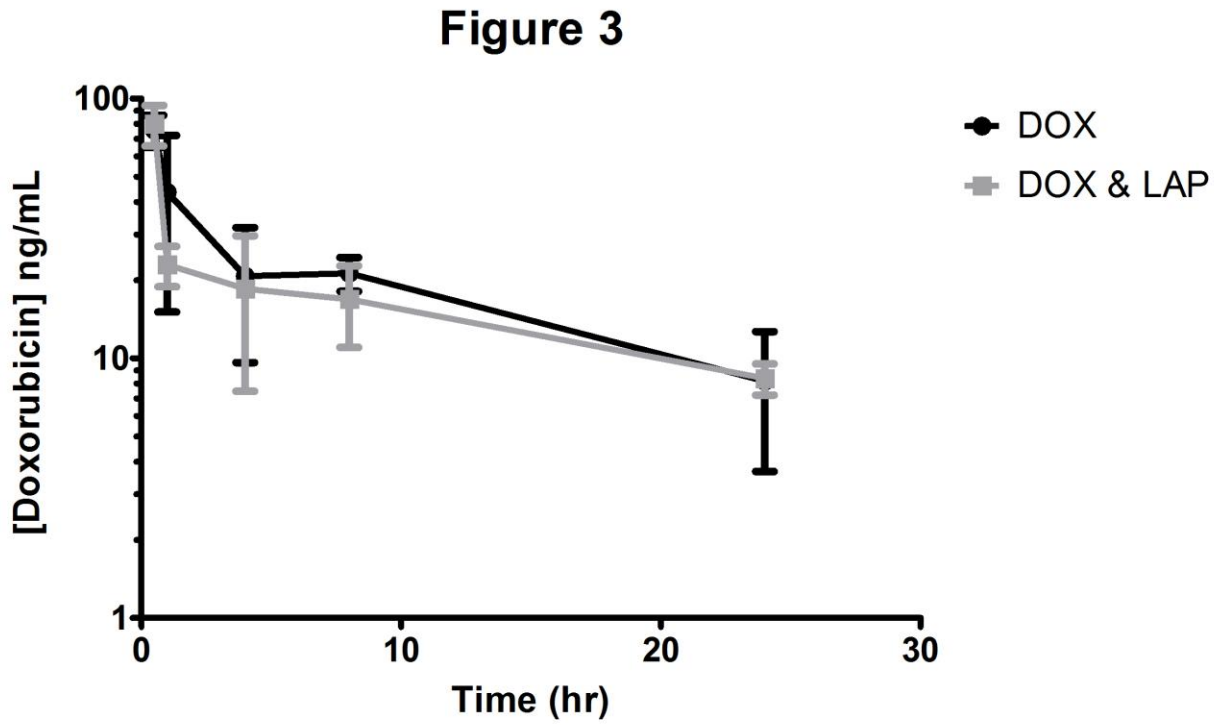

Figure 3: Mean ± standard deviation of plasma concentrations of DOXORUBICIN after combination LAPATINIB (oral gavage dose of 60 mg/kg) and DOXORUBICIN (i.v. dose of 6 mg/kg). n = 3 per timepoint.

Figure 4

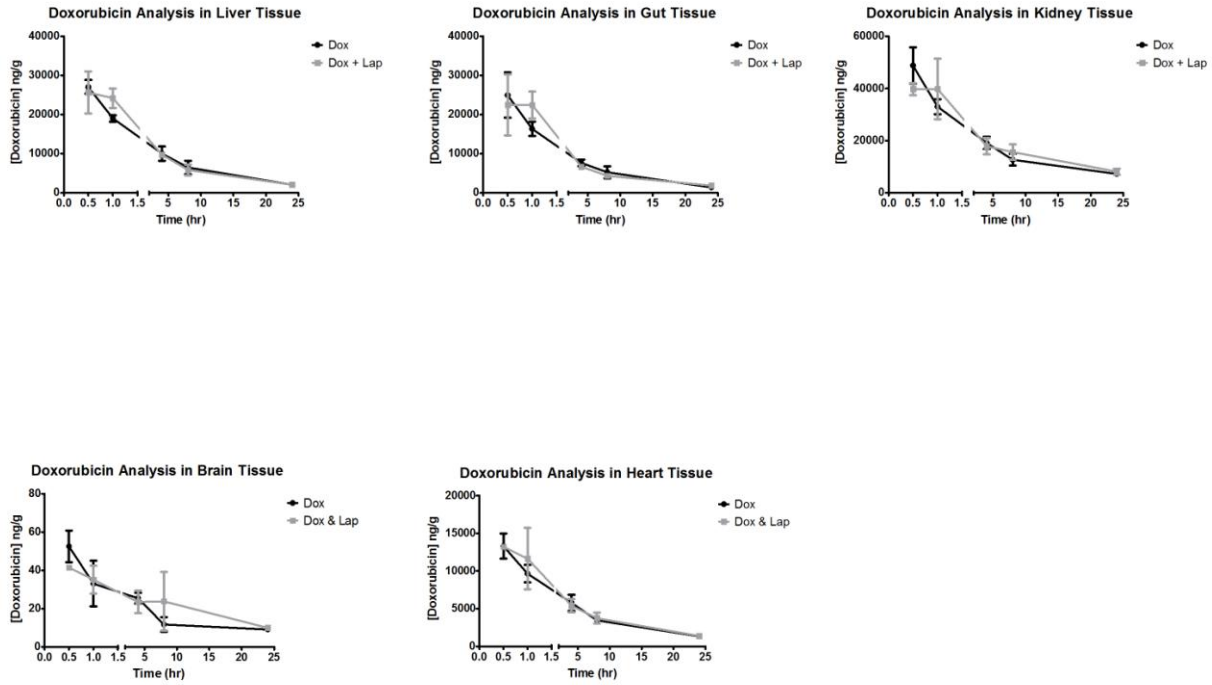

Figure 4: Mean ± standard deviation of tissue concentrations of DOXORUBICIN after combination LAPATINIB (oral gavage dose of 60 mg/kg) and DOXORUBICIN (i.v. dose of 6 mg/kg). n = 3 per timepoint.

Figure 5

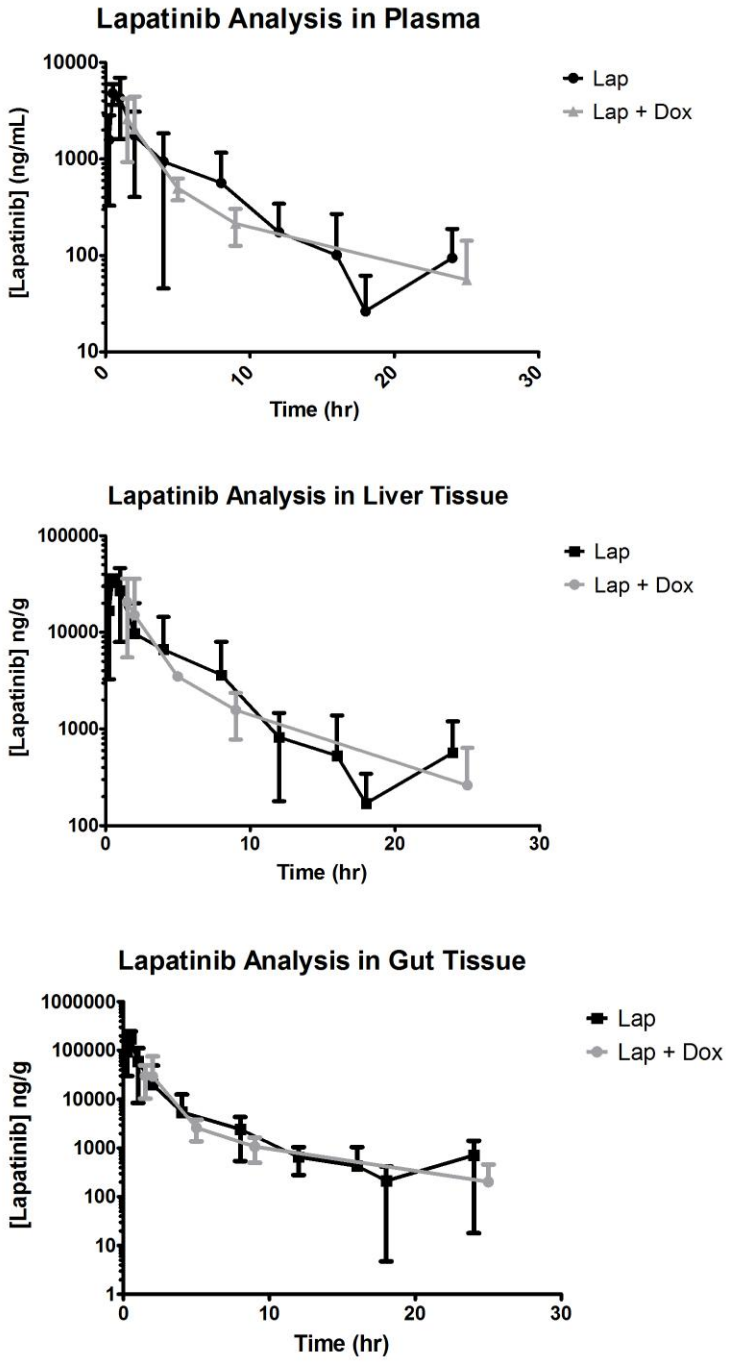

Figure 5: Mean ± standard deviation of plasma concentrations of LAPATINIB after combination LAPATINIB (oral gavage dose of 60 mg/kg) and DOXORUBICIN (i.v. dose of 6 mg/kg). n = 3 per timepoint.

Figure 6

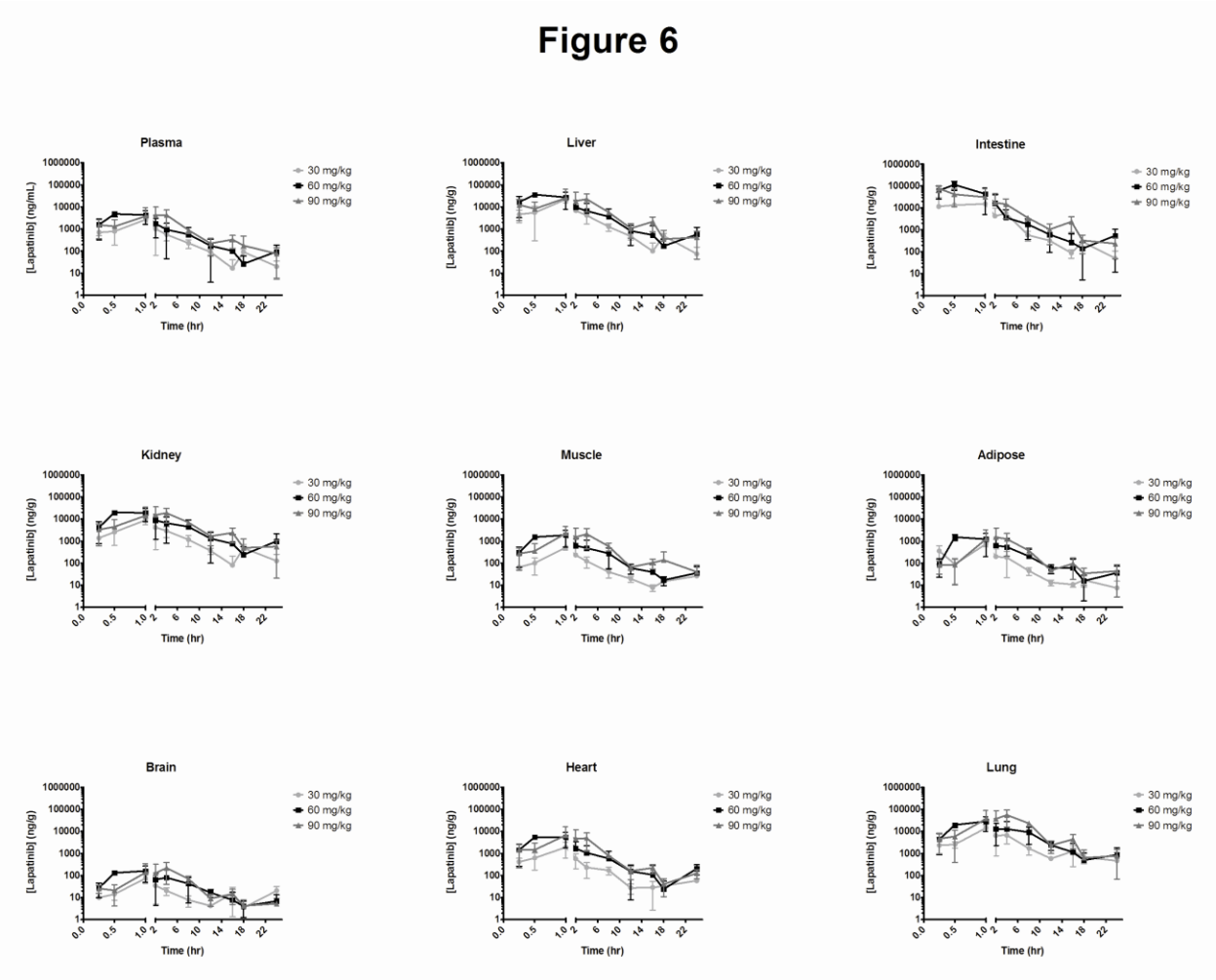

Figure 6: Mean ± standard deviation of tissue concentrations of LAPATINIB after oral gavage doses of 30, 60 and 90 mg/kg. n = 3 per timepoint.

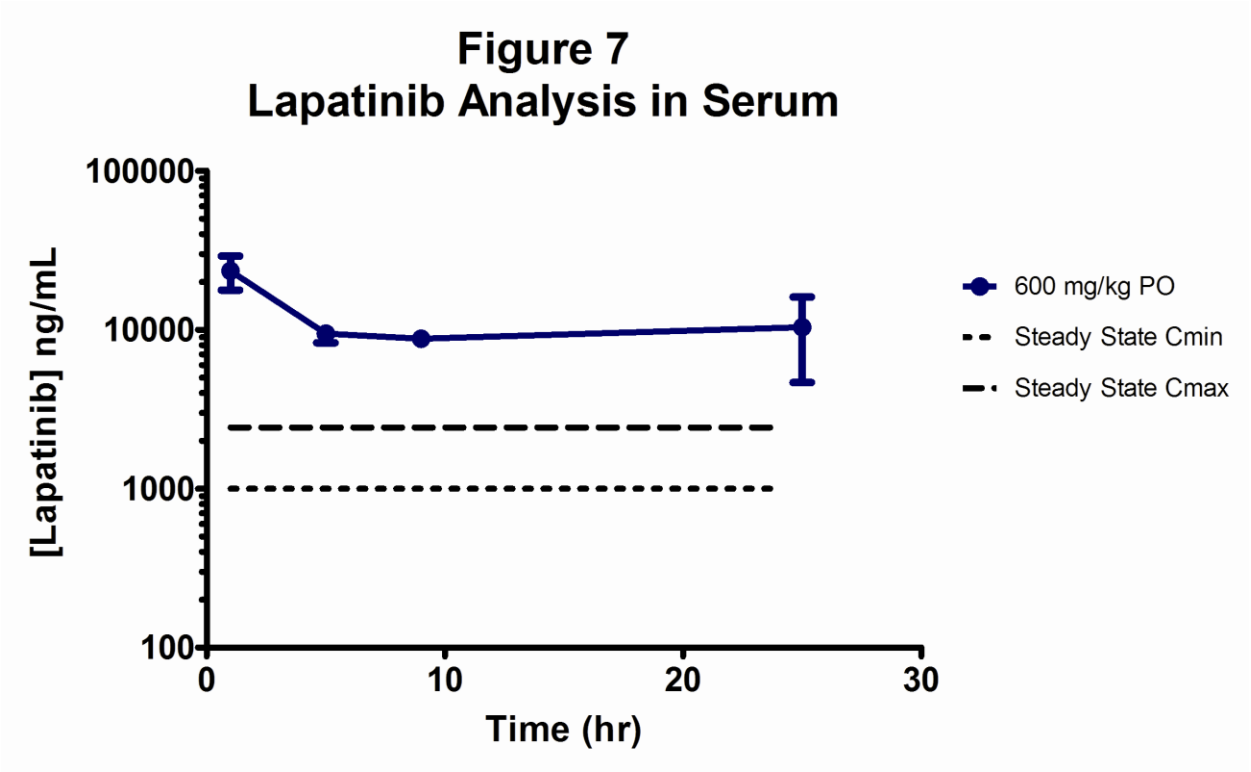

Figure 7: Mean ± standard deviation of serum concentrations of LAPATINIB after an oral gavage (PO) dose of 600 mg/kg in DMSO. Dashed lines represent the steady state peak (C_{max}) and trough (C_{min}) concentrations in humans, with our goal being to maintain LAPATINIB concentrations between these two concentrations for the duration of the PK study. n = 3 per timepoint.

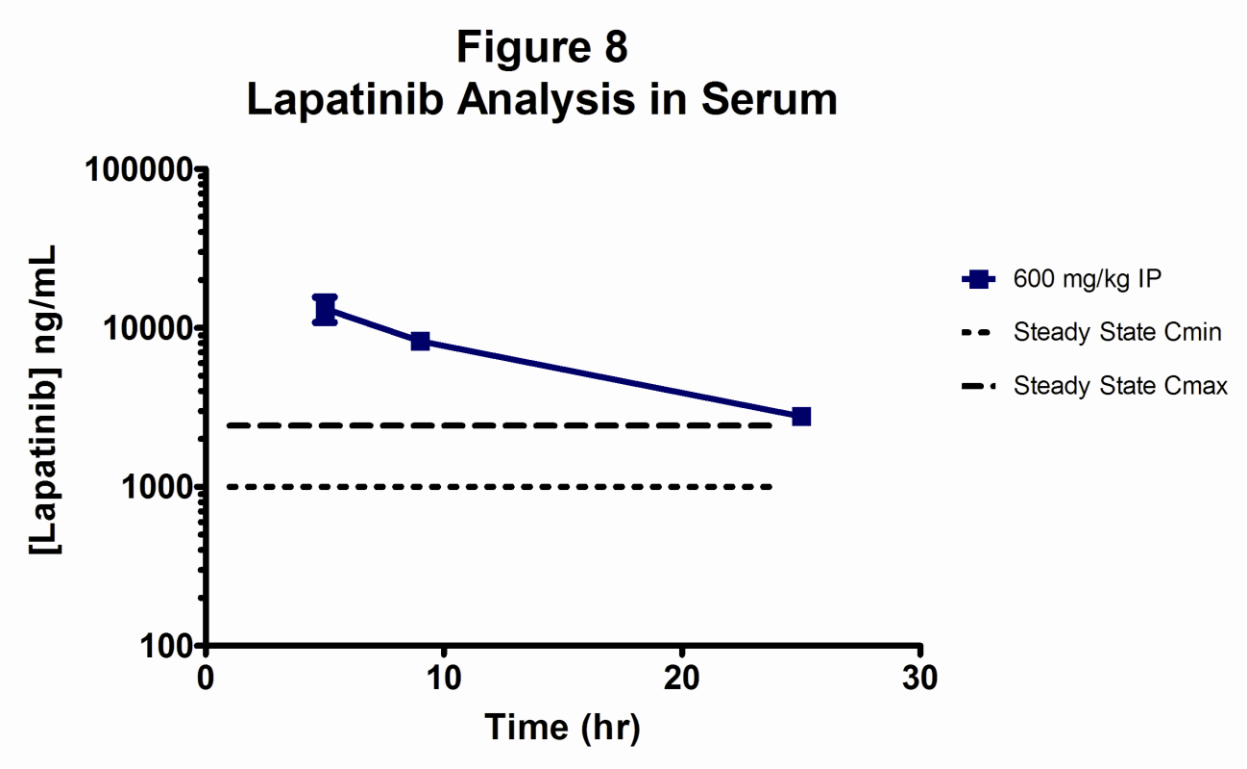

Figure 8: Mean ± standard deviation of serum concentrations of LAPATINIB after an intraperitoneal (IP) dose of 600 mg/kg in DMSO. Dashed lines represent the steady state peak (C_{max}) and trough (C_{min}) concentrations in humans, with our goal being to maintain LAPATINIB concentrations between these two concentrations for the duration of the PK study. n = 3 per timepoint.

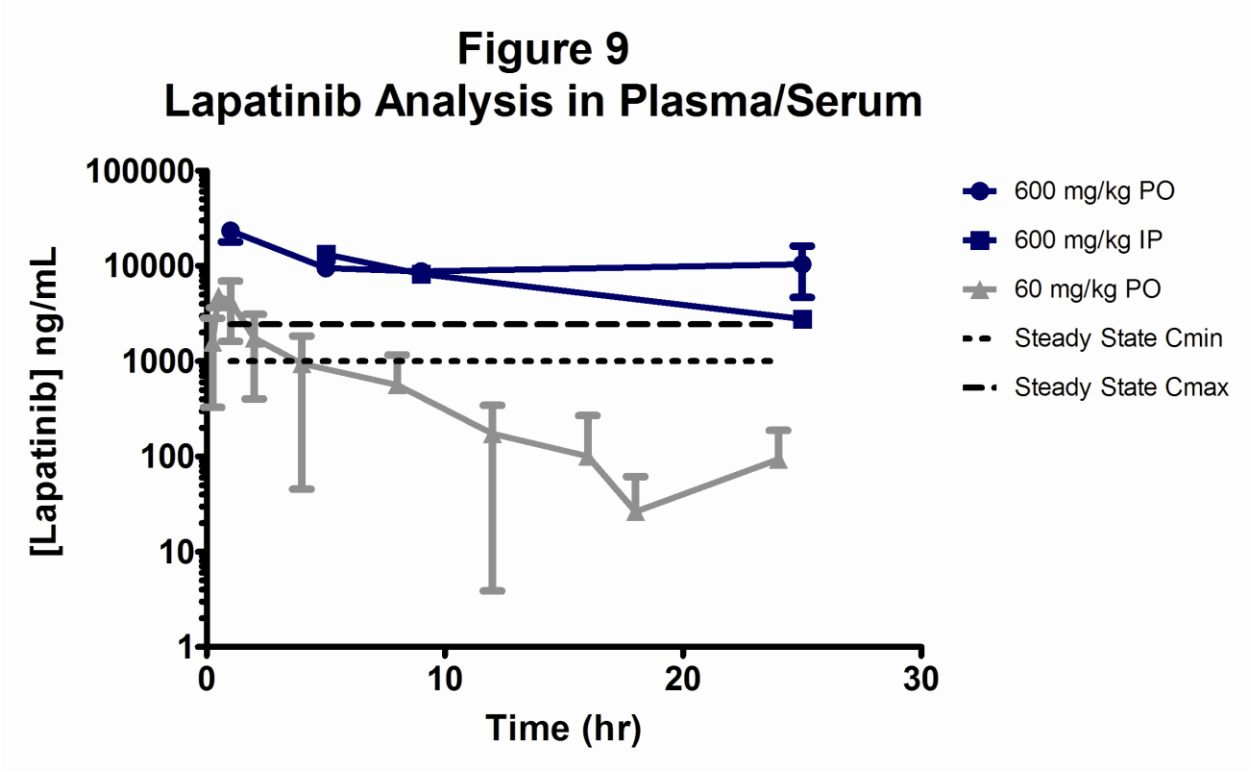

Figure 9: Mean ± standard deviation of serum concentrations of LAPATINIB after an oral gavage (PO) dose of 600 mg/kg in DMSO, an intraperitoneal (IP) dose of 600 mg/kg in DMSO or an oral gavage (PO) dose of 60 mg/kg in 0.5% hydroxypropyl methylcellulose: 0.1% Tween 80. Dashed lines represent the steady state peak (C_{max}) and trough (C_{min}) concentrations in humans, with our goal being to maintain LAPATINIB concentrations between these two concentrations for the duration of the PK study. n = 3 per timepoint.

Figure 10

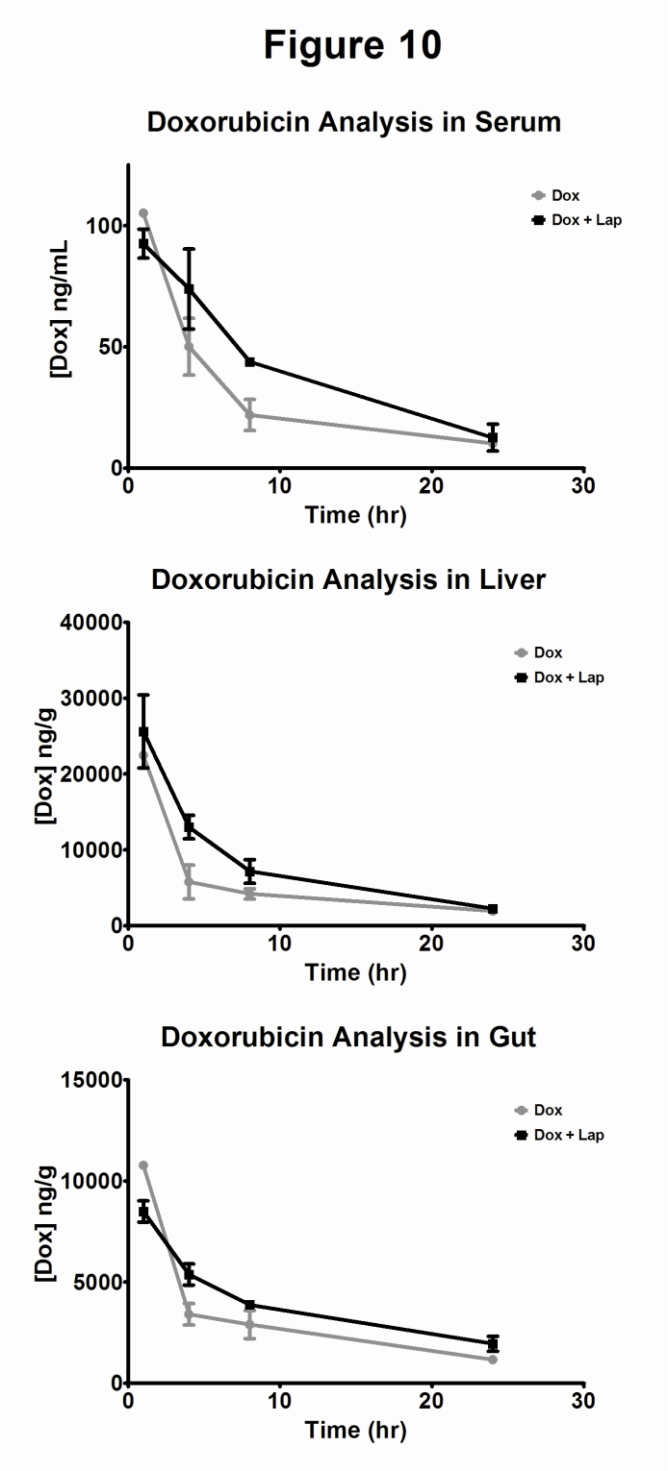

Figure 10: Mean ± standard deviation of tissue concentrations of DOXORUBICIN after combination LAPATINIB (oral gavage dose of 600 mg/kg in DMSO) and DOXORUBICIN (i.v. dose of 6 mg/kg). n = 3 per timepoint.

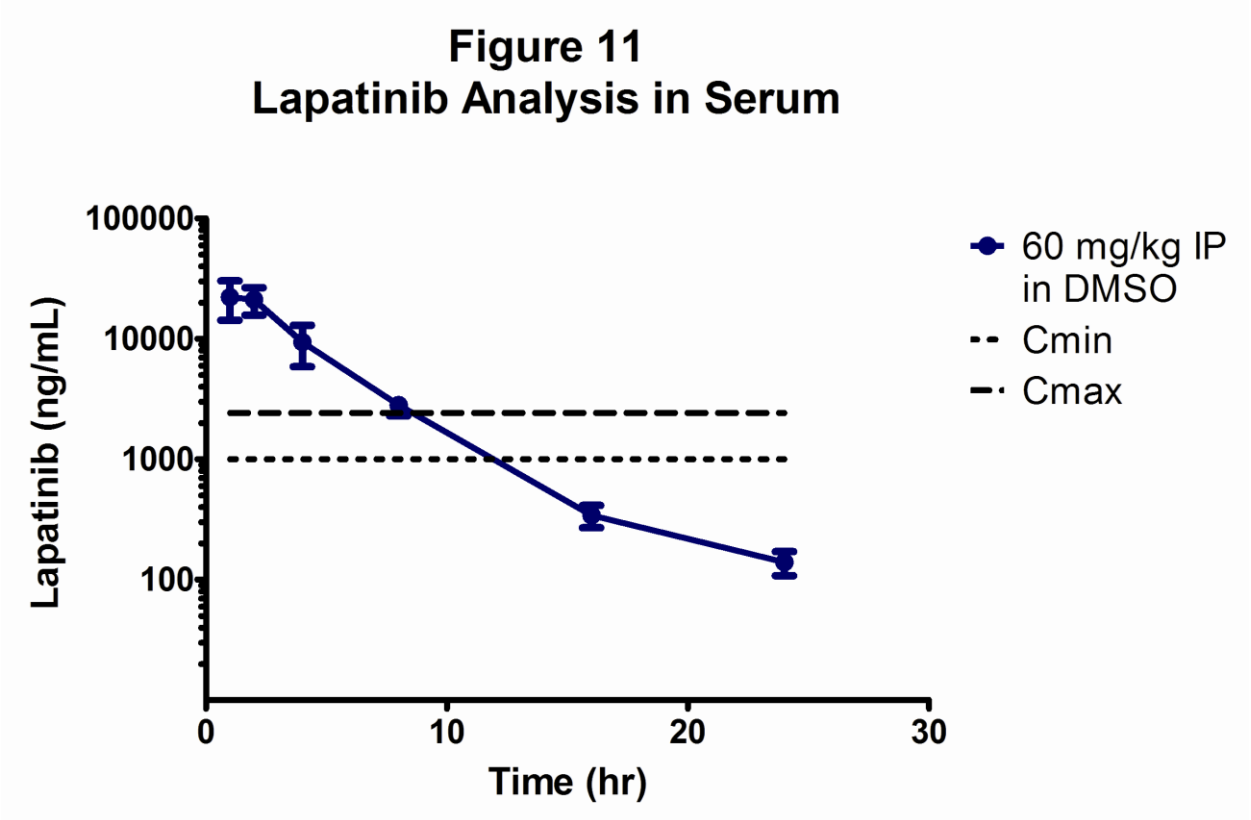

Figure 11: Mean ± standard deviation of serum concentrations of LAPATINIB after an intraperitoneal (IP) dose of 60 mg/kg in DMSO. Dashed lines represent the steady state peak (C_{max}) and trough (C_{min}) concentrations in humans, with our goal being to maintain LAPATINIB concentrations between these two concentrations for the duration of the PK study. n = 3 per timepoint.

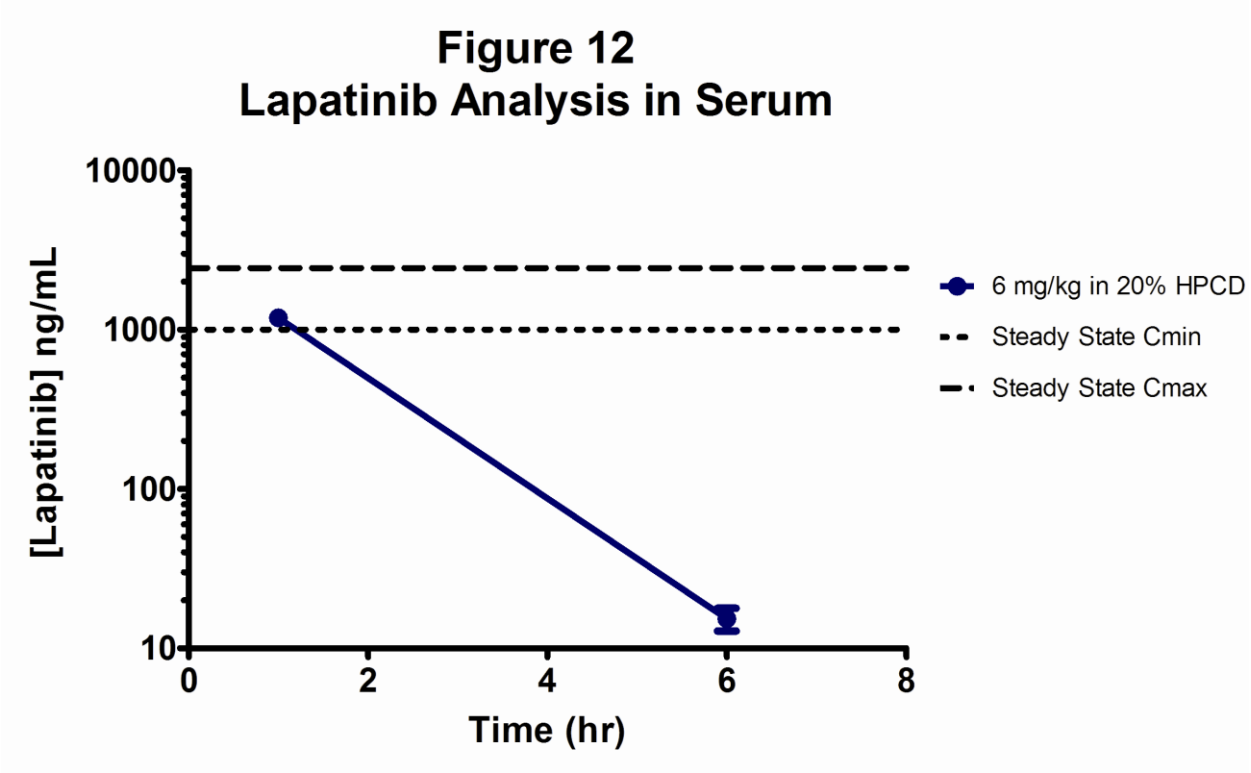

Figure 12: Mean ± standard deviation of serum concentrations of LAPATINIB after an intraperitoneal (IP) dose of 6 mg/kg in 20% hydroxypropyl beta cyclodextrin (HPCD). Dashed lines represent the steady state peak (C_{max}) and trough (C_{min}) concentrations in humans, with our goal being to maintain LAPATINIB concentrations between these two concentrations for the duration of the PK study. n = 3 per timepoint.

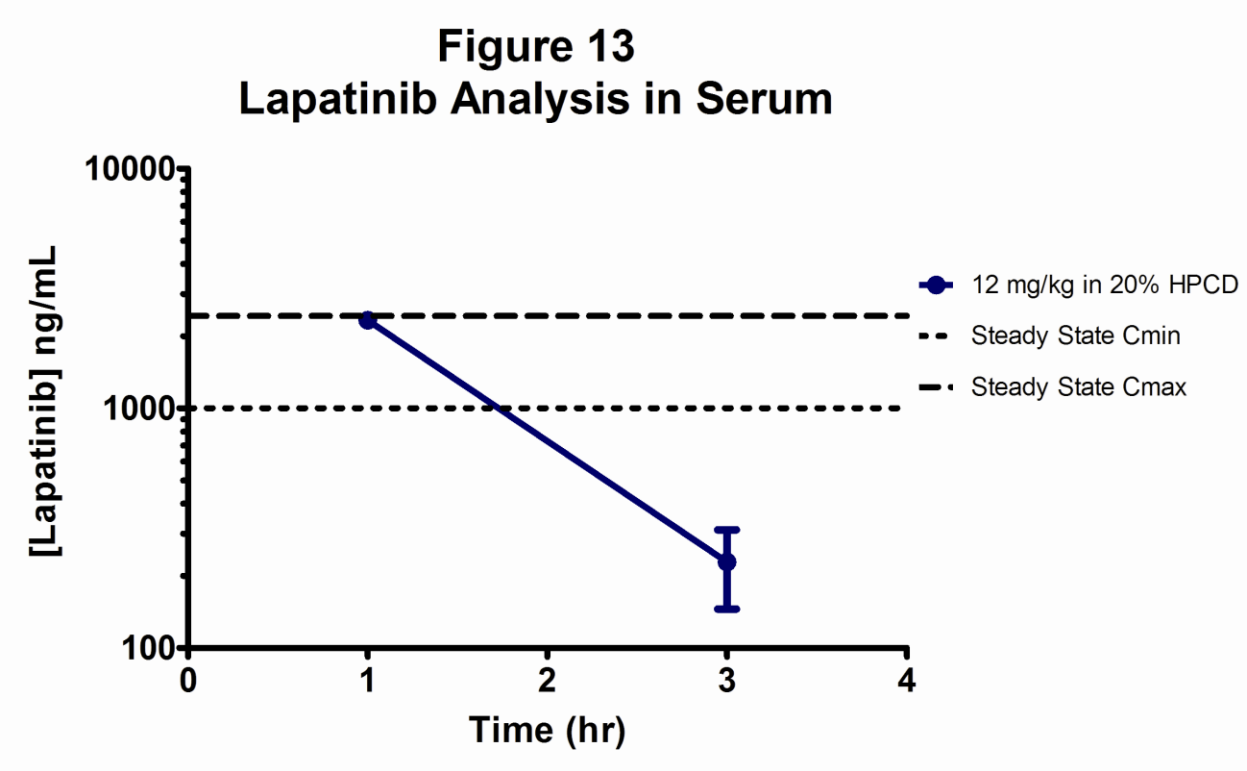

Figure 13: Mean ± standard deviation of serum concentrations of LAPATINIB after an intraperitoneal (IP) dose of 12 mg/kg in 20% hydroxypropyl beta cyclodextrin (HPCD). Dashed lines represent the steady state peak (C_{max}) and trough (C_{min}) concentrations in humans, with our goal being to maintain LAPATINIB concentrations between these two concentrations for the duration of the PK study. n = 3 per timepoint.

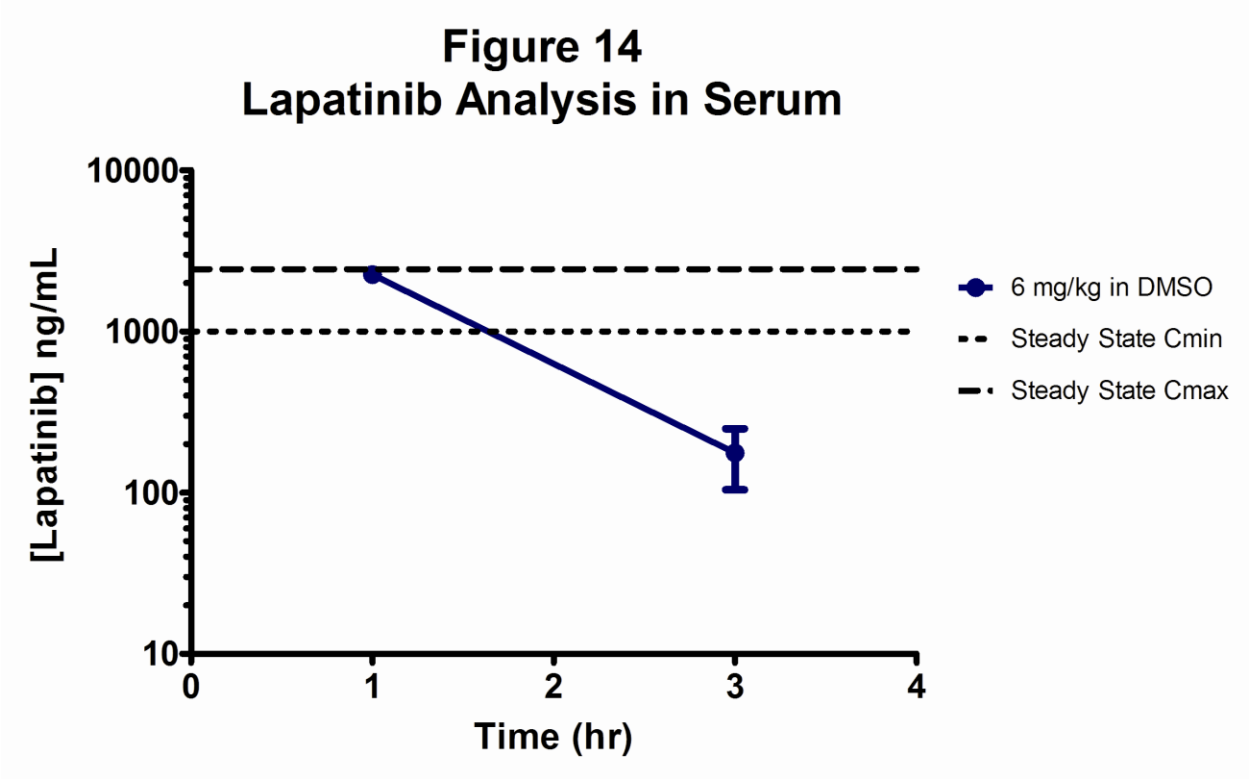

Figure 14: Mean ± standard deviation of serum concentrations of LAPATINIB after an intraperitoneal (IP) dose of 6 mg/kg in DMSO. Dashed lines represent the steady state peak (C_{max}) and trough (C_{min}) concentrations in humans, with our goal being to maintain LAPATINIB concentrations between these two concentrations for the duration of the PK study. n = 3 per timepoint.

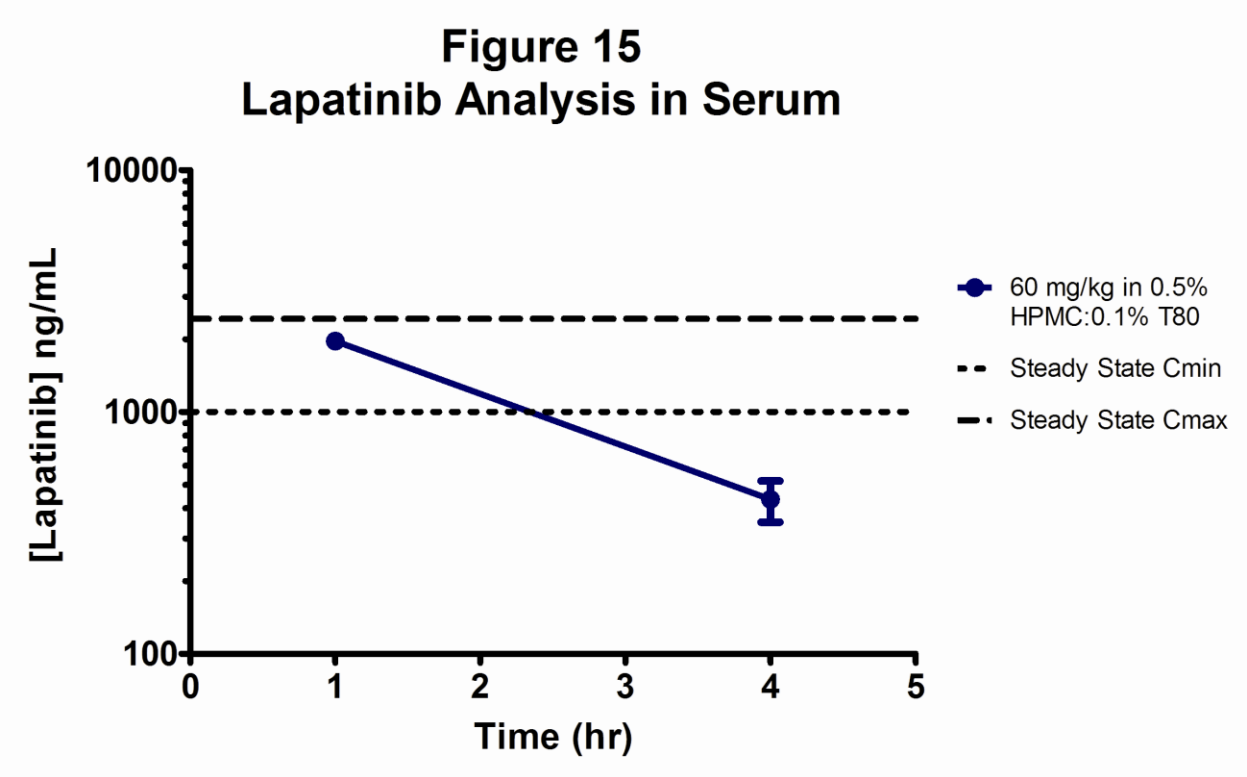

Figure 15: Mean ± standard deviation of serum concentrations of LAPATINIB after an intraperitoneal (IP) dose of 60 mg/kg in 0.5% hydroxypropyl methylcellulose: 0.1% Tween 80. Dashed lines represent the steady state peak (C_{max}) and trough (C_{min}) concentrations in humans, with our goal being to maintain LAPATINIB concentrations between these two concentrations for the duration of the PK study. n = 3 per timepoint.

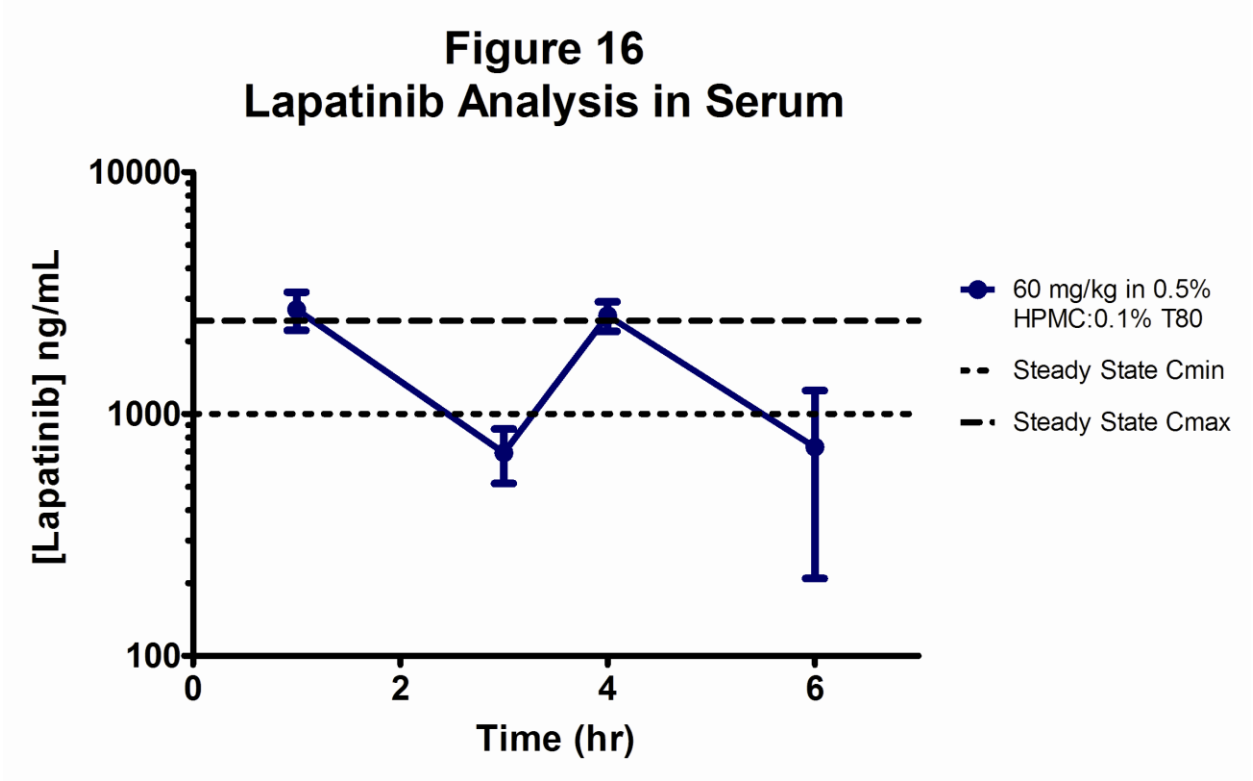

Figure 16: Mean ± standard deviation of serum concentrations of LAPATINIB after multiple intraperitoneal (IP) doses (every 3 hrs) of 60 mg/kg in 0.5% hydroxypropyl methylcellulose: 0.1% Tween 80. Dashed lines represent the steady state peak (C_{max}) and trough (C_{min}) concentrations in humans, with our goal being to maintain LAPATINIB concentrations between these two concentrations for the duration of the PK study. n = 3 per timepoint.

Figure 17

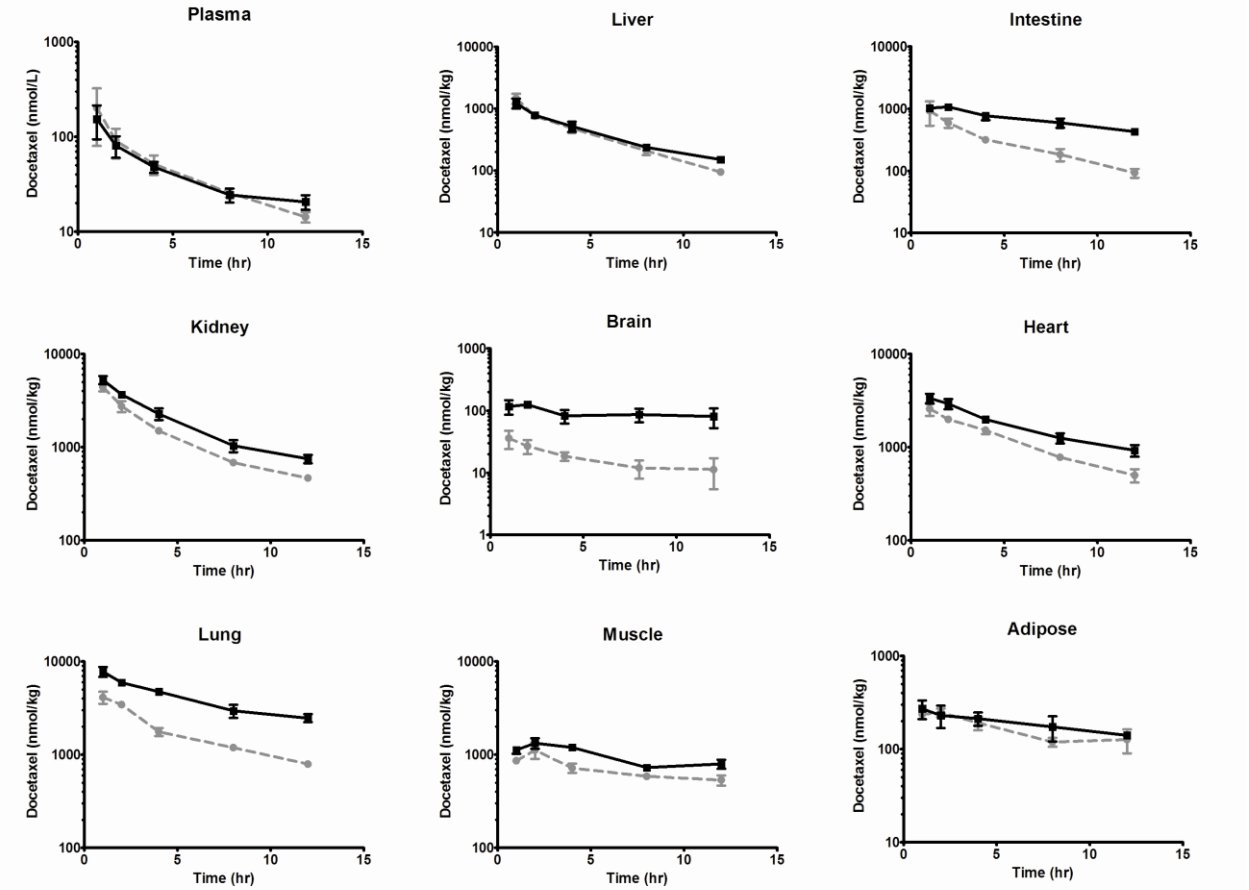

Figure 17: Mean ± standard deviation of plasma and tissue concentrations of docetaxel after an intravenous doses of 3 mg/kg to FVB wild-type (gray circles and dashed gray lines) and mdr1a/b (-/-) mice (black squares and solid black lines). n = 3 per timepoint.

Table 1. Lapatinibatinib plasma pharmacokinetic data modeled noncompartmentally and compartmentally (2 compartment) using WinNonLin.

PK Parameter	**AUC_{0-24}**	**CL/kg**	**Vz/kg**	**$t_{1/2}$**	**Tmax**	**Cmax**
Units	**hr*ng/mL**	**mL/hr/kg**	**mL/kg**	**hr**	**hr**	**ng/mL**
Noncompartmental	14462	4018	2020	3.5	0.5	4790
Compartmental	13417	4472	1118	3.4	0.6	5076

Table 2. Lapatinibatinib tissue pharmacokinetic data modeled noncompartmentally using WinNonLin.

Noncompartmental Analysis						
PK Parameter	**AUC_{0-24}**	**CL/kg**	**Vz/kg**	**$t_{1/2}$**	**Tmax**	**Cmax**
Units	**hr*ng/g**	**g/hr/kg**	**g/kg**	**hr**	**hr**	**ng/g**
Gut	196524	301	1240	2.9	0.5	174333
Lung	141541	409	2402	4.1	1	28217
Liver	94313	618	3013	3.4	0.5	36067
Kidney	84654	662	4033	4.2	0.5	19500
Heart	16249	3438	20015	4.0	1	5483
Muscle	6018	9661	52105	3.7	1	1849
Adipose	5492	10543	57645	3.8	0.5	1523
Brain	815	69665	463018	4.6	1	160

Table 3. Lapatinibatinib tissue pharmacokinetic data modeled compartmentally (2 compartment) using WinNonLin.

Compartmental Analysis						
PK Parameter	**AUC_{0-24}**	**CL/kg**	**Vz/kg**	**$t_{1/2}$**	**Tmax**	**Cmax**
Units	**hr*ng/g**	**g/hr/kg**	**g/kg**	**hr**	**hr**	**ng/g**
Gut						
Lung						
Liver	85127	705	1722	3.2	0.5	36889
Kidney	76782	781	2419	3.8	0.7	21363
Heart	16001	3750	14733	5.5	0.7	6133
Muscle	6038	9938	39434	5.2	0.7	1876
Adipose	4848	12376	27302	4.7	0.6	1479
Brain	849	70640	333939	5.6	0.7	158

Table 4: Tissue pharmacokinetics of lapatinibatinib in 5-6 week old female FVB mice after oral gavage dosing of 30, 60 and 90 mg/kg.

Tissue	Dose	AUC $_{0\rightarrow24}$	t $_{1/2}$	CL	Vz	T $_{max}$	C $_{max}$
	mg/kg	ng/g*hr	hr	g/hr/kg	g/kg	hr	ng/g
Plasma	30	7002.2	3.4	4224.7	20930.3	1.0	2706.7
Plasma	60	13949.1	3.7	4152.4	22206.9	0.5	4790.0
Plasma	90	27196.7	3.7	3261.0	17446.0	4.0	4308.7
Liver	30	47981.9	3.0	621.0	2725.1	1.0	22133.3
Liver	60	90502.5	3.4	643.2	3135.6	0.5	36066.7
Liver	90	145856.0	3.5	608.3	3031.6	1.0	25206.7
Intestine	30	42728.7	3.0	698.6	2985.4	1.0	15133.3
Intestine	60	130006.3	2.9	453.7	1870.3	0.5	115000.0
Intestine	90	147316.9	3.0	606.8	2621.2	0.3	75933.3
Kidney	30	30113.2	3.8	974.3	5275.8	1.0	8976.7
Kidney	60	82178.3	4.2	680.6	4145.8	0.5	19500.0
Kidney	90	131285.5	4.1	668.4	3966.2	4.0	18776.7
Lung	30	55877.6	4.9	507.1	3571.5	1.0	14466.7
Lung	60	136778.0	4.1	422.9	2482.3	1.0	28216.7
Lung	90	346612.3	3.4	256.8	1259.8	4.0	54866.7
Heart	30	4223.3	4.5	6522.3	42338.9	1.0	1897.7
Heart	60	15524.0	4.0	3587.5	20882.3	1.0	5483.3
Heart	90	29980.4	3.2	2944.6	13700.5	1.0	6661.7
Brain	30	335.7	10.7	45944.6	708709.7	1.0	75.8
Brain	60	789.0	4.6	71807.5	477259.0	1.0	160.2
Brain	90	1264.5	3.9	69537.4	390212.0	4.0	219.0
Muscle	30	1488.0	4.8	18003.7	123727.1	1.0	517.3
Muscle	60	5752.4	3.7	10091.9	54431.6	1.0	1848.7
Muscle	90	12892.6	3.8	6864.9	37419.8	1.0	2242.6
Adipose	30	1727.3	3.7	16973.6	91416.4	1.0	743.0
Adipose	60	5280.6	4.0	10926.9	63041.0	0.5	1523.3
Adipose	90	8618.9	3.8	10156.7	55662.3	2.0	1500.3

Table 5: Tissue $AUCs_{0-24}$ of doxorubicinorubicin in 5-6 week old female FVB mice after intravenous dosing of 6 mg/kg doxorubicinorubicin and combination oral gavage dosing of 600 mg/kg lapatinibatinib in DMSO and intravenous dosing of 6 mg/kg doxorubicinorubicin.

Tissue	DOXORUBICIN	DOXORUBICIN + LAPATINIB
Serum	633.8 ng/mL * hr	936.4 ng/mL * hr
Liver	111433 ng/g * hr	173562 ng/g * hr
Gut	66443 ng/g * hr	85916 ng/g * hr

Appendices

J Pharmacokinet Pharmacodyn
DOI 10.1007/s10928-012-9295-8

ORIGINAL PAPER

Physiologically based pharmacokinetic model of lapatinib developed in mice and scaled to humans

Susan F. Hudachek · Daniel L. Gustafson

Received: 19 July 2012 / Accepted: 22 December 2012

Abstract Lapatinib is an oral 4-anilinoquinazoline derivative that dually inhibits epidermal growth factor receptor and human epidermal growth factor receptor 2 (HER2). This drug is a mere decade old and has only been approved by the FDA for the treatment of breast cancer since 2007. Consequently, the intricacies of the pharmacokinetics are still being elucidated. In the work presented herein, we determined the biodistribution of orally administered lapatinib in mouse plasma, brain, heart, lung, kidney, intestine, liver, muscle and adipose tissue. Using this data, we subsequently developed a physiologically based pharmacokinetic (PBPK) model of lapatinib in mice that accurately predicted the tissue concentrations after doses of 30, 60 and 90 mg/kg. By taking into account interspecies differences in physiology and physiochemistry, we then extrapolated the mouse PBPK model to humans. Our model predictions closely reflected lapatinib plasma pharmacokinetics in healthy subjects. Additionally, we were also able to simulate the pharmacokinetics of this drug in the plasma of patients with solid malignancies by incorporating a decrease in liver metabolism into the model. Finally, our PBPK model also facilitated the estimation of various human tissue exposures to lapatinib, which harmonize with the organ-specific toxicities observed in clinical trials. This first-generation PBPK model of lapatinib can be further improved with a greater understanding of lapatinib absorption, distribution, metabolism and excretion garnered from subsequent in vitro and in vivo studies and expanded to include other pharmacokinetic determinants, including efflux transporters, metabolite generation, combination dosing, etc., to better predict lapatinib disposition in both mouse and man.

Keywords Breast cancer · Lapatinib · Physiologically based pharmacokinetic modeling · Tyrosine kinase inhibitor

Introduction

Lapatinib is an oral 4-anilinoquinazoline derivative that dually inhibits epidermal growth factor receptor (EGFR) and human epidermal growth factor receptor 2 (HER2) (estimated K_i^{app} values of 3 and 13 nM, respectively) by competing with ATP [1]. Aberrant signaling of these tyrosine kinases is prevalent in various types of solid tumors, thus making them attractive therapeutic targets. Presently, lapatinib is approved by the US Food and Drug Administration (FDA) in combination with capecitabine for the treatment of HER2 positive metastatic breast cancer and in combination with letrozole for the treatment of hormone receptor positive, HER2 positive metastatic breast cancer. In addition, there are approximately 250 current clinical trials in cancer patients involving this drug [2].

Numerous preclinical studies and clinical trials have investigated the plasma pharmacokinetics of lapatinib [3–15]. However, none have elucidated the biodistribution of this compound in tissues other than blood. Based on adverse reactions reported in humans (including cardiac, hepatic, gastrointestinal and lung toxicities), it can be presumed that there are significant levels of drug in these organs.

Electronic supplementary material The online version of this article (doi:10.1007/s10928-012-9295-8) contains supplementary material, which is available to authorized users.

S. F. Hudachek (✉) · D. L. Gustafson
Department of Clinical Sciences, Animal Cancer Center, Colorado State University, Fort Collins, CO, USA
e-mail: Susan.Hudachek@colostate.edu

Published online: 12 January 2013

To empirically determine both plasma and organ exposure to lapatinib, we developed a physiologically based pharmacokinetic (PBPK) model in mice and then scaled this model to humans. This type of pharmacologic modeling is a useful tool that facilitates the prediction of target tissue drug concentrations by incorporating mathematical descriptions of the uptake and disposition of chemicals based on quantitative interrelations among the critical determinants of physiological processes (i.e., absorption, metabolism, excretion and tissue solubility phenomena) [16]. Accordingly, PBPK models are comprised of compartments corresponding to discrete tissues or groupings of tissues with appropriate volumes, blood flows, and pathways for xenobiotic clearance including pertinent biochemical and physiochemical constants [17]. Each compartment in the model is described with a mass-balance differential equation whose terms mathematically represent biological processes; the set of equations is then solved by numerical integration to simulate tissue time-course concentrations of chemicals and their metabolites [17]. The PBPK model of lapatinib presented herein consisted of eight tissue compartments (plasma, brain, heart, lung, kidney, intestine, liver and slowly perfused tissues) and incorporated drug absorption, intestinal and hepatic metabolism and fecal elimination in both mouse and man.

Materials and methods

Chemicals

Lapatinib (GW572016) and GW572016AH were generously provided by GlaxoSmithKline. Hydroxypropyl methylcellulose and Tween® 80 were purchased from Sigma-Aldrich. All other reagents were of analytical grade.

Lapatinib pharmacokinetic studies in mice

Five to six-week-old female FVB mice were purchased from Taconic. Animals were housed in polycarbonate cages and kept on a 12 h light/dark cycle. Food and water were given ad libitum. All experimental procedures were approved by Colorado State University's Animal Care and Use Committee and the Department of Defense US Army Medical Research and Material Command (USAMRMC) Animal Care and Use Review Office (ACURO).

Upon arrival, mice acclimated for a minimum of seven days prior to any experimentation. After acclimation, a time course distribution study of lapatinib was conducted at doses of 30, 60 and 90 mg/kg. Lapatinib was formulated as a suspension in 0.5 % hydroxypropyl methylcellulose: 0.1 % Tween® 80 in Milli-Q water and was administered via oral gavage as a single bolus dose. Subsequently, three mice were sacrificed at 0.25, 0.5, 1, 2, 4, 8, 12 and 16 h by cardiac stick exsanguination under isoflurane anesthesia. Plasma, brain, liver, proximal small intestine, kidney, heart, lung, muscle and adipose tissue were immediately collected, rinsed with phosphate buffered saline, frozen in liquid nitrogen and stored at -80 °C until analysis.

Lapatinib high-pressure liquid chromatography-tandem mass spectrometry analysis

Analysis of lapatinib in plasma and tissue was done using high-pressure liquid chromatography-tandem mass spectrometry (LC/MS/MS) analysis based on the method of Bai et al. [18], modified as follows. Briefly, lapatinib was extracted from plasma by adding 210 μL of acetonitrile and 10 μL of internal standard (17.2 pmol GW572016AH) to 100 μL of unknown sample plasma, vortexing for 10 min and centrifuging at 18,000×*g* for 10 min at 4 °C. An aliquot of 20 μL of the supernatant was injected into the LC/MS/MS system for analysis. Tissues (brain, liver, proximal small intestine, kidney, heart, lung, muscle and adipose) were homogenized at 100 mg/mL in water and 100 μL of the homogenates were extracted using the method for plasma detailed above. Standards and quality control samples were prepared in the appropriate matrix and analyzed as described above.

The HPLC system consisted of an Agilent 1200 Series binary pump SL, vacuum degasser, thermostatted column compartment SL (Agilent Technologies, Santa Clara, CA, USA) and a CTC Analytics HTC PAL System autosampler (Leap Technologies, Carrboro, NC, USA). The HPLC column was a Waters Sunfire C8 column (4.6 × 50 mm I.D., 2.5 μm bead size) (Waters Corporation, Milford, MA, USA) protected by a SecurityGuard™ C18 cartridge (4 × 2.0 mm I.D.) (Phenomenex, Torrance, CA, USA) and maintained at room temperature. The mobile phase consisted of an aqueous component (A) of 20 mM ammonium formate in MilliQ water, pH 2.2 (with formic acid) and an organic component (B) of acetonitrile with 1 % formic acid. The 3.5 min run consisted of the following linear gradient elution: 95 % A and 5 % B at 0 min, 95 % A and 5 % B at 0.25 min, 25 % A and 75 % B at 0.35 min, 25 % A and 75 % B at 3.0 min, 95 % A and 5 % B at 3.1 min and 95 % A and 5 % B at 3.5 min. The system operated at a flow-rate of 0.75 mL/min.

Mass spectrometric detection was performed on an API 3200™ triple quadrupole instrument (Applied Biosystems Inc., Foster City, CA, USA) using multiple reaction monitoring (MRM). Ions were generated in positive ionization mode using an electrospray interface. Lapatinib compound-dependent parameters were as follows: declustering potential (DP): 60 V; entrance potential (EP): 10 V; collision cell entrance potential (CEP): 21 V; collision energy (CE): 51 V and collision cell exit potential (CXP): 5.8 V. GW572016AH

(internal standard) compound-dependent parameters were as follows: DP: 67 V; EP: 7.5 V; CEP: 23 V; CE: 49 V and CXP: 5.5 V. Source-dependent parameters were as follows: nebulizer gas (GS1): 50 psi; auxiliary (turbo) gas (GS2): 60 psi; turbo gas temperature (TEM): 500 °C; curtain gas [7]: 10 psi; collision-activated dissociation (CAD) gas (nitrogen): 6 psi; ionspray voltage (IS): 5,000 V and interface heater (IH): 500 °C. Peak areas ratios obtained from MRM of lapatinib (*m/z* 581 → 365.1) and GW572016AH (*m/z* 587 → 367) were used for quantification.

The lower limit of quantitation for this assay was 1 ng/mL for plasma and 5 ng/g for tissues. The accuracy for the assay was 95.61 ± 4.60 % in plasma and 95.83 ± 3.47 % in tissues. The precision of the assay was 1.97 % in plasma and 3.75 % in tissues.

PBPK model development

A PBPK model for lapatinib was developed incorporating absorption, intestinal and hepatic metabolism and fecal elimination. This flow-limited model was comprised of eight tissue compartments: plasma, brain, heart, lung, kidney, intestine, liver and slowly perfused tissue (Fig. 1). Physiological parameters (tissue volumes and tissue blood flows) were obtained from Brown et al. [19] and are shown in Table 1.

The unbound fraction of drug in the plasma was set at 0.01 (1 %), as lapatinib is highly bound (>99 %) to albumin and alpha-1 acid glycoprotein [1]. The arterial blood drug concentration available to all tissues except liver was considered to be the unbound lapatinib concentration in the blood. Both unbound and bound lapatinib were available for uptake into the liver.

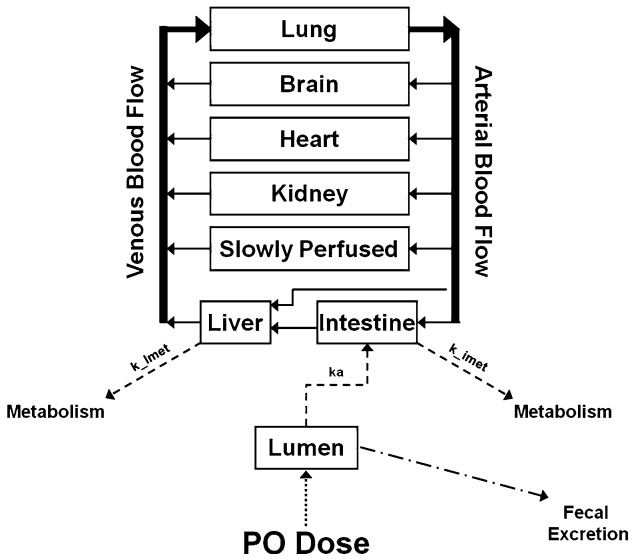

Fig. 1 Schematic representation of a physiologically based pharmacokinetic (PBPK) model of lapatinib. *Solid arrows* represent blood flow. *Dashed lines* represent first-order rate constants for absorption from intestinal lumen (*ka*), hepatic metabolism (*k_lmet*) and intestinal metabolism (k_imet). The *dotted line* represents lapatinib input into the system via per os (*p.o.*) dosing. Drug remaining in the lumen is eliminated via fecal excretion

Table 1 PBPK model parameter values

Parameter	Units	Mouse	Human
Lapatinib properties			
Molecular weight		581.06 g/mol	
Percent unbound		1 %	
Tissue volume[a]	% of body weight		
Blood		4.90	7.9
Brain		1.65	2.0
Heart		0.50	0.5
Lung		0.73	0.8
Kidney		1.67	0.4
Intestine		4.22	1.7
Liver		5.49	2.6
Slowly perfused[b]		80.84	84.1
Tissue blood flow[a]	% of cardiac output		
Brain		3.3	11.4
Heart		6.6	4.0
Lung		100	100
Kidney		9.1	17.5
Intestine		14.1	18.1
Liver		2.0	4.6
Slowly perfused[b]		64.9	44.4
Partition coefficients[c]	Ratio		
Brain:plasma		10 (19)	10
Heart:plasma		215 (22)	215
Lung:plasma		1,643 (19)	1,643
Kidney:plasma		1,064 (18)	1,064
Intestine:plasma		531 (31)	531
Liver:plasma		12 (20)	12
Slowly perfused:plasma		65 (20)	65
Absorption rate constants[d]	h^{-1}		
Lumen → Intestine		0.237 (2)	0.07 (6)
Metabolism rate constants	h^{-1}		
Liver[d]		127 (13)	75 (5)
Intestine		2.5[e]	0.975[f]

[a] Physiological parameters obtained from Brown et al. [19]

[b] Slowly perfused tissue parameters calculated as the remaining percent

[c] Determined by parameter estimation optimized for observed plasma and tissue concentrations from mouse 60 mg/kg dose cohort. Data is parameter estimate (CV%)

[d] First-order rate constants determined by parameter estimation optimized for observed plasma and tissue concentrations from mouse 60 mg/kg dose cohort for mouse model and observed plasma concentrations from healthy subject human data for human model. Data is parameter estimate (CV%)

[e] Calculated as 2 % of liver metabolism

[f] Calculated as 1.3 % of liver metabolism

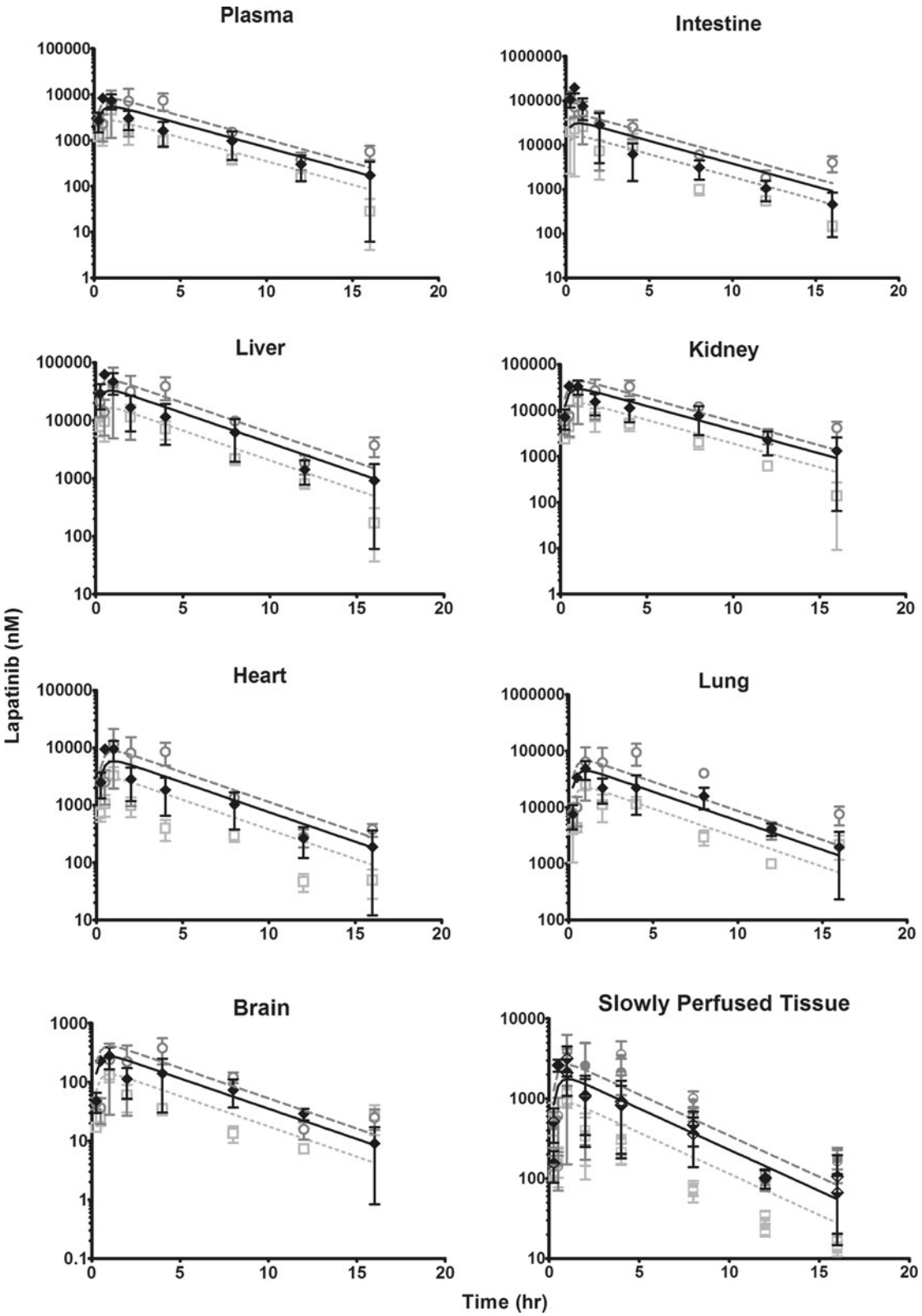
Plasma
Intestine
Liver
Kidney
Heart
Lung
Brain
Slowly Perfused Tissue
Lapatinib (nM)
Time (hr)

◀ **Fig. 2** Observed and model-simulated lapatinib concentrations in mouse plasma, intestine, liver, kidney, heart, lung, brain and slowly perfused tissue after oral gavage dosing of 30, 60 and 90 mg/kg. In all graphs except slowly perfused tissue, *open light gray squares*, *filled diamonds* and *open dark gray circles* represent the observed data from the 30, 60 and 90 mg/kg cohorts, respectively. In the slowly perfused tissue graph, the observed data from the 30 mg/kg dose cohort is represented by the *upper half-filled light gray squares* (adipose tissue) and *lower half-filled light gray squares* (muscle tissue); the observed data from the 60 mg/kg dose cohort is represented by *upper half-filled black diamonds* (adipose tissue) and *lower half-filled black diamonds* (muscle tissue); and the observed data from the 90 mg/kg dose cohort is represented by *upper half-filled dark gray circles* (adipose tissue) and *lower half-filled dark gray circles* (muscle tissue). For all observed data, error bars symbolize the standard error of the mean (SEM). *Light gray dotted lines*, *solid black lines*, and *dark gray dashed lines* represent model simulations for the 30, 60 and 90 mg/kg dose cohorts, respectively

Tissue:plasma partition coefficients were determined by parameter estimation, optimizing the fit for the observed plasma and tissue concentrations from the mouse 60 mg/kg dose cohort. These fitted values were compared with values calculated as detailed in Chen and Gross [44] using our experimental data (Online Resource 1). For these calculations, we used our concentration–time data from the mouse 60 mg/kg dose study and considered the terminal elimination phase to include the 4, 8, 12 and 16 h time points. The tissue:plasma partition coefficients were calculated as C_T^0/C_P^0, where C_T^0 and C_P^0 are the tissue and plasma intercepts (initial concentrations), respectively, from the concentration–time curves of the terminal elimination phase on a semilogarithmic plot. After the partition coefficients were determined, the values had to be adjusted because when we measured the plasma concentrations via LC/MS/MS, we analyzed both bound and unbound drug in the plasma. Thus, to correct the partition coefficients so they reflected only the unbound drug available for tissue uptake (1 % unbound), we multiplied the calculated value by 100. The Chen and Gross method [44] was applicable for the determination of kidney, lung and slowly perfused tissue (adipose and muscle were used as representative slowly perfused tissues) partition coefficients. However, for brain and heart partition coefficients, we were unable to utilize this method because the criteria for implementation of this equation were not met for these two tissues (K/Q was not $\ll 1$, where K is the organ clearance and Q is the blood flow). Additionally, for liver and intestine partition coefficients, Chen and Gross [44] describes unique equations, which we could not use because we did not have the values for all necessary variables. Therefore, because we were only able to determine three of the seven tissue partition coefficients using the Chen and Gross equations [44], we chose to estimate all partition coefficients by fitting these parameters to the model. For kidney, lung and slowly perfused tissue partition coefficients, the fitted values were 37, 7 and 12 % different than the calculated values, respectively. For brain, heart, liver and intestine partition coefficients, the fitted values were 10, 42, 29 and 16 % different than the calculated values, respectively.

The first-order rate constants for absorption from intestinal lumen and hepatic metabolism were determined by parameter estimation. For the mouse model, the fit was optimized for the observed plasma and tissue concentrations from the mouse 60 mg/kg dose cohort. For the human model, the fit was optimized for the observed plasma concentrations from a single 100 mg dose study conducted by GlaxoSmithKline in healthy subjects ($n = 21$).

The first-order rate constant for intestinal metabolism was estimated as a constant percentage of hepatic metabolism based on the ratio of total liver:intestinal CYP3A, the major cytochrome P450 enzyme sub-family responsible for lapatinib metabolism [1]. In mice, the mean quantity of immunoreactive CYP3A is 2.24 and 0.64 pmol/mg microsomal protein in liver and intestinal microsomes, respectively [45]. The total amount of microsomal protein in a 20 g mouse liver (5.49 % body weight [19] = 1.098 g) and small intestine is 38.9 mg (35.4 mg hepatic microsomal protein/g liver [46] × 1.098 g) and 2.67 mg [47], respectively. Accordingly, the total amount of CYP3A in a 20 g mouse liver and small intestine is 87.136 and 1.709 pmol, respectively. As a result, we concluded that the first-order rate constant for intestinal metabolism in mice is 2 % that of liver metabolism. In humans, total hepatic and small intestine (duodenum, jejunum and ileum) CYP3A was calculated to be 5,490 and 70.5 nmol, respectively [48]. Therefore, we represented the first-order rate constant for human intestinal metabolism as 1.3 % that of liver metabolism. This ratio held true for the microsomal intrinsic clearance of midazolam, a CYP3A-specific substrate, which was 15800 mL/min and 213.7 mL/min (or 1.35 %) in human liver and small intestine, respectively [48].

Table 1 lists all parameter values for both the mouse and human PBPK models.

The rate of change of the amount of drug in a generic storage tissue compartment mass balance equation is as follows:

$$\frac{dA_T}{dt} = Q_T \times (C_A - C_{VT})$$

where A_T is the amount of drug in the tissue compartment, t is time, Q_T is the blood flow to the tissue compartment, C_A is the arterial blood drug concentration entering the tissue compartment and C_{VT} is the venous blood drug concentration exiting the tissue compartment. Assuming venous equilibration, the drug concentration in the venous blood is:

$$C_{VT} = C_T/P_T$$

where C_T is the concentration of drug in the tissue compartment and P_T is the tissue:plasma partition coefficient.

Assuming the volume of the tissue (V_T) is constant, the drug concentration in the tissue is:

$$\frac{dC_T}{dt} = Q_T \times (C_A - C_{VT})/V_T$$

For metabolizing tissues (liver and intestine), the rate of change of the amount of drug metabolized (A_M) is as follows:

$$\frac{dA_M}{dt} = k \times C_{VT} \times V_T$$

where k is a first-order rate constant.

Computer simulation

For PBPK modeling, acslX Libero version 3.0.2.1 (The AEgis Technologies Group, Inc.) was used.

Pharmacokinetic analysis

Pharmacokinetic parameters were calculated using noncompartmental modeling performed with Microsoft Excel and standard equations for noncompartmental analysis.

Data analysis

The predictive capability of the model was evaluated by calculating the prediction error (PE%) as follows [20, 21]:

$$PE\% = \frac{Value_{predicted} - Value_{measured}}{Value_{measured}} \times 100$$

As a measure of the precision of the prediction, the median absolute prediction error (MAPE%) was calculated as follows:

$$MAPE\% = median(|PE\%1|,|PE\%2|, \ldots |PE\%n|)$$

As a measure of the bias of the prediction, the median prediction error (MPE%) was calculated as follows:

$$MPE\% = median(PE\%1, PE\%2, \ldots PE\%n)$$

Sensitivity analysis

A normalized sensitivity analysis was performed as described in Loccisano et al. [22] to assess the influence of each PBPK model parameter on the simulated plasma area under the concentration–time curve (AUC) for both the mouse and human models. Briefly, sensitivity coefficients were calculated with the original parameters and for those resulting from a 1 % change in each parameter value. The following equation was used to calculate the normalized sensitivity coefficient (SC):

$$SC = \frac{(A - B)/B}{(C - D)/D}$$

where A is the AUC resulting from the 1 % increase in the parameter value, B is the AUC resulting from the original parameter value, C is the parameter value increased by 1 % and D is the original parameter value.

Results

Lapatinib pharmacokinetics and model simulations in mice

A time course tissue distribution study of lapatinib was conducted in female FVB mice. Plasma and tissue concentrations were measured after single oral doses of 30, 60 and 90 mg/kg at 0.25, 0.5, 1, 2, 4, 8, 12 and 16 h post drug administration. These time points were chosen for sacrifice to provide multiple samplings during each pharmacokinetic phase (absorption, distribution and elimination).

The mouse PBPK model development was based on the concentration–time data from the 60 mg/kg dose cohort; partition coefficients and first-order rate constants were determined by parameter estimation, optimizing the fit for the observed plasma and tissue concentrations from this study. The concentration–time profiles of lapatinib in plasma, intestine, liver, kidney, heart, lung, slowly perfused tissue and brain and the resulting PBPK model simulations are shown in Fig. 2. For all tissues except intestine, the PBPK model simulations closely mirrored the observed data.

The model-predicted intestine concentrations for the first four time points (0.25, 0.5, 1 and 2 h) are significantly lower than the actual data. We suspect that the observed data is not an accurate measurement of the drug concentration in the intestinal epithelium. Instead, the measured values reflect both the lapatinib in the intestinal epithelium and unabsorbed lapatinib in the proximal intestinal lumen. As an attempt to circumvent this anticipated problem, we flushed the intestinal lumen with saline immediately after tissue collection; however, we still noted yellow aggregates of undissolved lapatinib within the lumen (resulting from administration of the drug as a suspension via oral gavage). Thus, the measured drug concentrations in the intestine are likely inflated due to the lapatinib suspension in the proximal intestinal lumen. After approximately 3 h, the model simulation accurately reflects the observed values. It is probable that the lapatinib suspension has moved through the intestinal lumen by this time, as the intestinal transit time in a mouse is approximately 3 h. Therefore, at these

Table 2 Observed and model-simulated lapatinib pharmacokinetic (PK) parameters in mice[a]

PK parameter	Dose		Plasma	Intestine	Liver	Kidney	Heart	Lung	Brain	Slowly perfused
$AUC_{0-16\ h}$ (nM × h)[b]	30	Observed	12,008	79,885	84,946	50,440	7,156	92,409	440.8	2,738
		Simulated	13,972	78,143	83,505	74,392	15,022	114,792	698.6	4,544
		Ratio	0.86	1.02	1.02	0.68	0.48	0.81	0.63	0.60
	60	Observed	24,052	235,114	157,288	137,624	26,545	233,760	1,315	9,519
		Simulated	27,944	156,284	167,010	148,784	30,044	229,583	1,397	9,087
		Ratio	0.86	1.50	0.94	0.92	0.88	1.02	0.94	1.05
	90	Observed	48,230	259,808	261,237	227,184	55,179	623,277	2,261	18,930
		Simulated	41,916	234,426	250,515	223,176	45,066	344,375	2,096	13,631
		Ratio	1.15	1.11	1.04	1.02	1.22	1.81	1.08	1.39
CL (L/h)[c]	30	Observed	0.09	0.01	0.01	0.02	0.14	0.01	2.34	0.38
		Simulated	0.07	0.01	0.01	0.01	0.07	0.01	1.48	0.23
		Ratio	1.16	0.98	0.98	1.47	2.10	1.24	1.58	1.66
	60	Observed	0.09	0.01	0.01	0.02	0.08	0.01	1.57	0.22
		Simulated	0.07	0.01	0.01	0.01	0.07	0.01	1.48	0.23
		Ratio	1.16	0.66	1.06	1.08	1.13	0.98	1.06	0.95
	90	Observed	0.06	0.01	0.01	0.01	0.06	0.005	1.37	0.16
		Simulated	0.08	0.03	0.01	0.01	0.07	0.01	1.48	0.22
		Ratio	0.78	0.45	0.96	0.98	0.79	0.55	0.93	0.73
$t_{1/2}$ (h)[d]	30	Observed	2.73	2.79	2.48	2.53	2.59	2.39	3.70	3.88
		Simulated	2.99	2.96	2.95	3.00	2.99	2.99	2.99	2.99
		Ratio	0.91	0.94	0.84	0.84	0.87	0.80	1.24	1.30
	60	Observed	3.42	3.05	2.75	3.57	3.05	3.04	3.12	2.57
		Simulated	2.99	2.96	2.95	3.00	2.99	2.99	2.99	2.99
		Ratio	1.14	1.03	0.93	1.19	1.02	1.02	1.04	0.86
	90	Observed	2.36	2.55	1.91	2.51	2.32	1.72	1.76	1.55
		Simulated	2.99	2.96	2.95	3.00	2.99	2.99	2.99	2.99
		Ratio	0.79	0.86	0.65	0.83	0.78	0.58	0.59	0.52

[a] PK parameters were calculated using noncompartmental modeling

[b] $AUC_{0-16\ h}$ is the area under the concentration–time curve from 0 to 16 h

[c] CL is clearance

[d] $t_{1/2}$ is the half-life for elimination as calculated from linear regression of the terminal elimination phase

later time points, the measured drug is presumably only lapatinib that has been absorbed into the intestinal epithelium.

After developing the mouse PBPK model with the 60 mg/kg dose cohort as a training set, we employed the other two dose cohorts (30 and 90 mg/kg) as test sets. The concentration–time data and the corresponding model simulations for these dose cohorts are also presented in Fig. 2. Again, the model simulations approximated the observed data with the exception of the early time points in the intestine, likely a result of the same phenomenon as described previously for the 60 mg/kg dose cohort.

The area under the concentration–time curve from 0 to 16 h ($AUC_{0-16\ h}$), clearance (CL) and elimination half-life ($t_{1/2}$) were calculated for both the observed and simulated data using noncompartmental analysis (Table 2). Lapatinib exhibits linear pharmacokinetics in all tissues within the 30–90 mg/kg dose range, as evidenced by a dose-dependent increase in $AUC_{0-16\ h}$ and constant CL (Fig. 3). To compare the actual and predicted data, we determined the ratio of the observed to model-predicted values (Table 2). The mean $AUC_{0-16\ h}$ ratio for all tissues was 1.00 and the range was 0.48 (heart from the 30 mg/kg dose cohort) to 1.81 (lung from the 90 mg/kg dose cohort), indicating that our model-predicted drug exposures reasonably mimicked the observed exposure for all tissues analyzed. As for CL, the model predictions also emulated the actual data; all ratios were between 0.45 (intestine from the 90 mg/kg dose cohort) and 2.10 (heart from the 30 mg/kg dose cohort), with the average ratio being 1.06. Lastly, all $t_{1/2}$ ratios were within the range of 0.52 (slowly perfused tissue from the 90 mg/kg dose cohort) and 1.24 (brain from the 30 mg/kg dose cohort), with an average ratio of 0.90. Overall, the PK

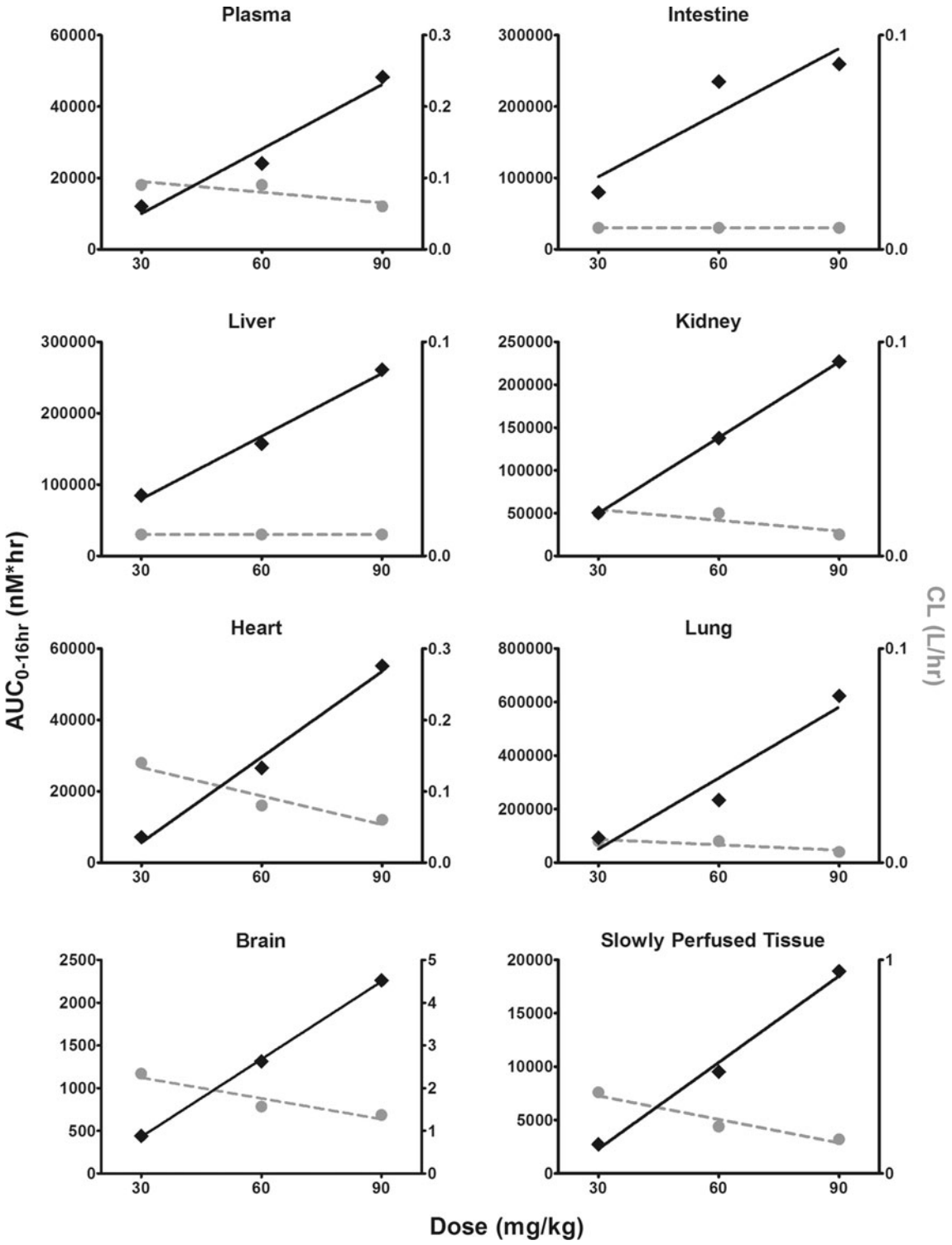

Fig. 3 Area under the concentration–time curve calculated from 0 to 16 h ($AUC_{0–16\ h}$) and clearance (CL) for the mouse 30, 60 and 90 mg/kg dose cohorts in plasma, intestine, liver, kidney, heart, lung, brain and slowly perfused tissue. $AUC_{0–16\ h}$ is presented on the *left y* axis and is represented by the *solid black diamonds*, with the corresponding linear regression trendline shown as the *solid black line*. CL is presented on the *right y* axis and is represented by the *solid gray circles* with the corresponding linear regression trendline shown as the *dashed gray line*. Both $AUC_{0–16\ h}$ and CL were determined by noncompartmental analysis

Table 3 Predictive performance for mouse PBPK model

	Concentrations		AUC^{a}_{0-16h}		$t^{b}_{1/2}$	
	MPE%[c]	MAPE%[d]	MPE%[c]	MAPE%[d]	MPE%[c]	MAPE%[d]
Plasma	28.53	43.36	16.18	16.18	9.57	12.64
Intestine	−8.40	68.10	9.77	−9.77	6.09	6.09
Liver	23.57	51.03	4.10	−1.70	19.11	19.11
Kidney	45.40	52.90	8.11	8.11	18.57	18.57
Heart	52.81	73.34	18.33	13.18	15.41	15.41
Lung	4.45	59.25	24.22	−1.79	25.14	25.14
Slowly perfused	28.77	47.40	27.99	−4.53	16.24	22.96
Brain	53.30	63.65	7.30	6.24	−4.29	19.16

[a] $AUC_{0-16\ h}$ is the area under the concentration–time curve from 0 to 16 h

[b] $t_{1/2}$ is the half-life for elimination as calculated from linear regression of the terminal elimination phase

[c] MPE% is the median prediction error, which is a measure of the bias of the prediction

[d] MAPE% is the median absolute prediction error, which is a measure of the precision of the prediction

parameters derived from the PBPK model simulations accurately mirrored the observed mouse data.

To further assess the predictive performance of the mouse model, we calculated the median prediction error (MPE%) and the median absolute prediction error (MAPE%) for the concentrations, $AUCs_{0-16\ h}$ and half-lives as measures of the bias and precision of the simulations, respectively (Table 3). Of these three variables, the concentrations were the most poorly predicted, with a mean MPE% of 28.6 and a mean MAPE% of 57.4. Although these prediction error assessments are not optimal, they are not surprising considering the large degree of variability in the data (mean concentration coefficient of variation of 78.6 %), likely due to the variable absorption of lapatinib when administered to unfasted animals. $AUC_{0-16\ h}$ and $t_{1/2}$ prediction errors were substantially better than the concentration prediction errors, feasibly because these parameters are derived from the cumulation of the concentration values and thus, the error of the individual points is muted. For $AUC_{0-16\ h}$, the average MPE% was 14.5 and the average MAPE% was 3.2. The MPE% for plasma and all tissue $AUCs_{0-16\ h}$ was less than 28.0 and the MAPE% was less than 16.2. Regarding half-life, the average MPE% was 13.2 and the average MAPE% was 17.4, with no individual plasma or tissue MPE% and MAPE% being more than ±25.2 and 25.2 %, respectively.

Lapatinib pharmacokinetics and model simulations in humans

The mouse PBPK model developed using the 60 mg/kg dose cohort was scaled to humans by using human parameters for tissue volumes and tissue blood flows and fitting the first-order rate constants for absorption and liver metabolism to the observed plasma concentrations from a single 100 mg dose study conducted by GlaxoSmithKline in healthy subjects ($n = 21$) (Table 1). The first-order rate constant for intestinal metabolism was set as 1.3 % that of liver metabolism as explained previously.

The concentration–time profiles of lapatinib in actual human plasma and the resulting PBPK model simulation are shown in Fig. 4a. The PBPK model prediction closely parallels the observed plasma concentration data. The MPE% and MAPE% for the lapatinib concentrations were −8.17 and 11.69, respectively. Regarding the actual and simulated plasma pharmacokinetic parameters, $AUCs_{0-60\ h}$ were 2,698 and 2,409 nM × h, CLs were 63.8 and 71.4 L/h and half-lives were 9.5 and 10.0 h, respectively. The $AUCs_{0-60\ h}$ for plasma and all tissues in the model are shown in Table 4. From largest to smallest, exposure to lapatinib ranked as follows: intestine, lung, liver, kidney, heart, plasma, slowly perfused tissue and brain.

Clinically, the recommended dose of lapatinib is 1,250 or 1,500 mg orally once daily continuously with either capecitabine (for advanced or metastatic breast cancer) or letrozole (for hormone receptor positive, HER2 positive metastatic breast cancer), respectively [1]. Thus, we modified our original model to incorporate multiple dosing of lapatinib. The resulting simulations of 1,250 and 1,500 mg doses of lapatinib q24 h for 8 days are shown in Fig. 4b. The steady-state area under the concentration–time curves calculated within the dosing interval from 0 to 24 h (AUC_{τ}) for plasma and all tissues in the model are shown in Table 4.

To further assess the predictive performance of the human model, we were not able to accrue concentration–time data for any other subjects/patients so we compared our model-predicted AUC, half-life, maximum concentration (C_{max}) and time of maximum concentration (T_{max}) values with those found in the literature for both healthy subjects [4, 24] and patients with solid tumors [5–13, 15].

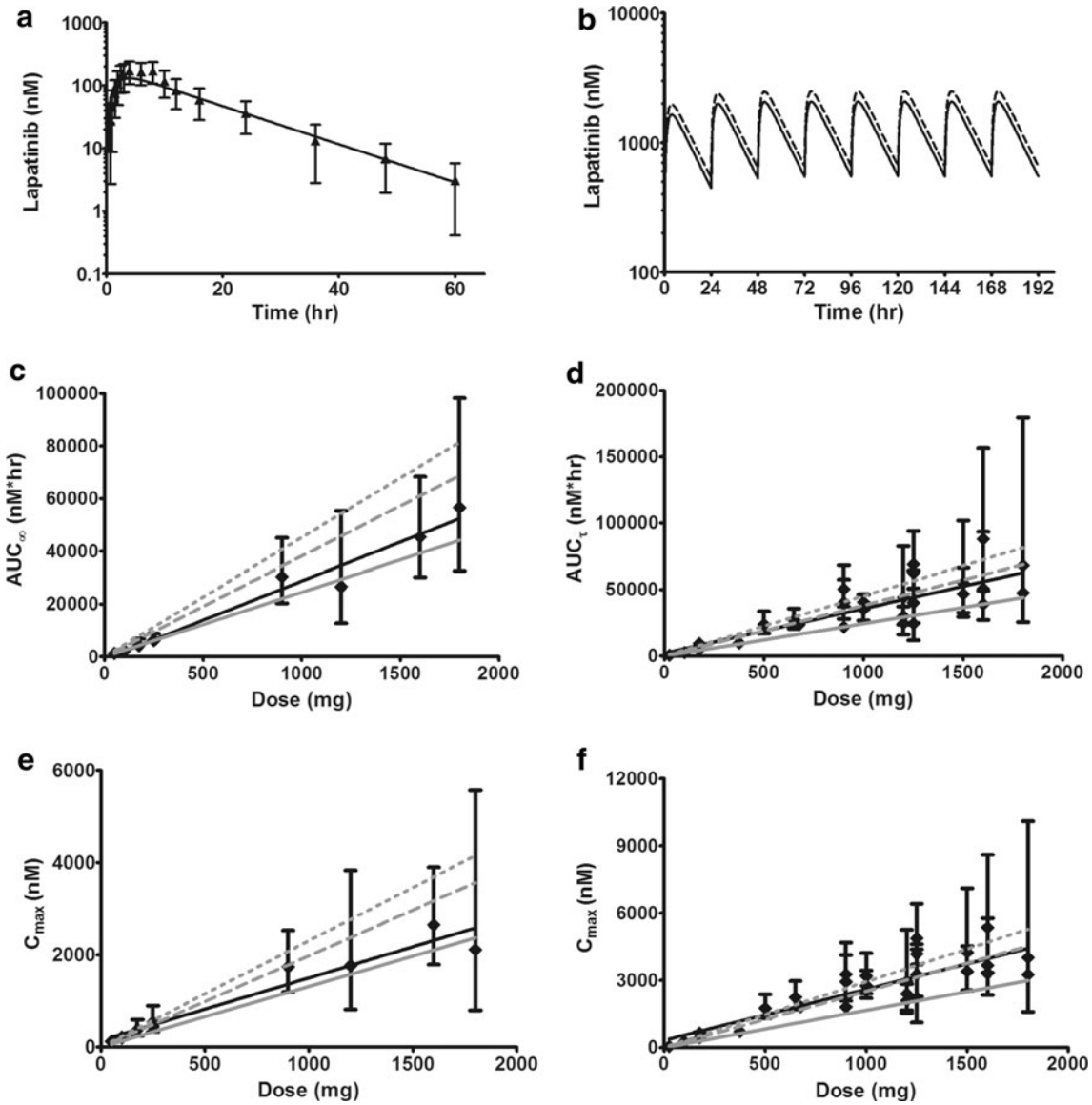

Fig. 4 Observed and model-simulated lapatinib concentrations, area under the concentration–time curve (AUC) and maximum concentration (C_{max}) in human plasma. **a** Single oral dose of 100 mg. *Filled black triangles* represent the observed data with *error bars* symbolizing the standard deviation (SD). The *solid black line* represents the model simulation. **b** Multiple doses (q24 h) for 8 days. *Solid black line* represents the model simulation for daily dosing of 1,250 mg. *Dashed black line* represents the model simulation for daily dosing of 1,500 mg. **c** After a single dose of lapatinib, *solid black diamonds* represent observed $AUCs_{\infty}$ (calculated from time 0 to infinity) with *error bars* symbolizing the 95 % confidence intervals and the *solid black line* is the corresponding linear regression trendline. The *solid gray line* represents the model-predicted $AUCs_{\infty}$. The *dashed gray line* represents simulated $AUCs_{\infty}$ from the model with moderate hepatic impairment. The *dotted gray line* represents simulated $AUCs_{\infty}$ from the model with severe hepatic impairment. **d** After multiple doses (q24 h) of lapatinib, *solid black diamonds* represent observed steady-state $AUCs_{\tau}$ (calculated within the dosing interval from time 0 to 24 h) with *error bars* symbolizing the 95 % confidence intervals and the *solid black line* is the corresponding linear regression trendline. The *solid gray line* represents the model-predicted $AUCs_{\infty}$. The *dashed gray line* represents simulated $AUCs_{\tau}$ from the model with moderate hepatic impairment. The *dotted gray line* represents simulated $AUCs_{\tau}$ from the model with severe hepatic impairment. **e** After a single dose of lapatinib, *solid black diamonds* represent observed C_{max} with *error bars* symbolizing the 95 % confidence intervals and the *black line* is the corresponding linear regression trendline. The *solid gray line* represents the model-predicted C_{max}. The *dashed gray line* represents simulated C_{max} from the model with moderate hepatic impairment. The *dotted gray lines* represents simulated C_{max} from the model with severe hepatic impairment. **f** After multiple doses (q24 h) of lapatinib, *solid black diamonds* represent observed C_{max} with *error bars* symbolizing the 95 % confidence intervals and the *solid black line* is the corresponding linear regression trendline. The *solid gray line* represents the model-predicted C_{max}. The *dashed gray line* represents simulated C_{max} from the model with moderate hepatic impairment. The *dotted gray line* represents simulated C_{max} from the model with severe hepatic impairment

Table 4 Human tissue AUCs for single and multiple (q24 h) lapatinib doses

	100 mg single dose $AUC^{a}_{0-60\ h}$ (nM × h)	1,250 mg multiple dose q24 h AUC^{b}_{τ} (nM × h)	1,500 mg multiple dose q24 h AUC^{b}_{τ} (nM × h)
Plasma	2,409	30,631	36,757
Intestine	21,884	277,286	332,744
Liver	14,470	183,723	220,468
Kidney	12,817	162,959	195,550
Heart	2,590	32,929	39,514
Lung	19,792	251,637	301,964
Brain	121	1,532	1,838
Slowly perfused	783	9,955	11,946

[a] $AUC_{0-60\ h}$ is the area under the concentration–time curve from 0 to 60 h

[b] AUC_{τ} is the steady-state area under the concentration–time curve within the dosing interval (0–24 h)

The results along with the subject/patient characteristics (disease state, fasted or not fasted when administered lapatinib, liver function and age) are presented in Table 5 (single dose lapatinib) and Tables 6, 7 (multiple dose lapatinib). Graphically, observed and predicted AUCs are depicted in Fig. 4c, d. For the single dose comparison, all of the prediction errors were less than ±27.2 %, with a MPE% of 0.29 and a MAPE% of 7.7. The single dose prediction errors were smaller for the area under the concentration–time curve calculated from time 0 to infinity ($AUCs_{\infty}$) of healthy subjects (MPE% of 1.5 and MAPE% of 2.5, $n = 6$ studies) than for the $AUCs_{\infty}$ of patients with solid tumors (MPE% of −17.8 and MAPE% of 17.8, $n = 4$ studies), which was not surprising given that our model was developed with data from healthy subjects who presumably cleared (metabolized) lapatinib more efficiently than the patients with advanced solid malignancies, as they were both younger and had normal liver function. Thus, our model tended to underpredict the AUC_{∞} for the patients with solid tumors, as indicated by the negative value of the MPE%. For the multiple dose lapatinib study, the prediction errors were larger, with a MPE% of −29.9 and a MAPE% of 29.9. Again, the negative MPE% was the result of our model simulations underpredicting lapatinib exposure, likely due to impaired hepatic function related to the age and disease state of the test population ($n = 24$ studies with cancer patients and only three studies with healthy subjects) versus the healthy training population used to develop the PBPK model.

Previously, lapatinib pharmacokinetics were assessed in subjects with moderate or severe hepatic impairment (Child-Pugh scores of 7–9, or greater than 9, respectively) and in 8 healthy control subjects; after a single oral dose of 100 mg, the lapatinib AUC increased approximately 56 and 85 % in subjects with moderate and severe hepatic impairment, respectively [25]. To imitate this liver dysfunction in our model, we decreased the first-order rate constant for liver metabolism by 35 and 45 % and, accordingly, achieved AUC increases of 56 and 85 %, respectively. Decreased liver metabolism of this magnitude has been observed in aged patients; a review of 16 cytochrome P450 (CYP) 3A substrates showed an average 37.2 % reduction in the clearance of these substrates by elderly versus young volunteers or patients [26]. The resulting AUC predictions from our modified model are graphed in Fig. 4c, d. The $AUCs_{\infty}$ resulting from hepatic impairment in the single dose studies both overpredicted exposure, conceivably because 60 % of the studies were done in healthy subjects. In contrast, the moderately impaired liver function simulation more correctly reflected the observed $AUCs_{\tau}$ from the multiple dose lapatinib clinical trials in which 86 % of the studies were done in cancer patients. Thus, decreasing the liver metabolism in our model improves the lapatinib exposure predictions for cancer patients.

In addition to actual and simulated human lapatinib exposures, we also wanted to evaluate concentration–time curve shape parameters. Accordingly, we compared observed and predicted half-life, C_{max} and T_{max} (Tables 8, 9, 10). For single dose lapatinib, the model-predicted and mean observed ($n = 10$ studies) half-lives were 10.0 and 10.3 h, respectively. For multiple dose lapatinib, the model predicted and mean observed ($n = 6$ studies) half-lives were 10.2 and 16.6 h, respectively. Overall, half-life MPE% was −8.1 and MAPE% was 28.1. In healthy subjects, the model overpredicted the half-life in 78 % of the studies (MPE% of 14.6) and in cancer patients, the model underpredicted the half-life in all studies (MPE% of −38.0).

For single dose lapatinib, our model-predicted T_{max} to be at 3.75 h post administration and the average observed T_{max} was 3.7 h. The MPE% and MAPE% were −6.3 and 9.6, respectively. For multiple dose lapatinib, our model-predicted steady-state T_{max} was 3.5 h and the mean observed T_{max} was 3.5 h. The MPE% and MAPE% were 1.6 and 14.6, respectively.

Regarding C_{max}, the actual values versus our model-simulated values are graphically shown in Fig. 4e, f. The single dose predictions directly paralleled the actual C_{max} (MPE% and MAPE% of −28.8 and 28.8, respectively). For the multiple dose predictions, our model underestimated steady-state C_{max} (MPE% and MAPE% of −33.9 and 33.9, respectively). However, when we decreased liver metabolism to mimic hepatic impairment (as we did with AUC), the predicted steady-state C_{max} for moderate liver dysfunction closely mirrored the observed data.

Table 5 Single dose lapatinib observed and predicted human AUC_∞ and subject characteristics

Dose (mg)	Observed AUC_∞ (nM × h)	Predicted AUC_∞ (nM × h)	AUC_∞ PE%[c]	Subjects	Food	Bilirubin[d]	AST[d]	ALT[d]	Age (years)[e]	Reference
50	1,170 (756–1,817)[a]	1,225	4.7	Healthy	Fasted	Normal	Normal	Normal	22 (18–53)	[4]
100	2,096 (1,492–2,941)[a]	2,450	16.9	Healthy	Fasted	Normal	Normal	Normal	22 (18–53)	[4]
100	2,459 (2,062–2,933)[b]	2,450	−0.4	Healthy	Not fasted	Normal	Normal	Normal	28 (20–47)	[14]
175	4,206 (2,588–6,834)[a]	4,288	1.9	Healthy	Fasted	Normal	Normal	Normal	22 (18–53)	[4]
250	6,313 (4,550–8,758)[a]	6,126	−3.0	Healthy	Fasted	Normal	Normal	Normal	22 (18–53)	[4]
250	6,068 (4,970–7,411)[b]	6,126	1.0	Healthy	Not fasted	Normal	Normal	Normal	29 (20–48)	[14]
900	30,250 (20,328–45,011)[a]	22,054	−27.1	Cancer	Fasted	≤1.5× ULN	≤2.5× ULN	≤2.5× ULN	60 (37–73)	[13]
1,200	26,574 (12,753–55,375)[a]	29,405	10.7	Cancer	Fasted	≤1.5× ULN	≤2.5× ULN	≤2.5× ULN	60 (37–73)	[13]
1,600	45,367 (30,150–68,263)[a]	39,207	−13.6	Cancer	Fasted	≤1.5× ULN	≤2.5× ULN	≤2.5× ULN	60 (37–73)	[13]
1,800	56,519 (32,499–98,293)[a]	44,108	−22.0	Cancer	Fasted	≤1.5× ULN	≤2.5× ULN	≤2.5× ULN	60 (37–73)	[13]

[a] AUC_∞ is the geometric mean (95 % confidence interval) of the area under the concentration–time curve calculated from time 0 to infinity

[b] AUC_∞ is the geometric mean (range) of the area under the concentration–time curve calculated from time 0 to infinity

[c] PE% is the prediction error

[d] Bilirubin, aspartate transaminase (AST) and alanine transaminase (ALT) are measures of liver function. ULN is upper limit of normal

[e] Median age (range)

Overall, our PBPK model properly predicted lapatinib pharmacokinetic parameters from actual populations. As our model was developed with data from healthy subjects, the predictions were better for studies which were conducted in healthy subjects versus patients with solid tumors. To improve our model simulations for cancer patients, we altered our liver metabolism parameter to reflect hepatic impairment resulting from disease and/or age. With this modification, the model more precisely reproduced actual AUCs and C_{max} from patients with solid tumors.

Sensitivity analysis

The normalized sensitivity coefficients for the mouse (60 mg/kg dose) and human (100 mg dose) PBPK models with respect to plasma AUC are shown in Fig. 5. Only parameters with sensitivity coefficients greater than 0.1 are shown. In both models, no normalized sensitivity coefficient was greater than ±1, indicating that there are no amplified parameter errors.

Discussion

Physiologically based pharmacokinetic models have been developed for numerous antineoplastic agents including methotrexate [27, 28], cisplatin [29], actinomycin-D [30], 5-fluorouracil [31], capecitabine [32], 1-β-D-arabinofuranosylcytosine [33], adriamycin [34–36], topotecan [37] and docetaxel [38]. The need for these types of pharmacokinetic models for chemotherapeutics is great because of the challenges presented by this class of pharmaceutical compounds, specifically the narrow therapeutic index which is governed by drug distribution in the body. With PBPK modeling, the dynamics of drug distribution can be predicted using basic information on physiochemical properties, transport, biotransformation and excretion, thus leading to a better understanding of target tissue exposure resulting in either a therapeutic or toxic effect.

We have successfully developed a first-generation PBPK model for the dual EGFR/HER2 tyrosine kinase inhibitor lapatinib. This drug is a mere decade old and has only been approved by the FDA for the treatment of breast cancer since 2007. Consequently, the intricacies of the pharmacokinetics are still being elucidated. To our knowledge, the details of mouse tissue distribution of lapatinib have been limited to plasma and brain [39, 40] whereas, in humans, only plasma concentrations have been determined [3–15]. The tissue distribution of [^{14}C] lapatinib was resolved by whole-body autoradiography in rats with detectable amounts quantified in the blood, brain, cerebrospinal fluid, harderian gland, heart, kidney, liver and muscle [41]. Our mouse data

Table 6 Multiple dose lapatinib (25–1,200 mg) observed and predicted human AUC_τ and subject characteristics

Dose (mg)	Observed AUC_τ (nM × h)[a]	Predicted AUC_τ (nM × h)	AUC_τ PE%[b]	Subjects	Food	Bilirubin[c]	AST[c]	ALT[c]	Age (years)[d]	Reference
25	515 (329–809)	613	19.1	Healthy	Fasted	Normal	Normal	Normal	22 (19–38)	[4]
100	25,68 (1,594–4,137)	2,450	−4.6	Healthy	Fasted	Normal	Normal	Normal	22 (19–38)	[4]
175	4,869 (3,313–7,154)	4,288	−11.9	Healthy	Fasted	Normal	Normal	Normal	22 (19–38)	[4]
175	9,431	4,288	−54.5	Cancer	Fasted	≤2 mg/dL	≤3.0× ULN	≤3.0× ULN	61 (25–80)	[15]
375	9,878	9,189	−7.0	Cancer	Fasted	≤2 mg/dL	≤3.0× ULN	≤3.0× ULN	62 (25–81)	[15]
500	23,922 (17,107–33,731)	12,252	−48.8	Cancer	Not fasted	≤2 mg/dL	≤3.0× ULN	≤3.0× ULN	56 (28–74)	[5]
650	27,020 (20,480–35,797)	15,928	−41.1	Cancer	Not fasted	≤2 mg/dL	≤3.0× ULN	≤3.0× ULN	60 (37–82)	[5]
675	23,578	16,540	−29.8	Cancer	Fasted	≤2 mg/dL	≤3.0× ULN	≤3.0× ULN	63 (25–82)	[15]
900	21,857	22,054	0.9	Cancer	Fasted	≤2 mg/dL	≤3.0× ULN	≤3.0× ULN	64 (25–83)	[15]
900	40,099 (28,052–57,481)	22,054	−45.0	Cancer	Not fasted	≤2 mg/dL	≤3.0× ULN	≤3.0× ULN	57 (34–82)	[5]
900	50,377 (37,204–68,217)	22,054	−56.2	Cancer	Fasted	≤1.5× ULN	≤2.5× ULN	≤2.5× ULN	60 (37–73)	[13]
1,000	40,615 (35,452–46,639)	24,504	−39.7	Cancer	Not fasted	≤2 mg/dL	≤3.0× ULN	≤3.0× ULN	53 (43–59)	[5]
1,000	35,280 (26,847–46,295)	24,504	−30.5	Cancer	Fasted	Adequate	Adequate	Adequate	53 (30–80)	[9]
1,200	24,610 (16,212–37,518)	29,405	19.5	Cancer	Not fasted	≤2 mg/dL	≤3.0× ULN	≤3.0× ULN	54 (37–67)	[5]
1,200	44,195 (23,626–82,673)	29,405	−33.5	Cancer	Fasted	≤1.5× ULN	≤2.5× ULN	≤2.5× ULN	60 (37–73)	[13]
1,200	29,773	29,405	−1.2	Cancer	Fasted	≤2 mg/dL	≤3.0× ULN	≤3.0× ULN	65 (25–84)	[15]

[a] AUC_τ is the geometric mean (95 % confidence interval) of the steady-state area under the concentration–time curve calculated within the dosing interval (0–24 h)

[b] PE% is the prediction error

[c] Bilirubin, aspartate transaminase (AST) and alanine transaminase (ALT) are measures of liver function. ULN is upper limit of normal

[d] Median age (range)

Table 7 Multiple dose lapatinib (1,250–1,800 mg) observed and predicted human AUC_τ and subject characteristics

Dose (mg)	Observed AUC_τ (nM × h)	Predicted AUC_τ (nM × h)	AUC_τ PE%[c]	Subjects	Food	Bilirubin[d]	AST[d]	ALT[d]	Age (years)[e]	Reference
1,250	62,300 (40,271–96,376)[a]	30,631	−50.8	Cancer	Not fasted	≤1.5 mg/dL	≤2.0× ULN	≤2.0× ULN	58.3 (2–79)	[7]
1,250	68,840 (50,425–94,138)[b]	30,631	−55.5	Cancer	Not fasted	Significant dysfunction excluded			58 (34–78)	[8]
1,250	24,438 (11,789–50,941)[b]	30,631	25.3	Cancer	Fasted	≤1.5 mg/dL	≤2.0× ULN	≤2.0× ULN	59 (19–74)	[10]
1,250	40,099 (24,954–64,193)[b]	30,631	−23.6	Cancer	Not fasted	≤2.0× ULN	≤5.0× ULN	≤5.0× ULN	57.5 (33–74)	[12]
1,500	46,639 (32,699–66,430)[b]	36,757	−21.2	Cancer	Not fasted	≤1.5 mg/dL	≤2.0× ULN	≤2.0× ULN	59.5 (39–73)	[6]
1,500	54,900 (29,601–101,833)[b]	36,757	−33.0	Cancer	Fasted	≤1.5 mg/dL	≤3.0× ULN	≤3.0× ULN	57 (31–73)	[11]
1,600	50,597 (27,364–93,450)[b]	39,207	−22.5	Cancer	Not fasted	≤2.0 mg/dL	≤3.0× ULN	≤3.0× ULN	55 (38–70)	[5]
1,600	87,941 (49,348–156,717)[b]	39,207	−55.4	Cancer	Fasted	≤1.5× ULN	≤2.5 × ULN	≤2.5× ULN	60 (37–73)	[13]
1,600	39,067[b]	39,207	0.4	Cancer	Fasted	≤2.0 mg/dL	≤3.0× ULN	≤3.0× ULN	66 (25–85)	[15]
1,800	47,671[b]	44,108	−7.5	Cancer	Fasted	≤2.0 mg/dL	≤3.0× ULN	≤3.0× ULN	67 (25–86)	[15]
1,800	67,895 (25,658–179,656)[b]	44,108	−35.0	Cancer	Fasted	≤1.5× ULN	≤2.5 × ULN	≤2.5× ULN	60 (37–73)	[13]

[a] AUC_τ is the mean (90 % confidence interval) of the steady-state area under the concentration–time curve calculated within the dosing interval (0–24 h)

[b] AUC_τ is the geometric mean (95 % confidence interval) of the steady-state area under the concentration–time curve calculated within the dosing interval (0–24 h)

[c] PE% is the prediction error

[d] Bilirubin, aspartate transaminase (AST) and alanine transaminase (ALT) are measures of liver function. ULN is upper limit of normal

[e] Median age (range)

Table 8 Single dose lapatinib observed and predicted human half-life ($t_{1/2}$), maximum concentration (C_{max}) and time of maximum concentration (T_{max})

Dose (mg)	Observed $t_{1/2}$ (h)	Predicted $t_{1/2}$ (h)	$T_{1/2}$ PE%[c]	Observed C_{max} (nM)	Predicted C_{max} (nM)	C_{max} PE%[c]	Observed T_{max} (h)	Predicted T_{max} (h)	T_{max} PE%[c]	Reference
50	6.0[a] (4.8–7.5)	10.0	66.7	124 (88–177)[d]	66	−46.7	3.0 (2.0–6.0)[f]	3.75	25.0	[4]
100	6.3[a] (5.6–7.0)	10.0	58.7	213 (148–308)[d]	132	−38.1	4.0 (2.5–5.9)[f]	3.75	−6.3	[4]
100	9.6[a] (8.5–10.7)	10.0	4.2	198 (174–224)[e]	132	−33.3	4.0 (2.5–8.0)[f]	3.75	−6.3	[14]
175	8.2[a] (6.7–9.9)	10.0	22.0	380 (241–599)[d]	231	−39.3	3.0 (2.0–4.0)[f]	3.75	25.0	[4]
250	8.8[a] (6.6–11.7)	10.0	13.6	546 (330–902)[d]	329	−39.7	4.0 (3.0–6.0)[f]	3.75	−6.3	[4]
250	10.2[a] (9.24–11.3)	10.0	−2.0	449 (360–563)[e]	329	−26.8	4.0 (2.5–6.0)[f]	3.75	−6.3	[14]
900	12.9[b] (10.1–18.3)	10.0	−22.5	1,740 (1,194–2,533)[d]	1,185	−31.9	4.0 (2.0–6.0)[g]	3.75	−6.3	[13]
1,200	11.5[b] (10.1–19.5)	10.0	−13.0	1,767 (816–3,833)[d]	1,581	−10.5	3.5 (2.1–6.0)[g]	3.75	7.1	[13]
1,600	13.9[b] (9.6–18.0)	10.0	−28.1	2,647 (1,793–3,903)[d]	2,107	−20.4	4.0 (2.0–8.0)[g]	3.75	−6.3	[13]
1,800	15.7[b] (11.0–133.1)	10.0	−36.3	2,112 (800–5,579)[d]	2,371	12.3	3.9 (3.0–8.0)[g]	3.75	−3.8	[13]

[a] $t_{1/2}$ is the terminal half-life geometric mean (95 % confidence interval)

[b] $t_{1/2}$ is the terminal half-life median (95 % confidence interval)

[c] PE% is the prediction error

[d] Is the geometric mean (95 % confidence interval) of C_{max}

[e] Is the geometric mean (range) of C_{max}

[f] Is the median (range) of T_{max}

[g] Is the median (95 % confidence interval) of T_{max}

demonstrated tissue:blood concentration ratios that were comparable to those presented by Polli et al. [41], indicating that lapatinib exhibits similar distribution dynamics in these two rodents. Considering the autoradiography data [41] and the work presented herein, we now have a comprehensive assessment of the biodistribution of lapatinib in rats and mice.

By incorporating the mouse tissue distribution data into a PBPK model, we were able to effectively predict lapatinib concentrations in mouse plasma, brain, heart, lung, kidney, intestine, liver and slowly perfused tissue after oral doses of 30, 60 and 90 mg/kg. Subsequently, by taking into account interspecies differences in physiology and physiochemistry, we extrapolated this PBPK model to humans. To validate the human model, we were only able to compare our model simulations with observed plasma lapatinib concentrations and pharmacokinetic parameters, as there is no data in the literature regarding human tissue levels. Our model correctly predicted plasma exposure [23], C_{max}, T_{max} and half-life following single doses of lapatinib ranging from 50 to 1,800 mg and following multiple doses of lapatinib ranging from 25 to 1,800 mg. After taking the clinical trial subject/patient characteristics into consideration, it was evident that our model predictions were more accurate for healthy subjects than for patients with solid tumors (whose AUCs and C_{max} were consistently underpredicted). This was not surprising given that our human PBPK model was developed with data from healthy subjects. In addition to the absence or presence of solid malignancies, the other major biological differences between these two populations were age and liver function. Both most likely contribute to hepatic impairment which results in a decrease in lapatinib clearance via metabolism and a subsequent increase in tissue exposure. When we altered our PBPK model to mimic hepatic impairment by decreasing the first-order rate constant for liver metabolism, the simulations for moderate hepatic impairment (incorporated as a 35 % decrease in liver metabolism) closely reflected the observed AUC and C_{max}

Table 9 Multiple dose lapatinib (25–1,200 mg) observed and predicted human half-life ($t_{1/2}$), maximum concentration (C_{max}) and time of maximum concentration (T_{max})

Dose (mg)	Observed $t_{1/2}$ (h)	Predicted $t_{1/2}$ (h)	$t_{1/2}$ PE%[c]	Observed C^{d}_{max} (nM)	Predicted C_{max} (nM)	C_{max} PE%[c]	Observed T_{max} (h)	Predicted T_{max} (h)	T_{max} PE%[c]	Reference
25	7.9[a] (6.4–9.8)	10.2	29.1	55 (38–81)	42	−23.7	2.7 (2.5–4.0)[e]	3.5	29.6	[4]
100	8.9[a] (6.1–12.9)	10.2	14.6	251 (150–420)	166	−33.9	3.0 (2.0–6.0)[e]	3.5	16.7	[4]
175	11.1[a] (7.3–16.8)	10.2	−8.1	429 (270–678)	290	−32.3	4.0 (3.0–6.0)[e]	3.5	−12.5	[4]
175	ND	10.2	NA	637	290	−54.5	ND	3.5	NA	[15]
375	ND	10.2	NA	706	622	−11.8	ND	3.5	NA	[15]
500	ND	10.2	NA	1,755 (1,308–2,375)	830	−52.7	ND	3.5	NA	[5]
650	ND	10.2	NA	2,237 (1,687–2,960)	1,078	−51.8	ND	3.5	NA	[5]
675	ND	10.2	NA	1,824	1,120	−38.6	ND	3.5	NA	[15]
900	ND	10.2	NA	1,807	1,493	−17.4	ND	3.5	NA	[15]
900	ND	10.2	NA	2,926 (2,082–4,130)	1,493	−49.0	ND	3.5	NA	[5]
900	23.1[b] (9.8–38.2)	10.2	−55.8	3,261 (2,270–4,683)	1,493	−54.2	4.0 (3.0–6.0)[f]	3.5	–12.5	[13]
1,000	ND	10.2	NA	3,184 (2,409–4,216)	1,659	−47.9	ND	3.5	NA	[5]
1,000	ND	10.2	NA	2,754 (2,203–3,442)	1,659	–39.8	ND	3.5	NA	[9]
1,200	ND	10.2	NA	2,100 (1,549–2,840)	1,990	−5.2	ND	3.5	NA	[5]
1,200	16.9[b] (15.1–34.3)	10.2	−39.6	2,952 (1,661–5,246)	1,990	−32.6	3.6 (3.0–7.9)[f]	3.5	−2.8	[13]
1,200	ND	10.2	NA	2,392	1,990	−16.8	ND	3.5	NA	[15]

ND not determined, *NA* not applicable

[a] $t_{1/2}$ is the terminal half-life geometric mean (95 % confidence interval)

[b] $t_{1/2}$ is the terminal half-life median (95 % confidence interval)

[c] PE% is the prediction error

[d] Is the geometric mean (95 % confidence interval) of C_{max}

[e] Is the median (range) of T_{max}

[f] Is the median (95 % confidence interval) of T_{max}

Table 10 Multiple dose lapatinib (1,250–1,800 mg) observed and predicted human half-life ($t_{1/2}$), maximum concentration (C_{max}) and time of maximum concentration (T_{max})

Dose (mg)	Observed $t_{1/2}$ (h)[a]	Predicted $t_{1/2}$ (h)	$t_{1/2}$ PE%[b]	Observed $C^{\S}_{max}$ (nM)	Predicted C_{max} (nM)	C_{max} PE%[b]	Observed T_{max} (h)	Predicted T_{max} (h)	T_{max} PE%[b]	Reference
1,250	ND	10.2	NA	4,182 (2,702–6,488)[c]	2,073	−50.4	3.5 (2.0–10)[e]	3.5	0	[7]
1,250	ND	10.2	NA	4,870 (3,700–6,419)[d]	2,073	−57.4	ND	3.5	NA	[8]
1,250	ND	10.2	NA	2,220 (1,119–4,389)[d]	2,073	−6.6	3.0 (1.5–8.0)[f]	3.5	16.7	[10]
1,250	ND	10.2	NA	3,253 (2,289–4,612)[d]	2,073	−36.3	3.0 (2.6–8.0)[f]	3.5	16.7	[12]
1,500	ND	10.2	NA	3,390 (2,547–4,526)[d]	2,488	−26.6	3.4 (0.0–6.0)[f]	3.5	3.2	[6]
1,500	ND	10.2	NA	4,251 (2,530–7,108)[d]	2,488	−41.5	3.0 (0.0–12.2)[f]	3.5	16.7	[11]
1,600	ND	10.2	NA	3,666 (2,341–5,765)[d]	2,654	−27.6	ND	3.5	NA	[5]
1,600	26.2 (12.9–48.3)	10.2	−61.1	5,354 (3,334–8,598)[d]	2,654	−50.4	5.1 (0.9–8.0)[g]	3.5	−31.4	[13]
1,600	ND	10.2	NA	3,304[d]	2,654	−19.7	ND	3.5	NA	[15]
1,800	ND	10.2	NA	3,253[d]	2,986	−8.2	ND	3.5	NA	[15]
1,800	21.8 (18.5–104.5)	10.2	−53.2	4,015 (1,595–10,102)[d]	2,986	−25.6	3.9 (3.0–7.9)[g]	3.5	−10.3	[13]

ND not determined, *NA* not applicable

[a] $t_{1/2}$ is the terminal half-life median (95 % confidence interval)

[b] PE% is the prediction error

[c] Is the mean (90 % confidence interval) of C_{max}

[d] Is the geometric mean (95 % confidence interval) of C_{max}

[e] Is the median (90 % confidence interval) of T_{max}

[f] Is the median (range) of T_{max}

[g] Is the median (95 % confidence interval) of T_{max}

in cancer patients. Thus, our model can not only predict lapatinib plasma pharmacokinetics in healthy subjects but, with a minor metabolic alteration, can also predict the pharmacokinetics of this drug in the plasma of patients with solid malignancies.

The human PBPK model additionally facilitates the estimation of tissue levels of lapatinib. There is incredible utility in this application of the model, as it is not feasible to collect actual tissue concentration data from humans. Based on the adverse reactions to lapatinib observed in clinical trials, we can speculate as to the organ distribution of this drug. It is probable that the heart, liver, intestine and lung are exposed to significant levels of lapatinib as patients administered this compound have experienced decreased left ventricular ejection fraction, QT prolongation, hepatotoxicity, diarrhea and interstitial lung disease/pneumonitis. From largest to smallest, our multiple dose (1,250 mg q24 h) model-predicted ratios of lapatinib tissue:plasma $AUCs_{\tau}$ were intestine (9.1), lung (8.2), liver (6.0), kidney (5.3), heart (1.1), slowly perfused tissue (0.3) and brain (0.05). Thus, for all organs in which adverse reactions to lapatinib have been noted, our model predicted tissue:plasma AUC ratios greater than 1, indicating substantial distribution into these tissues. Regarding brain, our model predicted low levels of lapatinib, which is consistent with the poor central nervous system (CNS) penetration observed in mice, owing to ABCB1- and ABCB2-mediated efflux [39]. Despite low lapatinib exposure in normal brain tissue, this drug has been shown to reduce the burden of metastatic breast cancer cells in the brains of mice [42] and have a modest CNS antitumor activity in human patients with brain metastases from HER2-positive breast cancer [43].

In summary, we have been able to successfully develop a PBPK model of lapatinib in mice, scale this model to humans and accurately predict the pharmacokinetics of this drug in human plasma over a wide range of doses. Additionally, our

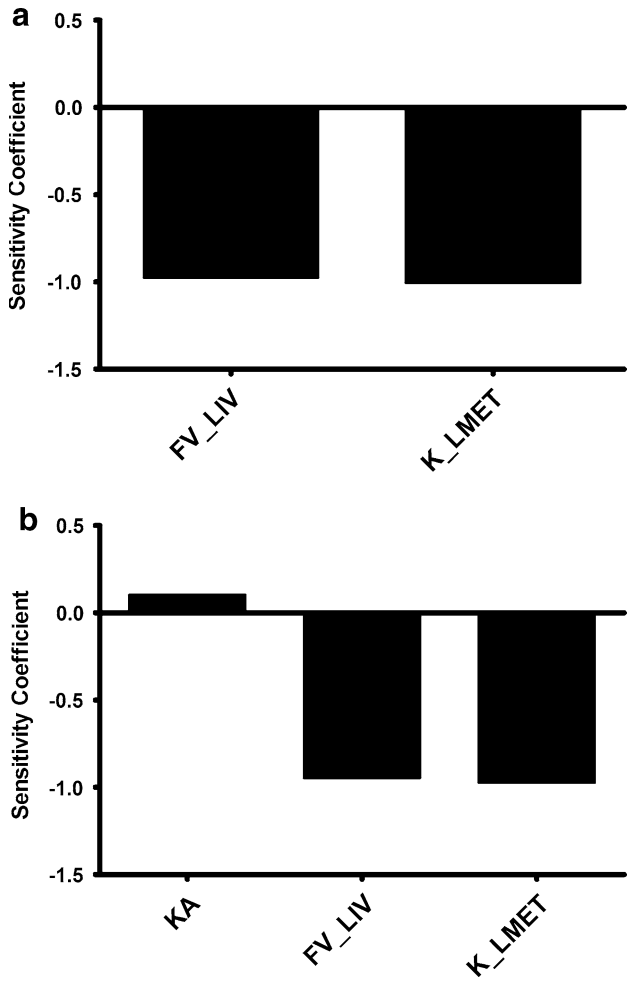

Fig. 5 Calculated sensitivity coefficients for PBPK model parameters with respect to plasma AUC for the (**a**) mouse model and (**b**) human single dose model. Only parameters with sensitivity coefficients >0.1 are shown. *FV_LIV* fractional volume of liver, *K_LMET* first-order rate constant for liver metabolism; and *KA* first-order rate constant for absorption from intestinal lumen

model also facilitated the estimation of various tissue exposures to lapatinib, which harmonize with the organ-specific toxicities documented in clinical trials. We acknowledge that this is a first-generation PBPK model which can be further improved with a greater understanding of lapatinib absorption, distribution, metabolism and excretion garnered from subsequent in vitro and in vivo studies. Moreover, our base model can be expanded to include other pharmacokinetic determinants, including efflux transporters, metabolite generation, combination dosing, etc., to make this PBPK model even more beneficial for the prediction of lapatinib disposition in both mouse and man.

Acknowledgments We are grateful to Jerry L. Campbell (Center for Human Health Assessment, The Hamer Institutes for Health Sciences, Research Triangle Park, Durham, NC, USA), Conrad Housand (The AEgis Technologies Group, Oshawa, ON, USA) and Robin McDougall (The AEgis Technologies Group, Oshawa, ON, USA) for all of their help and guidance with this project. This work was supported in part by Grant number W81XWH-09-1-0457 from the Department of Defense (DOD) Breast Cancer Research Program (BCRP) of the Office of the Congressionally Directed Medical Research Programs (CDMRP).

Conflict of interest The authors declare that they have no conflict of interest.

References

1. GlaxoSmithKline (2012) Tykerb prescribing information. http://us.gsk.com/products/assets/us_tykerb.pdf. Accessed 01 July 2012
2. www.clinicaltrials.gov
3. Gaul MD, Guo Y, Affleck K, Cockerill GS, Gilmer TM, Griffin RJ, Guntrip S, Keith BR, Knight WB, Mullin RJ, Murray DM, Rusnak DW, Smith K, Tadepalli S, Wood ER, Lackey K (2003) Discovery and biological evaluation of potent dual ErbB-2/EGFR tyrosine kinase inhibitors: 6-thiazolylquinazolines. Bioorg Med Chem Lett 13(4):637–640
4. Bence AK, Anderson EB, Halepota MA, Doukas MA, DeSimone PA, Davis GA, Smith DA, Koch KM, Stead AG, Mangum S, Bowen CJ, Spector NL, Hsieh S, Adams VR (2005) Phase I pharmacokinetic studies evaluating single and multiple doses of oral GW572016, a dual EGFR-ErbB2 inhibitor, in healthy subjects. Invest New Drugs 23(1):39–49
5. Burris HA III, Hurwitz HI, Dees EC, Dowlati A, Blackwell KL, O'Neil B, Marcom PK, Ellis MJ, Overmoyer B, Jones SF, Harris JL, Smith DA, Koch KM, Stead A, Mangum S, Spector NL (2005) Phase I safety, pharmacokinetics, and clinical activity study of lapatinib (GW572016), a reversible dual inhibitor of epidermal growth factor receptor tyrosine kinases, in heavily pretreated patients with metastatic carcinomas. J Clin Oncol 23(23):5305–5313
6. Siegel-Lakhai WS, Beijnen JH, Vervenne WL, Boot H, Keessen M, Versola M, Koch KM, Smith DA, Pandite L, Richel DJ, Schellens JH (2007) Phase I pharmacokinetic study of the safety and tolerability of lapatinib (GW572016) in combination with oxaliplatin/fluorouracil/leucovorin (FOLFOX4) in patients with solid tumors. Clin Cancer Res 13(15 Pt 1):4495–4502
7. Chu QS, Schwartz G, de Bono J, Smith DA, Koch KM, Versola MJ, Pandite L, Arya N, Curtright J, Fleming RA, Ho PT, Rowinsky EK (2007) Phase I and pharmacokinetic study of lapatinib in combination with capecitabine in patients with advanced solid malignancies. J Clin Oncol 25(24):3753–3758
8. Midgley RS, Kerr DJ, Flaherty KT, Stevenson JP, Pratap SE, Koch KM, Smith DA, Versola M, Fleming RA, Ward C, O'Dwyer PJ, Middleton MR (2007) A phase I and pharmacokinetic study of lapatinib in combination with infusional 5-fluorouracil, leucovorin and irinotecan. Ann Oncol 18(12):2025–2029
9. Storniolo AM, Pegram MD, Overmoyer B, Silverman P, Peacock NW, Jones SF, Loftiss J, Arya N, Koch KM, Paul E, Pandite L, Fleming RA, Lebowitz PF, Ho PT, Burris HA 3rd (2008) Phase I dose escalation and pharmacokinetic study of lapatinib in combination with trastuzumab in patients with advanced ErbB2-positive breast cancer. J Clin Oncol 26(20):3317–3323
10. LoRusso PM, Jones SF, Koch KM, Arya N, Fleming RA, Loftiss J, Pandite L, Gadgeel S, Weber BL, Burris HA III (2008) Phase I and pharmacokinetic study of lapatinib and docetaxel in patients with advanced cancer. J Clin Oncol 26(18):3051–3056
11. Chu QS, Cianfrocca ME, Goldstein LJ, Gale M, Murray N, Loftiss J, Arya N, Koch KM, Pandite L, Fleming RA, Paul E,

Rowinsky EK (2008) A phase I and pharmacokinetic study of lapatinib in combination with letrozole in patients with advanced cancer. Clin Cancer Res 14(14):4484–4490
12. Molina JR, Kaufmann SH, Reid JM, Rubin SD, Galvez-Peralta M, Friedman R, Flatten KS, Koch KM, Gilmer TM, Mullin RJ, Jewell RC, Felten SJ, Mandrekar S, Adjei AA, Erlichman C (2008) Evaluation of lapatinib and topotecan combination therapy: tissue culture, murine xenograft, and phase I clinical trial data. Clin Cancer Res 14(23):7900–7908
13. Nakagawa K, Minami H, Kanezaki M, Mukaiyama A, Minamide Y, Uejima H, Kurata T, Nogami T, Kawada K, Mukai H, Sasaki Y, Fukuoka M (2009) Phase I dose-escalation and pharmacokinetic trial of lapatinib (GW572016), a selective oral dual inhibitor of ErbB-1 and -2 tyrosine kinases, in Japanese patients with solid tumors. Jpn J Clin Oncol 39(2):116–123
14. Smith DA, Koch KM, Arya N, Bowen CJ, Herendeen JM, Beelen A (2009) Effects of ketoconazole and carbamazepine on lapatinib pharmacokinetics in healthy subjects. Br J Clin Pharmacol 67(4):421–426
15. Burris HA III, Taylor CW, Jones SF, Koch KM, Versola MJ, Arya N, Fleming RA, Smith DA, Pandite L, Spector N, Wilding G (2009) A phase I and pharmacokinetic study of oral lapatinib administered once or twice daily in patients with solid malignancies. Clin Cancer Res 15(21):6702–6708
16. Krishnan K, Loizou GD, Spendiff M, Lipscomb JC, Andersen ME (2010) PBPK modeling: a primer. In: Krishnan K, Andersen ME (eds) Quantitative modeling in toxicology, vol 17. Wiley, Chichester, p 485
17. Andersen ME, Yang RSH, Clewell HJ III, Reddy MB (2005) Introduction: a historical perspective of the development and applications of PBPK models. In: Reddy MB, Yang RSH, Clewell HJ III, Andersen ME (eds) Physiologically based pharmacokinetic modeling: science and applications, vol 19. Wiley-Interscience, Hoboken, p 420
18. Bai F, Freeman BB III, Fraga CH, Fouladi M, Stewart CF (2006) Determination of lapatinib (GW572016) in human plasma by liquid chromatography electrospray tandem mass spectrometry (LC-ESI-MS/MS). J Chromatogr B Analyt Technol Biomed Life Sci 831(1–2):169–175
19. Brown RP, Delp MD, Lindstedt SL, Rhomberg LR, Beliles RP (1997) Physiological parameter values for physiologically based pharmacokinetic models. Toxicol Ind Health 13(4):407–484
20. Sheiner LB, Beal SL (1981) Some suggestions for measuring predictive performance. J Pharmacokinet Biopharm 9(4):503–512
21. Wu G (1995) Calculating predictive performance: a user's note. Pharmacol Res 31(6):393–399
22. Loccisano AE, Campbell JL Jr, Butenhoff JL, Andersen ME, Clewell HJ III (2012) Comparison and evaluation of pharmacokinetics of PFOA and PFOS in the adult rat using a physiologically based pharmacokinetic model. Reprod Toxicol 33(4):452–467
23. Castellino S, O'Mara M, Koch K, Borts DJ, Bowers GD, MacLauchlin C (2012) Human metabolism of lapatinib, a dual kinase inhibitor: implications for hepatotoxicity. Drug Metab Dispos 40(1):139–150
24. Kwara A, Lartey M, Sagoe KW, Rzek NL, Court MH (2009) CYP2B6 (c.516G–>T) and CYP2A6 (*9B and/or *17) polymorphisms are independent predictors of efavirenz plasma concentrations in HIV-infected patients. Br J Clin Pharmacol 67(4):427–436
25. GlaxoSmithKline (2010) Tyverb prescribing information. http://www.ema.europa.eu/docs/en_GB/document_library/EPAR_-_Product_Information/human/000795/WC500044957.pdf. Accessed 01 July 2012
26. Cotreau MM, von Moltke LL, Greenblatt DJ (2005) The influence of age and sex on the clearance of cytochrome P450 3A substrates. Clin Pharmacokinet 44(1):33–60
27. Bischoff KB, Dedrick RL, Zaharko DS (1970) Preliminary model for methotrexate pharmacokinetics. J Pharm Sci 59(2):149–154
28. Bischoff KB, Dedrick RL, Zaharko DS, Longstreth JA (1971) Methotrexate pharmacokinetics. J Pharm Sci 60(8):1128–1133
29. Evans WE, Crom WR, Tsiatis A, Green AA, Hayes FA, Pratt CB (1982) Pharmacokinetic modeling of cisplatin disposition in children and adolescents with cancer. Cancer Chemother Pharmacol 10(1):22–26
30. Lutz RJ, Galbraith WM, Dedrick RL, Shrager R, Mellett LB (1977) A model for the kinetics of distribution of actinomycin-D in the beagle dog. J Pharmacol Exp Ther 200(3):469–478
31. Collins JM, Dedrick RL, King FG, Speyer JL, Myers CE (1980) Nonlinear pharmacokinetic models for 5-fluorouracil in man: intravenous and intraperitoneal routes. Clin Pharmacol Ther 28(2):235–246
32. Tsukamoto Y, Kato Y, Ura M, Horii I, Ishitsuka H, Kusuhara H, Sugiyama Y (2001) A physiologically based pharmacokinetic analysis of capecitabine, a triple prodrug of 5-FU, in humans: the mechanism for tumor-selective accumulation of 5-FU. Pharm Res 18(8):1190–1202
33. Dedrick RL, Forrester DD, Ho DH (1972) In vitro-in vivo correlation of drug metabolism—deamination of 1- -D-arabinofuranosylcytosine. Biochem Pharmacol 21(1):1–16
34. Harris PA, Gross JF (1975) Preliminary pharmacokinetic model for adriamycin (NSC-123127). Cancer Chemother Rep 59(4):819–825
35. Chan KK, Cohen JL, Gross JF, Himmelstein KJ, Bateman JR, Tsu-Lee Y, Marlis AS (1978) Prediction of adriamycin disposition in cancer patients using a physiologic, pharmacokinetic model. Cancer Treat Rep 62(8):1161–1171
36. Gustafson DL, Rastatter JC, Colombo T, Long ME (2002) Doxorubicin pharmacokinetics: macromolecule binding, metabolism, and excretion in the context of a physiologic model. J Pharm Sci 91(6):1488–1501
37. Sung C, Blaney SM, Cole DE, Balis FM, Dedrick RL (1994) A pharmacokinetic model of topotecan clearance from plasma and cerebrospinal fluid. Cancer Res 54(19):5118–5122
38. Bradshaw-Pierce EL, Eckhardt SG, Gustafson DL (2007) A physiologically based pharmacokinetic model of docetaxel disposition: from mouse to man. Clin Cancer Res 13(9):2768–2776
39. Polli JW, Olson KL, Chism JP, John-Williams LS, Yeager RL, Woodard SM, Otto V, Castellino S, Demby VE (2009) An unexpected synergist role of P-glycoprotein and breast cancer resistance protein on the central nervous system penetration of the tyrosine kinase inhibitor lapatinib (*N*-{3-chloro-4-[(3-fluorobenzyl)oxy]phenyl}-6-[5-({[2-(methylsulfonyl)ethyl]amino}methyl)-2-furyl]-4-quinazolinamine; GW572016). Drug Metab Dispos 37(2):439–442
40. Taskar KS, Rudraraju V, Mittapalli RK, Samala R, Thorsheim HR, Lockman J, Gril B, Hua E, Palmieri D, Polli JW, Castellino S, Rubin SD, Lockman PR, Steeg PS, Smith QR (2012) Lapatinib distribution in HER2 overexpressing experimental brain metastases of breast cancer. Pharm Res 29(3):770–781
41. Polli JW, Humphreys JE, Harmon KA, Castellino S, O'Mara MJ, Olson KL, John-Williams LS, Koch KM, Serabjit-Singh CJ (2008) The role of efflux and uptake transporters in [*N*-{3-chloro-4-[(3-fluorobenzyl)oxy]phenyl}-6-[5-({[2-(methylsulfonyl)ethyl]amino}methyl)-2-furyl]-4-quinazolinamine (GW572016, lapatinib) disposition and drug interactions. Drug Metab Dispos 36(4):695–701
42. Gril B, Palmieri D, Bronder JL, Herring JM, Vega-Valle E, Feigenbaum L, Liewehr DJ, Steinberg SM, Merino MJ, Rubin SD, Steeg PS (2008) Effect of lapatinib on the outgrowth of metastatic breast cancer cells to the brain. J Natl Cancer Inst 100(15):1092–1103
43. Lin NU, Dieras V, Paul D, Lossignol D, Christodoulou C, Stemmler HJ, Roche H, Liu MC, Greil R, Ciruelos E, Loibl S, Gori S, Wardley A, Yardley D, Brufsky A, Blum JL, Rubin SD,

Dharan B, Steplewski K, Zembryki D, Oliva C, Roychowdhury D, Paoletti P, Winer EP (2009) Multicenter phase II study of lapatinib in patients with brain metastases from HER2-positive breast cancer. Clin Cancer Res 15(4):1452–1459

44. Chen HS, Gross JF (1979) Estimation of tissue-to-plasma partition coefficients used in physiological pharmacokinetic models. J Pharmacokinet Biopharm 7(1):117–125
45. Perloff MD, Von Moltke LL, Greenblatt DJ (2003) Differential metabolism of midazolam in mouse liver and intestine microsomes: a comparison of cytochrome P450 activity and expression. Xenobiotica 33(4):365–377
46. Hietanen E, Vainio H (1973) Interspecies variations in small intestinal and hepatic drug hydroxylation and glucuronidation. Acta Pharmacol Toxicol (Copenh) 33(1):57–64
47. Zhang QY, Dunbar D, Kaminsky LS (2003) Characterization of mouse small intestinal cytochrome P450 expression. Drug Metab Dispos 31(11):1346–1351
48. Paine MF, Khalighi M, Fisher JM, Shen DD, Kunze KL, Marsh CL, Perkins JD, Thummel KE (1997) Characterization of interintestinal and intraintestinal variations in human CYP3A-dependent metabolism. J Pharmacol Exp Ther 283(3):1552–1562

Cancer Chemotherapy and Pharmacology

Co-administration of lapatinib increases exposure to docetaxel but not doxorubicin in the small intestine of mice

Journal:	*Cancer Chemotherapy and Pharmacology*
Manuscript ID:	CCP-13-0029
Manuscript Type:	Original Article
Date Submitted by the Author:	15-Jan-2013
Complete List of Authors:	Hudachek, Susan; Colorado State University, Clinical Sciences Gustafson, Daniel; Colorado State University, Clinical Sciences
Keywords:	Breast Cancer, Docetaxel, Doxorubicin, Lapatinib

Title: Co-administration of lapatinib increases exposure to docetaxel but not doxorubicin in the small intestine of mice

Authors: Susan F. Hudachek and Daniel L. Gustafson

Affiliations: Animal Cancer Center, Department of Clinical Sciences, Colorado State University, Fort Collins, Colorado

Corresponding Author:
Susan F Hudachek
Address: 1620 Campus Delivery, Fort Collins CO, 80523
Phone: (970) 297-4056
Email: Susan.Hudachek@colostate.edu

Conflicts of Interest: DISCLOSURES: NONE

Abstract:

Purpose: Combination therapy is increasingly utilized for the treatment of metastatic breast cancer. However, co-administration of drugs, particularly agents that are substrates for or inhibitors of p-glycoprotein, can result in increased tissue toxicity. Unfortunately, determining levels of chemotherapeutics in human tissues is challenging and plasma drug concentrations are not always indicative of tissue toxicokinetics or toxicodynamics, especially when tissue penetration is altered.

Methods: The aim of the work presented herein was to determine if concomitant administration of compounds currently being combined in clinical trials for metastatic breast cancer treatment alters plasma and tissue pharmacokinetics in mice if both agents are p-glycoprotein substrates and/or inhibitors. Accordingly, we investigated the pharmacokinetic interactions of the classic cytotoxics and p-glycoprotein substrates docetaxel and doxorubicin when given concurrently with the targeted agent and p-glycoprotein inhibitor lapatinib.

Results: Our time course plasma and tissue distribution studies showed that co-administration of lapatinib with doxorubicin did not appreciably alter the pharmacokinetics of this anthracycline in the plasma or six tissues evaluated in mice, presumably because, at doses relevant to human exposure, lapatinib inhibition of p-glycoprotein did not significantly alter doxorubicin transport out of these tissue compartments.

Conclusions: However, combining lapatinib with docetaxel dramatically increased intestinal exposure to this chemotherapeutic, which has clinical implications for enhancing gastrointestinal toxicity. The significant lapatinib-docetaxel interaction is likely CYP3A4-mediated, suggesting that caution should be taken when this combination is administered, particularly to patients with compromised CYP3A activity, and recipients should be closely monitored for enhanced toxicity, particularly for adverse effects on the intestine.

Introduction:

The treatment of metastatic breast cancer is increasingly turning towards the use of combination therapy to optimize clinical outcomes [1-3]. Although additive or synergistic activity of agents is clearly advantageous for enhancing efficacy, a concurrent increase in toxicity may also result from the combination. The latter is particularly likely when the co-administered compounds are substrates for or inhibitors of ATP-binding cassette (ABC) transporters, which have a critical role in protecting cells from xenobiotics.

One of the best characterized ABC transporters is P-glycoprotein (PGP), discovered in 1976 [4]. Consistent with its role as a toxin efflux pump, PGP is highly expressed on the apical surface of epithelial cells with excretory roles, such as cells lining the colon, small intestine, pancreatic ductules, bile ductules, kidney proximal tubules and the adrenal gland [5,6]. The transporter is also located on the endothelial cells of the blood-brain barrier [7], the blood-testis barrier [8] and the blood-mammary tissue barrier [9]. Impairing the ability of PGP to export drugs out of these tissues, either by direct or competitive inhibition, could result in increased intracellular drug concentrations and, accordingly, increased tissue toxicity.

Data regarding human tissue levels of chemotherapeutics is sparse and unfortunately, plasma drug concentrations are not always indicative of the drug's concentration in tissues, especially when tissue penetration is altered. In mice, the disconnect between plasma and tissue pharmacokinetics has been observed when a PGP substrate was administered to mdr1a (-/-) mice [10] and when two PGP substrates were administered in combination [11]. Concerning the PGP substrate doxorubicin, the latter paper concluded that "monitoring of plasma levels of doxorubicin, when used in combination with another drug that is a PGP substrate, will not reflect actual pharmacokinetic changes occurring in other tissues". Thus, identifying whether the co-administration of compounds will result in increased tissue exposure and consequent enhanced toxicity based on an agent's plasma profile alone is problematic.

To address tissue-specific drug exposure resulting from combination therapy, we conducted studies in mice. The aim of the work presented herein was to determine if the co-administration of compounds commonly combined for metastatic breast cancer treatment alters plasma and tissue pharmacokinetics if both agents are PGP substrates and/or inhibitors. Accordingly, we investigated the pharmacokinetic interactions of the classic cytotoxics and PGP substrates docetaxel and doxorubicin when given concomitantly with the targeted agent and PGP inhibitor lapatinib, as both combinations are being explored clinically for the treatment of metastatic breast cancer. There is precedent to suggest that drug-drug interactions involving PGP could be significant for these combinations; *in vitro* studies have shown that lapatinib increased the intracellular accumulation of docetaxel 4.2-fold and doxorubicin 3.6-fold in the ABCB1-overexpressing DLKP-A [12] and MCF7/adr [13] cell lines, respectively. By understanding the plasma and tissue dynamics of these combination therapies in mice, we can then correspondingly dose adjust in humans to mitigate potential increases in toxicity so that the benefit of treatment outweighs the burden.

Materials and Methods:

Chemicals

Docetaxel (Winthrop U.S.) was acquired from the University of Colorado Hospital Pharmacy. Doxorubicin was acquired from the Colorado State University Veterinary Teaching Hospital Pharmacy. Lapatinib (GW572016) and GW572016AH were generously provided by GlaxoSmithKline. Hydroxypropyl methylcellulose, Tween® 80 and daunorubicin were purchased from Sigma-Aldrich. All other reagents were of analytical grade.

Animals

Five to six-week-old female FVB mice were purchased from Taconic. Animals were housed in polycarbonate cages and kept on a 12 hr light/dark cycle. Food and water were given *ad libitum*. Upon arrival, mice acclimated for a minimum of seven days prior to any experimentation.

All experimental procedures were approved by Colorado State University's Animal Care and Use Committee and the Department of Defense US Army Medical Research and Material Command (USAMRMC) Animal Care and Use Review Office (ACURO).

Lapatinib pharmacokinetic study

A time course distribution study of lapatinib was conducted. Lapatinib was formulated as a suspension of 12 mg/mL in 0.5% hydroxypropyl methylcellulose: 0.1% Tween® 80 in Milli-Q water and administered via intraperitoneal injection as a bolus dose of 60 mg/kg. Lapatinib was dosed every 3 hours for a total of 5 doses (q3hr × 5). Subsequently, three mice were sacrificed at each post-dose C_{max} (determined from previous studies to be 1 hr post-dose) and C_{min} (3 hrs post-dose). For the fifth dose, we only sacrificed mice at the C_{max}. All sacrifices were done by cardiac stick exsanguination under isoflurane anesthesia. Plasma was immediately collected, frozen in liquid nitrogen and stored at -80°C until analysis.

Docetaxel pharmacokinetic study

A time course distribution study of docetaxel with both single dose and multiple dose lapatinib was conducted. Docetaxel was acquired as an initial solution of 20 mg/mL in 50/50 (v/v) ratio polysorbate 80/dehydrated alcohol, further diluted to a solution of 0.6 mg/mL in 0.9% sodium chloride and administered via intravenous tail vein injection as a single bolus dose of 3 mg/kg. Lapatinib was formulated as a suspension of 12 mg/mL in 0.5% hydroxypropyl methylcellulose: 0.1% Tween® 80 in Milli-Q water and administered via intraperitoneal injection

as a bolus dose of 60 mg/kg. Vehicle was 0.5% hydroxypropyl methylcellulose: 0.1% Tween® 80 in Milli-Q water.

For the combination docetaxel and single dose lapatinib study, docetaxel was injected one hour after the single lapatinib or vehicle administration. Subsequently, three mice were sacrificed at 1, 2, 4, 8 and 12 hr post docetaxel injection. For the combination docetaxel and multiple dose lapatinib study, lapatinib or vehicle was dosed q3hr × 5. Docetaxel was injected one hour after the first lapatinib or vehicle dose. Subsequently, three mice were sacrificed at 4, 8 and 12 hrs post docetaxel injection. All sacrifices were done by cardiac stick exsanguination under isoflurane anesthesia. Plasma, brain, liver, proximal small intestine, kidney, heart, lung, muscle and adipose tissue were immediately collected, frozen in liquid nitrogen and stored at -80°C until analysis.

Doxorubicin pharmacokinetic study

A time course distribution study of doxorubicin with both single dose and multiple dose lapatinib was conducted. Doxorubicin was acquired as an initial solution of 2 mg/mL in 0.9% sodium chloride, further diluted to a solution of 1.2 mg/mL in 0.9% sodium chloride and administered via intravenous tail vein injection as a single bolus dose of 6 mg/kg. Lapatinib and vehicle were formulated and administered as for docetaxel studies.

For the combination doxorubicin and single dose lapatinib study, doxorubicin was injected one hour after the single lapatinib or vehicle administration. Subsequently, three mice were sacrificed at 1, 2, 4, 8, 12, 24 and 48 hrs post doxorubicin injection. For the combination doxorubicin and multiple dose lapatinib study, lapatinib or vehicle was dosed q3hr × 5. Doxorubicin was injected one hour after the first lapatinib or vehicle dose. Subsequently, three mice were sacrificed at 4, 8, 12, 24 and 48 hr post doxorubicin injection. Sacrifices, tissue collection and storage were done as for docetaxel studies.

Lapatinib high-pressure liquid chromatography-tandem mass spectrometry analysis

Analysis of lapatinib in plasma was done using high-pressure liquid chromatography-tandem mass spectrometry (LC/MS/MS) analysis based on the method of Bai et al. [14], modified as follows. Briefly, lapatinib was extracted from plasma by adding 210 uL of acetonitrile and 10 uL of internal standard (17.2 pmol GW572016AH) to 100 uL of unknown sample plasma, vortexing for 10 min and centrifuging at 18,000 x g for 10 min at 4°C. An aliquot of 20 uL of the supernatant was injected into the LC/MS/MS system for analysis. Standards and quality control samples were prepared in mouse plasma and analyzed as described above.

The HPLC system consisted of an Agilent 1200 Series binary pump SL, vacuum degasser, thermostatted column compartment SL (Agilent Technologies, Santa Clara, CA, USA) and a CTC Analytics HTC PAL System autosampler (Leap Technologies, Carrboro, NC, USA). The HPLC column was a Waters Sunfire C8 column (4.6 × 50 mm I.D., 2.5 µm bead size) (Waters Corporation, Milford, MA, USA) protected by a SecurityGuard™ C18 cartridge (4 × 2.0 mm I.D.) (Phenomenex, Torrance, CA, USA) and maintained at room temperature. The mobile phase consisted of an aqueous component (A) of 20mM ammonium formate in MilliQ water, pH 2.2 (with formic acid), and an organic component (B) of acetonitrile with 1% formic acid. The 3.5 min run consisted of the following linear gradient elution: 95% A and 5% B at 0 min, 95% A and 5% B at 0.25 min, 25% A and 75% B at 0.35 min, 25% A and 75% B at 3.0 min, 95% A and 5% B at 3.1 min and 95% A and 5% B at 3.5 min. The system operated at a flow-rate of 0.75 mL/min.

Mass spectrometric detection was performed on an API 3200™ triple quadrupole instrument (Applied Biosystems Inc, Foster City, CA, USA) using multiple reaction monitoring (MRM). Ions were generated in positive ionization mode using an electrospray interface. Lapatinib compound-dependent parameters were as follows: declustering potential (DP): 60 V;

entrance potential (EP): 10 V; collision cell entrance potential (CEP): 21 V; collision energy (CE): 51 V and collision cell exit potential (CXP): 5.8 V. GW572016AH (internal standard) compound-dependent parameters were as follows: DP: 67 V; EP: 7.5 V; CEP: 23 V; CE: 49 V and CXP: 5.5 V. Source-dependent parameters were as follows: nebulizer gas (GS1): 50 psi; auxiliary (turbo) gas (GS2): 60 psi; turbo gas temperature (TEM): 500°C; curtain gas [15]: 10 psi; collision-activated dissociation gas (nitrogen) (CAD): 6 psi; ionspray voltage (IS): 5000 V and interface heater (IH): 500°C. Peak areas ratios obtained from MRM of lapatinib (*m/z* 581 → 365.1) and GW572016AH (*m/z* 587 → 367) were used for quantification.

Docetaxel high-pressure liquid chromatography-tandem mass spectrometry analysis

Analysis of docetaxel in plasma and tissues was done using high-pressure liquid chromatography-tandem mass spectrometry (HPLC/MS/MS) analysis based on a method previously developed in our laboratory [16,17], modified as follows. Briefly, docetaxel was extracted from plasma by adding 1000 uL of ethyl acetate to 100 uL of unknown sample plasma, vortexing for 10 min and centrifuging at 18,000 x g for 10 min at 4°C. 800 uL of the organic phase was collected and evaporated to dryness using a rotary evaporator. Dried samples were reconstituted in 200 uL of 80/20 0.1% formic acid in water/acetonitrile, vortexed for 10 min and centrifuged at 18,000 x g for 10 min at 4°C. An aliquot of 60 uL of the supernatant was injected into the LC/MS/MS system for analysis. Tissues were homogenized at 100 mg/mL in water and 100 uL of the homogenates was extracted using the method for plasma detailed above. Standards and quality control samples were prepared in the appropriate matrix and analyzed as described above.

The HPLC and autosampler systems were the same as used with lapatinib. The HPLC column was a Waters Sunfire C8 column (2.1 × 150 mm I.D., 5.0 µm bead size) (Waters Corporation, Milford, MA, USA) protected by a SecurityGuard™ C18 cartridge (4 × 2.0 mm I.D.)

(Phenomenex, Torrance, CA, USA) and maintained at room temperature. The mobile phase consisted of an aqueous component (A) of 0.1% formic acid in MilliQ water and an organic component (B) of acetonitrile. The 4.0 min run consisted of the following linear gradient elution: 50% A and 50% B at 0 min, 50% A and 50% B at 0.5 min, 2% A and 98% B at 1.25 min, 2% A and 98% B at 3.0 min, 50% A and 50% B at 3.5 min and 50% A and 50% B at 4.0 min. The system operated at a flow-rate of 0.5 mL/min.

The mass spectrometric system was the same as used with lapatinib. Docetaxel compound-dependent parameters were as follows: DP: 21 V; EP: 4.5 V; CEP: 71 V; CE: 23 V and CXP: 3.5 V. Source-dependent parameters were as follows: GS1: 40 psi; GS2: 60 psi; TEM: 400°C; CUR: 30 psi; CAD: 2 psi; IS: 4500 V and IH: 500°C. Peak areas ratios obtained from MRM of docetaxel (*m/z* 808.5 → 226) were used for quantification.

Doxorubicin high-pressure liquid chromatography (HPLC)-fluorescence analysis

Analysis of doxorubicin in plasma and tissues was done using HPLC-fluorescence analysis based on a method previously developed in our laboratory [18,19], modified as follows. Briefly, doxorubicin was extracted from plasma by adding 600 uL of methanol and 10 uL of internal standard (1000 ng/mL daunorubicin) to 100 uL of unknown sample plasma, vortexing for 10 min, adding 250 uL of 12 mM phosphoric acid, vortexing for 10 min and centrifuging at 18,000 x g for 10 min at 4°C. An aliquot of 100 uL of the supernatant was injected into the HPLC system for analysis. Tissues were homogenized at 100 mg/mL in water and 100 uL of the homogenates was extracted using the method for plasma detailed above. Standards and quality control samples were prepared in the appropriate matrix and analyzed as described above.

The HPLC system consisted of a Shimadzu prominence LC-20AD binary pump, prominence DGU-20A_3 vacuum degasser, prominence CTO-20A column oven, prominence SIL-20AC auto sampler, prominence CBM-20A communications bus module and an RF-10A_{XL}

fluorescence detector with excitation and emission wavelengths set at 480 and 580 nm, respectively (Shimadzu, Columbia, MD, USA). The HPLC column was a Waters Sunfire C18 column (4.6 × 50 mm I.D., 2.5 µm bead size) (Waters Corporation, Milford, MA, USA) protected by a SecurityGuard™ C18 cartridge (4 × 2.0 mm I.D.) (Phenomenex, Torrance, CA, USA) and maintained at room temperature. The mobile phase consisted of an aqueous component (A) of 15 mM sodium phosphate in MilliQ water, pH 2.2 (with orthophosphoric acid), and an organic component (B) of acetonitrile. The 7.5 min run consisted of the following linear gradient elution: 80% A and 20% B at 0 min, 80% A and 20% B at 1.5 min, 50% A and 50% B at 6.5 min, 80% A and 20% B at 7.0 min, and 80% A and 20% B at 7.5 min. The system operated at a flow-rate of 0.75 mL/min.

Pharmacokinetic Analysis

Pharmacokinetic parameters were calculated using noncompartmental modeling performed with Microsoft Excel and standard equations for noncompartmental analysis.

Statistical Analysis

Statistical analysis was performed using GraphPad Prism v5.01 (GraphPad Software, San Diego, California). For the comparison of concentration means, two-tailed unpaired *t*-tests were used.

Results:

Combination lapatinib and chemotherapy clinical trials

To determine the effect of lapatinib on the pharmacokinetics of multiple classes of chemotherapeutics in humans, we reviewed all phase I clinical trials to date that involved drugs administered in combination with lapatinib and included pharmacokinetic data. In these eight

clinical trials [20-25,15,26], the plasma pharmacokinetics of eleven drugs and metabolites were reported; only three of these compounds exhibited statistically significant alterations in pharmacokinetic parameters upon concomitant administration with lapatinib (Table 1). When dosed with lapatinib, the plasma area under the concentration-time curve [27] of SN-38 and topotecan increased by 45% and 18%, respectively. The authors of both studies suggested that the decreased clearance was likely due to the interaction of lapatinib with efflux transporters, particularly PGP. Lapatinib has been shown to be both a substrate for PGP and breast cancer resistance protein (BCRP) and an inhibitor of PGP, BRCP and organic anion transporting polypeptide 1B1 (OATP1B1) [28]. As an inhibitor, lapatinib could prevent PGP from transporting xenobiotics out of the cell, thus increasing exposure to compounds that are PGP substrates. As a substrate, lapatinib could act as a competitor for PGP efflux.

To determine if the other chemotherapeutics used in the clinical trials are PGP substrates, we utilized Althotas Virtual Laboratory [29]. The support vector machine (SVM) method predicted that 4 of the 10 compounds assessed are substrates of PGP (Table 1). Of these, two drugs (SN-38 and topotecan) exhibited an increase in exposure when given with lapatinib whereas two (irinotecan and docetaxel) did not.

To further investigate the relationship with PGP, we also used Althotas Virtual Laboratory [29] to calculate the docking energies of human PGP-ligand interactions. The lowest free energy of docking to PGP for each compound is presented in Table 1. In comparison, the lowest free energy of docking to PGP for lapatinib is -10.3 kcal/mol. The significance of these energies is unclear. The geometries of the human PGP-ligand interactions are shown in Supplementary Figures 1 and 2.

In the human clinical trials, although the plasma pharmacokinetics were altered for only 27.3% of the compounds evaluated, all combination regimens caused an increase in toxicity. In 6 of the trials, dose reduction [25,24,21,15,22] or the addition of pegfilgrastim [23] was

warranted. Thus, the plasma pharmacokinetic data was not indicative of tissue pharmacokinetics or toxicodynamics.

Currently, there are 114 breast cancer clinical trials involving concomitant lapatinib [30]. Of all trials, 69% (n = 79) involve another drug that is a PGP substrate (as determined by Althotas Virtual Laboratory [29]). Of these, 57% (n = 45) include a taxane (docetaxel or paclitaxel) and/or an anthracycline (doxorubicin or epirubicin) (Supplementary Spreadsheet 1). Hence, taxanes and anthracyclines are commonly administered with lapatinib for the treatment of breast cancer and are also PGP substrates. Therefore, we chose to further explore the plasma and tissue pharmacokinetics of docetaxel and doxorubicin when given in combination with lapatinib in mice.

Human equivalent dosing of lapatinib in mice

For the subsequent combination studies, our aim was to administer a dose of lapatinib to mice that would result in plasma exposure equivalent to the steady-state plasma exposure in humans when given the recommended dose of lapatinib (1250 mg/day). We determined that dosing mice intraperitoneally with 60 mg/kg lapatinib every 3 hours for a total of 5 doses resulted in maximum concentrations (C_{max}) and minimum concentrations (C_{min}) of lapatinib that were similar to human peak (2430 ng/mL at 4 hr) and trough levels (1000 ng/mL) (Figure 1A). Extrapolating the mouse steady-state concentrations (achieved after 5 doses) out to 24 hours, this dosing regimen resulted in an AUC of 39.9 μg/mL × hr which is comparable to both the calculated human AUC_{τ} of 41.2 μg/mL × hr (Figure 1B) and the observed human geometric mean AUC_{τ} of 36.2 μg/mL × hr [31]. Accordingly, we used this mouse dosing regimen for the following combination studies.

Combination lapatinib and docetaxel studies in mice

Two time course plasma and tissue distribution studies of combination lapatinib and docetaxel were conducted in female FVB mice, which were administered either a single or multiple (q3hr × 5) intraperitoneal 60 mg/kg doses of lapatinib. In both experiments, a single intravenous injection of 3 mg/kg docetaxel was given one hour after the first lapatinib dose. Samples were collected at 1, 2, 4, 8 and 12 hrs post docetaxel administration.

After a single dose of lapatinib, there was a statistically significant increase in the concentration of docetaxel in kidney at 1 hr (10.6%) and 12 hrs (18.3%), intestine at 2 hrs (72.4%) and adipose tissue at 8 hrs (41.1%) versus docetaxel following vehicle. After multiple doses of lapatinib, there was a statistically significant increase (versus vehicle) in the concentration of docetaxel in kidney at 8 hrs (25.5%), intestine at 4 hrs (19.4%) and 8 hrs (89.7%), muscle at 8 hrs (23.4%) and plasma at 8 hrs (21.8%) (Figure 2).

In terms of exposure, combination therapy resulted in >25% increases in intestine and adipose tissue (Table 2). In intestine, there was a 32.8% and 44.6% increase after single and multiple dose lapatinib, respectively. In adipose tissue, there was a 35.4% and a 25.2% increase after single and multiple dose lapatinib, respectively.

In addition to exposure, we also evaluated the effect of lapatinib on docetaxel concentration-time curve shape parameters by comparing half-life and C_{max} values (Supplementary Tables 1 and 2). For the former, half-lives differed by ±25% after multiple dose lapatinib in muscle (-42.5%) and brain (+144.0%). However, for terminal half-life calculations using nonlinear regression, our curve was comprised of only 3 time points (4, 8 and 12 hrs) and for the brain and muscle multiple dose lapatinib curves, the r square (weighted) goodness-of-fit values for the regression lines were suboptimal. Specifically, in muscle, the r square (weighted) values were 0.5740 and 0.6994 for docetaxel alone and combination lapatinib and docetaxel, respectively. In brain, the r square (weighted) values were 0.8515 and 0.5249 for docetaxel alone and combination lapatinib and docetaxel, respectively. Thus, the half-life calculations from

these curves are flawed and, as such, the differences are likely misrepresentations. Regarding C_{max} values, there were no statistically significant differences.

Plasma concentrations of lapatinib in the combination single dose lapatinib and docetaxel study and the multiple dose lapatinib and docetaxel study are shown in Figures 1C and 1D, respectively. In the single dose lapatinib and docetaxel study, the C_{max} (700 ng/mL) was below the human trough concentration. In the multiple dose lapatinib and docetaxel study, all three lapatinib concentrations measured were within the targeted range (between the human steady state C_{max} and C_{min} following the recommended dose of lapatinib (1250 mg/day)).

Combination lapatinib and doxorubicin studies in mice

Two time course plasma and tissue distribution studies of combination lapatinib and doxorubicin were conducted in female FVB mice, which were administered either a single or multiple (q3hr × 5) intraperitoneal 60 mg/kg doses of lapatinib. In both experiments, a single intravenous injection of 6 mg/kg doxorubicin was given one hour after the first lapatinib dose. Samples were collected at 1, 2, 4, 8, 12, 24 and 48 hrs post doxorubicin administration.

After a single dose of lapatinib, there was a statistically significant increase in the concentration of doxorubicin in adipose tissue at 4 hrs (65.5%) and a statistically significant decrease at 24 hrs (40.4%) versus doxorubicin following vehicle (Figure 3). There were no statistically significant differences in doxorubicin concentrations in plasma or tissues after multiple dose lapatinib versus vehicle. Doxorubicin levels in the brain could not be evaluated because all sample peaks were below our lower limit of quantitation (50 ng/g).

Pertaining to exposure, the only change greater than ±25% was a decrease in adipose tissue (26.0%) after multiple dose lapatinib. There was also a 46.2% decrease and a 28.6% increase in adipose tissue terminal half-lives (calculated from the 12, 24 and 48 hr time points) after single and multiple dose lapatinib, respectively. As with docetaxel, these half-lives are

likely distorted as the r square (weighted) values for these regression lines were substandard. As for C_{max} values, we found no statistically significant differences.

Plasma concentrations of lapatinib in the combination single dose lapatinib and doxorubicin study and the multiple dose lapatinib and doxorubicin study are shown in Figures 1E and 1F, respectively. In the single dose lapatinib and doxorubicin study, the C_{max} (553 ng/mL) was below the human trough concentration. In the multiple dose lapatinib and doxorubicin study, all three lapatinib concentrations measured during the multiple dosing period were within the targeted range (between the human steady state C_{max} and C_{min} following the recommended dose of lapatinib (1250 mg/day)).

Discussion:

Cytotoxic and biologic combinations for the treatment of metastatic breast cancer have been approved by the US Food and Drug Administration (FDA) and several investigational drug combinations are currently undergoing evaluation in clinical trials [1]. While there are clear advantages to combining therapies, there is also the potential disadvantage of increasing the toxicity burden to the patient with only moderate improvements in efficacy and benefit [2]. In our evaluation of eight clinical trials involving co-administration of lapatinib with cytotoxic agents, all combinations caused an increase in toxicity versus the regimen without lapatinib, indicating that concomitant administration increased tissue drug exposure beyond a tolerable level. However, plasma pharmacokinetics were altered for only 27.3% of the compounds evaluated, demonstrating that chemotherapeutic concentrations in plasma alone were not indicative of adverse drug-drug interactions in tissues.

Drug-drug interactions are often mediated by competition for or inhibition of efflux proteins. As lapatinib is both a substrate for and inhibitor of PGP [28], we combined this drug with cytotoxic agents that are PGP substrates and used clinically in conjunction with lapatinib for

the treatment of metastatic breast cancer. Our study of lapatinib and docetaxel in mice showed that co-administration resulted in intestinal docetaxel exposure increases of 32.8% and 44.6% after single dose and multiple dose lapatinib, respectively. Although we did not evaluate toxicodynamics because of the short duration of our pharmacokinetic studies (12 hrs), this amplified intestinal exposure likely would have clinical ramifications, as the gastrointestinal tract is a major site of reported docetaxel-related adverse events. In patients treated with docetaxel as a single agent for various tumor types (n = 2045), nausea (39%), diarrhea (39%) and vomiting (22%) were observed; other gastrointestinal events included anorexia, taste perversion, constipation, abdominal pain, gastrointestinal bleeding and esophagitis [32].

Regarding the increased docetaxel exposure in adipose tissue (35.4% and a 25.2% after single and multiple dose lapatinib, respectively), this may also have clinically significant consequences given that adipose tissue could theoretically serve as a reservoir of docetaxel (since many lipid-soluble drugs are stored in fat) and thereby contribute to the significant increases in plasma, kidney, muscle and intestine docetaxel concentrations at later time points (8 and 12 hrs).

In a phase I study of lapatinib and docetaxel in patients with advanced cancer, the plasma pharmacokinetics of both compounds in combination were not significantly different than the drug profiles when administered separately; however, there was an increase in toxicity [23]. Specifically, the drug-related adverse events reported by most patients were diarrhea (56%), rash (52%), fatigue (27%) and nausea (25%). The authors could not characterize the diarrhea, nausea or rash as specific to either lapatinib or docetaxel but, in light of the data from our mouse study, we can conjecture that the gastrointestinal toxicities were likely due to an increase in docetaxel exposure in the enterocytes. Neutropenia, a frequent toxicity associated with docetaxel, also occurred during the phase I trial and necessitated the addition of pegfilgrastin to

the dosing regimen. The authors suggest that lapatinib increased the sensitivity to this toxicity, possibly by inhibiting PGP-mediated efflux of docetaxel from bone marrow stem cells [23].

In contrast to docetaxel, lapatinib did not significantly alter the pharmacokinetics of doxorubicin in plasma or tissues commonly associated with doxorubicin-related toxicity, such as heart, intestine and liver [33]. However, increases in doxorubicin $AUC_{0\rightarrow24hr}$ in these tissues (24% in heart, 65% in intestine and 339% in liver) and were observed in mice lacking mdr1a versus wild-type mice, implicating PGP as a causative factor in the alteration of doxorubicin pharmacokinetics in these tissues. This proposition is further support by additional rodent combination studies of doxorubicin with PGP inhibitors cyclosporin A [34,35] and SDZ PSC 833 [36], in which co-administration resulted in significant increases in tissue levels of doxorubicin. Thus, our study suggests that lapatinib is a weaker inhibitor of PGP than cyclosporin A and SDZ PSC 833. MDCKII-MDR1 monolayer efflux studies using 3H-digoxin as a probe substrate reported half maximal inhibitory concentrations of 3.9 [28] and 1.6 μM [37] for lapatinib and cyclosporin A, respectively, indicating that cyclosporin A is ~2.5 times more potent than lapatinib as a PGP inhibitor.

In addition to altering the pharmacokinetics of doxorubicin, cyclosporin A has also been shown to increase the plasma exposure of oral docetaxel 9-fold [38]. However, only a 3-fold increase was observed when docetaxel was administered per os to mdr1a/1b (-/-) mice compared to wild-type [39], suggesting that PGP inhibition was not the major factor accountable for the magnified systemic AUC when docetaxel was administered in combination with cyclosporin A. Alternatively, the increase in exposure was likely more resultant of competitive inhibition of cytochrome P450 enzymes by cyclosporin A, as both this immunosuppresant and docetaxel are substrates for CYP3A4 [40-42]. In mice, this is evidenced by a 12-fold plasma docetaxel exposure increase in cyp3a(-/-)versus wild-type mice after oral dosing [39]. Moreover,

after docetaxel dosing, the cyp3a(-/-) mice exhibited moderate toxicity in the small intestine whereas this was only mild in mrd1a/b(-/-) mice [39].

Further evidence that CYP3A metabolism plays a more important role than PGP-mediated efflux in docetaxel elimination comes from studies of intravenous injection of docetaxel in wild-type and mdr1a/b (-/-) mice, which resulted in no difference in systemic exposure to docetaxel [38]. Co-administration of cyclosporin A, however, increased plasma docetaxel AUC by 3-fold in both wild-type and mdr1a/b (-/-) mice [38], presumably due to the effect of cyclosporin A on docetaxel metabolism by CYP3A4.

Similar to cyclosporin A, lapatinib is not only an inhibitor of PGP but this targeted agent is also a CYP3A4 substrate and inhibitor [31,43]. As the latter, we propose that lapatinib competitively inhibits docetaxel intestinal metabolism by CYP3A4 and, consequently, is responsible for the considerable increase in docetaxel exposure that we observed in the small intestine of mice. A similar escalation was not seen in the liver because hepatic CYP3A is much more abundant than intestinal CYP3A, which is only ~2% of that in the liver [44-46]. Thus, these metabolic enzymes in the liver are not as susceptible to saturation as those in the small intestine. However, the importance of intestinal CYP3A metabolism of docetaxel should not be understated and is illustrated by a 16.6-fold versus a 2.2-fold decrease in docetaxel plasma exposure after oral administration to cyp3a (-/-) mice with human CYP3A4 in only the intestine or only the liver, respectively [47]. In contrast to docetaxel, a CYP3A4-mediated effect of lapatinib on doxorubicin exposure was not noted because this anthracycline is primarily metabolized to doxorubicinol by cytoplasmic aldo-keto and carbonyl reductases [48,49].

In conclusion, co-administration of lapatinib with doxorubicin did not appreciably alter the pharmacokinetics of this cytotoxic in the plasma or six tissues evaluated in mice, presumably because, at doses relevant to human exposure, lapatinib inhibition of PGP did not significantly alter doxorubicin export from these compartments and lapatinib inhibition of CYP3A4 was

inconsequential for doxorubicin metabolism to doxorubicinol. However, combining lapatinib with docetaxel dramatically increased intestinal exposure to this chemotherapeutic, which has clinical implications for enhancing gastrointestinal toxicity. The significant lapatinib-docetaxel interaction is likely CYP3A4-mediated and thus, our study suggests that caution should be taken when this combination is administered, particularly to patients with compromised CYP3A activity. As co-administration of these two agents is protocol for clinical trials that are either recruiting or active, we recommend closely monitoring the recipients of combined lapatinib and docetaxel for enhanced toxicity, particularly for adverse effects on the intestine.

Acknowledgements:

We are grateful to AJ Beaupre for performing all of the intravenous tail vein injections in both the docetaxel and doxorubicin mouse studies.

Grant Support: This work was supported in part by grant number W81XWH-09-1-0457 from the Department of Defense (DOD) Breast Cancer Research Program (BCRP) of the Office of the Congressionally Directed Medical Research Programs (CDMRP).

References:

1. Tkaczuk KH (2009) Review of the contemporary cytotoxic and biologic combinations available for the treatment of metastatic breast cancer. Clin Ther 31 Pt 2:2273-2289

2. Miles D, von Minckwitz G, Seidman AD (2002) Combination versus sequential single-agent therapy in metastatic breast cancer. Oncologist 7 Suppl 6:13-19

3. Cianfrocca M, Gradishar WJ (2007) Counterpoint: the argument for combination chemotherapy in the treatment of metastatic breast cancer. J Natl Compr Canc Netw 5 (8):673-675

4. Juliano RL, Ling V (1976) A surface glycoprotein modulating drug permeability in Chinese hamster ovary cell mutants. Biochim Biophys Acta 455 (1):152-162

5. Thiebaut F, Tsuruo T, Hamada H, Gottesman MM, Pastan I, Willingham MC (1987) Cellular localization of the multidrug-resistance gene product P-glycoprotein in normal human tissues. Proc Natl Acad Sci U S A 84 (21):7735-7738

6. Croop JM, Raymond M, Haber D, Devault A, Arceci RJ, Gros P, Housman DE (1989) The three mouse multidrug resistance (mdr) genes are expressed in a tissue-specific manner in normal mouse tissues. Mol Cell Biol 9 (3):1346-1350

7. Beaulieu E, Demeule M, Ghitescu L, Beliveau R (1997) P-glycoprotein is strongly expressed in the luminal membranes of the endothelium of blood vessels in the brain. Biochem J 326 (Pt 2):539-544

8. Melaine N, Lienard MO, Dorval I, Le Goascogne C, Lejeune H, Jegou B (2002) Multidrug resistance genes and p-glycoprotein in the testis of the rat, mouse, Guinea pig, and human. Biol Reprod 67 (6):1699-1707

9. Edwards JE, Alcorn J, Savolainen J, Anderson BD, McNamara PJ (2005) Role of P-glycoprotein in distribution of nelfinavir across the blood-mammary tissue barrier and blood-brain barrier. Antimicrob Agents Chemother 49 (4):1626-1628

10. van Asperen J, van Tellingen O, Tijssen F, Schinkel AH, Beijnen JH (1999) Increased accumulation of doxorubicin and doxorubicinol in cardiac tissue of mice lacking mdr1a P-glycoprotein. Br J Cancer 79 (1):108-113

11. Gustafson DL, Merz AL, Long ME (2005) Pharmacokinetics of combined doxorubicin and paclitaxel in mice. Cancer Lett 220 (2):161-169

12. Collins DM, Crown J, O'Donovan N, Devery A, O'Sullivan F, O'Driscoll L, Clynes M, O'Connor R Tyrosine kinase inhibitors potentiate the cytotoxicity of MDR-substrate anticancer agents independent of growth factor receptor status in lung cancer cell lines. Invest New Drugs 28 (4):433-444

13. Dai CL, Tiwari AK, Wu CP, Su XD, Wang SR, Liu DG, Ashby CR, Jr., Huang Y, Robey RW, Liang YJ, Chen LM, Shi CJ, Ambudkar SV, Chen ZS, Fu LW (2008) Lapatinib (Tykerb, GW572016) reverses multidrug resistance in cancer cells by inhibiting the activity of ATP-binding cassette subfamily B member 1 and G member 2. Cancer Res 68 (19):7905-7914

14. Bai F, Freeman BB, 3rd, Fraga CH, Fouladi M, Stewart CF (2006) Determination of lapatinib (GW572016) in human plasma by liquid chromatography electrospray tandem mass spectrometry (LC-ESI-MS/MS). J Chromatogr B Analyt Technol Biomed Life Sci 831 (1-2):169-175

15. Chu QS, Schwartz G, de Bono J, Smith DA, Koch KM, Versola MJ, Pandite L, Arya N, Curtright J, Fleming RA, Ho PT, Rowinsky EK (2007) Phase I and pharmacokinetic study of lapatinib in combination with capecitabine in patients with advanced solid malignancies. J Clin Oncol 25 (24):3753-3758

16. Bradshaw-Pierce EL, Eckhardt SG, Gustafson DL (2007) A physiologically based pharmacokinetic model of docetaxel disposition: from mouse to man. Clin Cancer Res 13 (9):2768-2776

17. Gustafson DL, Long ME, Zirrolli JA, Duncan MW, Holden SN, Pierson AS, Eckhardt SG (2003) Analysis of docetaxel pharmacokinetics in humans with the inclusion of later sampling time-points afforded by the use of a sensitive tandem LCMS assay. Cancer Chemother Pharmacol 52 (2):159-166

18. Gustafson DL, Rastatter JC, Colombo T, Long ME (2002) Doxorubicin pharmacokinetics: Macromolecule binding, metabolism, and excretion in the context of a physiologic model. J Pharm Sci 91 (6):1488-1501

19. de Jong J, Guerand WS, Schoofs PR, Bast A, van der Vijgh WJ (1991) Simple and sensitive quantification of anthracyclines in mouse atrial tissue using high-performance liquid chromatography and fluorescence detection. J Chromatogr 570 (1):209-216

20. Chu QS, Cianfrocca ME, Goldstein LJ, Gale M, Murray N, Loftiss J, Arya N, Koch KM, Pandite L, Fleming RA, Paul E, Rowinsky EK (2008) A phase I and pharmacokinetic study of lapatinib in combination with letrozole in patients with advanced cancer. Clin Cancer Res 14 (14):4484-4490

21. Molina JR, Kaufmann SH, Reid JM, Rubin SD, Galvez-Peralta M, Friedman R, Flatten KS, Koch KM, Gilmer TM, Mullin RJ, Jewell RC, Felten SJ, Mandrekar S, Adjei AA, Erlichman C (2008) Evaluation of lapatinib and topotecan combination therapy: tissue culture, murine xenograft, and phase I clinical trial data. Clin Cancer Res 14 (23):7900-7908

22. Kimball KJ, Numnum TM, Kirby TO, Zamboni WC, Estes JM, Barnes MN, Matei DE, Koch KM, Alvarez RD (2008) A phase I study of lapatinib in combination with carboplatin in women with platinum sensitive recurrent ovarian carcinoma. Gynecol Oncol 111 (1):95-101

23. LoRusso PM, Jones SF, Koch KM, Arya N, Fleming RA, Loftiss J, Pandite L, Gadgeel S, Weber BL, Burris HA, 3rd (2008) Phase I and pharmacokinetic study of lapatinib and docetaxel in patients with advanced cancer. J Clin Oncol 26 (18):3051-3056

24. Storniolo AM, Pegram MD, Overmoyer B, Silverman P, Peacock NW, Jones SF, Loftiss J, Arya N, Koch KM, Paul E, Pandite L, Fleming RA, Lebowitz PF, Ho PT, Burris HA, 3rd (2008) Phase I dose escalation and pharmacokinetic study of lapatinib in combination with trastuzumab in patients with advanced ErbB2-positive breast cancer. J Clin Oncol 26 (20):3317-3323

25. Midgley RS, Kerr DJ, Flaherty KT, Stevenson JP, Pratap SE, Koch KM, Smith DA, Versola M, Fleming RA, Ward C, O'Dwyer PJ, Middleton MR (2007) A phase I and pharmacokinetic study of lapatinib in combination with infusional 5-fluorouracil, leucovorin and irinotecan. Ann Oncol 18 (12):2025-2029

26. Siegel-Lakhai WS, Beijnen JH, Vervenne WL, Boot H, Keessen M, Versola M, Koch KM, Smith DA, Pandite L, Richel DJ, Schellens JH (2007) Phase I pharmacokinetic study of the safety and tolerability of lapatinib (GW572016) in combination with oxaliplatin/fluorouracil/leucovorin (FOLFOX4) in patients with solid tumors. Clin Cancer Res 13 (15 Pt 1):4495-4502

27. Castellino S, O'Mara M, Koch K, Borts DJ, Bowers GD, MacLauchlin C Human metabolism of lapatinib, a dual kinase inhibitor: implications for hepatotoxicity. Drug Metab Dispos 40 (1):139-150

28. Polli JW, Humphreys JE, Harmon KA, Castellino S, O'Mara MJ, Olson KL, John-Williams LS, Koch KM, Serabjit-Singh CJ (2008) The role of efflux and uptake transporters in [N-{3-chloro-4-[(3-fluorobenzyl)oxy]phenyl}-6-[5-({[2-(methylsulfonyl)ethyl]amino }methyl)-2-furyl]-4-quinazolinamine (GW572016, lapatinib) disposition and drug interactions. Drug Metab Dispos 36 (4):695-701

29. Bikadi Z, Hazai I, Malik D, Jemnitz K, Veres Z, Hari P, Ni Z, Loo TW, Clarke DM, Hazai E, Mao Q Predicting P-glycoprotein-mediated drug transport based on support vector machine and three-dimensional crystal structure of P-glycoprotein. PLoS One 6 (10):e25815

30. . www.clinicaltrials.gov.

31. GlaxoSmithKline (2012) Tykerb prescribing information. http://us.gsk.com/products/assets/us_tykerb.pdf.

32. Sanofi-Aventis (2011) Taxotere Product Mongraph. http://products.sanofi.ca/en/taxotere.pdf.

33. Pfizer (2012) Adriamycin Product Mongraph. http://www.pfizer.ca/en/our_products/products/monograph/150.

34. Bellamy WT, Peng YM, Odeleye A, Ellsworth L, Xu MJ, Grogan TM, Weinstein RS (1995) Cardiotoxicity in the SCID mouse following administration of doxorubicin and cyclosporin A. Anticancer Drugs 6 (6):736-743

35. Colombo T, Zucchetti M, D'Incalci M (1994) Cyclosporin A markedly changes the distribution of doxorubicin in mice and rats. J Pharmacol Exp Ther 269 (1):22-27

36. Gonzalez O, Colombo T, De Fusco M, Imperatori L, Zucchetti M, D'Incalci M (1995) Changes in doxorubicin distribution and toxicity in mice pretreated with the cyclosporin analogue SDZ PSC 833. Cancer Chemother Pharmacol 36 (4):335-340

37. Rautio J, Humphreys JE, Webster LO, Balakrishnan A, Keogh JP, Kunta JR, Serabjit-Singh CJ, Polli JW (2006) In vitro p-glycoprotein inhibition assays for assessment of clinical drug interaction potential of new drug candidates: a recommendation for probe substrates. Drug Metab Dispos 34 (5):786-792

38. Bardelmeijer HA, Ouwehand M, Buckle T, Huisman MT, Schellens JH, Beijnen JH, van Tellingen O (2002) Low systemic exposure of oral docetaxel in mice resulting from extensive first-pass metabolism is boosted by ritonavir. Cancer Res 62 (21):6158-6164

39. van Waterschoot RA, Lagas JS, Wagenaar E, van der Kruijssen CM, van Herwaarden AE, Song JY, Rooswinkel RW, van Tellingen O, Rosing H, Beijnen JH, Schinkel AH (2009) Absence of both cytochrome P450 3A and P-glycoprotein dramatically increases docetaxel oral bioavailability and risk of intestinal toxicity. Cancer Res 69 (23):8996-9002

40. Marre F, Sanderink GJ, de Sousa G, Gaillard C, Martinet M, Rahmani R (1996) Hepatic biotransformation of docetaxel (Taxotere) in vitro: involvement of the CYP3A subfamily in humans. Cancer Res 56 (6):1296-1302

41. Shou M, Martinet M, Korzekwa KR, Krausz KW, Gonzalez FJ, Gelboin HV (1998) Role of human cytochrome P450 3A4 and 3A5 in the metabolism of taxotere and its derivatives: enzyme specificity, interindividual distribution and metabolic contribution in human liver. Pharmacogenetics 8 (5):391-401

42. Niel N, Rechencq E, Muller A, Vidal JP, Escale R, Durand T, Girard JP, Rossi JC, Bonne C (1992) Synthesis and contractile activity of new pseudopeptido and thioaromatic analogues of leukotriene D4. Prostaglandins 43 (1):45-54

43. Teng WC, Oh JW, New LS, Wahlin MD, Nelson SD, Ho HK, Chan EC Mechanism-based inactivation of cytochrome P450 3A4 by lapatinib. Mol Pharmacol 78 (4):693-703

44. Perloff MD, Von Moltke LL, Greenblatt DJ (2003) Differential metabolism of midazolam in mouse liver and intestine microsomes: a comparison of cytochrome P450 activity and expression. Xenobiotica 33 (4):365-377

45. Hietanen E, Vainio H (1973) Interspecies variations in small intestinal and hepatic drug hydroxylation and glucuronidation. Acta Pharmacol Toxicol (Copenh) 33 (1):57-64

46. Paine MF, Khalighi M, Fisher JM, Shen DD, Kunze KL, Marsh CL, Perkins JD, Thummel KE (1997) Characterization of interintestinal and intraintestinal variations in human CYP3A-dependent metabolism. J Pharmacol Exp Ther 283 (3):1552-1562

47. van Herwaarden AE, Wagenaar E, van der Kruijssen CM, van Waterschoot RA, Smit JW, Song JY, van der Valk MA, van Tellingen O, van der Hoorn JW, Rosing H, Beijnen JH, Schinkel AH (2007) Knockout of cytochrome P450 3A yields new mouse models for understanding xenobiotic metabolism. J Clin Invest 117 (11):3583-3592

48. Robert J, Gianni L (1993) Pharmacokinetics and metabolism of anthracyclines. Cancer Surv 17:219-252

49. Loveless H, Arena E, Felsted RL, Bachur NR (1978) Comparative mammalian metabolism of adriamycin and daunorubicin. Cancer Res 38 (3):593-598

50. Andersen ME, Yang RSH, Clewell HJ, 3rd, Reddy MB (2005) Introduction: a historical perspective of the development and applications of PBPK models. In: Reddy MB, Yang RSH, Clewell HJ, 3rd, Andersen ME (eds) Physiologically based pharmacokinetic modeling : science and applications. Wiley-Interscience, Hoboken, N.J., pp xix, 420 p.

Figure Legend:

Figure 1: Lapatinib concentrations in mouse plasma. (A) Time course of maximum and minimum lapatinib concentrations after five 60 mg/kg intraperitoneal doses (at times 0, 3, 6, 9 and 12 hrs). Maximum and minimum concentrations were achieved 1 and 3 hrs post dose, respectively. Filled black diamonds represent mean concentrations and error bars represent standard deviations (n = 3). (B) Filled black diamonds and error bars as in (A). Open grey diamonds represent extrapolated maximum and minimum lapatinib concentrations with continued q3hr dosing after achievement of steady-state. Filled black circles represent human steady-state maximum (2430 ng/mL) and minimum (1000 ng/mL) concentrations (achieved 4 and 24 hrs post dose, respectively). (C) Time course of lapatinib concentrations after a single dose of 60 mg/kg intraperitoneal lapatinib administered at time -1 hr (arrow) followed by a single dose of 3 mg/kg intravenous docetaxel administered at time 0 hr. Filled black diamonds represent mean concentrations and error bars represent standard deviations (n = 3). (D) Time course of lapatinib concentrations after five 60 mg/kg intraperitoneal doses (at times -1, 2, 5, 8 and 11 hrs (arrows)) followed by a single dose of 3 mg/kg intravenous docetaxel administered at time 0 hr. Filled black diamonds represent mean concentrations and error bars represent

standard deviations (n = 3). (E) Time course of lapatinib concentrations after a single dose of 60 mg/kg intraperitoneal lapatinib administered at time -1 hr (arrow) followed by a single dose of 6 mg/kg intravenous doxorubicin administered at time 0 hr. Filled black diamonds represent mean concentrations and error bars represent standard deviations (n = 3). (F) Time course of lapatinib concentrations after five 60 mg/kg intraperitoneal doses (at times -1, 2, 5, 8 and 11 hrs (arrows)) followed by a single dose of 6 mg/kg intravenous doxorubicin administered at time 0 hr. Filled black diamonds represent mean concentrations and error bars represent standard deviations (n = 3). In all graphs, dashed lines represent the human steady-state maximum concentration (2430 ng/mL) and dotted lines represent the human steady-state minimum concentration (1000 ng/mL) after administration of the recommended dose of lapatinib (1250 mg/day).

Figure 2: Time courses of docetaxel concentrations in mouse plasma and tissues after a single dose of 3 mg/kg intravenous docetaxel administered at time 0 hr. For the single dose lapatinib study, one hour prior to docetaxel administration (at time -1 hr), mice were administered either single dose intraperitoneal vehicle (solid white bars) or single dose 60 mg/kg intraperitoneal lapatinib (horizontally striped bars). For the multiple dose lapatinib study, one hour prior to docetaxel administration (at time -1 hr) and again at times 2, 5, 8 and 11 hrs, mice were administered either intraperitoneal vehicle (solid black bars) or 60 mg/kg intraperitoneal lapatinib (diagonally striped bars). All bars represent mean concentrations and error bars represent standard deviations (n = 3). Asterisks represent statistically significance differences ($p < 0.05$).

Figure 3: Time courses of doxorubicin concentrations in mouse plasma and tissues after a single dose of 6 mg/kg intravenous doxorubicin administered at time 0 hr. For the single dose lapatinib study, one hour prior to doxorubicin administration (at time -1 hr), mice were

administered either single dose intraperitoneal vehicle (solid white bars) or single dose 60 mg/kg intraperitoneal lapatinib (horizontally striped bars). For the multiple dose lapatinib study, one hour prior to doxorubicin administration (at time -1 hr) and again at times 2, 5, 8 and 11 hrs, mice were administered either intraperitoneal vehicle (solid black bars) or 60 mg/kg intraperitoneal lapatinib (diagonally striped bars). All bars represent mean concentrations and error bars represent standard deviations (n = 3). Asterisks represent statistically significance differences ($p < 0.05$).

Supplementary Figure Legend:

Supplementary Figure 1: Docking geometry of P glycoprotein (PGP) and ligands. Docking geometry of PGP and (A) lapatinib, (B) irinotecan, (C) SN-38, (D) topotecan, (E) docetaxel and (F) doxorubicin. PGP cartoon rendering is grey. Ligands are represented as colored spheres. Atoms are carbon (green), hydrogen (grey), oxygen [50], nitrogen (blue), chlorine [20], fluorine (aqua) and sulfur (yellow).

Supplementary Figure 2: Docking geometry of P glycoprotein (PGP) interacting side chains and ligands. (A) lapatinib, (B) irinotecan, (C) SN-38, (D) topotecan, (E) docetaxel and (F) doxorubicin. PGP interacting side chains are rendering in a color ramp that goes from blue (at the N-terminus) to green to yellow (at the C-terminus). Ligands are represented as red spheres.

Table 1. Clinical, Pharmacokinetic and PGP Evaluation of Drugs Administered in Combination with Lapatinib in Phase I Clinical Trials

Clinical Trial	Drug	Number of Patients	Lapatinib Dose (mg/day)	Increased Toxicity	PK Parameter	Statistically Significant % Change[a]	PGP Substrate[b]	Docking Energy (kcal/mol)[c]	Ref
lapatinib + FOLFIRI	irinotecan	12	1250	Yes	AUC_{∞}, CL, V_{ss}	None	yes	-12.0	24
lapatinib + FOLFIRI	SN-38	12	1250	Yes	$AUC_{0\text{-}24hr}$	+44.9%	yes	-10.0	24
lapatinib + FOLFIRI	SN-38	12	1250	Yes	C_{max}	+27.0%	yes	-10.0	24
lapatinib + topotecan	topotecan	9	1250	Yes	$AUC_{0\text{-}24hr}$	+18.1%	yes	-9.4	20
lapatinib + topotecan	topotecan	9	1250	Yes	CL	-15.7%	yes	-9.4	20
lapatinib + topotecan	topotecan	9	1250	Yes	C_{max}, $t_{1/2}$, V_{ss}	None	yes	-9.4	20
lapatinib + docetaxel	docetaxel	8	1250	Yes	AUC_{∞}, CL, V_{ss}	None	yes	-9.2	22
lapatinib + letrozole	letrozole	8	1500	Yes	AUC_{τ}, C_{max}, T_{max}, C_{τ}	None	no	NA	19
lapatinib + capecitabine	capecitabine	19	1250	Yes	AUC_{τ}, C_{max}, T_{max}	None	no	NA	25
lapatinib + FOLFOX4	unbound platinum	17	1500	Yes	AUC, C_{max}, T_{max}, $t_{1/2}$, CL, V_{ss}	None	no	NA	26
lapatinib + FOLFIRI	5-fluorouracil	12	1250	Yes	C_{ss}	None	no	NA	24
lapatinib + capecitabine	5-fluorouracil	19	1250	Yes	AUC, T_{max}	None	no	NA	25
lapatinib + capecitabine	5-fluorouracil	19	1250	Yes	C_{max}	-20.6%	no	NA	25
lapatinib + FOLFOX4	5-fluorouracil	17	1500	Yes	C_{ave}, CL	None	no	NA	26
lapatinib + carboplatin	carboplatin	10	750	Yes	AUC	None	no	NA	21
lapatinib + capecitabine	α-fluoro-β-alanine	19	1250	Yes	AUC, C_{max}, T_{max}	None	no	NA	25
lapatinib + trastuzumab	trastuzumab	27	1000	Yes	$AUC_{0\text{-}24hr}$, C_{max}	None	NA[d]	NA[d]	23

Abbreviations: FOLFIRI, 5-fluorouracil, leucovorin and irinotecan; FOLFOX4, oxaliplatin, leucovorin and 5-fluorouracil; AUC, area under the concentration-time curve; $AUC_{0\text{-}24hr}$, area under the concentration-time curve from 0 to 24 hrs; AUC_{∞}, area under the concentration-time curve from 0 to infinity; AUC_{τ}, area under the concentration-time curve within a steady-state dosing interval; C_{max}, maximum concentration; C_{τ}, concentration at the end of a dosing interval; CL, clearance; C_{ss}, concentration at steady-state; C_{ave}, time-averaged concentration at steady-state; T_{max}, time of maximum concentration; $t_{1/2}$, half-life; V_{ss}, volume of distribution at steady-state; NA, not applicable.

[a]Percent (%) change was calculated as $100 \times \left(\left(Combination\,AUC \right) - \left(Single\,Agent\,AUC \right) \Big/ Single\,Agent\,AUC \right)$.

[b]PGP substrate determination of the ligand in column 2 was calculated with the support vector machine (SVM) method at http://pgp.althotas.com (21991360).

[c]Docking energy of ligand in column 2 with human PGP was calculated at http://pgp.althotas.com (21991360).

[d]Althotas (21991360) did not have information available regarding trastuzumab.

Table 2. Comparison of AUCs from Combination Lapatinib and Docetaxel Pharmacokinetic Studies in Mice

Sample	Single Dose Vehicle + Docetaxel $AUC_{0\text{-}12hr}$	Single Dose Lapatinib + Docetaxel $AUC_{0\text{-}12hr}$	% Change[e]	Multiple Dose Vehicle + Docetaxel $AUC_{4\text{-}12hr}$	Multiple Dose Lapatinib + Docetaxel $AUC_{4\text{-}12hr}$	% Change[c]
Lung[a]	15085	15442	+2.4%	9211	9987	+8.4%
Kidney[a]	12303	12974	+5.5%	5930	6964	+17.4%
Heart[a]	9989	9481	-5.1%	5601	5548	-0.9%
Muscle[a]	5283	4878	-7.7%	3084	3546	+15.0%
Intestine[a]	3511	4664	+32.8%	1957	2830	+44.6%
Liver[a]	3096	3471	+12.1%	1517	1668	+10.0%
Adipose[a]	1911	2587	+35.4%	1351	1691	+25.2%
Plasma[b]	378.6	423.2	+11.8%	179.5	185.3	+3.2%
Brain[a]	167.9	162	-3.5%	91.45	88.01	-3.8%

Abbreviations: $AUC_{0\text{-}12hr}$, area under the concentration-time curve from 0 to 12 hrs; $AUC_{4\text{-}12hr}$, area under the concentration-time curve from 4 to 12 hrs.
[a]Tissue AUC values are ng/g × hr.
[b]Plasma AUC values are ng/mL × hr.
[c]Percent (%) change was calculated as $100 \times \left(\left(Lapatinib + Docetaxel\ AUC \right) - \left(Vehicle + Docetaxel\ AUC \right) \Big/ Vehicle + Docetaxel\ AUC \right)$.

Table 3. Comparison of AUCs from Combination Lapatinib and Doxorubicin Pharmacokinetic Studies in Mice

Sample	Single Dose Vehicle + Doxorubicin $AUC_{0\text{-}48hr}$	Single Dose Lapatinib + Doxorubicin $AUC_{0\text{-}48hr}$	% Change[a]	Multiple Dose Vehicle + Doxorubicin $AUC_{4\text{-}48hr}$	Multiple Dose Lapatinib + Doxorubicin $AUC_{4\text{-}48hr}$	% Change[a]
Kidney[b]	238066	225903	-5.1%	194490	204623	+5.2%
Lung[b]	222640	211633	-4.9%	169515	175490	+3.5%
Liver[b]	126709	130778	+3.2%	78636	87168	+10.8%
Heart[b]	74829	71633	-4.3%	52493	52137	-0.7%
Intestine[b]	68936	62982	-8.6%	50136	58130	+15.9%
Adipose[b]	21058	17796	-15.5%	15555	11506	-26.0%
Plasma[c]	490.4	543.9	+10.9%	343.3	369.0	+7.5%

Abbreviations: $AUC_{0\text{-}48hr}$, area under the concentration-time curve from 0 to 48 hrs; $AUC_{4\text{-}48hr}$, area under the concentration-time curve from 4 to 48 hrs.

[a]Percent (%) change was calculated as $100 \times \left(\left(Lapatinib + Doxorubicin\,AUC \right) - \left(Vehicle + Doxorubicin\,AUC \right) \Big/ Vehicle + Doxorubicin\,AUC \right)$.

[b]Tissue AUC values are ng/g▪hr.

[c]Plasma AUC values are ng/mL▪hr.

Figure 1

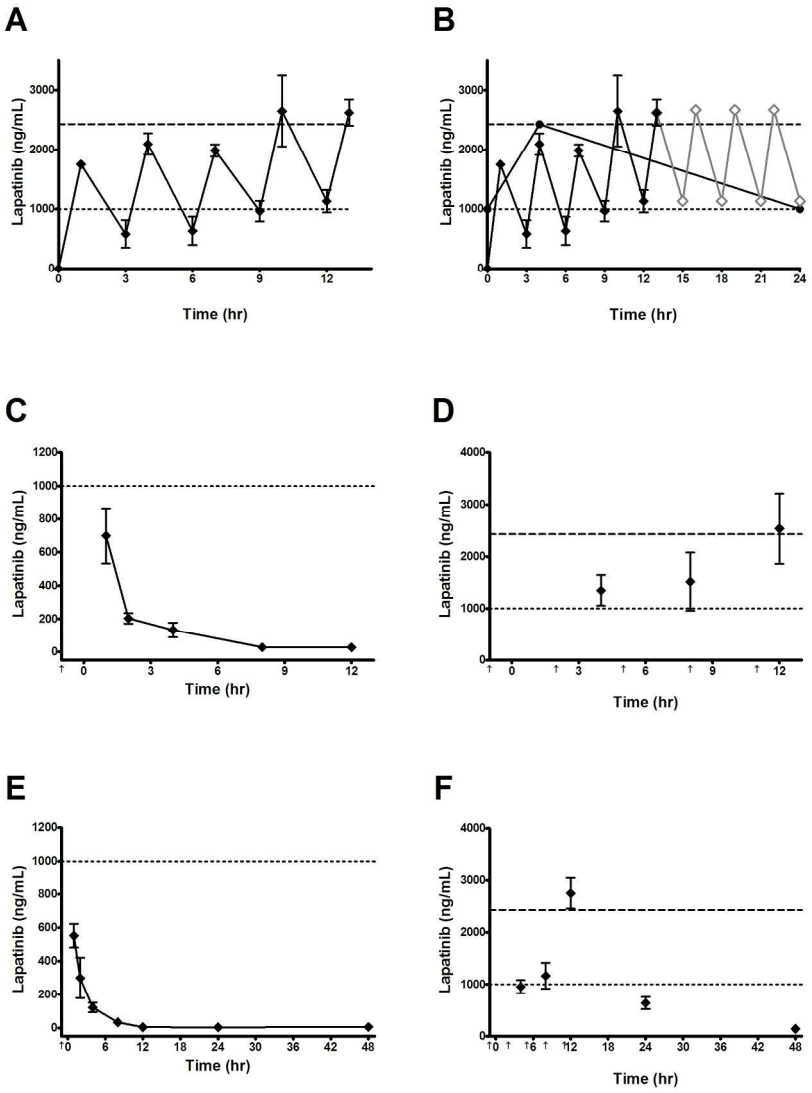

186x258mm (300 x 300 DPI)

Figure 2

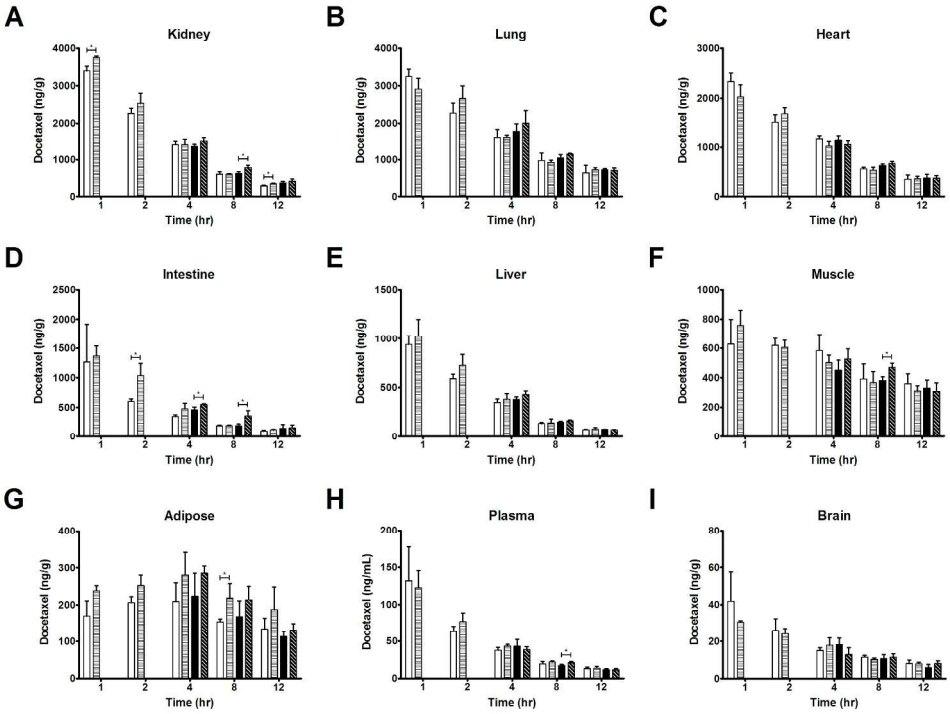

255x199mm (300 x 300 DPI)

Figure 3

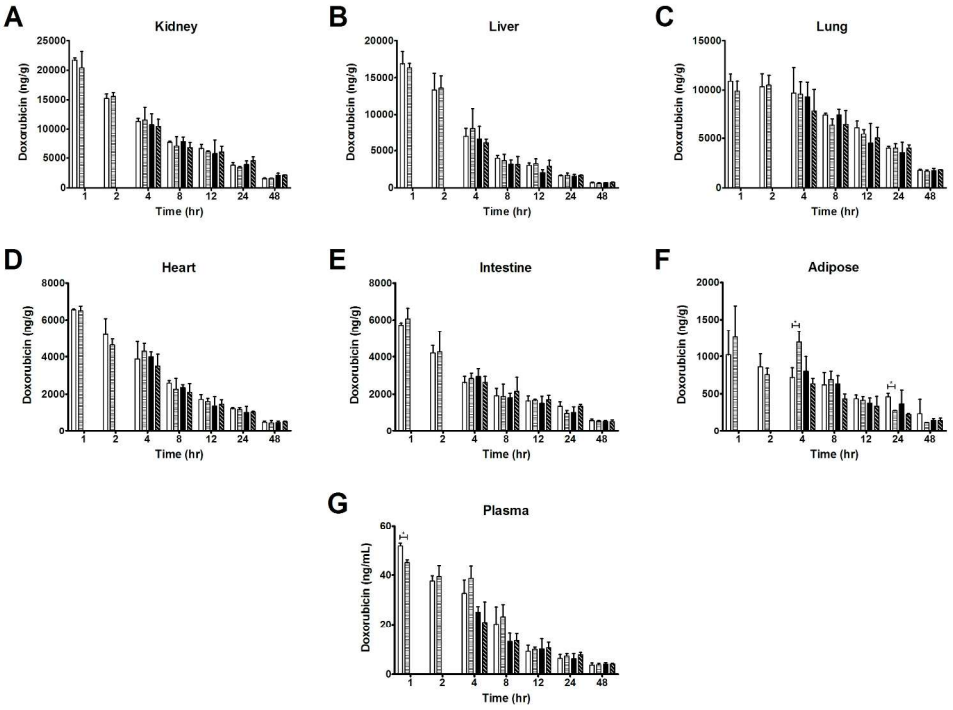

252x198mm (300 x 300 DPI)

Supplementary Table 1. Comparison of Half-lives from Combination Lapatinib and Docetaxel Pharmacokinetic Studies in Mice

Sample	Single Dose Vehicle + Docetaxel $t_{1/2}$	Single Dose Lapatinib + Docetaxel $t_{1/2}$	% Change[a]	Multiple Dose Vehicle + Docetaxel $t_{1/2}$	Multiple Dose Lapatinib + Docetaxel $t_{1/2}$	% Change[a]
Adipose	12.6 (7.0-66.0)	13.8 (6.5-∞)	+9.5%	8.2 (5.1-20.8)	7.2 (5.4-10.8)	-12.2%
Muscle	11.4 (6.2-70.0)	11.5 (7.4-26.1)	+0.9%	18.1 (10.2-81.6)	10.4 (6.8-22.0)	-42.5%
Brain	8.8 (6.1-16.2)	6.8 (4.9-11.0)	-22.7%	5 (3.7-7.7)	12.2 (6.5-94.7)	+144.0%
Lung	6.0 (4.1-10.8)	6.9 (5.5-9.1)	+15.0%	6.1 (5.1-7.5)	5.3 (4.4-6.6)	-13.1%
Plasma	5.2 (4.1-7.3)	4.9 (4.1-6.0)	-5.8%	4.3 (3.3-6.0)	4.6 (3.9-5.5)	+7.0%
Heart	4.5 (3.6-6.0)	5.3 (4.3-6.8)	+17.8%	4.9 (4.1-6.1)	6.1 (4.1-11.7)	+24.5%
Intestine	4.4 (3.8-5.3)	4.0 (3.3-5.2)	-9.1%	4.8 (3.2-9.9)	4.4 (3.2-6.9)	-8.3%
Liver	3.5 (3.1-4.2)	3.5 (2.8-4.9)	0.0%	3.4 (3.1-3.7)	3.1 (2.9-3.4)	-8.8%
Kidney	3.5 (3.2-3.9)	4.0 (3.4-4.7)	+14.3%	4.3 (3.7-5.0)	4.3 (3.8-5.1)	0.0%

Abbreviations: $t_{1/2}$, terminal half-life (95% confidence interval) in hr.

[a]Percent (%) change was calculated as $100 \times \left(\left(Lapatinib + Docetaxel\, t_{1/2} \right) - \left(Vehicle + Docetaxel\, t_{1/2} \right) \Big/ Vehicle + Docetaxel\, t_{1/2} \right)$.

Supplementary Table 2. Comparison of Maximum Concentrations from Combination Lapatinib and Docetaxel Pharmacokinetic Studies in Mice

Sample	Single Dose Vehicle + Docetaxel C_{max}	Single Dose Lapatinib + Docetaxel C_{max}	% Change[a]	Multiple Dose Vehicle + Docetaxel C_{max}[e]	Multiple Dose Lapatinib + Docetaxel C_{max}[e]	% Change[a]
Kidney[b]	3396.7 (130.1)[d]	3756.7 (35.1)[d]	+10.6%	1350.0 (60.8)	1500.0 (121.2)	+11.1%
Lung[b]	3250.0 (194.7)[d]	2913.3 (284.3)[d]	-10.4%	1786.7 (200.1)	2000.0 (340.4)	+11.9%
Heart[b]	2336.7 (172.1)[d]	2033.3 (240.1)[d]	-13.0%	1163.3 (86.2)	1053.3 (76.4)	-9.5%
Intestine[b]	1268.7 (647.7)[d]	1366.7 (171.6)[d]	+7.7%	458.3 (47.5)	547.3 (18.6)	+19.4%
Liver[b]	938.0 (94.6)[d]	1025.3 (171.4)[d]	+9.3%	381.7 (25.8)	431.0 (35.5)	+12.9%
Muscle[b]	628.3 (170.7)[d]	759.3 (102.0)[d]	+20.8%	450.0 (68.4)	526.3 (69.3)	+17.0%
Adipose[b]	209.3 (50.5)[e]	280.3 (61.1)[e]	+33.9%	223.3 (62.1)	285.7 (19.2)	-27.9%
Plasma[c]	132.0 (45.5)[d]	122.3 (23.1)[d]	-7.3%	43.2 (9.1)	38.7 (3.9)	-10.4%
Brain[b]	42.0 (15.5)[d]	30.7 (0.8)[d]	-26.9%	18.2 (3.5)	12.9 (3.7)	-29.1%

Abberviations: C_{max}, maximum concentration (standard deviation).

[a]Percent (%) change was calculated as $100 \times \left(\left(Lapatinib + Docetaxel C_{\max} \right) - \left(Vehicle + Docetaxel C_{\max} \right) \Big/ Vehicle + Docetaxel C_{\max} \right)$.

[b]Tissue C_{max} values are ng/g.
[c]Plasma C_{max} values are ng/mL.
[d]C_{max} was at 1 hr.
[e]C_{max} was at 4 hr.

Supplementary Table 3. Comparison of Half-lives from Combination Lapatinib and Doxorubicin Pharmacokinetic Studies in Mice

Sample	Single Dose Vehicle + Doxorubicin $t_{1/2}$	Single Dose Lapatinib + Doxorubicin $t_{1/2}$	% Change[a]	Multiple Dose Vehicle + Doxorubicin $t_{1/2}$	Multiple Dose Lapatinib + Doxorubicin $t_{1/2}$	% Change[a]
Adipose	37.0 (16.6-∞)	19.9 (18.2-22.0)	-46.2%	23.4 (13.4-94.0)	30.1 (18.8-75.4)	+28.6%
Plasma	27.3 (18.4-52.5)	25.3 (20.4-33.1)	-7.3%	29.3 (17.1-102)	26.2 (20.6-36.0)	-10.6%
Intestine	23.6 (17.9-34.4)	23.0 (19.0-29.3)	-2.5	24.9 (17.3-44.6)	21.0 (17.2-27.1)	-15.7%
Heart	20.1 (17.1-24.2)	19.9 (16.0-26.6)	-1.0%	23.6 (15.5-49.2)	24.8 (20.9-30.4)	+5.1%
Lung	20.0 (18.1-22.4)	20.7 (18.0-24.3)	+3.5%	25.3 (16.1-59.5)	24.0 (19.0-32.3)	-5.1%
Kidney	17.4 (15.4-20.0)	19.2 (17.4-21.4)	+10.3%	25.3 (17.4-46.4)	24.0 (19.7-30.6)	-5.1%
Liver	16.9 (14.8-19.8)	15.1 (12.6-18.9)	-10.7%	21.8 (17.3-29.4)	18.5 (15.1-24.0)	-15.1%

Abbreviations: $t_{1/2}$, terminal half-life (95% confidence interval) in hr.

[a]Percent (%) change was calculated as $100 \times \left(\left(Lapatinib + Doxorubicin\, t_{1/2} \right) - \left(Vehicle + Doxorubicin\, t_{1/2} \right) \Big/ Vehicle + Doxorubicin\, t_{1/2} \right)$.

Supplementary Table 4. Comparison of Maximum Concentrations from Combination Lapatinib and Doxorubicin Pharmacokinetic Studies in Mice

Sample	Single Dose Vehicle + Doxorubicin C_{max}	Single Dose Lapatinib + Doxorubicin C_{max}	% Change[a]	Multiple Dose Vehicle + Doxorubicin C_{max}[e]	Multiple Dose Lapatinib + Doxorubicin C_{max}[e]	% Change[a]
Kidney[b]	21710.1 (385.9)[d]	20422.4 (2733.6)[d]	-5.9%	10749.4 (1891.6)	10486.4 (1217.8)	-2.4%
Liver[b]	16855.7 (1658.0)[d]	16343.8 (582.4)[d]	-3.0%	6553.3 (1862.7)	6045.4 (513.0)	-7.8%
Lung[b]	10893.6 (703.2)[d]	9871.9 (1006.4)[d]	-9.4%	9316.9 (1483.6)	7856.1 (2192.4)	-15.7%
Heart[b]	6546.8 (48.5)[d]	6490.2 (260.6)[d]	-0.9%	3995.0 (263.5)	3495.2 (641.3)	-12.5%
Intestine[b]	5726.7 (106.1)[d]	6072.6 (562.8)[d]	+6.0%	2944.0 (416.3)	2629.5 (320.3)	-10.7%
Adipose[b]	1021.4 (326.1)[e]	1259.0 (427.0)[e]	+23.3%	802.0 (194.6)	635.4 (69.8)	-20.8%
Plasma[c]	51.7 (1.1)[d]	45.0 (1.1)[d]	-13.0%	25.1 (2.3)	20.8 (8.3)	-17.1%

Abberviations: C_{max}, maximum concentration (standard deviation).

[a]Percent (%) change was calculated as $100 \times \left(\left(Lapatinib + Docetaxel C_{\max} \right) - \left(Vehicle + Docetaxel C_{\max} \right) \Big/ Vehicle + Docetaxel C_{\max} \right)$.

[b]Tissue C_{max} values are ng/g.
[c]Plasma C_{max} values are ng/mL.
[d]C_{max} was at 1 hr.
[e]C_{max} was at 4 hr.

Supplementary Figure 1

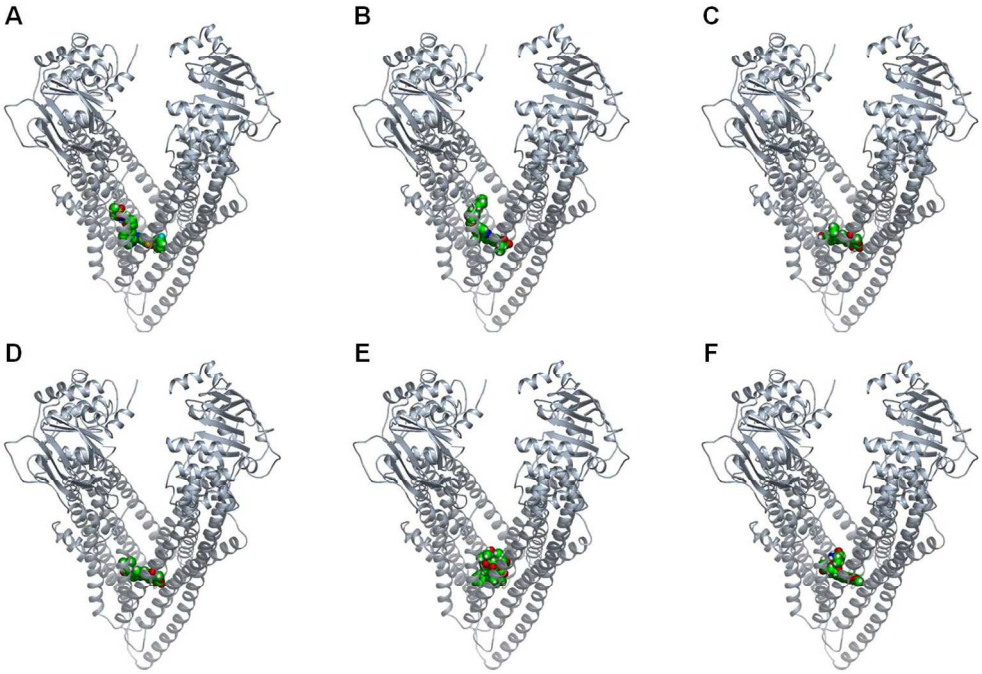

255x188mm (150 x 150 DPI)

Supplementary Figure 2

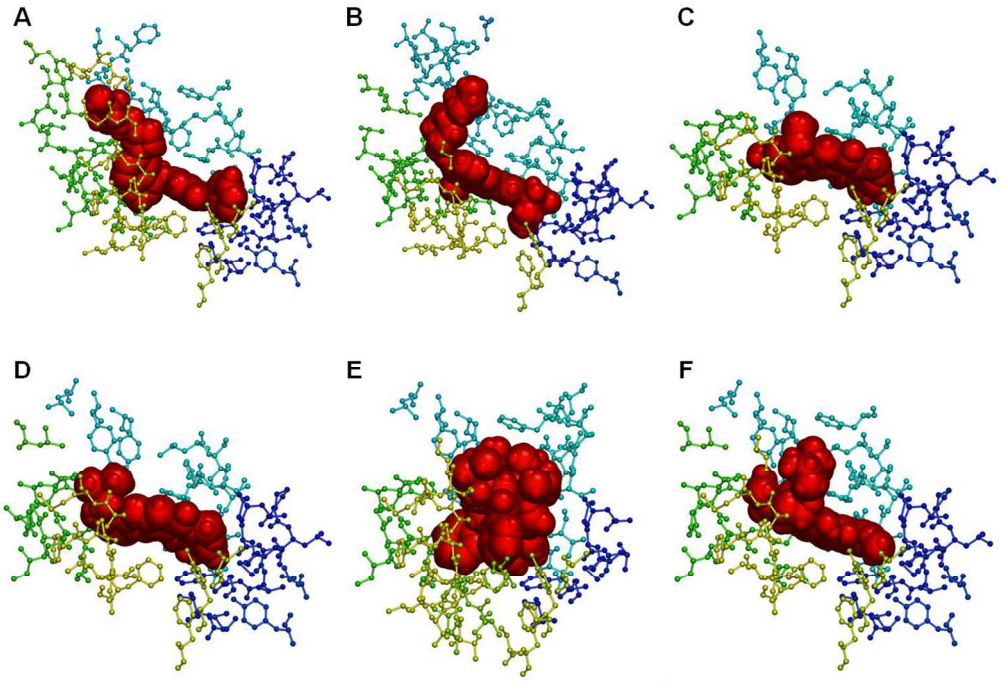

248x182mm (150 x 150 DPI)

Title	Recruitment	Study Results	PGP Substrate	Drug	Docking Energy	Interventions
Safety Study of AMG 386 to Treat HER2-positive Locally Recurrent or Metastatic Breast Cance	Recruiting	No Results Available	NO			Drug: AMG 386|Drug: Capecitabine|Drug: Lapatinib|Drug: Paclitaxel|Drug: Trastuzumab
Capecitabine (Xeloda) and Lapatinib (Tykerb) as First-line Therapy in HER2/Neu-positive Breast Cance	Active, not recruiting	No Results Available	NO			Drug: Capecitabine|Drug: Lapatinib
Continued HER2 Suppression With Lapatinib Plus Trastuzumab Versus Trastuzumab Alone	Recruiting	No Results Available	NO			Drug: Lapatinib|Biological: Trastuzumab
A Phase Ib/II Study of BEZ235 and Trastuzumab in Patients With HER2-positive Breast Cancer Who Failed Prior to Trastuzumab	Recruiting	No Results Available	NO			Drug: BEZ235|Drug: Trastuzumab|Drug: Lapatinib|Drug: Capecitabine
GW572016 Combined With Trastuzumab For The Treatment Of Previously Trastuzumab-Treated Breast Cancer	Completed	No Results Available	NO			Drug: Lapatinib
Lapatinib in Combination With Trastuzumab in Patients With HER2-Positive, Metastatic Breast Cancer	Recruiting	No Results Available	NO			Drug: Lapatinib|Drug: Herceptin
Lapatinib in Combination With Capecitabine in Japanese Patients With Metastatic Breast Cancer	Completed	Has Results	NO			Drug: Lapatinib|Drug: Capecitabine
ELBA: Exemestane and Lapatinib in Advanced Breast Cancer	Withdrawn	No Results Available	NO			Drug: Exemestane|Drug: Lapatinib
Lapatinib Plus Capecitabine Versus Trastuzumab Plus Capecitabine in ErbB2 (HER2) Positive Metastatic Breast Cancer	Recruiting	No Results Available	NO			Drug: Capecitabine|Drug: Lapatinib|Drug: Trastuzumab
Capecitabine and Lapatinib With or Without Cixutumumab in Treating Patients With Previously Treated HER2-Positive Stage IIIB, Stage IIIC, or Stage IV Breast Cancer	Active, not recruiting	No Results Available	NO			Drug: Cixutumumab|Drug: Capecitabine|Drug: Lapatinib ditosylate
Vorinostat and Lapatinib in Advanced Solid Tumors and Advanced Breast Cancer to Evaluate Response and Biomarkers	Recruiting	No Results Available	NO			Drug: Vorinostat|Drug: Lapatinib
Letrozole In Combination With Lapatinib In Neoadjuvant Treatment Of Early Breast Cancer	Recruiting	No Results Available	NO			Drug: Lapatinib|Drug: Letrozole
PhII Neo-Adjuvant Letrozole & Lapatinib in Pts w/HER2+ & Hormone Receptor+ Operable Breast CA SPORE	Terminated	Has Results	NO			Drug: Lapatinib ditosylate|Drug: Letrozole
Capecitabine (XELODA) With Or Without Lapatinib (GW572016) For Women With Refractory Advanced or Metastatic Breast Cancer	Completed	No Results Available	NO			Drug: Capecitabine|Drug: Lapatinib
Lapatinib Ditosylate and Capecitabine in Treating Patients With Stage IV Breast Cancer and Brain Metastases	Recruiting	No Results Available	NO			Drug: Capecitabine|Drug: Lapatinib ditosylate
Novel Capecitabine Dosing Schedule in Combination With Lapatinib, Based on the Norton-Simon Mathematical Method in Patients With HER2 Overexpressed/Amplified, Trastuzumab (Herceptin) -Refractory, Metastatic Breast Cance	Active, not recruiting	No Results Available	NO			Drug: Capecitabine|Drug: Lapatinib
Lapatinib and Temozolomide for the Treatment of Progressive Brain Disease in HER-2 Positive Breast Cance	Active, not recruiting	No Results Available	NO			Drug: Lapatinib|Drug: Temozolomide
Neoadjuvant Combined Endocrine and HER2 Target Therapy in Postmenopausal Women With ER and Her2 Positive Breast Cancer	Recruiting	No Results Available	NO			Drug: Letrozole|Drug: Lapatinib
Evaluating Lapatinib + Capecitabine in Patients Aged 70 and Over With HER2 Metastatic Breast Cancer	Active, not recruiting	No Results Available	NO			Drug: Lapatinib|Drug: Capecitabine
An Open-Label Study of Trastuzumab Emtansine (T-DM1) vs Capecitabine+Lapatinib in Patients With HER2-Positive Locally Advanced or Metastatic Breast Cancer (EMILIA	Recruiting	No Results Available	NO			Drug: Trastuzumab|Drug: Emtansine|Drug: Lapatinib|Drug: Capecitabine
Tolerability of the Combination of Lapatinib and Trastuzumab in Adults Age 60 or Older With HER2 Positive Metastatic Breast Cancer	Recruiting	No Results Available	NO			Drug: Lapatinib|Drug: Trastuzumab
Lapatinib and Trastuzumab With or Without Endocrine Therapy	Active, not recruiting	Has Results	NO			Drug: Lapatinib|Drug: Trastuzumab|Drug: Endocrine
ALTTO (Adjuvant Lapatinib And/Or Trastuzumab Treatment Optimisation) Study: BIG 2-06/N063D	Active, not recruiting	No Results Available	NO			Drug: Lapatinib|Drug: Trastuzumab
Extension Study of Lapatinib Plus Herceptin With or Without Endocrine Therapy	Recruiting	No Results Available	NO			Drug: Herceptin|Drug: Lapatinib|Drug: Letrozole
Lapatinib With Trastuzumab in Treating Patients With HER2-Negative/HER2 Mutant Metastatic Breast Cancer	Not yet recruiting	No Results Available	NO			Drug: Lapatinib ditosylate|Drug: Trastuzumab
GW572016 and Trastuzumab in Treating Patients With Metastatic Breast Cancer That Overexpresses HER2/Neu	Completed	No Results Available	NO			Drug: Trastuzumab|Drug: Lapatinib ditosylate
Modulation of Response to Hormonal Therapy With Lapatinib and/or Metformin in Patients With Metastatic Breast Cancer	Recruiting	No Results Available	NO			Drug: Lapatinib|Drug: Metformin
Role of Early Versus Late Switch to Lapatinib-Capecitabine (TYCO	Recruiting	No Results Available	NO			Drug: Lapatinib|Drug: Capecitabine
Lapatinib +Capecitabine Treatment for Advanced Metastatic Breast Cancer in Women From China	Active, not recruiting	Has Results	NO			Drug: Lapatinib|Drug: Capecitabine
Study Comparing GW572016 And Letrozole Versus Letrozole In Subjects With Advanced Or Metastatic Breast Cancer	Active, not recruiting	Has Results	NO			Drug: Lapatinib|Drug: Letrozole
EAP (Expanded Access Protocol) Of Lapatinib Combined With Capecitabine In Metastatic Breast Cancer	Recruiting	No Results Available	NO			Drug: Lapatinib|Drug: Capecitabine
Lapatinib and Bevacizumab for Metastatic Breast Cancer	Active, not recruiting	Has Results	NO			Drug: Lapatinib|Drug: Bevacizumab
Study to Assess dHER2+AS15 Cancer Vaccine Given in Combination With Lapatinib to Patients With Metastatic Breast Cancer	Active, not recruiting	No Results Available	NO			Drug: dHER2 + AS15 ASCI|Drug: Lapatinib
Lapatinib In Combination With Trastuzumab Versus Lapatinib Monotherapy In Subjects With HER2-positive Metastatic Breast Cancer	Completed	Has Results	NO			Drug: Lapatinib|Drug: Trastuzumab
A Study to Compare the Safety and Efficacy of an Aromatase Inhibitor in Combination With Lapatinib, Trastuzumab or Both for the Treatment of Hormone Receptor Positive, HER2+ Metastatic Breast Cance	Recruiting	No Results Available	NO			Drug: Lapatinib|Drug: Trastuzumab|Drug: Aromatase inhibitor|Drug: lapatinib
Efficacy and Tolerability of Eribulin Plus Lapatinib in Patients With Metastatic Breast Cancer (E-VITA	Recruiting	No Results Available	YES	eribulin	-12.4	Drug: Lapatinib|Drug: Eribulin
Study To Examine The Effects Of Lapatinib On The Pharmacokinetics Of Digoxin In Subjects w/ ErbB2 Positive Breast Cancer	Completed	No Results Available	YES	digoxin	-11.5	Drug: Lapatinib|Drug: Digoxin
Study of Foretinib in Combination With Lapatinib in Patients With Metastatic Breast Cancer	Recruiting	No Results Available	YES	foretinib	-11.4	Drug: Foretinib|Drug: Lapatinib
Pazopanib Plus Lapatinib Compared To Lapatinib Alone In Subjects With Inflammatory Breast Cancer	Completed	Has Results	YES	pazopanib	-10.9	Drug: Lapatinib|Drug: Pazopanib
Pazopanib Plus Lapatinib Compared To Lapatinib Alone In Subjects With Advanced Or Metastatic Breast Cancer	Active, not recruiting	Has Results	YES	pazopanib	-10.9	Drug: Pazopanib|Drug: Lapatinib
Lapatinib Ditosylate and MK2206 in Treating Women With Metastatic Breast Cancer	Recruiting	No Results Available	YES	MK2206	-10.7	Drug: MK2206|Drug: Lapatinib ditosylate
MK2206 in Combination With Lapatinib Ditosylate in Patients With Advanced or Metastatic Solid Tumors or Breast Cancer	Not yet recruiting	No Results Available	YES	MK2206	-10.7	Drug: MK2206|Drug: Lapatinib ditosylate
A Study of MK2206 in Combination With Trastuzumab and Lapatinib for the Treatment of HER2+ Solid Tumors (2206-015)	Completed	No Results Available	YES	MK2206	-10.7	Drug: MK2206|Drug: Trastuzumab|Drug: Lapatinib
LBH589 in Combination With Capecitabine Plus/Minus (As) Lapatinib in Breast Cancer Patients	Active, not recruiting	No Results Available	YES	LBH589	-10.5	Drug: LBH589|Drug: Capecitabine|Drug: Lapatinib
Entinostat and Lapatinib Ditosylate in Patients With Locally Recurrent or Distant Relapsed Metastatic Breast Cancer Previously Treated With Trastuzumab	Recruiting	No Results Available	YES	entinostat	-10	Drug: Entinostat|Drug: Lapatinib ditosylate
Lapatinib and Tamoxifen in Treating Patients With Advanced or Metastatic Breast Cancer	Active, not recruiting	No Results Available	YES	tamoxifen	-9.7	Drug: Lapatinib ditosylate|Drug: Tamoxifen citrate
Lapatinib and Tamoxifen in Treating Patients With Locally Advanced or Metastatic Breast Cancer That Did Not Respond to Previous Tamoxifen	Active, not recruiting	No Results Available	YES	tamoxifen	-9.7	Drug: Lapatinib ditosylate|Drug: Tamoxifen citrate
AUY922 With Lapatinib and Letrozole for ER+ HER2+ Advanced Breast Cancer	Recruiting	No Results Available	YES	AUY922	-9.7	Drug: Lapatinib|Drug: Letrozole
Lapatinib and Vinorelbine in Treating Women With HER2-Overexpressing Locally Advanced or Metastatic Breast Cancer	Recruiting	No Results Available	YES	vinorelbine	-9.6	Drug: Lapatinib ditosylate|Drug: Vinorelbine tartrate
A Study Evaluating the Efficacy and Safety of Lapatinib + Vinorelbine in ErbB2 Positive Metastatic Breast Cancer Patients	Recruiting	No Results Available	YES	vinorelbine	-9.6	Drug: Lapatinib|Drug: Vinorelbine
Vinorelbine Metronomic Plus Lapatinib for Overexpressing HER-2 Metastatic Breast Cance	Withdrawn	No Results Available	YES	vinorelbine	-9.6	Drug: Vinorelbine|Drug: Lapatinib
Lapatinib in Combination With Oral Vinorelbine for Metastatic Breast Cancer	Recruiting	No Results Available	YES	vinorelbine	-9.6	Drug: Lapatinib|Drug: Vinorelbine
Lapatinib + Vinorelbine in ErbB2 Overexpressing, First or Second Line Metastatic Breast Cancer Subjects	Active, not recruiting	No Results Available	YES	vinorelbine	-9.6	Drug: Lapatinib|Drug: Vinorelbine
Safety Study in Subjects With Metastatic Breast Cancer Who Progressed After Taxanes Treatment	Recruiting	No Results Available	YES	vinorelbine	-9.6	Drug: Lapatinib|Drug: Vinorelbine|Drug: Capecitabine|Drug: Gemcitabine
Lapatinib in Combination With Vinorelbine	Active, not recruiting	No Results Available	YES	vinorelbine	-9.6	Drug: Lapatinib|Drug: Vinorelbine
Dose Finding Study for Combination of Capecitabine, Lapatinib and Vinorelbine in Metastatic Breast Cancer	Recruiting	No Results Available	YES	vinorelbine	-9.6	Drug: Lapatinib|Drug: Capecitabine|Drug: Vinorelbine
Lapatinib in Combination With Vinorelbine	Active, not recruiting	No Results Available	YES	vinorelbine	-9.6	Drug: Vinorelbine|Drug: Lapatinib|Drug: Capecitabine
Safety and Efficacy of BKM120 and Lapatinib in HER2+/PI3K-activated, Trastuzumab-resistant Advanced Breast Cancer	Recruiting	No Results Available	YES	BKM120	-9.5	Drug: BKM120|Drug: Lapatinib
Phase I Study of Ixabepilone Plus Lapatinib With or Without Capecitabine in the Treatment of Human Epidermal Growth Factor Receptor 2 (HER2)-Positive Breast Cancer	Terminated	Has Results	YES	ixabepilone	-9.4	Drug: Ixabepilone|Drug: Lapatinib|Drug: Capecitabine
Brain Metastases In ErbB2-Positive Breast Cancer	Terminated	No Results Available	YES	topotecan	-9.4	Drug: Lapatinib|Drug: Capecitabine|Drug: Topotecan
APRICOT-B: Study to Evaluate Apricoxib in Combination With Lapatinib and Capecitabine in the Treatment of HER2/Neu+ Breast Cancer (TP2001-202)	Terminated	No Results Available	YES	apricoxib	-9.2	Drug: Apricoxib|Drug: Lapatinib|Drug: Capecitabine
Fulvestrant With or Without Lapatinib and/or Aromatase Inhibitor Therapy in Treating Postmenopausal Women With Metastatic Breast Cancer That Progressed After Previous Aromatase Inhibitor Therapy	Recruiting	No Results Available	YES	fulvestrant	-9.2	Drug: Anastrozole|Drug: Exemestane|Drug: Fulvestrant|Drug: Lapatinib ditosylate|Drug: Letrozole
Fulvestrant With or Without Lapatinib in Treating Postmenopausal Women With Stage III or Stage IV Breast Cancer That is Hormone Receptor-Positive	Active, not recruiting	No Results Available	YES	fulvestrant	-9.2	Drug: Lapatinib ditosylate|Drug: Fulvestrant
A Study of Lapatinib in Combination With Everolimus in Patients With Advanced, Triple Negative Breast Cancer	Recruiting	No Results Available	YES	everolimus	-9.1	Drug: Lapatinib|Drug: Everolimus
Study of How Well Letrozole Works in Combination With Lapatinib Followed by an Addition of Everolimus in Postmenopausal Women With Advanced Endocrine Resistant Breast Cancer	Recruiting	No Results Available	YES	everolimus	-9.1	Drug: Letrozole|Drug: Lapatinib|Drug: Everolimus
Lapatinib and RAD-001 for HER2 Positive Metastatic Breast Cancer	Recruiting	No Results Available	YES	RAD-001	-9.1	Drug: Lapatinib|Drug: RAD-001
Study Evaluating Neratinib Versus Lapatinib Plus Capecitabine For ErbB2 Positive Advanced Breast Cancer	Active, not recruiting	No Results Available	YES	neratinib	-9	Drug: Neratinib|Drug: Lapatinib|Drug: Capecitabine
Efficacy and Safety of BMS-690514 in Combination With Letrozole to Treat Metastatic Breast Cancer	Completed	No Results Available	YES	BMS-690514	-8.6	Drug: BMS-690514|Drug: Lapatinib|Drug: Letrozole
A Study to Examine the Effects of Esomeprazole on the Pharmacokinetics of Orally Administered Lapatinib in Subjects With Metastatic ErbB2 Positive Breast Cancer	Completed	No Results Available	YES	esomeprazole	-7.5	Drug: Lapatinib ditosylate|Drug: Esomeprazole
Phase II Neoadjuvant in Inflammatory Breast Cancer	Active, not recruiting	No Results Available	YES	TAXANE OR ANTHRACYCLINE		Drug: Lapatinib|Drug: Paclitaxel|Drug: 5-Fluorouracil|Drug: Epirubicin|Drug: Cyclophosphamide
Study Of Lapatinib In Combination With Paclitaxel In The Treatment Of Newly Diagnosed Inflammatory Breast Cancer	Completed	No Results Available	YES	TAXANE OR ANTHRACYCLINE		Drug: Lapatinib|Drug: Paclitaxel
Abraxane and Lapatinib in Treating Patients With Stage I, Stage II, or Stage III Breast Cancer	Active, not recruiting	No Results Available	YES	TAXANE OR ANTHRACYCLINE		Drug: Lapatinib ditosylate|Drug: Paclitaxel
Lapatinib and Epirubicin in Treating Patients With Metastatic Breast Cancer	Active, not recruiting	No Results Available	YES	TAXANE OR ANTHRACYCLINE		Drug: Epirubicin hydrochloride|Drug: Lapatinib ditosylate
Phase I/II Study of Neoadjuvant Lapatinib in Breast Cancer	Recruiting	No Results Available	YES	TAXANE OR ANTHRACYCLINE		Drug: Docetaxel|Drug: Lapatinib|Drug: Trastuzumab
Docetaxel, Carboplatin, and Trastuzumab and/or Lapatinib in Treating Women With Stage I, Stage II, or Stage III Breast Cancer That Can Be Removed by Surgery	Recruiting	No Results Available	YES	TAXANE OR ANTHRACYCLINE		Drug: Trastuzumab|Drug: Carboplatin|Drug: Docetaxel|Drug: Lapatinib ditosylate
Lapatinib in Combination With Docetaxel in Patients With HER-2 Positive Advanced or Metastatic Breast Cancer	Recruiting	No Results Available	YES	TAXANE OR ANTHRACYCLINE		Drug: Lapatinib|Drug: Docetaxel
Lapatinib Combined With Paclitaxel For Patients With First-Line ErbB2-Amplified Metastatic Breast Cancer	Active, not recruiting	No Results Available	YES	TAXANE OR ANTHRACYCLINE		Drug: Lapatinib|Drug: Paclitaxel
Chemotherapy and Lapatinib or Trastuzumab in Treating Women With HER2/Neu-Positive Metastatic Breast Cancer	Active, not recruiting	No Results Available	YES	TAXANE OR ANTHRACYCLINE		Drug: Trastuzumab|Drug: Docetaxel|Drug: Lapatinib ditosylate|Drug: Paclitaxe
A Study of AC Followed by a Combination of Paclitaxel Plus Trastuzumab or Lapatinib or Both Given Before Surgery to Patients With Operable HER2 Positive Invasive Breast Cance	Active, not recruiting	No Results Available	YES	TAXANE OR ANTHRACYCLINE		Drug: Doxorubicin|Drug: Cyclophosphamide|Drug: Paclitaxel|Drug: Trastuzumab|Drug: Lapatinib
Paclitaxel and Trastuzumab With or Without Lapatinib in Treating Patients With Stage II or Stage III Breast Cancer That Can Be Removed by Surgery	Active, not recruiting	No Results Available	YES	TAXANE OR ANTHRACYCLINE		Drug: Trastuzumab|Drug: Lapatinib ditosylate|Drug: Paclitaxel
Paclitaxel With / Without GW572016 (Lapatinib) As First Line Therapy For Women With Advanced Or Metastatic Breast Cancer	Completed	No Results Available	YES	TAXANE OR ANTHRACYCLINE		Drug: Paclitaxel|Drug: Lapatinib
Lapatinib Plus Caelyx in Patients With Advanced Metastatic Breast Cancer Following Failure of Trastuzumab Therapy	Active, not recruiting	No Results Available	YES	TAXANE OR ANTHRACYCLINE		Drug: Doxorubicin hydrochloride|Drug: Lapatinib
A Phase III Trials Program Exploring the Integration of Bevacizumab, Everolimus (RAD001), and Lapatinib Into Current Neoadjuvant Chemotherapy Regimes for Primary Breast Cance	Active, not recruiting	No Results Available	YES	TAXANE OR ANTHRACYCLINE		Drug: Epirubicin|Drug: Cyclophosphamide|Drug: Docetaxel|Drug: Epirubicin|Drug: Bevacizumab|Drug: Paclitaxel|Drug: Everolimus|Drug: Trastuzumat
Lapatinib and Doxorubicin Hydrochloride Liposome in Treating Patients With Metastatic Breast Cancer	Active, not recruiting	No Results Available	YES	TAXANE OR ANTHRACYCLINE		Drug: Lapatinib ditosylate|Drug: Doxil
Docetaxel, Carboplatin, Trastuzumab, and Lapatinib in Treating Patients With Early Stage Breast Cancer	Completed	No Results Available	YES	TAXANE OR ANTHRACYCLINE		Drug: Trastuzumab|Drug: Carboplatin|Drug: Docetaxel|Drug: Lapatinib ditosylate
Study In Women And Men With Metastatic Breast Cancer That Have Overexpression Of ErbB2	Active, not recruiting	Has Results	YES	TAXANE OR ANTHRACYCLINE		Drug: Lapatinib|Drug: Paclitaxel
Lapatinib In Combination With Chemotherapy In Subjects With Relapsed Breast Cancer	Terminated	Has Results	YES	TAXANE OR ANTHRACYCLINE		Drug: Lapatinib|Drug: Capecitabine|Drug: Docetaxel|Drug: nab-Paclitaxe
Doxorubicin and Cyclophosphamide Followed by Paclitaxel, Trastuzumab, and Lapatinib in Treating Patients With HER2/Neu-Overexpressed Breast Cance	Active, not recruiting	No Results Available	YES	TAXANE OR ANTHRACYCLINE		Drug: Trastuzumab|Drug: Cyclophosphamide|Drug: Doxorubicin hydrochloride|Drug: Lapatinib ditosylate|Drug: Paclitaxe
Trastuzumab and Cyclophosphamide Followed By Trastuzumab, Paclitaxel, and Lapatinib in Treating Patients With Early-Stage HER2-Positive Breast Cancer That Has Been Removed By Surger	Completed	No Results Available	YES	TAXANE OR ANTHRACYCLINE		Drug: Trastuzumab|Drug: Cyclophosphamide|Drug: Doxorubicin hydrochloride|Drug: Lapatinib ditosylate|Drug: Paclitaxe
Phase II Neoadjuvant Doxorubicin and Cyclophosphamide -> Docetaxel With Lapatinib in Stage II/III Her2Neu+ Breast Cancer	Completed	No Results Available	YES	TAXANE OR ANTHRACYCLINE		Drug: Lapatinib|Drug: Doxorubicin|Drug: Cyclophosphamide|Drug: Docetaxel|Drug: Pegfilgrastim|Drug: Filgrastim|Drug: Dexamethasone|Drug: Trastuz
A Phase II Neo-adjuvant Study Assessing TCH (Docetaxel, Carboplatin and Trastuzumab), TCL (Docetaxel, Carboplatin and Lapatinib) and the Combination of TCHL (Docetaxel,Carboplatin, Trastuzumab and Lapatinib) in HER-2 Positive Breast Cancer Patient	Recruiting	No Results Available	YES	TAXANE OR ANTHRACYCLINE		Drug: Docetaxel|Drug: Carboplatin|Drug: Trastuzumab|Drug: Lapatinib
ErbB2 Positive Metastatic Breast Cancer	Recruiting	No Results Available	YES	TAXANE OR ANTHRACYCLINE		Drug: Lapatinib|Drug: Lipo-Dox
A Randomized Study of TH Versus THL in First Line Treatment of HER2-positive Metastatic Breast Cance	Recruiting	No Results Available	YES	TAXANE OR ANTHRACYCLINE		Drug: Trastuzumab|Drug: Paclitaxel|Drug: Lapatinib
Study of Preoperative Weekly Paclitaxel and Carboplatin With Lapatinib (TykerbA®) in Patients With ErbB2-Positive Stage I-III Breast Cancer	Recruiting	No Results Available	YES	TAXANE OR ANTHRACYCLINE		Drug: Paclitaxel|Drug: Carboplatin|Drug: Lapatinib
Lapatinib/Carboplatin/Paclitaxel in Previously Treated Ovarian or Breast Cancer Patients	Completed	No Results Available	YES	TAXANE OR ANTHRACYCLINE		Drug: Lapatinib|Drug: Carboplatin|Drug: Paclitaxel
Preoperative Chemotherapy With Paclitaxel, Gemcitabine, and Lapatinib (TykerbA®) (PGT	Completed	No Results Available	YES	TAXANE OR ANTHRACYCLINE		Drug: Paclitaxel|Drug: Gemcitabine|Drug: Lapatinib
Primary Chemotherapy in Patients With HER2-positive Early Breast Cancer	Recruiting	No Results Available	YES	TAXANE OR ANTHRACYCLINE		Drug: Lapatinib
DETECT III - A Multicenter, Phase III Study to Compare Standard Therapy +/- Lapatinib in HER2-ve MBC-Patients With HER2+ve CTCs	Recruiting	No Results Available	YES	TAXANE OR ANTHRACYCLINE		Drug: Docetaxel|Drug: Paclitaxel|Drug: Vinorelbine|Drug: Capecitabine|Drug: Doxorubicin|Drug: Anastrozole|Drug: Letrozole|Drug: Exemestane|Drug:
Trastuzumab Versus Lapatinib as Neoadjuvant Treatment for Her2+ Patients	Active, not recruiting	No Results Available	YES	TAXANE OR ANTHRACYCLINE		Drug: Epirubicin|Drug: Cyclophosphamide|Drug: Taxotere|Drug: Herceptin|Drug: Lapatinib
The Myocet/Lapatinib Study	Recruiting	No Results Available	YES	TAXANE OR ANTHRACYCLINE		Drug: Myocet|Drug: Lapatinib
Lapatinib and Paclitaxel in Treating Patients With Advanced Solid Tumors	Active, not recruiting	No Results Available	YES	TAXANE OR ANTHRACYCLINE		Drug: Lapatinib ditosylate|Drug: Paclitaxel
GW572016 With Docetaxel and Trastuzumab for the Treatment Of Untreated ErbB2 Over-Expressing Metastatic Breast Cancer	Active, not recruiting	No Results Available	YES	TAXANE OR ANTHRACYCLINE		Drug: Lapatinib|Drug: Docetaxel|Drug: Trastuzumab
ErbB2 Over-expressing Metastatic Breast Cancer Study Using Paclitaxel, Trastuzumab, and Lapatinib	Active, not recruiting	No Results Available	YES	TAXANE OR ANTHRACYCLINE		Drug: Lapatinib|Drug: Paclitaxel|Drug: Trastuzumab
Combination Of Lapatinib With Carboplatin, Paclitaxel and Trastuzumab In Metastatic Breast Cancer	Active, not recruiting	No Results Available	YES	TAXANE OR ANTHRACYCLINE		Drug: Lapatinib|Drug: Carboplatin|Drug: Trastuzumab|Drug: Paclitaxel
Lapatinib or Trastuzumab Given Prior to Surgery With Chemotherapy in Patients With Early Breast Cancer	Withdrawn	No Results Available	YES	TAXANE OR ANTHRACYCLINE		Drug: Lapatinib|Drug: Trastuzumab|Drug: Epirubicin|Drug: Cyclophosphamide|Drug: Paclitaxel
A Phase II, Randomized, Open-label Study of Lapatinib Plus Chemotherapy Versus Trastuzumab Plus Chemotherapy in HER2-positive and p95HER2-positive Metastatic Breast Cancer	Not yet recruiting	No Results Available	YES	TAXANE OR ANTHRACYCLINE		Drug: Lapatinib|Drug: Trastuzumab|Drug: Docetaxel|Drug: Paclitaxel|Drug: Vinorelbine
Neoadjuvant Study With Chemotherapy, Lapatinib And Trastuzumab In Breast Cancer	Completed	No Results Available	YES	TAXANE OR ANTHRACYCLINE		Drug: Lapatinib|Drug: Trastuzumab|Drug: Paclitaxel|Drug: Fluorouracil|Drug: Epidoxorubicin|Drug: Cyclophosphamide
Lapatinib +/- Trastuzumab In Addition To Standard Neoadjuvant Breast Cancer Therapy	Active, not recruiting	Has Results	YES	TAXANE OR ANTHRACYCLINE		Drug: Trastuzumab|Drug: Paclitaxel|Drug: FEC75|Drug: Lapatinib
Addition of Carboplatin to Neoadjuvant Therapy for Triple-negative and HER2-positive Early Breast Cance	Recruiting	No Results Available	YES	TAXANE OR ANTHRACYCLINE		Drug: Carboplatin|Drug: Paclitaxel|Drug: Doxorubicin|Drug: Trastuzumab|Drug: Bevacizumab|Drug:
Neo ALTTO (Neoadjuvant Lapatinib and/or Trastuzumab Treatment Optimisation) Study	Active, not recruiting	Has Results	YES	TAXANE OR ANTHRACYCLINE		Drug: Lapatinib|Drug: Trastuzumab|Drug: Paclitaxel
Phase II Lapatinib Plus Nab-Paclitaxel As First And Second Line Therapy In her2+ MBC	Active, not recruiting	Has Results	YES	TAXANE OR ANTHRACYCLINE		Drug: Lapatinib|Drug: nab-Paclitaxel
Phase I/II Study of Lapatinib in Combination With Paclitaxel as 1L Chemotherapy for ErbB2-positive MBC	Active, not recruiting	No Results Available	YES	TAXANE OR ANTHRACYCLINE		Drug: Lapatinib|Drug: Paclitaxel
Continuation Study of Lapatinib Monotherapy or Lapatinib in Combination With Other Anti-cancer Agents	Recruiting	No Results Available	YES	TAXANE OR ANTHRACYCLINE		Drug: Lapatinib|Drug: Paclitaxel|Drug: Letrozole|Drug: Capecitabine|Drug: Oxaliplatin|Drug: Gemcitabine|Drug: Docetaxel|Drug: Trastuzumab|Drug: Le
Pazopanib (VOTRIENT) Plus Paclitaxel (TAXOL), Pazopanib Plus Paclitaxel (TAXOL) Plus Carboplatin (PARAPLATIN), and Pazopanib Plus Paclitaxel (TAXOL) Plus Lapatinib (TYKERB	Completed	No Results Available	YES	TAXANE OR ANTHRACYCLINE		Drug: Pazopanib|Drug: Lapatinib|Drug: Paclitaxel|Drug: Carboplatin

Journal of Pharmacokinetics and Pharmacodynamics

Incorporation of ABCB1-Mediated Transport into a Physiologically-Based Pharmacokinetic Model of Docetaxel in Mice

--Manuscript Draft--

Manuscript Number:	
Full Title:	Incorporation of ABCB1-Mediated Transport into a Physiologically-Based Pharmacokinetic Model of Docetaxel in Mice
Article Type:	Original Article
Keywords:	docetaxel; ABCB1; MDR1; PGP; physiologically-based pharmacokinetic modeling
Corresponding Author:	Susan Hudachek Colorado State University Fort Collins, UNITED STATES
Corresponding Author Secondary Information:	
Corresponding Author's Institution:	Colorado State University
Corresponding Author's Secondary Institution:	
First Author:	Susan Hudachek
First Author Secondary Information:	
Order of Authors:	Susan Hudachek
	Daniel Gustafson
Order of Authors Secondary Information:	
Abstract:	Docetaxel is one of the most widely used anticancer agents. While this taxane has proven to be an effective chemotherapeutic drug, noteworthy challenges exist in relation to docetaxel administration due to the considerable interindividual variability in efficacy and toxicity associated with the use of this compound, largely attributable to differences between individuals in their ability to metabolize and eliminate docetaxel. Regarding the latter, the ATP-binding cassette transporter B1 (ABCB1, PGP, MDR1) is primarily responsible for docetaxel elimination. To further understand the role of ABCB1 in the biodistribution of docetaxel in mice, we utilized physiologically-based pharmacokinetic (PBPK) modeling that included ABCB1-mediated transport in relevant tissues. Transporter function was evaluated by studying docetaxel pharmacokinetics in wild-type FVB and Mdr1a/b constitutive knockout (KO) mice and incorporating this concentration-time data into a PBPK model comprised of eight tissue compartments (plasma, brain, heart, lung, kidney, intestine, liver and slowly perfused tissues) and, in addition to ABCB1-mediated transport, included intravenous drug administration, specific binding to intracellular tubulin, intestinal and hepatic metabolism, glomerular filtration and tubular reabsorption. For all tissues in both the FVB and KO cohorts, the PBPK model simulations closely mirrored the observed data. Furthermore, both models predicted AUC values that were with 15% of the observed AUC values, indicating that our model-simulated drug exposures accurately reflected the observed tissue exposures. Overall, our PBPK model furthers the understanding of the role of ABCB1 in the biodistribution of docetaxel. Additionally, this exemplary model structure can be applied to investigate the pharmacokinetics of other ABCB1 transporter substrates.
Opposed Reviewers:	

Title: Incorporation of ABCB1-Mediated Transport into a Physiologically-Based Pharmacokinetic Model of Docetaxel in Mice

Authors: Susan F. Hudachek and Daniel L. Gustafson

Affiliations: Flint Animal Cancer Center, Department of Clinical Sciences, Colorado State University, Fort Collins, Colorado

Keywords: docetaxel; ABCB1; MDR1; PGP; physiologically-based pharmacokinetic modeling

Corresponding Author:

Daniel L Gustafson

Address: 1678 Campus Delivery, Fort Collins CO, 80523

Phone: (970) 297-1278

Email: Daniel.Gustafson@colostate.edu

Abstract:

Docetaxel is one of the most widely used anticancer agents. While this taxane has proven to be an effective chemotherapeutic drug, noteworthy challenges exist in relation to docetaxel administration due to the considerable interindividual variability in efficacy and toxicity associated with the use of this compound, largely attributable to differences between individuals in their ability to metabolize and eliminate docetaxel. Regarding the latter, the ATP-binding cassette transporter B1 (ABCB1, PGP, MDR1) is primarily responsible for docetaxel elimination. To further understand the role of ABCB1 in the biodistribution of docetaxel in mice, we utilized physiologically-based pharmacokinetic (PBPK) modeling that included ABCB1-mediated transport in relevant tissues. Transporter function was evaluated by studying docetaxel pharmacokinetics in wild-type FVB and Mdr1a/b constitutive knockout (KO) mice and incorporating this concentration-time data into a PBPK model comprised of eight tissue compartments (plasma, brain, heart, lung, kidney, intestine, liver and slowly perfused tissues) and, in addition to ABCB1-mediated transport, included intravenous drug administration, specific binding to intracellular tubulin, intestinal and hepatic metabolism, glomerular filtration and tubular reabsorption. For all tissues in both the FVB and KO cohorts, the PBPK model simulations closely mirrored the observed data. Furthermore, both models predicted AUC values that were with 15% of the observed AUC values, indicating that our model-simulated drug exposures accurately reflected the observed tissue exposures. Overall, our PBPK model furthers the understanding of the role of ABCB1 in the biodistribution of docetaxel. Additionally, this exemplary model structure can be applied to investigate the pharmacokinetics of other ABCB1 transporter substrates.

Introduction:

Docetaxel (Taxotere®) is one of the most widely used anticancer agents. This compound, the first semisynthetic taxoid, was initially approved for use in 1996 for the treatment of metastatic breast cancer. Since then, docetaxel has been approved for a variety of indications, including common cancers such as breast, prostate and lung, as well as less common malignancies, such as gastric and head and neck cancer. While this taxane has proven to be an effective chemotherapeutic drug, noteworthy challenges exist in relation to docetaxel administration due to the considerable interindividual variability in efficacy and toxicity associated with the use of this agent [1]. The pharmacokinetic and pharmacodynamic variability of docetaxel is largely attributable to differences between individuals in their ability to metabolize and eliminate this compound. Docetaxel metabolism is primarily through the cytochrome P450 family member CYP3A4 and the ATP-binding cassette transporter B1 (ABCB1, PGP, MDR1) is responsible for elimination [2-4].

ABCB1 is a membrane-localized, energy-dependent drug efflux ATP-binding cassette (ABC) transporter with very broad substrate specificity. In mice, there are two genes that encode drug-transporting ABCB1, namely mdr1a and mdr1b [5-7]. The mouse mdr1a gene is predominantly expressed in intestine, liver, and blood capillaries of brain and testis whereas the mdr1b gene is principally found in the adrenal gland, placenta, ovaries and pregnant uterus [8]. Both mdr1a and mdr1b are expressed in the kidney [8]. In contrast, humans have only one isoform of ABCB1, which is prominent in the brush border of renal proximal tubules, in the biliary membrane of hepatocytes, in the apical membrane of mucosal cells in the intestine, in capillary endothelial cells of the brain and testis, in the adrenal gland and in placental trophoblasts [9-11]. In both mice and humans, ABCB1 functions to export xenobiotic compounds into the urine, bile and intestinal lumen and to prevent the accumulation of toxic agents in tissues such as the

brain, testis and placenta. Additionally, expression of ABCB1 in tumor cells is known to confer drug resistance by pumping anticancer drugs out of the cell [12, 13].

To further understand the role of ABCB1 in the biodistribution of docetaxel in mice, we utilized physiologically-based pharmacokinetic (PBPK) modeling in mice that included ABCB1-mediated transport in relevant tissues. This type of pharmacologic modeling is a useful tool that facilitates the prediction of target tissue drug concentrations by incorporating mathematical descriptions of the uptake and disposition of chemicals based on quantitative interrelations among the critical determinants of physiological processes (i.e., absorption, distribution, metabolism and excretion) [14]. Accordingly, PBPK models are comprised of compartments corresponding to discrete tissues or groupings of tissues with appropriate volumes, blood flows, and pathways for xenobiotic clearance including pertinent biochemical and physiochemical constants [15]. Each compartment in the model is described with a mass-balance differential equation whose terms mathematically represent biological processes; the set of equations is then solved by numerical integration to simulate tissue time-course concentrations of chemicals and their metabolites [15]. The value of PBPK modeling is becoming increasingly apparent and this approach is now intensively used throughout the process of drug discovery and development [16, 17].

The PBPK model of docetaxel presented herein is comprised of eight tissue compartments (plasma, brain, heart, lung, kidney, intestine, liver and slowly perfused tissues) and, in addition to ABCB1-mediated transport, incorporates intravenous drug administration, specific binding to intracellular tubulin, intestinal and hepatic metabolism, glomerular filtration and tubular reabsorption. To evaluate the contribution of ABCB1 to the biodistribution of docetaxel, wild-type FVB and Mdr1a/b constitutive knockout (KO) mice were studied [18].

Materials and Methods:

Chemicals

Docetaxel (Winthrop U.S.) was acquired from the University of Colorado Hospital Pharmacy. All other reagents were of analytical grade.

Animals

Five to six-week-old female FVB mice and four to eight-week-old female Mdr1a/b constitutive knockout (KO) mice were purchased from Taconic. Animals were housed in polycarbonate cages and kept on a 12 hr light/dark cycle. Food and water were given *ad libitum*. Upon arrival, mice acclimated for a minimum of seven days prior to any experimentation. All experimental procedures were approved by Colorado State University's Animal Care and Use Committee and the Department of Defense US Army Medical Research and Material Command (USAMRMC) Animal Care and Use Review Office (ACURO).

Docetaxel pharmacokinetic studies in mice

A time course tissue and feces distribution study of docetaxel was conducted in both FVB and KO mice. Docetaxel was acquired as an initial solution of 20 mg/mL in 50/50 (v/v) ratio polysorbate 80/dehydrated alcohol, further diluted to a solution of 0.6 mg/mL in 0.9% sodium chloride and administered via intravenous tail vein injection as a single bolus dose of 3 mg/kg. Subsequently, three mice from each cohort were sacrificed at 1, 2, 4, 8 and 12 hrs post docetaxel injection by cardiac stick exsanguination under isoflurane anesthesia. Plasma, brain, liver, proximal small intestine, kidney, heart, and lung tissue were immediately collected, rinsed with phosphate buffered saline, frozen in liquid nitrogen and stored at -80°C until analysis. Feces was collected from the mice sacrificed at 12 hrs. For this purpose, mice from each cohort (n = 3) were housed together and the pooled feces were collected for the duration of the study.

In addition, feces below the cecum were also collected upon sacrifice. All fecal samples were stored at -80°C until analysis.

Docetaxel high-pressure liquid chromatography-tandem mass spectrometry analysis

Analysis of docetaxel in plasma and tissues was done using high-pressure liquid chromatography-tandem mass spectrometry (HPLC/MS/MS) analysis based on a method previously developed in our laboratory [19, 20] modified as follows. Briefly, docetaxel was extracted from plasma by adding 1000 µL of ethyl acetate to 100 µL of unknown sample plasma, vortexing for 10 min and centrifuging at 18,000 x g for 10 min at 4°C. 800 µL of the organic phase was collected and evaporated to dryness using a rotary evaporator. Dried samples were reconstituted in 200 µL of 80/20 0.1% formic acid in water/acetonitrile, vortexed for 10 min and centrifuged at 18,000 x g for 10 min at 4°C. An aliquot of 60 µL of the supernatant was injected into the LC/MS/MS system for analysis.

Tissues were homogenized at 100 mg/mL in water and 100 µL of the homogenate was extracted using the method for plasma detailed above. Fecal samples were lyophilized and drug was extracted by homogenizing the lyophilized feces at 25 mg/mL in ethyl acetate. 1000 µL of this feces mixture was then analyzed using the method for plasma and tissues illustrated above. Standards and quality control samples were prepared in the appropriate matrix and analyzed as described above.

The HPLC system consisted of an Agilent 1200 Series binary pump SL, vacuum degasser, thermostatted column compartment SL (Agilent Technologies, Santa Clara, CA, USA) and a CTC Analytics HTC PAL System autosampler (Leap Technologies, Carrboro, NC, USA). The HPLC column was a Waters Sunfire C8 column (2.1 × 150 mm I.D., 5.0 µm bead size) (Waters Corporation, Milford, MA, USA) protected by a SecurityGuard™ C18 cartridge (4 × 2.0 mm I.D.) (Phenomenex, Torrance, CA, USA) and maintained at room temperature. The mobile

phase consisted of an aqueous component (A) of 0.1% formic acid in Milli-Q water and an organic component (B) of acetonitrile. The 4.0 min run consisted of the following linear gradient elution: 50% A and 50% B at 0 min, 50% A and 50% B at 0.5 min, 2% A and 98% B at 1.25 min, 2% A and 98% B at 3.0 min, 50% A and 50% B at 3.5 min and 50% A and 50% B at 4.0 min. The system operated at a flow-rate of 0.5 mL/min.

Mass spectrometric detection was performed on an API 3200™ triple quadrupole instrument (Applied Biosystems Inc, Foster City, CA, USA) using multiple reaction monitoring (MRM). Ions were generated in positive ionization mode using an electrospray interface. Docetaxel compound-dependent parameters were as follows: declustering potential (DP): 21 V; entrance potential (EP): 4.5 V; collision cell entrance potential (CEP): 71 V; collision energy (CE): 23 V and collision cell exit potential (CXP): 3.5 V. Source-dependent parameters were as follows: nebulizer gas (GS1): 40 psi; auxiliary (turbo) gas (GS2): 60 psi; turbo gas temperature (TEM): 400°C; curtain gas (CUR): 30 psi; collision-activated dissociation (CAD) gas (nitrogen): 2 psi; ionspray voltage (IS): 4500 V and interface heater (IH): 400°C. Peak areas obtained from MRM of docetaxel (*m/z* 808.5 → 226) were used for quantification.

Pharmacokinetic Analysis

Pharmacokinetic parameters were calculated using noncompartmental modeling performed with Microsoft Excel and standard equations for noncompartmental analysis.

PBPK model development

A PBPK model for docetaxel was developed based on a model previously described by Bradshaw-Pierce et al. [19]. The modified model presented herein incorporated intravenous drug administration, specific binding to intracellular tubulin, ABCB1 transport, intestinal and hepatic metabolism, glomerular filtration and tubular reabsorption. This flow-limited model was

comprised of eight tissue compartments: plasma, brain, heart, lung, kidney, intestine, liver and slowly perfused tissues.

Physiological parameters (tissue volumes and tissue blood flows) were obtained from Brown et al.[21].

The value used for the unbound fraction of docetaxel in the blood was 0.07, as docetaxel is highly bound (93%) to plasma proteins [22]. The arterial blood drug concentration available to all tissues was considered to be the unbound docetaxel concentration in the blood.

Tissue:plasma partition coefficients were determined by parameter estimation, optimizing the fit for both the FVB and KO observed plasma and tissue concentrations.

The tubulin binding capacity for colchicine in various tissues was determined by Wierzba et al. [23]. These values were used in the present work for docetaxel tubulin binding capacities in the represented tissues (with the exception of the slowly perfused tissue tubulin binding capacity, which was determined by parameter estimation), as both colchicine and docetaxel bind to assembled tubulin with a stoichiometry of one mole ligand per one mole αβ subunit [23, 24].

For docetaxel tubulin binding affinity (Kd), the number used in our PBPK model was 19 nM. This value was derived from data indicating that paclitaxel (a structurally similar compound) binds reversibly to microtubules reassembled *in vitro* with high affinity (Kd of 10 nM) whereas the binding affinity for docetaxel, which is slightly more water soluble, is approximately 1.9-fold higher [24, 25].

The fraction of kidney blood flow filtered at the glomerulus was calculated using a glomerular filtration rate of 0.405 mL/min and 0.275 mL/min in FVB and KO mice, respectively [26]. Assuming that 9.1% of the cardiac output goes to the kidneys [21], 26.5% and 18.7% of the kidney blood flow is filtered at the glomerulus in FVB and KO mice, respectively.

The first-order rate constant for tubular reabsorption in the FVB mouse model was determined by parameter estimation, optimizing the fit for the FVB observed plasma and tissue concentrations. For the KO mouse model, the first-order rate constant for tubular reabsorption was also determined by parameter estimation, optimizing the fit for the KO observed plasma and tissue concentrations.

The first-order rate constant for hepatic CYP3A4 metabolism was determined by parameter estimation, optimizing the fit for both the FVB and KO observed plasma and tissue concentrations.

To describe intestinal CYP3A4 metabolism, a first-order rate constant was used for the FVB mouse model. This value was determined by parameter estimation, optimizing the fit for the FVB observed plasma and tissue concentrations.

For the KO mouse model, Michaelis-Menten kinetics were used to describe saturable intestinal CYP3A4 metabolism. The K_m and V_{max} values for CYP3A4 metabolism of docetaxel to an alcohol docetaxel (M2, resulting from oxidation of the *tert*-butyl ester side group) were obtained from van Herwaarden et al. [27]. From this work, the K_m was determined to be 600 nM. The reported V_{max} was 14 pmol/min/mg microsomal protein. This *in vitro* number was scaled for use *in vivo* by converting mg of microsomal protein to grams of intestine (3.16 mg intestinal microsomal protein/g intestine [28]) and correcting units for compatibility with the model, resulting in a V_{max} value of 2654 nM/hr.

ABCB1 transport was described as a saturable process in the lung, kidney, heart, brain and slowly perfused tissue compartments. The K_m and V_{max} values were determined by parameter estimation, optimizing the fit for the FVB observed plasma and tissue concentrations.

PBPK model equations

The rate of change of the amount of drug in a generic tissue compartment with ABCB1 transport and drug metabolism is as follows:

$$\frac{dA_T}{dt} = \left(Q_T \times \left(C_A - C_{VT}\right)\right) - dA_{PGP} - dA_{MET}$$

where A_T is the amount of drug in the tissue compartment, t is time, Q_T is the blood flow to the tissue compartment, C_A is the arterial blood drug concentration entering the tissue compartment, C_{VT} is the venous blood drug concentration exiting the tissue compartment, A_{PGP} is the amount of drug transported out of the tissue compartment by ABCB1 and A_{MET} is the amount of drug metabolized in the tissue compartment.

The rate of change of the amount of drug transported out of the tissue compartment by ABCB1 is as follows:

$$\frac{dA_{PGP}}{dt} = \left(Vmax_T \times C_{VT}\right) \Big/ \left(KM_T + C_{VT}\right)$$

where $Vmax_T$ is the maximum velocity of ABCB1 transport out of the tissue compartment and KM_T is the Michaelis-Menten constant (K_m) for ABCB1 transport out of the tissue compartment.

The rate of change of the amount of drug metabolized by a first order reaction in the tissue compartment is as follows:

$$\frac{dA_{MET}}{dt} = k \times C_{VT} \times V_T$$

where k is a first-order rate constant and V_T is the volume of the tissue compartment.

The rate of change of the amount of drug metabolized by a saturable reaction in the tissue compartment is as follows:

$$\frac{dA_{MET}}{dt} = \left(Vmax_M \times C_{VT}\right) \Big/ \left(KM_M + C_{VT}\right)$$

where $Vmax_M$ is the maximum velocity of metabolism and KM_M is the Michaelis-Menten constant (K_m) for metabolism.

Assuming venous equilibration and specific tubulin binding, the drug concentration in the venous blood is:

$$C_{VT} = C_T \Big/ \left(\left(P_T \times fu \right) + \left(TBC_T / \left(TBA + C_{VT} \right) \right) \right)$$

where C_T is the concentration of drug in the tissue compartment, P_T is the tissue:plasma partition coefficient, fu is the unbound fraction of drug in the blood, TBC_T is the tubulin binding capacity of the tissue compartment and TBA is the tubulin binding affinity.

Assuming the volume of the tissue is constant, the drug concentration in the tissue is:

$$\frac{dC_T}{dt} = A_T / V_T$$

Computer Simulation

For PBPK modeling, acslX Libero version 3.0.2.1 (The AEgis Technologies Group, Inc.) was used.

Statistical Analysis

Statistical analysis was performed using GraphPad Prism v5.01 (GraphPad Software, San Diego, California). For the comparison of concentration means, two-tailed unpaired *t*-tests were used.

Sensitivity Analysis

A normalized sensitivity analysis was performed as described in Loccisano et al. [29] to assess the influence of each PBPK model parameter on the simulated plasma area under the concentration-time curve (AUC) for the FVB mouse model. Briefly, sensitivity coefficients were calculated with the original parameters and for those resulting from a 1% change in each

parameter value. The following equation was used to calculate the normalized sensitivity coefficient (SC):

$$SC = \frac{(A-B)/B}{(C-D)/D}$$

where A is the AUC resulting from the 1% increase in the parameter value, B is the AUC resulting from the original parameter value, C is the parameter value increased by 1% and D is the original parameter value.

Results:

Docetaxel pharmacokinetics in FVB and KO mice

A time course biodistribution study of docetaxel was conducted in female FVB and KO mice. Plasma and tissue concentrations were measured 1, 2, 4, 8 and 12 hrs after a single intravenous bolus dose of 3 mg/kg. In addition, total unchanged docetaxel excreted in the feces was determined for the duration of the pharmacokinetic study (12 hrs).

Following docetaxel administration, there was a statistically significant increase in the concentration of docetaxel at 2, 4, 8 and 12 hours in the lung, kidney, heart, intestine and brain of the KO versus FVB mice (Figure 1). Additionally, a statistically significant increase was observed in the lung and brain tissue of KO versus FVB mice at 1 hour post injection. Conversely, we did not note differences in docetaxel plasma concentrations between FVB and KO mice during the study. Furthermore, liver concentrations did not vary significantly between KO and FVB mice except at 12 hrs, when there was a 59% increase in the docetaxel concentration in the liver of the KO versus FVB mice.

In terms of exposure, the loss of ABCB1 transporter function in the KO mice resulted in increased exposure (AUC) in all tissues with the exception of plasma (Table 1). These increases ranged from a modest 6% in liver to a profound 444% in brain.

Docetaxel PBPK model simulations in FVB and KO mice

PBPK model development was based on the concentration-time data from docetaxel pharmacokinetic studies in FVB and KO mice. A schematic representation of the model is shown in Figure 2. Values of the parameters used in this model were both mined from the literature when available and fitted to the observed plasma and tissue concentrations from the pharmacokinetic studies. As detailed in the Materials and Methods, data collected from previous work included tissue volumes and tissue blood flows, fraction of docetaxel bound to plasma proteins, tubulin binding capacities, tubulin binding affinity, glomerular filtration rate, and K_m and V_{max} values for intestinal metabolism in KO mice. Also described in the Materials and Methods, values determined by parameter estimation were tissue:plasma partition coefficients, the first-order rate constant for hepatic metabolism, the first-order rate constant for intestinal metabolism in FVB mice, the first-order rate constants for tubular reabsorption and K_m and V_{max} values for ABCB1 transport. All parameter values are listed in Table 2.

Notably, different enzyme kinetics were used to describe intestinal metabolism in the FVB and KO mouse models. In the FVB mouse model, we represented CYP3A4 intestinal metabolism as a first-order process. Although the total amount of CYP3A in the intestine of mice is only ~2% of that present in the liver [30] and, thus, is likely saturable at relatively low concentrations of substrate, a possible synergistic action of intestinal ABCB1 and CYP3A has been suggested that prevents enzyme saturation. Firstly, according to this mechanism, ABCB1 functions to lower the intracellular enterocyte concentration of a substrate, thereby precluding saturation of CYP3A by maintaining the substrate concentration within the linear range of the CYP3A metabolizing capacity; consequently, a larger fraction of the intracellular substrate is metabolized and overall intestinal metabolism is increased [31]. Second, the export function of ABCB1 combined with subsequent drug re-uptake results in repeated and therefore prolonged

exposure of the substrate to enterocyte CYP3A, thereby increasing the probability that the substrate will be metabolized; this repeated cycling of substrate increases total metabolism, regardless of saturating or nonsaturating CYP3A kinetics [32]. Conceptually, these complex processes were incorporated into the present PBPK model with consideration for the principle of parsimony. Overall, the collective effect of the proposed synergism between intestinal ABCB1 and CYP3A is to increase intestinal metabolism. Thus, in the FVB mouse model, we eliminated ABCB1 transport out of the intestine and added compensatory first-order (nonstaurable) intestinal CYP3A metabolism kinetics. In the KO mouse model, this synergism is absent because these mice lack ABCB1; therefore, intestinal CYP3A metabolism was described by saturation (Michaelis-Menten) kinetics.

In our FVB mouse model, we also considered ABCB1 transport out of the liver to be negligible and, consequently, set the V_{max} value for hepatic ABCB1 transport to zero. By setting this value to zero, we simplified complex processes for the purpose of modeling. Physiologically, while ABCB1 transporters are present in the liver, it is likely that a relatively small amount of docetaxel is actually exported because the majority of this drug is metabolized by CYP3A prior to interacting with ABCB1. An insignificant role for ABCB1 transport of docetaxel into the bile is evidence by cannulated gallbladder studies, in which equivalent amounts of unchanged docetaxel (3-4% of the dose) were recovered in the bile of both FVB and KO mice following intravenous drug administration [33]. Similar results were observed after paclitaxel administration; in cannulated gallbladder studies, biliary excretion of unchanged paclitaxel did not differ between FVB and KO mice (5.9 and 5.2% of the dose, respectively) [18]. Hepatic ABCB1 transport is likely minimal for the taxanes because these compounds are extensively metabolized by CYP3A4 in the liver.

Correspondingly, with our FVB mouse model void of intestinal ABCB1 transport into the lumen and hepatic ABCB1 transport into the bile, the first-order rate constant for enterohepatic

recycling was zero, as the model did not allow for transport of docetaxel into the lumen. As a consequence, neither the FVB nor the KO model predicted any fecal elimination of docetaxel. This reflected our observed unchanged docetaxel recovered in the feces, which was less than 1.5% of the administered dose in both cohorts of mice.

The concentration-time profiles of docetaxel in plasma, lung, kidney, heart, liver, intestine and brain and the resulting PBPK model simulations are shown in Figure 3. For all tissues in both the FVB and KO cohorts, the PBPK model simulations closely mirrored the observed data.

Regarding docetaxel metabolism, 77% and 80% of the administered dose was metabolized according to the FVB and KO PBPK model simulations, respectively. The PBPK model predicted that the liver and intestine metabolized 69 and 8 percent, respectively, in the FVB mice. Conversely, in the KO mice, the intestine only metabolized 2% of the dose while the liver metabolized 78% (Figure 3).

The PBPK model-predicted AUCs were compared with the observed AUCs for both the FVB and KO mouse cohorts (Table 1). For this comparison, the percent difference between the observed and predicted values was calculated (Table 1). The FVB mouse model AUC predictions were all within 10% of the observed AUCs, except for the predicted heart AUC, which was 11.3% less than the observed AUC. For the KO mouse model, all predicted AUCs were less than 5.2% different from the observed AUCs with the exception of plasma and brain AUCs, which were both 14.8% greater than the observed AUCs. Overall, both models predicted AUC values that were with 15% of the observed AUC values, indicating that our model-simulated drug exposures accurately reflected the observed exposure in lung, kidney, heart, liver, intestine, plasma and brain.

Sensitivity Analysis

The normalized sensitivity coefficients for the FVB mouse PBPK model with respect to plasma AUC are shown in Fig. 4. Only parameters with sensitivity coefficients greater than 0.01 are shown. In this model, no normalized sensitivity coefficient was greater than 0.6, indicating that there are no amplified parameter errors.

Discussion:

PBPK models have been developed for numerous antineoplastic agents including methotrexate [34-36], cisplatin [37], actinomycin-D [38], 5-fluorouracil [39], capecitabine [40], 1-β-D-arabinofuranosylcytosine [41], adriamycin [42-44], topotecan [45] and docetaxel [19]. The need for these types of pharmacokinetic models for chemotherapeutics is great because of the challenges presented by this class of pharmaceutical compounds, specifically the narrow therapeutic index that is governed by drug distribution in the body. With PBPK modeling, the dynamics of drug distribution can be predicted using basic information on physiochemical properties, transport, biotransformation and excretion, thus leading to a better understanding of target tissue exposure resulting in either a therapeutic or toxic effect.

For use in PBPK model development, the role of ABCB1 in the biodistribution of docetaxel was evaluated by studying the differences in the plasma and tissue concentrations between wild-type FVB and Mdr1a/b constitutive knockout (KO) mice. Our work showed that docetaxel exposure increased by at least 100% in the lung, intestine and brain of the ABCB1 deficient KO mice versus the wild-type mice. In contrast, plasma and liver exposure to docetaxel remained relatively unchanged between the two cohorts. These results compare closely with a similar experiment done by Kemper et al. [46], in which a statistically significant increase in exposure was found in the brain and lungs but not in the plasma or liver of KO versus FVB mice. In both studies, the largest increase in docetaxel exposure was observed in the brain (+444% and +516% in the former and latter work, respectively).

By integrating the FVB and KO mouse tissue distribution data into a PBPK model, we were able to effectively predict docetaxel concentrations in plasma, brain, heart, lung, kidney, intestine, liver and slowly perfused tissues after an intravenous dose of 3 mg/kg. To include ABCB1 transport and metabolism into our PBPK models, we considered the lumen-to-enterocyte recycling process (the entry and exit of a compound across the intestinal epithelium multiple times which leads to in an increase in drug residency time within the enterocyte) [47-49]. The results from the development of a PBPK model which incorporated CYP3A metabolism and ABCB1 transport for the prediction of intestinal drug absorption support the notion of a drug 'cycling' effect that ABCB1 efflux imposes on the intestine which causes enhanced drug metabolism [48]. This PBPK model used seven luminal compartments to represent the small intestine wherein each luminal compartment was associated with a unique enterocyte compartment, with no transit of drug between adjacent enterocyte compartments. Additionally, each luminal compartment was assigned a unique ABCB1 abundance factor, CYP3A4 abundance factor, transit rate constant, absorption rate constant and basolateral to apical transfer rate constant. As docetaxel-specific rate constants necessary for the implementation of this segmented intestinal model are not yet available, we simplified the lumen-to-enterocyte recycling phenomenon in our model by eliminating ABCB1 transport out of the intestine in the wild-type mice and, as compensation, representing intestinal metabolism as a first-order, nonsaturable process. In our KO mouse model, lumen-to-enterocyte recycling is nonexistent, as these mice lack ABCB1. Thus, KO mice do not demonstrate a compensatory increase in intestinal metabolism and, consequently, CYP3A4 metabolism in the intestine was described by saturation kinetics in this cohort.

By permitting first-order intestinal metabolism in the FVB mouse model, the predicted amount of docetaxel metabolized in the intestine was 8% whereas the liver was responsible for metabolizing 69% of the administered dose. Physiologically, these numbers are relevant as

evidenced by a study in which CYP3A4-transgenic mice were generated that either expressed CYP3A4 in the intestine or in the liver [27]. Mice with CYP3A4 expression in only the intestine were able to clear 21% of the docetaxel cleared from the plasma by wild-type mice. Additionally, in these transgenic mice with no CYP3A4 expression in the liver, 13.5% of docetaxel metabolites M1-4 were recovered in the small intestine relative to wild-type mice. Thus, this data demonstrates that the intestine alone is capable of metabolizing a significant amount of docetaxel and our FVB mouse model-simulated value of 8% is physiologically plausible.

Our KO mouse model does not incorporate ABCB1 transport and the consequent lumen-to-enterocyte recycling process; therefore, with saturable (Michaelis-Menten) intestinal metabolism kinetics, the intestine was predicted to only metabolize 2.6% of the docetaxel metabolized by the liver in these mice. This value is in accordance with the total amount of CYP3A present in the intestine of mice, which is only ~2% of that present in the liver [30].

Overall, our pharmacokinetic study and PBPK model highlight the importance of ABCB1 transport in the biodistribution of docetaxel. As is well known, many therapeutic agents are ABCB1 substrates and, thus, likely are subject to similar pharmacokinetic changes when ABCB1 function is altered. To our knowledge, the only other whole-body mouse PBPK model that incorporates ABCB1 transport (but only in non-eliminating tissues, namely brain and heart) is a model of domperidone, an antiemetic drug associated with cardiac toxicity [50]. Both this and our work clearly illustrate the utility of PBPK modeling for further understanding the physiological mechanics of drug distribution in tissues expressing ABCB1.

An in-depth comprehension of the effects of ABCB1 transport on drug pharmacokinetics and pharmacodynamics is advantageous to human medicine because large interindividual differences in ABCB1 expression have been reported. While no null alleles have been found for ABCB1 in humans thus far, single nucleotide polymorphisms (SNPs) that affect the structure and function of the transporter have been discovered [51]. One of the most frequently found set

of variants is the 1236C>T (G412G), 2677G>T (A893S) and 3435C>T (I1145I) haplotype that is found in roughly 25-40% of Caucasians and Asians [52]. In a study comprising the pharmacogenetic screening of CYP3A and ABCB1 in relation to population pharmacokinetics of docetaxel, the homozygous 1236C>T polymorphism in the ABCB1 gene was significantly correlated with a 25% decrease in docetaxel clearance [53]. This is in contrast to work that found polymorphisms in the CYP3A genes but not in ABCB1 had a profound effect on docetaxel exposure [54]. Thus, the former study suggests that dose-adaptation based on characterization of the 1236C>T status of ABCB1 may result in reduced interindividual variation of docetaxel pharmacokinetics while the latter study argues against screening for ABCB1 polymorphisms. However, a critical limitation of both studies is that docetaxel analysis was performed only in human plasma, which, of course, is common as it is not feasible to collect actual tissue concentration data from humans.

As shown by our work, although plasma docetaxel concentrations are virtually the same in FVB and KO mice, there are significant differences in tissue exposure to this taxane that are directly related to ABCB1 transport. And, it is in these tissues that docetaxel-associated toxicities occur. Thus, it is of the utmost importance to understand not only the plasma but also the tissue distribution of docetaxel (as well as other drugs) to truly assess the necessity of dose modifications based on protein functionality. For this purpose, PBPK modeling is an ideal tool. Our data and model suggest that adjusting the dose of docetaxel in relation to ABCB1 function is imperative to minimize detrimental tissue exposure and toxicity related to this compound. To determine the pertinence of this type of dose modification to humans, the present mouse PBPK model can be scaled to humans by taking into account interspecies differences in physiology and physiochemistry. In this way, we can estimate the affect of ABCB1 transport on both the plasma and tissue distribution of docetaxel in humans and subsequently use *in silico*

experimentation prior to clinical trials for optimization of the administration of docetaxel to maximize efficacy and minimize toxicity.

Acknowledgements:

We are grateful to AJ Beaupre for performing all of the intravenous tail vein injections for the mouse studies. Additionally, we are grateful to Robin McDougall (The AEgis Technologies Group, Oshawa, ON, USA) for all of his help and guidance with the PBPK modeling.

Grant Support:

This work was supported by grant number W81XWH-09-1-0457 from the Department of Defense (DOD) Breast Cancer Research Program (BCRP) of the Office of the Congressionally Directed Medical Research Programs (CDMRP).

Figure Legend:

Figure 1: Observed docetaxel concentrations in mouse lung, kidney, heart, liver, intestine, plasma and brain and observed total docetaxel amount in feces following an intravenous dose of 3 mg/kg. Black bars represent the data from FVB mice. White bars represent the data from Mdr1a/b knockout (KO) mice. For all observed data, error bars symbolize standard deviation (SD).

Figure 2: Schematic representation of a physiologically-based pharmacokinetic (PBPK) model of docetaxel incorporating intravenous drug administration, intestinal and hepatic metabolism, enterohepatic recycling (EHR), glomerular filtration, tubular reabsorption, urinary and fecal elimination and ABCB1 transport.

Figure 3: Observed and PBPK model-simulated docetaxel concentrations in mouse lung, kidney, heart, liver, intestine, plasma and brain and model-predicted intestinal and hepatic metabolism following an intravenous dose of 3 mg/kg. Black diamonds represent the observed data from FVB mice. White diamonds represent the observed data from Mdr1a/b knockout (KO) mice. For all observed data, error bars symbolize standard deviation (SD). Solid lines and dashed lines indicate PBPK model predictions for FVB and KO mice, respectively.

Figure 4: Calculated sensitivity coefficients for PBPK model parameters with respect to plasma area under the concentration-time curve (AUC) for the FVB mouse model. Only parameters with sensitivity coefficients > 0.01 are shown. FQ_KID: fractional blood flow to kidney, FV_INT: fractional volume of intestine, FV_BLD: fractional volume of blood, K_LMET: first-order rate constant for hepatic metabolism, KMT: Michaelis-Menten constant (Km) for ABCB1 transport, VMAXT_KID: maximum rate (Vmax) of ABCB1 transport from kidney, FV_KID: fractional volume of kidney, FU: unbound fraction of docetaxel in the blood and FQ_INT: fractional blood flow to intestine.

References:

1. Bruno, R., et al., *A population pharmacokinetic model for docetaxel (Taxotere): model building and validation.* J Pharmacokinet Biopharm, 1996. **24**(2): p. 153-72.

2. Bruno, R. and G.J. Sanderink, *Pharmacokinetics and metabolism of Taxotere (docetaxel).* Cancer Surv, 1993. **17**: p. 305-13.

3. Marre, F., et al., *Hepatic biotransformation of docetaxel (Taxotere) in vitro: involvement of the CYP3A subfamily in humans.* Cancer Res, 1996. **56**(6): p. 1296-302.

4. Shirakawa, K., et al., *Interaction of docetaxel ("Taxotere") with human P-glycoprotein.* Jpn J Cancer Res, 1999. **90**(12): p. 1380-6.

5. Gros, P., J. Croop, and D. Housman, *Mammalian multidrug resistance gene: complete cDNA sequence indicates strong homology to bacterial transport proteins.* Cell, 1986. **47**(3): p. 371-80.

6. Hsu, S.I., L. Lothstein, and S.B. Horwitz, *Differential overexpression of three mdr gene family members in multidrug-resistant J774.2 mouse cells. Evidence that distinct P-glycoprotein precursors are encoded by unique mdr genes.* J Biol Chem, 1989. **264**(20): p. 12053-62.

7. Devault, A. and P. Gros, *Two members of the mouse mdr gene family confer multidrug resistance with overlapping but distinct drug specificities.* Mol Cell Biol, 1990. **10**(4): p. 1652-63.

8. Croop, J.M., et al., *The three mouse multidrug resistance (mdr) genes are expressed in a tissue-specific manner in normal mouse tissues.* Mol Cell Biol, 1989. **9**(3): p. 1346-50.

9. Thiebaut, F., et al., *Cellular localization of the multidrug-resistance gene product P-glycoprotein in normal human tissues.* Proc Natl Acad Sci U S A, 1987. **84**(21): p. 7735-8.

10. Cordon-Cardo, C., et al., *Multidrug-resistance gene (P-glycoprotein) is expressed by endothelial cells at blood-brain barrier sites.* Proc Natl Acad Sci U S A, 1989. **86**(2): p. 695-8.

11. Sugawara, I., et al., *Tissue distribution of P-glycoprotein encoded by a multidrug-resistant gene as revealed by a monoclonal antibody, MRK 16.* Cancer Res, 1988. **48**(7): p. 1926-9.

12. Dano, K., *Active outward transport of daunomycin in resistant Ehrlich ascites tumor cells.* Biochim Biophys Acta, 1973. **323**(3): p. 466-83.

13. Szakacs, G., et al., *Targeting multidrug resistance in cancer.* Nat Rev Drug Discov, 2006. **5**(3): p. 219-34.

14. Krishnan, K., et al., *PBPK modeling: a primer*, in *Quantitative modeling in toxicology*, K. Krishnan and M.E. Andersen, Editors. 2010, John Wiley & Sons: Chichester, West Sussex. p. xvii, 485 p.

15. Andersen, M.E., et al., *Introduction: a historical perspective of the development and applications of PBPK models*, in *Physiologically based pharmacokinetic modeling : science and applications*, M.B. Reddy, et al., Editors. 2005, Wiley-Interscience: Hoboken, N.J. p. xix, 420 p.

16. Norris, D.A., et al., *Development of predictive pharmacokinetic simulation models for drug discovery.* J Control Release, 2000. **65**(1-2): p. 55-62.

17. Theil, F.P., et al., *Utility of physiologically based pharmacokinetic models to drug development and rational drug discovery candidate selection.* Toxicol Lett, 2003. **138**(1-2): p. 29-49.

18. Schinkel, A.H., et al., *Normal viability and altered pharmacokinetics in mice lacking mdr1-type (drug-transporting) P-glycoproteins.* Proc Natl Acad Sci U S A, 1997. **94**(8): p. 4028-33.

19. Bradshaw-Pierce, E.L., S.G. Eckhardt, and D.L. Gustafson, *A physiologically based pharmacokinetic model of docetaxel disposition: from mouse to man.* Clin Cancer Res, 2007. **13**(9): p. 2768-76.

20. Gustafson, D.L., et al., *Analysis of docetaxel pharmacokinetics in humans with the inclusion of later sampling time-points afforded by the use of a sensitive tandem LCMS assay.* Cancer Chemother Pharmacol, 2003. **52**(2): p. 159-66.

21. Brown, R.P., et al., *Physiological parameter values for physiologically based pharmacokinetic models.* Toxicol Ind Health, 1997. **13**(4): p. 407-84.

22. Urien, S., et al., *Docetaxel serum protein binding with high affinity to alpha 1-acid glycoprotein.* Invest New Drugs, 1996. **14**(2): p. 147-51.

23. Wierzba, K., et al., *Tubulin as a major determinant of tissue distribution of vincristine.* J Pharm Sci, 1987. **76**(12): p. 872-5.

24. Diaz, J.F. and J.M. Andreu, *Assembly of purified GDP-tubulin into microtubules induced by taxol and taxotere: reversibility, ligand stoichiometry, and competition.* Biochemistry, 1993. **32**(11): p. 2747-55.

25. Chabner, B. and D.L. Longo, *Cancer chemotherapy and biotherapy : principles and practice*. 5th ed., Philadelphia: Wolters Kluwer Health/Lippincott Williams & Wilkins. xv, 812 p.

26. Huls, M., et al., *P-glycoprotein-deficient mice have proximal tubule dysfunction but are protected against ischemic renal injury.* Kidney Int, 2007. **72**(10): p. 1233-41.

27. van Herwaarden, A.E., et al., *Knockout of cytochrome P450 3A yields new mouse models for understanding xenobiotic metabolism.* J Clin Invest, 2007. **117**(11): p. 3583-92.

28. Zhang, Q.Y., D. Dunbar, and L.S. Kaminsky, *Characterization of mouse small intestinal cytochrome P450 expression.* Drug Metab Dispos, 2003. **31**(11): p. 1346-51.

29. Loccisano, A.E., et al., *Comparison and evaluation of pharmacokinetics of PFOA and PFOS in the adult rat using a physiologically based pharmacokinetic model.* Reprod Toxicol. **33**(4): p. 452-67.

30. Hudachek, S.F. and D.L. Gustafson, *Physiologically based pharmacokinetic model of lapatinib developed in mice and scaled to humans.* J Pharmacokinet Pharmacodyn.

31. van Waterschoot, R.A. and A.H. Schinkel, *A critical analysis of the interplay between cytochrome P450 3A and P-glycoprotein: recent insights from knockout and transgenic mice.* Pharmacol Rev. **63**(2): p. 390-410.

32. Benet, L.Z., *The drug transporter-metabolism alliance: uncovering and defining the interplay.* Mol Pharm, 2009. **6**(6): p. 1631-43.

33. Bardelmeijer, H.A., et al., *Low systemic exposure of oral docetaxel in mice resulting from extensive first-pass metabolism is boosted by ritonavir.* Cancer Res, 2002. **62**(21): p. 6158-64.

34. Bischoff, K.B., R.L. Dedrick, and D.S. Zaharko, *Preliminary model for methotrexate pharmacokinetics.* J Pharm Sci, 1970. **59**(2): p. 149-54.

35. Bischoff, K.B., et al., *Methotrexate pharmacokinetics.* J Pharm Sci, 1971. **60**(8): p. 1128-33.

36. Zaharko, D.S., et al., *Methotrexate tissue distribution: prediction by a mathematical model.* J Natl Cancer Inst, 1971. **46**(4): p. 775-84.

37. Evans, W.E., et al., *Pharmacokinetic modeling of cisplatin disposition in children and adolescents with cancer.* Cancer Chemother Pharmacol, 1982. **10**(1): p. 22-6.

38. Lutz, R.J., et al., *A model for the kinetics of distribution of actinomycin-D in the beagle dog.* J Pharmacol Exp Ther, 1977. **200**(3): p. 469-78.

39. Collins, J.M., et al., *Nonlinear pharmacokinetic models for 5-fluorouracil in man: intravenous and intraperitoneal routes.* Clin Pharmacol Ther, 1980. **28**(2): p. 235-46.

40. Tsukamoto, Y., et al., *A physiologically based pharmacokinetic analysis of capecitabine, a triple prodrug of 5-FU, in humans: the mechanism for tumor-selective accumulation of 5-FU.* Pharm Res, 2001. **18**(8): p. 1190-202.

41. Dedrick, R.L., D.D. Forrester, and D.H. Ho, *In vitro-in vivo correlation of drug metabolism--deamination of 1- -D-arabinofuranosylcytosine.* Biochem Pharmacol, 1972. **21**(1): p. 1-16.

42. Harris, P.A. and J.F. Gross, *Preliminary pharmacokinetic model for adriamycin (NSC-123127).* Cancer Chemother Rep, 1975. **59**(4): p. 819-25.

43. Chan, K.K., et al., *Prediction of adriamycin disposition in cancer patients using a physiologic, pharmacokinetic model.* Cancer Treat Rep, 1978. **62**(8): p. 1161-71.

44. Gustafson, D.L., et al., *Doxorubicin pharmacokinetics: Macromolecule binding, metabolism, and excretion in the context of a physiologic model.* J Pharm Sci, 2002. **91**(6): p. 1488-501.

45. Sung, C., et al., *A pharmacokinetic model of topotecan clearance from plasma and cerebrospinal fluid.* Cancer Res, 1994. **54**(19): p. 5118-22.

46. Kemper, E.M., et al., *Improved penetration of docetaxel into the brain by co-administration of inhibitors of P-glycoprotein.* Eur J Cancer, 2004. **40**(8): p. 1269-74.

47. Padowski, J.M. and G.M. Pollack, *Pharmacokinetic and pharmacodynamic implications of P-glycoprotein modulation.* Methods Mol Biol. **596**: p. 359-84.

48. Badhan, R., et al., *Methodology for development of a physiological model incorporating CYP3A and P-glycoprotein for the prediction of intestinal drug absorption.* J Pharm Sci, 2009. **98**(6): p. 2180-97.

49. Kivisto, K.T., M. Niemi, and M.F. Fromm, *Functional interaction of intestinal CYP3A4 and P-glycoprotein.* Fundam Clin Pharmacol, 2004. **18**(6): p. 621-6.

50. Fenneteau, F., et al., *Assessing drug distribution in tissues expressing P-glycoprotein through physiologically based pharmacokinetic modeling: model structure and parameters determination.* Theor Biol Med Model, 2009. **6**: p. 2.

51. Robey, R.W., et al., *ABC transporters: unvalidated therapeutic targets in cancer and the CNS.* Anticancer Agents Med Chem. **10**(8): p. 625-33.

52. Fung, K.L. and M.M. Gottesman, *A synonymous polymorphism in a common MDR1 (ABCB1) haplotype shapes protein function.* Biochim Biophys Acta, 2009. **1794**(5): p. 860-71.

53. Bosch, T.M., et al., *Pharmacogenetic screening of CYP3A and ABCB1 in relation to population pharmacokinetics of docetaxel.* Clin Cancer Res, 2006. **12**(19): p. 5786-93.

54. Baker, S.D., et al., *Pharmacogenetic pathway analysis of docetaxel elimination.* Clin Pharmacol Ther, 2009. **85**(2): p. 155-63.

Table 1
Click here to download Table: Table 1.doc

Table 1. Comparison of docetaxel exposure (AUC) in FVB and Mdr1a/b knockout (KO) mice.

Sample	Observed FVB $AUC_{1\text{-}12hr}$ (nM×hr)	Predicted FVB $AUC_{1\text{-}12hr}$ (nM×hr)	Observed KO $AUC_{1\text{-}12hr}$ (nM×hr)	Predicted KO $AUC_{1\text{-}12hr}$ (nM×hr)	% Difference between Observed FVB AUC & Observed KO AUC[a]	% Difference between Observed FVB AUC & Predicted FVB AUC[b]	% Difference between Observed KO AUC & Predicted KO AUC[c]
Lung	18866	17368	43833	46082	+132%	-7.9%	+5.1%
Kidney	14497	15408	20665	20514	+43%	+6.3%	-0.7%
Heart	12952	11483	18895	19442	+46%	-11.3%	+2.9%
Liver	4344	3969	4605	4741	+6%	-8.6%	+3.0%
Intestine	3214	3113	7648	7665	+138%	-3.1%	+0.2%
Plasma	523	508	481	552	-8%	-2.9%	+14.8%
Brain	184	176	1001	1149	+444%	-4.3%	+14.8%

Abbreviations: $AUC_{1\text{-}12hr}$, area under the concentration-time curve from 1 to 12 hrs.

[a]Percent (%) difference was calculated as $100\times\left(\left(KOAUC_{observed}-FVBAUC_{observed}\right)\Big/\left(FVBAUC_{observed}\right)\right)$.

[b]Percent (%) difference was calculated as $100\times\left(\left(FVBAUC_{predicted}-FVBAUC_{observed}\right)\Big/\left(FVBAUC_{observed}\right)\right)$.

[c]Percent (%) difference was calculated as $100\times\left(\left(KOAUC_{predicted}-KOAUC_{observed}\right)\Big/\left(KOAUC_{observed}\right)\right)$.

Table 2
Click here to download Table: Table 2.doc

Table 2. PBPK model parameter values.

Parameter	Value
Docetaxel molecular weight[a]	581.06 g/mol
Fraction of docetaxel bound to plasma proteins[a]	0.93
Tissue volumes	% of body weight
Blood[a]	4.90
Brain[a]	1.65
Heart[a]	0.50
Lung[a]	0.73
Kidney[a]	1.67
Intestine[a]	4.22
Liver[a]	5.49
Slowly perfused[a]	80.84
Tissue blood flows	% of cardiac output
Brain[a]	3.3
Heart[a]	6.6
Lung[a]	100
Kidney[a]	9.1
Intestine[a]	14.1
Liver[a]	2.0
Slowly perfused[a]	64.9
Partition coefficients	ratio
Brain:plasma[b]	58
Heart:plasma[b]	990
Lung:plasma[b]	2376
Kidney:plasma[b]	995
FVB intestine:plasma[b]	195
KO intestine:plasma[b]	397
Liver:plasma[b]	7088
Slowly perfused:plasma[b]	748
Tubulin binding capacities	nmol/kg
Brain[a]	10710
Heart[a]	1970
Lung[a]	2580
Kidney[a]	1470
Intestine[a]	1080
Liver[a]	3510
Slowly perfused[b]	521
Tubulin binding affinity[a]	19 nM
Metabolism	
First-order liver metabolism rate constant[b]	3664 hr^{-1}
First-order FVB intestine metabolism rate constant[b]	19 hr^{-1}
Saturable KO intestine metabolism K_m[a]	600 nmol/kg
Saturable KO intestine metabolism V_{max}[a]	2654 nmol/hr/kg
Glomerular filtration and tubular reabsorption	
FVB fraction kidney blood flow filtered at glomerulus[a]	0.265
KO fraction kidney blood flow filtered at glomerulus[a]	0.187
FVB tubular reabsorption rate constant[b]	0.02 hr^{-1}
KO tubular reabsorption rate constant[b]	1.8 hr^{-1}
PGP transport	
K_m[b]	28 nmol/kg
Brain V_{max}[b]	14581 nmol/hr/kg
Heart V_{max}[b]	14599 nmol/hr/kg
Lung V_{max}[b]	340176 nmol/hr/kg
Kidney V_{max}[b]	3003 nmol/hr/kg
Slowly perfused V_{max}[b]	10 nmol/hr/kg

[a]Values obtained from the literature.
[b]Values determined by parameter estimation.

Figure 1
Click here to download Figure: Figure 1.pdf

Figure 1

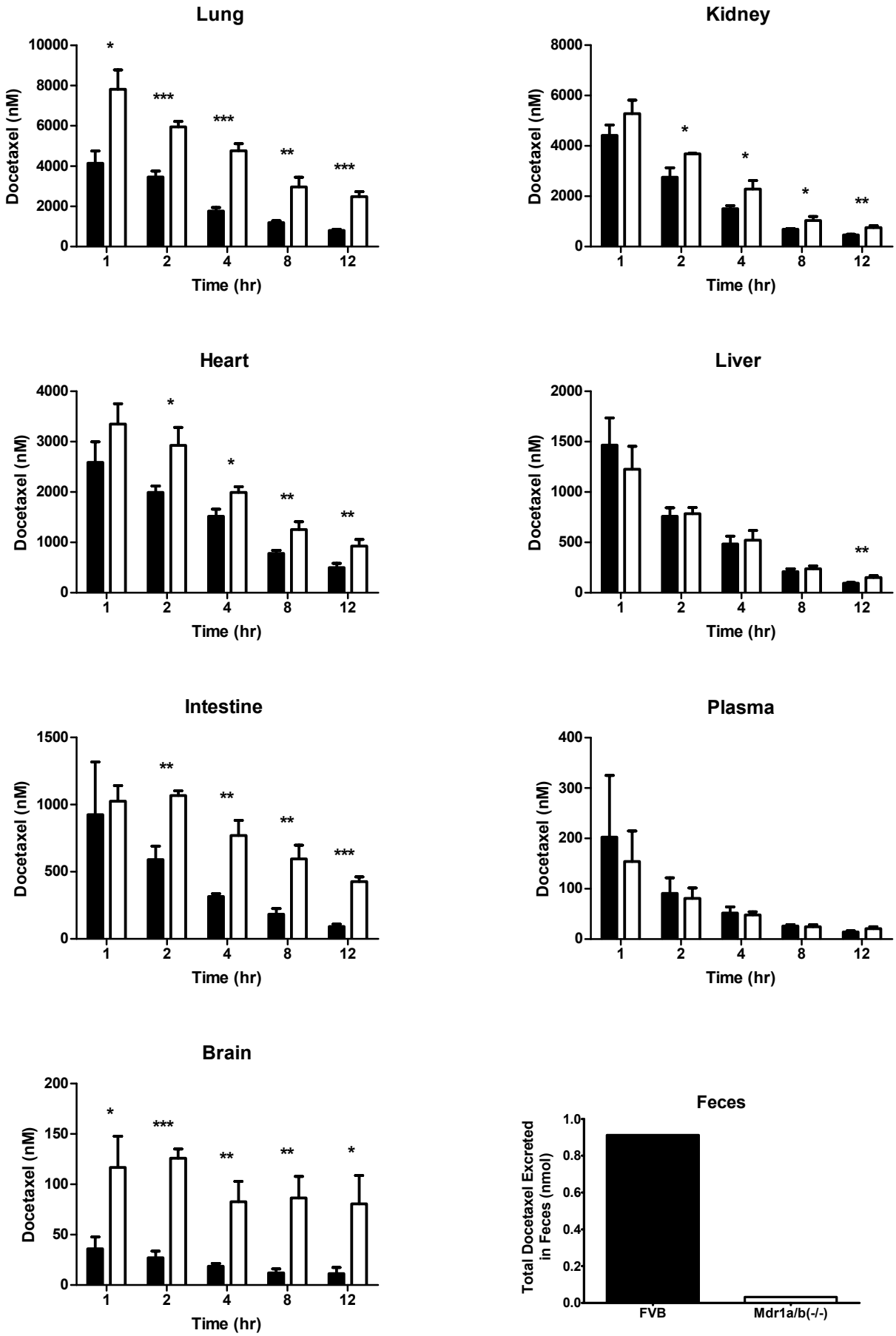

Figure 2

Figure 2

Click here to download Figure: Figure 2.pdf

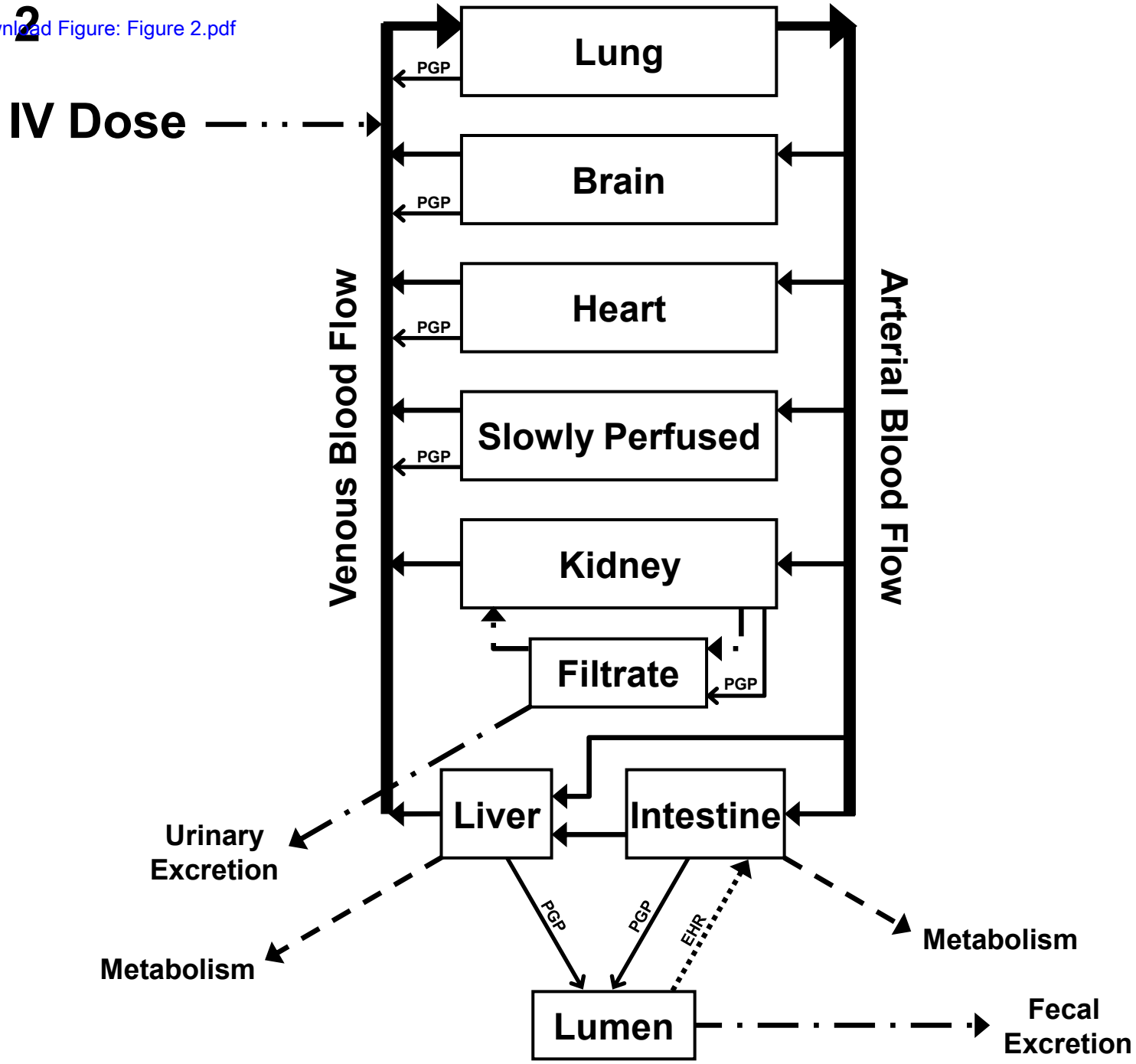

Figure 3
Click here to download Figure: Figure 3.pdf

Figure 3

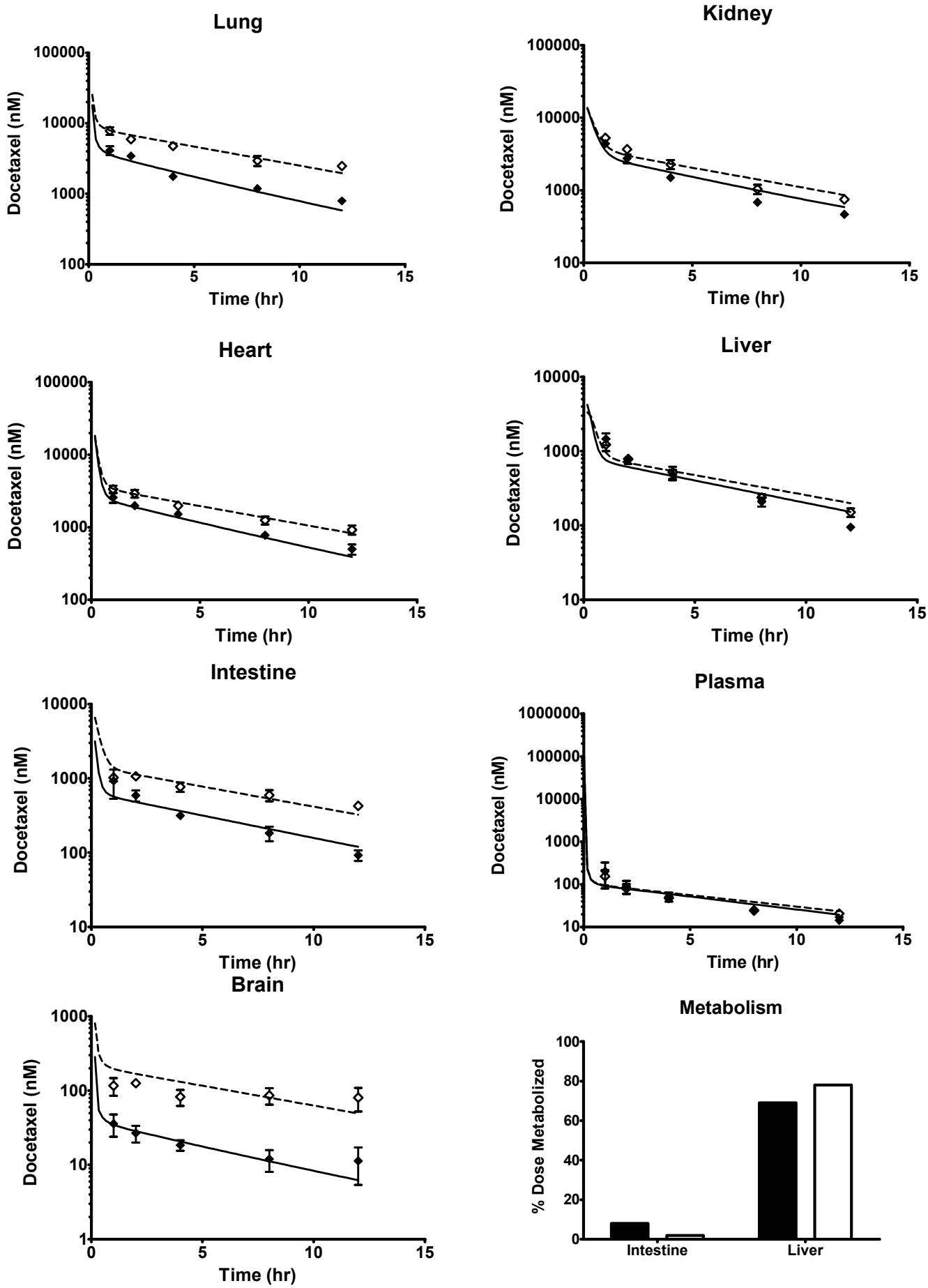

Figure 4
Click here to download Figure: Figure 4.pdf

Figure 4

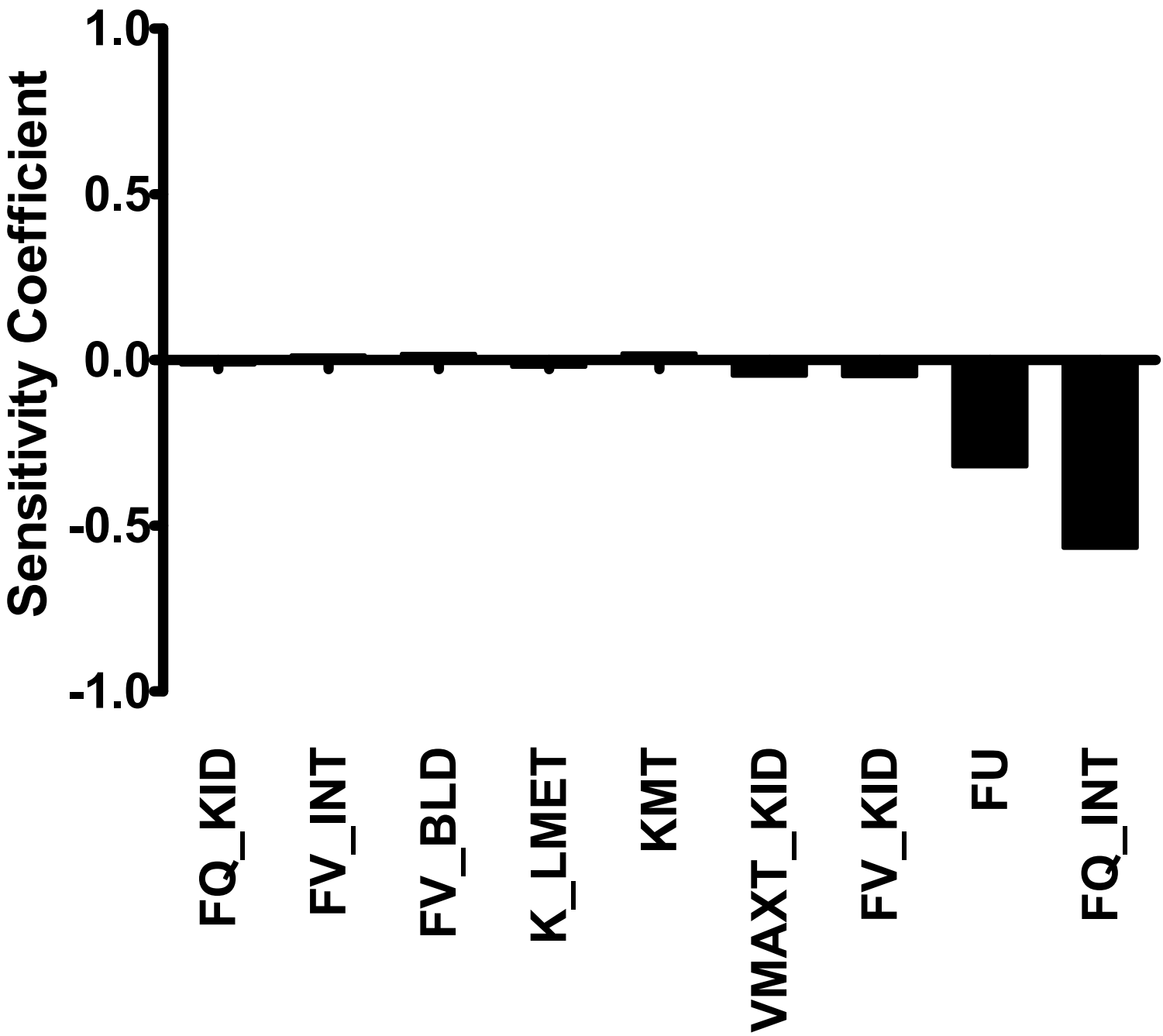

Electronic Supplementary Material

Click here to download Electronic Supplementary Material: Model Code.doc

```
program: FVB PBPK Mouse Model of Docetaxel including PGP Transport Mice !file: DTX_Mouse_FINAL_FVB.csl

initial

!Gear's Stiff Integration Algorithm
algorithm ialg = 2

!Dosing parameters
      constant Dose = 3 !intravenous dose; UNITS: mg/kg; tail vein injection
      constant MW = 861.9 !UNITS: g/mol
      DDose = (Dose*1000000*BW)/MW !delivered dose; UNITS: nmol; scaled to bodyweight
      constant fu = 0.07 !fraction docetaxel unbound in blood; 93% bound to plasma proteins from 8913835

!Timing Commands
      constant TSTOP = 12 !length of experiment; UNITS: hr
      constant POINTS = 72 !number of points
      CINT = TSTOP/POINTS !interval of data collection (every 10 min); UNITS: hr

!Organ blood flow parameters
      CO = 0.275*(BW**0.75)*60 !cardiac output; UNITS: L/hr; from Brown (9249929) page 440
      constant FQ_liv = 0.020 !flow to liver; UNITS: fraction CO; liver hepatic artery from Brown (9249929) page 438
      constant FQ_int = 0.141 !flow to intestine; UNITS: fraction CO; liver portal vein from Brown (9249929) page 438
      constant FQ_kid = 0.091 !flow to kidneys; UNITS: fraction CO; from Brown (9249929) page 438
      constant FQ_brn = 0.033 !flow to brain; UNITS: fraction CO; from Brown (9249929) page 438
      constant FQ_hrt = 0.066 !flow to heart; UNITS: fraction CO; from Brown (9249929) page 438
      constant FQ_lng = 1.000 !flow to lungs; UNITS: fraction CO; from Brown (9249929) page 445

!Organ volume parameters
      constant BW = 0.020 !bodyweight; UNITS: kg
      constant FV_liv = 0.0549 !volume of liver; UNITS: fraction BW; from Brown (9249929) page 416
      constant FV_int = 0.0422 !volume of intestinal tract; UNITS: fraction BW; from Brown (9249929) page 416
      constant FV_kid = 0.0167 !volume of kidneys; UNITS: fraction BW; from Brown (9249929) page 416
      constant FV_brn = 0.0165 !volume of brain; UNITS: fraction BW; from Brown (9249929) page 416
      constant FV_hrt = 0.0050 !volume of heart; UNITS: fraction BW; from Brown (9249929) page 416
      constant FV_lng = 0.0073 !volume of lungs; UNITS: fraction BW; from Brown (9249929) page 416
      constant FV_bld = 0.0490 !volume of blood; UNITS: fraction BW: from Brown (9249929) page 435

!Mass balance parameters
      FQ_sp = 1-FQ_liv-FQ_int-FQ_kid-FQ_brn-FQ_hrt !flow to slowly perfused tissue; UNITS: fraction CO
```

```
      FV_sp = 1-FV_liv-FV_int-FV_kid-FV_brn-FV_hrt-FV_lng-FV_bld !volume slowly perfused tissue; UNITS: fraction BW

!Partition coefficients
      constant P_liv = 7088 !liver:plasma partition coefficient; from PE
      constant P_kid = 995 !kidney:plasma partition coefficient; from PE
      constant P_brn = 58 !brain:plasma partition coefficient; from PE
      constant P_hrt = 990 !heart:plasma partition coefficient; from PE
      constant P_lng = 2376 !lungs:plasma partition coefficient; from PE
      constant P_sp =  748 !slowly perfused tissues:plasma partition coefficient; from PE
      constant P_int_fvb = 195 !intestine:plasma partition coefficient for FVB mice; from PE
      constant P_int_ko  = 397 !intestine:plasma partition coefficient for KO mice; from PE

!Tubulin binding capacities
      constant TB_liv = 3510 !liver tubulin binding capacity; UNITS: nmol/kg; from 3440929
      constant TB_int = 1080 !intestine tubulin binding capacity; UNITS: nmol/kg; from 3440929
      constant TB_kid = 1470 !kidney tubulin binding capacity; UNITS: nmol/kg; from 3440929
      constant TB_brn = 10710 !brain tubulin binding capacity; UNITS: nmol/kg; from 3440929
      constant TB_hrt = 1970 !heart tubulin binding capacity; UNITS: nmol/kg; from 3440929
      constant TB_lng = 2580 !lung tubulin binding capacity; UNITS: nmol/kg; from 3440929
      constant TB_sp = 521 !slowly perfused tissue tubulin binding capacity; UNITS: nmol/kg; from PE

!Tubulin binding affinity; from Cancer Chemotherapy and Biotherapy: Principles and Practice by Bruce A Chabner and
Dan L. Longo, page 234, and 8096151
      constant KD = 19 !UNITS: nmol/L

!Metabolism parameters
      constant KMM_int_ko = 600 !Michaelis-Menten constant for intestinal metabolism in KO mice; UNITS: nmol/kg; from
17975676
      constant VMAXM_int_ko = 2654 !Maximum rate of intestinal metabolism in KO mice; UNITS: nmol/hr/kg; from
17975676 and 14570766
      constant K_IMET_fvb = 19 !First-order rate constant for intestinal metabolism in FVB mice; UNITS: 1/hr; from PE
      constant K_LMET = 3664 !First-order rate constant for hepatic metabolism; UNITS: 1/hr; from PE

!PGP transport
      constant KMT = 28 !Michaelis-Menten constant for PGP transport; UNITS: nmol/kg; from PE
      constant VMAXT_brn = 14581 !Maximum rate of PGP transport from brain to blood; UNITS: nmol/hr/kg; from PE
      constant VMAXT_hrt = 14599 !Maximum rate of PGP transport from heart to blood; UNITS: nmol/hr/kg; from PE
      constant VMAXT_lng = 340176 !Maximum rate of PGP transport from lung to blood; UNITS: nmol/hr/kg; from PE
      constant VMAXT_sp = 10 !Maximum rate of PGP transport from muscle to blood; UNITS: nmol/hr/kg; from PE
```

```
      constant VMAXT_kid = 3003 !Maximum rate of PGP transport from kidney to urine; UNITS: nmol/hr/kg; from PE
      constant VMAXT_int = 0 !Maximum rate of PGP transport from intestine to lumen; UNITS: nmol/hr/kg; set to zero
      constant VMAXT_liv = 0 !!Maximum rate of PGP transport from liver to lumen; UNITS: nmol/hr/kg; set to zero

!Glomerular filtration
      constant fgf_fvb = 0.265 !Fraction of kidney blood flow filtered at the glomerulus in FVB mice; UNITS: fraction
CO; from 17851469
      constant fgf_ko  = 0.187 !Fraction of kidney blood flow filtered at the glomerulus in KO mice; UNITS: fraction
CO; from 17851469

!First-order reabsorption from urine into kidney
      constant k_rabs_fvb = 0.02 !First-order reabsorption from urine into kidney in FVB mice; UNITS: 1/hr; from PE
      constant k_rabs_ko = 1.8 !First-order reabsorption from urine into kidney in KO mice; UNITS: 1/hr; from PE

!First-order enterohepatic recycling
      constant k_ehr = 0 !UNITS: 1/hr; set to zero

!Flags
      constant VMAXT_flag = 1 !FVB = 1, KO = 0
      constant VMAXM_flag_fvb = 1 !FVB = 1, KO = 0
      constant VMAXM_flag_ko = 0 !FVB = 0, KO = 1
      constant P_int_flag = 1 !FVB = 1, KO = 0
      constant fgf_flag = 1 !FVB = 1, KO = 0
      constant k_rabs_flag = 1 !FVB = 1, KO = 0

      if(P_int_flag==1)then
      P_int = P_int_fvb
      else
      P_int = P_int_ko
      endif

      if(fgf_flag==1)then
      fgf = fgf_fvb
      else
      fgf = fgf_ko
      endif

      if(k_rabs_flag==1)then
      k_rabs = k_rabs_fvb
```

```
      else
      k_rabs = k_rabs_ko
      endif

!Scaled blood flow parameters in L/hr
      Q_liv = FQ_liv*CO
      Q_int = FQ_int*CO
      Q_kid = FQ_kid*CO
      Q_brn = FQ_brn*CO
      Q_hrt = FQ_hrt*CO
      Q_lng = FQ_lng*CO
      Q_sp = FQ_sp*CO

!Scaled volume parameters in kg
      V_liv = FV_liv*BW
      V_int = FV_int*BW
      V_kid = FV_kid*BW
      V_brn = FV_brn*BW
      V_hrt = FV_hrt*BW
      V_lng = FV_lng*BW
      V_sp = FV_sp*BW
      V_bld = FV_bld*BW
      V_pl = V_bld/2

!Scaled tubulin binding capacities in nmol
      STB_liv = TB_liv*V_liv
      STB_int = TB_int*V_int
      STB_kid = TB_kid*V_kid
      STB_brn = TB_brn*V_brn
      STB_hrt = TB_hrt*V_hrt
      STB_lng = TB_lng*V_lng
      STB_sp = TB_sp*V_sp

!Scaled metabolism and transport parameters
      SVMAXM_int_ko = VMAXM_int_ko*V_int !UNITS: nmol/hr
      SVMAXT_brn = VMAXT_brn*V_brn !UNITS: nmol/hr
      SVMAXT_hrt = VMAXT_hrt*V_hrt !UNITS: nmol/hr
      SVMAXT_lng = VMAXT_lng*V_lng !UNITS: nmol/hr
      SVMAXT_sp = VMAXT_sp*V_sp !UNITS: nmol/hr
```

```
      SVMAXT_kid = VMAXT_kid*V_kid !UNITS: nmol/hr
      SVMAXT_int = VMAXT_int*V_int !UNITS: nmol/hr
      SVMAXT_liv = VMAXT_liv*V_liv !UNITS: nmol/hr

!Mass balance checks
      FQ_total = FQ_liv+FQ_int+FQ_kid+FQ_brn+FQ_hrt+FQ_sp !should equal 1
      FV_total = FV_liv+FV_int+FV_kid+FV_brn+FV_hrt+FV_lng+FV_bld+FV_sp !should equal 1
      Q_total = Q_liv+Q_int+Q_kid+Q_brn+Q_hrt+Q_sp !should equal CO
      V_total = V_liv+V_int+V_kid+V_brn+V_hrt+V_lng+V_sp+V_bld !should equal BW

end

derivative

!Brain concentration
      dA_brn = (Q_brn*(C_art-C_v_brn))-dA_btp !Rate of change of amount in brain; UNITS: nmol/hr
      C_v_brn = C_brn/((P_brn*fu)+(STB_brn/(KD+C_v_brn))) !Concentration in brain venous blood; UNITS: nmol/L
      A_brn = integ(dA_brn,0.0) !Amount in brain; UNITS: nmol
      C_brn = A_brn/V_brn !Concentration in brain; UNITS: nmol/L
      AUC_brn = integ(C_brn,0.0) !AUC in the brain; UNITS: nmol/L * hr

!Brain transport
      dA_btp = ((SVMAXT_brn*C_v_brn)/(KMT+C_v_brn))*VMAXT_flag !Rate of PGP transport from brain into blood; UNITS:
nmol/hr
      A_btp = integ(dA_btp,0.0) !Amount transported by brain PGP; UNITS: nmol

!Heart concentration
      dA_hrt = (Q_hrt*(C_art-C_v_hrt))-dA_htp !Rate of change of amount in heart; UNITS: nmol/hr
      C_v_hrt = C_hrt/((P_hrt*fu)+(STB_hrt/(KD+C_v_hrt))) !Concentration in heart venous blood; UNITS: nmol/L
      A_hrt = integ(dA_hrt,0.0) !Amount in heart; UNITS: nmol
      C_hrt = A_hrt/V_hrt !Concentration in heart; UNITS: nmol/L
      AUC_hrt = integ(C_hrt,0.0) !AUC in heart; UNITS: nmol/L * hr

!Heart transport
      dA_htp = ((SVMAXT_hrt*C_v_hrt)/(KMT+C_v_hrt))*VMAXT_flag !Rate of PGP transport from heart into blood; UNITS:
nmol/hr
      A_htp = integ(dA_htp,0.0) !Amount transported by heart PGP; UNITS: nmol

!Lung concentration
```

```
      dA_lng = (Q_lng*(C_ven-C_v_lng))-dA_lngtp !Rate of change of amount in lungs; UNITS: nmol/hr
      C_v_lng = C_lng/((P_lng*fu)+(STB_lng/(KD+C_v_lng))) !Concentration in lung venous blood; UNITS: nmol/L
      A_lng = integ(dA_lng,0.0) !Amount in lungs; UNITS: nmol
      C_lng = A_lng/V_lng !Concentration in lungs; UNITS: nmol/L
      AUC_lng = integ(C_lng,0.0) !AUC in lungs; UNITS: nmol/L * hr

!Lung transport
      dA_lngtp = ((SVMAXT_lng*C_v_lng)/(KMT+C_v_lng))*VMAXT_flag !Rate of PGP transport from lung into blood; UNITS:
nmol/hr
      A_lngtp = integ(dA_lngtp,0.0) !Amount transported by lung PGP; UNITS: nmol

!Slowly perfused tissue concentration
      dA_sp = (Q_sp*(C_art-C_v_sp))-dA_sptp !Rate of change of amount in slowly perfused tissues; UNITS: nmol/hr
      C_v_sp = C_sp/((P_sp*fu)+(STB_sp/(KD+C_v_sp))) !Concentration in slowly perfused tissue venous blood; UNITS:
nmol/L
      A_sp = integ(dA_sp,0.0) !Amount in slowly perfused tissues; UNITS: nmol
      C_sp = A_sp/V_sp !Concentration in slowly perfused tissues: UNITS: nmol/L
      AUC_sp = integ(C_sp,0.0) !AUC in slowly perfused tissues; UNITS: nmol/L * hr

!Slowly perfused tissue transport
      dA_sptp = ((SVMAXT_sp*C_v_sp)/(KMT+C_v_sp))*VMAXT_flag !Rate of PGP transport from slowly perfused tissue into
blood; UNITS: nmol/hr
      A_sptp = integ(dA_sptp,0.0) !Amount transported by slowly perfused tissue PGP; UNITS: nmol

!Kidney concentration
      dA_kid = Q_kid*(C_art-C_v_kid)+dA_rabs-dA_ktp !Rate of change of amount in kidney; UNITS: nmol/hr
      C_v_kid = C_kid/((P_kid*fu)+(STB_kid/(KD+C_v_kid))) !Concentration in kidney venous blood; UNITS: nmol/L
      A_kid = integ(dA_kid,0.0) !Amount in kidney; UNITS: nmol
      C_kid = A_kid/V_kid !Concentration in kidney: UNITS: nmol/L
      AUC_kid = integ(C_kid,0.0) !AUC in kidney; UNITS: nmol/L * hr

!Kidney transport
      dA_ktp = ((SVMAXT_kid*C_v_kid)/(KMT+C_v_kid))*VMAXT_flag !Rate of PGP transport from kidney into urine; UNITS:
nmol/hr
      A_ktp = integ(dA_ktp,0.0) !Amount transported by kidney PGP; UNITS: nmol

!Glomerular filtration
      dA_gfr = Q_kid*(C_art*fu)*fgf !Rate of glomerular filtration; UNITS: nmol/hr
      A_gfr = integ(dA_gfr,0.0) !Amount filtered at the glomerulus; UNITS: nmol
```

```
!Urine concentration
      dA_urn = dA_gfr-dA_rabs+dA_ktp !Rate of change of amount in urine; UNITS: nmol/hr
      A_urn = integ(dA_urn,0.0) !Amount excreted in urine; UNITS: nmol

!Reabsorption from urine
      dA_rabs = k_rabs*A_urn !Rate of reabsorption into the kidney from the urine; UNITS: nmol/hr
      A_rabs = integ(dA_rabs,0.0) !Amount reabsorbed into the kidney from the urine; UNITS: nmol

!Intestine concentration
      dA_int = Q_int*(C_art-C_v_int)-dA_imet_fvb-dA_imet_ko-dA_itp+dA_ehr !Rate of change of amount in intestine;
UNITS: nmol/hr
      C_v_int = C_int/((P_int*fu)+(STB_int/(KD+C_v_int))) !Concentration in intestine venous blood; UNITS: nmol/L
      A_int = integ(dA_int,0.0) !Amount in intestine; UNITS: nmol
      C_int = A_int/V_int !Concentration in intestine: UNITS: nmol/L
      AUC_int = integ(C_int,0.0) !AUC in intestine; UNITS: nmol/L * hr

!Intestine transport
      dA_itp = ((SVMAXT_int*C_v_int)/(KMT+C_v_int))*VMAXT_flag !Rate of intestinal PGP transport into lumen; UNITS:
nmol/hr
      A_itp = integ(dA_itp,0.0) !Amount transported by intestinal PGP; UNITS: nmol

!Intestine metabolism
      dA_imet_ko = ((SVMAXM_int_ko*C_v_int)/(KMM_int_ko+C_v_int))*VMAXM_flag_ko !Rate of intestinal metabolism in KO
mice; UNITS: nmol/hr
      A_imet_ko = integ(dA_imet_ko,0.0) !Amount metabolized by intestine in KO mice; UNITS: nmol
      dA_imet_fvb = (K_IMET_fvb*C_v_int*V_int)*VMAXM_flag_fvb !Rate of intestinal metabolism in FVB mice; UNITS:
nmol/hr
      A_imet_fvb = integ(dA_imet_fvb,0.0) !Amount metabolized by intestine in FVB mice; UNITS: nmol

!Amount of drug absorbed into intestine from enterohepatic recycling
      dA_ehr = k_ehr*A_lumen !Rate of change in amount recirculated; UNITS: nmol/hr
      A_ehr = integ(dA_ehr,0.0) !Amount recirculated; UNITS: nmol

!Liver concentration
      dA_liv = (Q_liv*C_art)+(Q_int*C_v_int)-((Q_liv+Q_int)*C_v_liv)-dA_lmet-dA_ltp !Rate of change of amount in
liver; UNITS: nmol/hr
      C_v_liv = C_liv/((P_liv*fu)+(STB_liv/(KD+C_v_liv))) !Concentration in liver venous blood; UNITS: nmol/L
      A_liv = integ(dA_liv,0.0) !Amount in liver; UNITS: nmol
```

```
      C_liv = A_liv/V_liv !Concentration in liver: UNITS: nmol/L
      AUC_liv = integ(C_liv,0.0) !AUC in liver; UNITS: nmol/L * hr

!Liver transport
      dA_ltp = ((SVMAXT_liv*C_v_liv)/(KMT+C_v_liv))*VMAXT_flag !Rate of hepatic PGP transport into bile/lumen; UNITS:
nmol/hr
      A_ltp = integ(dA_ltp,0.0) !Amount transported by hepatic PGP; UNITS: nmol

!Liver metabolism
      dA_lmet = K_LMET*C_v_liv*V_liv !Rate of liver metabolism; UNITS: nmol/hr
      A_lmet = integ(dA_lmet,0.0) !Amount metabolized by liver; UNITS: nmol

!Lumen concentration
      dA_lumen = dA_ltp+dA_itp-dA_ehr !Rate of change in lumen; UNITS: nmol/hr
      A_lumen = integ(dA_lumen,0.0) !Amount in lumen; UNITS: nmol

!Feces concentration
      dA_feces = dA_lumen !Rate of change in feces; UNITS: nmol/hr
      A_feces = integ(dA_feces,0.0) !Amount excreted in feces; UNITS: nmol

!Venous and arterial blood and plasma concentrations
      dA_ven = (Q_brn*C_v_brn)+(Q_hrt*C_v_hrt)+(Q_sp*C_v_sp)+(Q_kid*C_v_kid)+((Q_liv+Q_int)*C_v_liv)+(Q_lng*C_v_lng)-
(Q_brn*C_art)+dA_btp+dA_htp+dA_lngtp+dA_sptp-(Q_hrt*C_art)-(Q_sp*C_art)-(Q_kid*C_art)-(Q_int*C_art)-(Q_liv*C_art)-
(Q_lng*C_ven)-dA_gfr !Rate of change in venous blood; UNITS: nmol/hr
      A_ven = integ(dA_ven,DDose) !Amount in venous blood; UNITS: nmol
      C_ven = A_ven/V_bld !Concentration in venous blood; UNITS: nmol/L
      C_art = C_ven !Concentration in arterial blood; UNITS: nmol/L
      C_pl = A_ven/V_pl !Concentration in plasma; UNITS: nmol/L
      AUC_pl = integ(C_pl,0.0) !AUC in plasma; UNITS: nmol/L * hr

!Mass check
  TMass = A_brn+A_hrt+A_lng+A_sp+A_kid+A_int+A_liv+A_ven+A_imet_fvb+A_imet_ko+A_lmet+A_urn+A_feces !should equal
DDose
      Bal = DDose-TMass !should equal zero
      P_exc = ((A_urn+A_feces)/TMass)*100 !Percent excreted
      P_lmet = (A_lmet/TMass)*100 !Percent metabolized by liver
      P_imet = ((A_imet_fvb+A_imet_ko)/TMass)*100 !Percent metabolized by intestine
      P_met = P_lmet+P_imet !Total percent metabolized
```

```
  termt(t .ge. tstop, 'time limit')
end
end
```